

Diss. ETH No. 25595

**Treatment techniques for mixed beam
radiotherapy with simultaneously
optimized photon and electron beams**

Silvan Mueller

DISS. ETH NO. 25595

**Treatment techniques for mixed beam
radiotherapy with simultaneously
optimized photon and electron beams**

A thesis submitted to attain the degree of

DOCTOR OF SCIENCES of ETH ZURICH

(Dr. sc. ETH Zurich)

presented by

SILVAN MUELLER

MSc ETH Physics

born on 16.10.1987

citizen of Malters (LU) and Ruswil (LU)

accepted on the recommendation of

Prof. Dr. M.F.M. Stampanoni, examiner

Prof. Dr. P.J. Keall, co-examiner

PD Dr. P. Manser, co-examiner

2018

This thesis was carried out at the Division of Medical Radiation Physics, Inselspital, Bern University Hospital. This work was supported by Varian Medical Systems and by the Swiss Cancer League & Foundation Cancer Research Switzerland grant KFS-3279-08-2013.

The thesis consists of five papers published in high-ranked medical physics journals: two in *Physics in Medicine & Biology*, two in *Medical Physics* and one in *Biomedical Physics & Engineering Express*.

The publication presented in chapter 4 was the Editor's Choice of the corresponding issue in *Physics in Medicine & Biology*. In addition, the abstract of the preliminary work of the publication presented in chapter 6 received the Best in Physics award at the 59th annual meeting & exhibition of the American Association of Physicists in Medicine (AAPM) in 2017.

Contents

Abstract	5
Zusammenfassung	7
1. Introduction	11
2. Electron beam collimation with a photon MLC for standard electron treatments	23
3. A dosimetric evaluation of different levels of energy and intensity modulation for inversely planned multi-field MERT	55
4. Simultaneous optimization of photons and electrons for mixed beam radiotherapy	79
5. Part 1: Optimization and evaluation of dynamic trajectory radiotherapy	113
6. Part 2: Dynamic mixed beam radiotherapy (DYMBER): Photon dynamic trajectories combined with modulated electron beams	143
7. Discussion	177
8. Conclusions	187
Acknowledgements	189
Curriculum Vitae	191

Abstract

In radiotherapy, electron beams are well suited to treat superficial targets, while sparing distally located organs at risk (OARs) due to their dose fall-off. However, electron beams are limited to treat targets within 5 cm from the patient surface owing to their limited range for the available energies up to 22 MeV. Moreover, OARs located laterally to the target relative to beam direction cannot be spared adequately due to the large penumbra of the electron beams. In contrast to electron beams, photon beams have a very small penumbra and targets can be treated at all locations in the patient because of the exponential dose fall-off. However, this exponential fall-off also leads to a large dose contribution delivered to normal tissue. A treatment approach for mixed beam radiotherapy (MBRT) could merge the advantages of photons and electrons, while keeping their downsides at a minimum. A high potential for treating targets with at least a superficial part is hypothesized. Thus, the aim of this thesis was to develop and investigate treatment techniques for MBRT with simultaneously optimized photon and electron contributions that can be efficiently and accurately delivered using a conventional C-arm treatment unit.

Using the photon multileaf collimator (pMLC) for electron beam collimation instead of cut-outs placed in the electron applicator is suggested to make electron treatments more efficient and to facilitate advanced treatment techniques for modulated electron radiotherapy (MERT) and MBRT. It was shown that today's single electron field treatment plans using cut-out collimation can be replaced by plans of similar treatment plan quality using pMLC collimation with accurately calculated dose distributions at a large source-to-surface distance range of 70-100 cm. Next, the impact of intensity and energy modulation enabled by the pMLC was investigated for MERT plans of the breast, skin, parotid and larynx. Energy modulation was found to be of substantially larger value than intensity modulation to increase treatment plan quality for MERT.

To explore the dosimetric potential of MBRT, a treatment planning process (TPP) was developed allowing to generate pMLC based step and shoot MBRT plans (ssMBRT) with simultaneously optimized and Monte Carlo (MC) calculated photon and

electron contributions. A simulated annealing based direct aperture optimization was implemented and applied for the purpose of simultaneous optimization. ssMBRT plans generated for a left chest wall and a squamous cell carcinoma case dosimetrically outperformed plans for MERT, photon intensity modulated radiation therapy (IMRT) and volumetric modulated arc therapy (VMAT).

Beside of electron beams, conventional C-arm treatment units offer also other degrees of freedom (DoFs), which are not utilized with the current state-of-the-art treatment techniques. Thus, a non-coplanar treatment technique for dynamic trajectory radiotherapy (DTRT) was developed, which utilizes combined dynamic gantry, table and collimator rotations during beam on of a photon beam. For two head and neck, a lung, an esophagus and a prostate case, it was shown that DTRT improves treatment plan quality compared to VMAT. Combining photon dynamic trajectories with step and shoot modulated electron beams, called dynamic mixed beam radiotherapy (DYMBER), would result in a treatment technique utilizing more DoFs than any other treatment technique presented before for conventional C-arm treatment units. Thus, a TPP was developed, which allows to create DYMBER plans. This TPP was applied for a brain and two head and neck cases and the resulting DYMBER plans are dosimetrically superior than DTRT and VMAT plans. Furthermore, MC calculated dose distributions of the DYMBER plans agree very well with absolute dose measurements performed with gafchromic films placed in an anthropomorphic phantom.

In conclusion, this thesis demonstrates the dosimetric value of combining particle types for radiotherapy for the case of photons and electrons. The results of the efficiently and accurately deliverable MBRT plans suggest using MBRT for future clinical applications to treat targets with at least a superficial part of any treatment site with improved treatment plan quality compared to photon-only techniques.

Zusammenfassung

In der Radiotherapie sind Elektronenstrahlen gut geeignet, um oberflächliche Zielvolumen zu bestrahlen, währenddessen tiefer gelegene Risikoorgane (OARs) aufgrund deren Dosisabfall verschont bleiben. Elektronenstrahlen sind für die Behandlung jedoch auf Zielvolumen bis zu einer Tiefe von 5 cm zur Patientenoberfläche limitiert aufgrund deren limitierter Reichweite mit den verfügbaren Strahlenenergien von bis zu 22 MeV. Zudem können OARs seitlich zum Zielvolumen relativ zur Strahlrichtung nicht ausreichend geschont werden wegen der grossen Penumbra von Elektronenstrahlen. Im Kontrast zu Elektronenstrahlen haben Photonenstrahlen eine sehr kleine Penumbra und Zielvolumen können aufgrund des exponentiellen Dosisabfalls an allen Stellen im Patienten behandelt werden. Dieser exponentielle Dosisabfall führt allerdings auch zu grossen Dosisanteilen bei gesundem Gewebe. Ein Behandlungsansatz mit gemischten Strahlen in der Radiotherapie (MBRT) könnte die Vorteile von Photonen und Elektronen vereinen und dabei deren Nachteile auf ein Minimum beschränken. Ein grosses Potential ist für die Behandlung von Zielvolumen mit mindestens einem oberflächlichen Teilvolumen vermutet. Das Ziel dieser Dissertation war es daher Behandlungstechniken für MBRT mit simultan optimierten Photonen- und Elektronenanteilen, welche auf einer konventionellen C-Arm Bestrahlungseinheit effizient und genau abgestrahlt werden können, zu entwickeln und zu untersuchen.

Das Verwenden des Photonen Multilamellenkollimator (pMLC) ist vorgeschlagen anstelle von im Elektronen Applikator platzierten Blöcken für die Kollimation von Elektronenstrahlen um Elektronenbehandlungen effizienter zu machen und fortgeschrittene Behandlungstechniken wie modulierte Elektronenradiotherapie (MERT) und MBRT zu ermöglichen. Es wurde gezeigt, dass die heutigen Pläne mit einem blockkollimierten Feld für Elektronenbehandlungen durch Pläne mit ähnlicher Qualität unter Verwendung von pMLC Kollimation mit genau berechneten Dosisverteilungen für Distanzen zwischen der Strahlquelle zur Patientenoberfläche von 70-100 cm ersetzt werden können. Als Nächstes wurde der Einfluss von Intensitäts- und

Energiemodulierung, welche durch den pMLC ermöglicht wurden, auf MERT Pläne für Brust, Haut, Parotis und Larynx untersucht. Es wurde herausgefunden, dass Energiemodulierung von erheblich höherem Nutzen ist als Intensitätsmodulierung um die Qualität von Behandlungsplänen für MERT zu erhöhen.

Um das dosimetrische Potential von MBRT zu erforschen wurde ein Prozess für die Behandlungsplanung (TPP) entwickelt, welcher es erlaubt pMLC segmentierte MBRT Pläne (ssMBRT) mit simultan optimierten und Monte Carlo (MC) berechneten Photonen- und Elektronenanteilen zu erstellen. Ein "Simulated Annealing" Algorithmus wurde für die direkte Segmentoptimierung (DAO) implementiert und für den Zweck der simultanen Optimierung verwendet. ssMBRT Pläne für einen Fall der linken Brustwand und einen Fall eines Plattenepithelkarzinoms übertrafen dosimetrisch Pläne für MERT, intensitätsmodulierte Photonenradiotherapie (IMRT) und volumetrisch modulierte Bogentherapie (VMAT).

Neben Elektronenstrahlen bieten konventionelle C-Arm Bestrahlungseinheiten weitere Freiheitsgrade (DoFs), welche mit den heutigen modernen Behandlungstechniken nicht verwendet werden. Daher wurde eine nicht-koplanare Behandlungstechnik für Radiotherapie mit dynamischen Trajektorien (DTRT) entwickelt, welche dynamische Rotationen von Bestrahlungsgerät, Behandlungstisch und Kollimator während der Bestrahlung mit Photonenstrahlen kombiniert. Für zwei Kopf- und Halsfälle, ein Lungen-, ein Oesophagus- und ein Prostatafall wurde gezeigt, dass DTRT die Qualität des Behandlungsplans verglichen zu VMAT erhöht. Die Kombination von dynamischen Trajektorien für Photonenstrahlen und mit Segmenten modulierte Elektronenstrahlen, genannt dynamische und gemischte Strahlen für Radiotherapie (DYMBER), wäre eine Bestrahlungstechnik, die mehr DoFs benutzt als je eine andere präsentierte Technik für konventionelle C-Arm Bestrahlungseinheiten zuvor. Daher wurde ein TPP entwickelt, welcher es erlaubt DYMBER Pläne zu erstellen. Dieser TPP wurde für einen Hirnfall und zwei Hals- und Kopffälle angewendet und die resultierenden DYMBER Pläne waren dosimetrisch überlegen gegenüber DTRT und VMAT Plänen. Die MC berechneten Dosisverteilungen der DYMBER Pläne stimmten zudem sehr gut mit absoluten Dosismessungen überein, welche mit

gafchromic Filmen durchgeführt wurden, die in einem anthropomorphen Phantom platziert wurden.

In dieser Dissertation wurde für den Fall von Photonen und Elektronen der dosimetrische Wert von kombinierten Teilchentypen für die Radiotherapie demonstriert. Die Resultate der effizient und genau abstrahlbaren MBRT Pläne suggerieren MBRT für zukünftige klinische Anwendungen zu verwenden, um Zielvolumen mit zumindest einem oberflächlichen Teilvolumen jeglicher Behandlungsstelle mit verbesserter Qualität der Bestrahlungspläne zu behandeln im Vergleich zu Techniken, die ausschliesslich Photonen verwenden.

1

Introduction

Cancer is responsible for 8.2 million of deaths worldwide in 2012 (IARC and Cancer Research UK 2014). In the same year, an estimated 14.1 million of new cases occurred making cancer a leading cause of disease. Radiotherapy is one of the three main modalities for treatments against cancer besides surgery and chemotherapy and is applied for curative and palliative treatments. In case of palliative treatments, radiotherapy may be used to relieve pain from patients. Other approaches such as immune therapy, targeted therapy and antihormone therapy are also applied for treatments against cancer. For many indications, treatment modalities are combined. The choice of treatment modality is mainly dependent on type, stage and characteristics of cancer, as well as the age and health of the patient.

Radiotherapy uses ionizing radiation in order to eradicate tumor cells, while sparing normal tissue such as healthy organs. The energy deposited in the tumor cells by radiotherapy is quantified by the dose, which is defined as the absorbed energy per mass of tissue (unit: 1 Gy = 1 J / kg). The radiation delivered to the target volume originates either from an external or an internal source. Brachytherapy and radioisotope therapy use internal sources in form of radioactive isotopes either sealed or unsealed, respectively. For external beam radiotherapy, most often a linear accelerator is used to accelerate electrons to finally produce photon or electron beams. The linear accelerator is mounted either on a C-arm gantry, ring or robotic treatment unit. C-arm gantry treatment units are the most commonly used treatment unit type and are called conventional treatment units throughout the whole thesis. A smaller fraction of external beam radiotherapy is carried out using protons, heavy ions or neutrons.

Nowadays, for most external beam radiotherapy treatments, only photon beams are used. However, there are indications in which electron beams are used in combination with photon beams or alone. In 2017, for 10% of all patients treated with conventional treatment units at the Inselspital – Bern University Hospital, Radio-Onkologiezentrum

Biel – Seeland – Berner Jura AG, Radio-Onkologie Berner Oberland AG and Radio-Onkologie Solothurn AG, electron beams were used at least partly. Most of these patients underwent breast treatments.

1.1. Dosimetry of photon and electron beams

Photons are bosonic, massless and electrically uncharged elementary particles and the force carrier for the electromagnetic force, while electrons are fermionic elementary particles with a rest mass of about 511 keV and carrier of one negative elementary electric charge. Due to the different physical properties of photons and electrons, they behave differently in material. Electrons are directly ionizing particles, because of their electric charge. Within short distance, they undergo many Coulomb interactions with the orbital electrons of the atoms in a medium. The energy loss in the medium per pathlength of electrons through these interactions can be described by the Bethe-Bloch equation. Photons on the other side are indirectly ionizing particles. This means that they first release electrons or positrons in the medium mainly through photoelectric effect, Compton scattering and pair production with probabilities dependent on the energy of the photon and the material constitution of the medium. The attenuation of a photon beam through these interactions can be well described by the Beer-Lambert law, which tells us that the number of photons is exponentially reduced in the medium. The electrons and positrons released by the photons do then deposit the energy in a second step.

The relative biological effectiveness (RBE) of radiation is dependent on the dose, the dose rate, the biological system and the radiation quality, which is described by the linear energy transfer (LET). LET is dependent on the particle type and its energy. For photon beams, the energy deposition is mainly performed by the released electrons and therefore the same particle type as for electron beams. Furthermore, the typically available beam energies on conventional treatment units of 4-18 MV for photon beams and 4-22 MeV for electron beams are all sparsely ionizing beams. This means that the mean distance between interactions of the electrons with the medium are far away from each other (low LET values). For sparsely ionizing beams, the RBE is considered to be

the same in clinical practice. Thus, the dose delivered by photon and electron beams does not need to be corrected for RBE with respect to the other beam type.

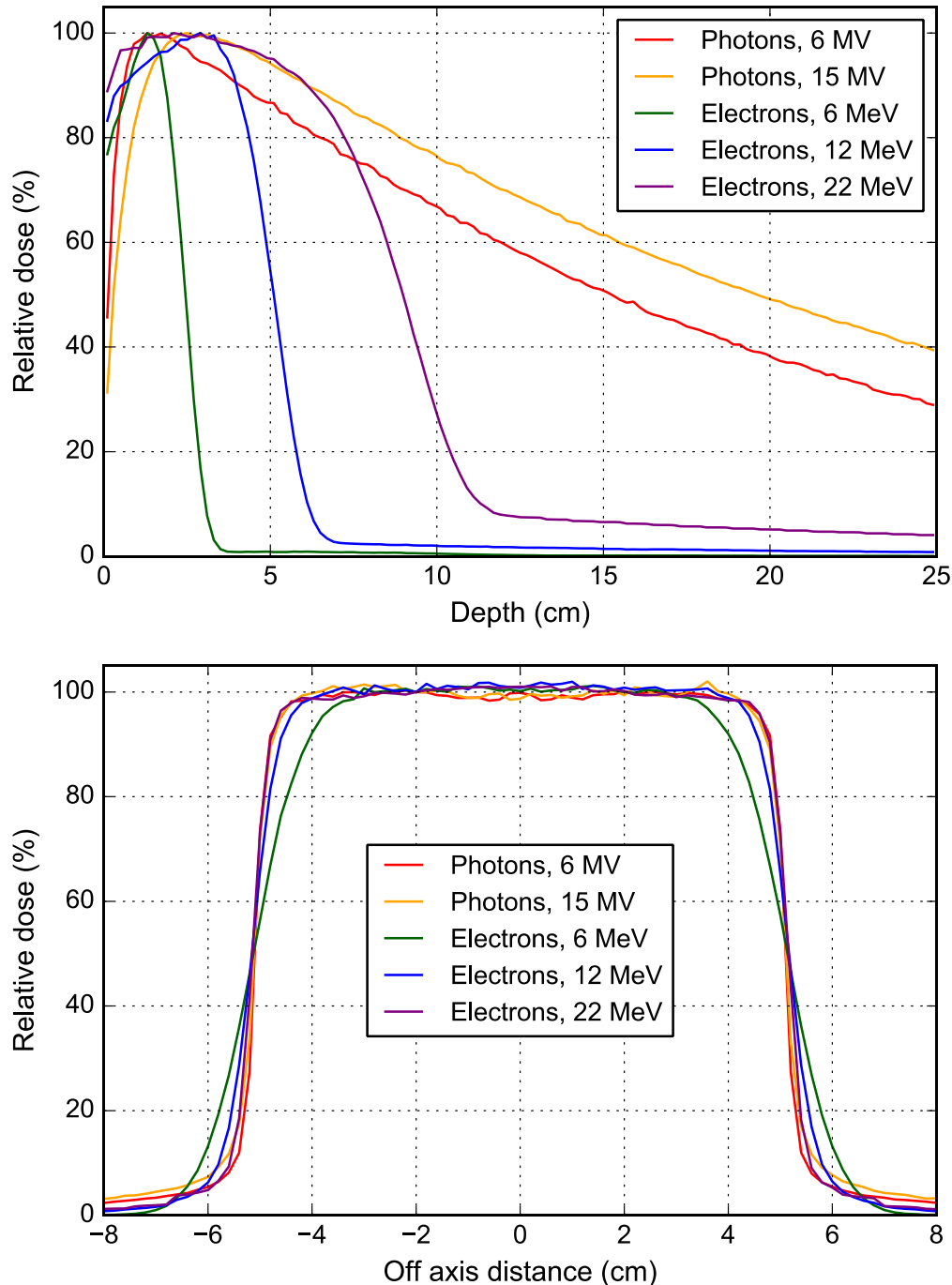


Figure 1. Calculated depth dose curves (top) and crossplane dose profiles (bottom) in water at a depth of 2 cm for several photon and electron beams with a field size of $10 \times 10 \text{ cm}^2$ at a source-to-surface distance of 100 cm. The photon beams are collimated with the secondary collimator jaws and the electron beams with a standard insert placed in an electron applicator. The dose is calculated for a TrueBeam (Varian Medical Systems, Palo Alto, CA) using VMC++ (Kawrakow and Fippel 2000) within the framework of the Swiss Monte Carlo Plan (SMCP) (Fix *et al* 2007) for photon beams and using the commercially available electron Monte Carlo (eMC) (Varian Medical Systems, Palo Alto, CA) for electron beams.

Due to the different physical behavior in material, the dose distributions of photon and electron beams are fundamentally different. In figure 1, depth dose curves and dose profiles are shown for some selected beam energies in the energy ranges available for conventional treatment units.

MV photon beams have a low surface dose compared to the maximal dose leading to a skin sparing effect. The higher the energy and the smaller the field size, the lower is the surface dose. A dose buildup region follows until reaching the depth of maximal dose z_{\max} , which is primarily beam energy and secondarily field size dependent. Deeper than z_{\max} , an exponential dose fall-off is given due to the exponential attenuation of the photon beam. Shallower than z_{\max} , this is not the case, because the charged particle equilibrium (CPE) is not given there. The depth dose curves of the MV photon beams demonstrate that the dose can be delivered to any depth in the patient's body. However, this exponential fall-off also leads to a large dose contribution delivered to normal tissue.

The depth dose curves of the electron beams are different to the photon beams. According to the Bethe-Bloch equation, a Bragg-peak would be expected for the depth dose curves of the electron beams. However, due to the relatively small rest mass of electrons compared to other charged particles like protons or heavy ions, particle scattering is more pronounced and therefore the Bragg-peak is less distinct. Though, there is still a distal dose fall-off at an energy dependent depth as visible in figure 1. The dose fall-off is less steep for higher beam energy and smaller field size. Compared with MV photon beams, the electron beams have a high surface dose. In case of a target volume reaching the surface, this is advantageous. For other targets, skin is less spared than with photon beams. The depth dose curves have a bremsstrahlung tail after the distal dose fall-off, which is larger for higher beam energies. These bremsstrahlung photons are mainly produced in the scattering foils of the treatment head, but also in other beam modifiers and the patient itself. Due to the distal dose fall-off, electron beams are suited to spare normal tissue for treatments of superficial targets. However, the available beam energies limit their application to targets within 5 cm from the patient surface such that the dose is still homogeneously distributed in the target.

The profiles of the photon beams have a smaller penumbra than the electron beams. One reason for this is that the electrons scatter much more in air than photons and thus,

the beam impinging on the patient is less defined. This also means, that the electron beam penumbra is more dependent on the source-to-surface distance (SSD) than the photon beam penumbra, because with increased SSD, the distance between the last collimation device and the patient increases and therefore the electrons undergo more in-air scatter. The electron beam penumbra at a certain depth is larger for lower energies and increases with depth. The photon beam penumbra is much less dependent on beam energy and depth. Based on these characteristics, OARs located laterally close to the target with respect to beam direction are spared less using electron than photon beams.

1.2. Motivation for mixed beam radiotherapy

In the following, the dosimetric advantages and disadvantages of photon and electron beams mentioned in the previous subchapter are illustratively discussed based on an academic situation. Figure 2 shows a transversal view of an academic situation with a cylindrical phantom including contours of a target to be treated and two OARs to be spared. The target has a superficial and a distal part with respect to the closest phantom surface. Both OARs are closely located to the target. One of them is distally and the other is laterally located with respect to the closest phantom surface. The superficial part could be well treated using electron beams in the range of 6-12 MeV, while sparing the distal OAR. For treating the distal part, higher beam energies would be necessary. However, the distal part of the target is up to 7.5 cm deep located making it impossible to deliver the dose homogeneously to the whole target with electron beams up to 22 MeV. Moreover, the lateral OAR cannot be spared adequately due to the large electron beam penumbra. MV photon beams could deliver the dose homogeneously to the whole target by using multiple beam directions around the phantom. The exponential dose fall-off of photon beams makes this possible, but there are also downsides connected to it: Covering the superficial part of the target would probably lead to large dose values delivered to the lateral OAR (for tangential photon beams) and the distal OAR (for enface photon beams). Moreover, a large low dose bath would be delivered to normal tissue if the distal part is covered.

For such a scenario, a treatment approach for mixed beam radiotherapy (MBRT) could take advantage of both photon and electron beams, while keeping their downsides

at a minimum to increase treatment plan quality. Many clinical cases treated by radiotherapy of sites such as head and neck and breast have targets with a superficial part and could therefore potentially benefit of MBRT.

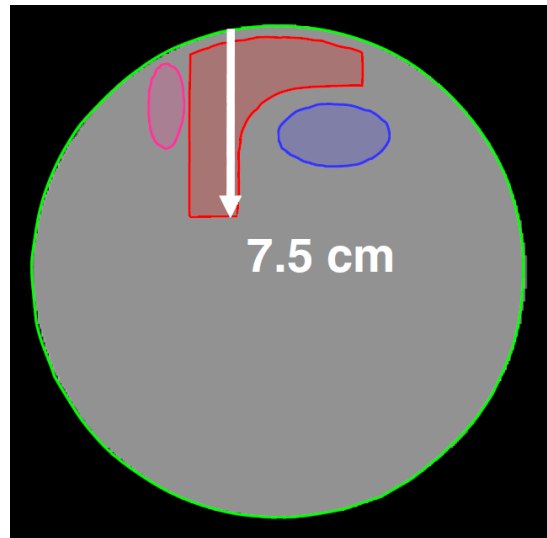


Figure 2. A transversal view of an academic situation with a cylindrical water phantom. A target (red), a lateral OAR (magenta) and a distal OAR (blue) are contoured.

1.3. Requirements for a treatment technique

Generally, treatment plans are expected to have a high treatment plan quality, delivery efficiency and accuracy. Thus, these three properties would also be required for plans of a treatment technique for MBRT. In the following, these requirements and potential approaches to achieve them are further elaborated for the scope of MBRT.

The tumor control probability (TCP) and the normal tissue complication probability (NTCP) are highly dependent on the dose delivered. Furthermore, the therapeutic window in which the TCP is higher than the NTCP is typically very narrow. Thus, it is of high value for the clinical outcome that the prescribed dose is delivered to the tumor with a high accuracy. High accuracy requirements follow for the treatment unit and for the monitor unit (MU) determination of the fields to be applied. The MUs to be applied are determined based on the dose calculation of the treatment plan. For this, analytical or Monte Carlo (MC) methods are applied based on the planning computed tomography (CT) image set. MC simulates nature by transporting particles randomly and repeatedly through the treatment head and the patient according to the cross sections of the physical interactions. Irregular and small fields, inhomogeneous tissue and different SSDs can be

considered accurately with MC. Better agreements with dose measurements are reported for MC than for analytical methods for both photon and electron beams (Carrasco *et al* 2004, Ding *et al* 2005). The downside of MC are large computation times to reach a low statistical uncertainty. However, variance reduction techniques such as Macro Monte Carlo (MMC) (Neuenschwander and Born 1992) and simultaneous transport of particle sets (STOPS) (Kawrakow and Fippel 2000) are applied to increase calculation efficiency.

A high treatment plan quality means that the dose is homogeneously delivered to the target and that the OARs and other normal tissue receive as low dose values as possible. These two goals are conflicting and thus, a compromise needs to be found. Since about twenty years, inverse treatment planning is used in clinics to find an appropriate compromise as mentioned above for the treatment plan generation of techniques such as photon intensity modulated radiation therapy (IMRT). This allows to increase treatment plan quality compared to 3D conformal radiation therapy (3DCRT) (Bortfeld *et al* 2006). The inverse problem is usually formulated by defining the desired dose distribution. In practice, this means that the planner defines dose objectives for the target and healthy structures such as OARs. Next, an optimization approach is applied to modulate the intensities of the irradiation fields such that the objectives are fulfilled as good as possible. To quantify the plan quality, an objective function is evaluated, which sums the deviations of the plan's dose distribution to the dose objectives. A treatment unit enabling intensity modulation is required to deliver such plans. For photon IMRT, conventional treatment units are equipped with a photon multileaf collimator (pMLC) consisting of multiple pairs of leaves, which can be moved independently of each other. They are built out of material with a high atomic number Z like tungsten such that beams are well collimated. The optimized intensity maps can then be delivered by moving the leaves accordingly or by delivering multiple static segments. In the scope of MBRT, a similar or the same solution enabling intensity modulation for both particle types is desirable to increase plan quality.

Conventional treatment units can deliver both photon and electron beams. To generate a flattened photon beam, the accelerated electrons are impinging on a high Z target producing bremsstrahlung photons, which are then attenuated by a flattening

filter. For the generation of a flattened electron beam, the target and the flattening filter are moved away, and scattering foils are placed instead. Thus, a conventional treatment unit is appropriate for an efficient delivery of MBRT as the whole plan can be delivered on the same treatment unit. Moreover, the conventional treatment units support typically 5-6 electron beams of different energies making energy modulation feasible. Treatment techniques for modulated electron radiotherapy (MERT) were well studied in research with different collimation devices enabling intensity modulation such as a few leaf electron collimator (FLEC) (Al-Yahya *et al* 2005), an electron multileaf collimator (eMLC) (Gauer *et al* 2008) or a pMLC (du Plessis *et al* 2006).

The level the dosimetric potential of MBRT is elaborated is strongly dependent on the techniques used for treatment plan generation (Xiong *et al* 2004). In research, different optimization approaches were applied for MBRT. Most of them optimized the photon and electron contributions in a sequential manner and thus, the advantages of these two particle types are not merged optimally (Mu *et al* 2004). A simultaneous optimization of photon and electron contributions would result in superior treatment plan quality (Xiong *et al* 2004, Alexander *et al* 2012, Palma *et al* 2012). However, the previous results are either based on using inefficient delivery techniques, non-deliverable plans or using a treatment unit, which is out-of-date. Moreover, only breast treatments are investigated with deliverable plans so far.

1.4. Aim and outline of the thesis

The aim of this thesis is to develop treatment techniques for MBRT with simultaneously optimized photon and electron contributions and to investigate the dosimetric potential of MBRT for several treatment sites. The generated MBRT treatment plans are aimed to be efficiently and accurately deliverable using a conventional treatment unit.

Using the pMLC for electron beam collimation would make intensity and energy modulation feasible for electron beams. Beside of that, clinical workflow would be substantially improved not only for MERT and MBRT, but also for today's standard electron treatments using typically a single electron field. However, electron treatments are nowadays still performed using standard or molded patient-specific cut-outs placed in the electron applicator. Thus, in chapter 2, the dosimetric characteristics of treatment

plans with a single electron-field, either collimated with a cut-out or with the pMLC are compared for standard electron treatment situations.

To evaluate the dosimetric gain of using the pMLC for electron beams, the impact of intensity and energy modulation for pMLC based MERT is studied in chapter 3. For this, different levels of intensity and energy modulation are systematically investigated for several treatment sites.

In chapter 4, an MC based treatment planning process (TPP) for an pMLC based step and shoot MBRT treatment technique (ssMBRT) is developed. Core element of this TPP is a simultaneous optimization of photon and electron beams, which allows to merge the advantages of photons and electrons. The main purpose of this development is to demonstrate the dosimetric potential of ssMBRT in comparison to MERT and the photon-only treatment techniques IMRT and volumetric modulated arc therapy (VMAT).

Beside of electron beams, conventional treatment units offer also other degrees of freedom (DoFs), which are not utilized by the state-of-the-art treatment technique VMAT. Dynamic collimator rotation would allow to rotate the pMLC favorably during beam on and dynamic table rotation would even allow to utilize a non-coplanar beam setup. Thus, a treatment technique called dynamic trajectory radiotherapy (DTRT) is developed in chapter 5, which combines dynamic gantry, table and collimator rotations for photon beams.

Combining the DoFs utilized by DTRT with intensity and energy modulated electron beams would result in a treatment technique utilizing more DoFs of a conventional treatment unit than ever presented before. In chapter 6, an MC based TPP is developed to create treatment plans for such a treatment technique, called dynamic mixed beam radiotherapy (DYMBER). The dosimetric benefit of DYMBER and its deliverability is demonstrated.

In chapter 7, several aspects of the developed MBRT treatment techniques are discussed and chapter 8 contains the conclusions of the thesis.

References

- Al-Yahya K, Schwartz M, Shenouda G, Verhaegen F, Freeman C and Seuntjens J 2005 Energy modulated electron therapy using a few leaf electron collimator in combination with IMRT and 3D-CRT: Monte Carlo-based planning and dosimetric evaluation *Med. Phys.* **32** 2976–86
- Alexander A, Soisson E, Renaud M-A and Seuntjens J 2012 Direct aperture optimization for FLEC-based MERT and its application in mixed beam radiotherapy *Med. Phys.* **39** 4820–31
- Bortfeld T 2006 IMRT: a review and preview *Phys. Med. Biol.* **51** R363–79
- Carrasco P, Jornet N, Duch M A, Weber L, Ginjaume M, Eudaldo T, Jurado D, Ruiz A and Ribas M 2004 Comparison of dose calculation algorithms in phantoms with lung equivalent heterogeneities under conditions of lateral electronic disequilibrium *Med. Phys.* **31** 2899-911
- Ding G X, Cygler J E, Yu C W, Kalach N I and Daskalov G 2005 A comparison of electron beam dose calculation accuracy between treatment planning systems using either a pencil beam or a Monte Carlo algorithm *Int. J. Radiation Oncology Biol. Phys.* **63** 622-33
- du Plessis F C P, Leal A, Stathakis S, Xiong W and Ma C-M 2006 Characterization of megavoltage electron beams delivered through a photon multi-leaf collimator (pMLC) *Phys. Med. Biol.* **51** 2113–29
- Fix M K, Manser P, Frei D, Volken W, Mini R and Born E J 2007 An efficient framework for photon Monte Carlo treatment planning *Phys. Med. Biol.* **52** N425-37
- Gauer T, Sokoll J, Cremers F, Harmansa R, Luzzara M and Schmidt R 2008 Characterization of an add-on multileaf collimator for electron beam therapy *Phys. Med. Biol.* **53** 1071–85
- International Agency for Research on Cancer and Cancer Research UK 2014 World Cancer Factsheet *Cancer Research UK*
- Kawrakow I and Fippel M 2000 VMC++, a fast MC algorithm for radiation treatment planning *The Use of Computers in Radiotherapy, 8th Int. Conf. (Heidelberg,*

- Germany*) ed W Schlegel and T Bortfeld (Heidelberg: Springer) (<https://doi.org/10.1007/978-3-642-59758-9>)
- Mu X, Olofsson L, Karlsson M, Sjögren R and Zackrisson B 2004 Can photon IMRT be improved by combination with mixed electron and photon techniques? *Acta Oncol.* **43** 727–35
- Neuenschwander H and Born E J 1992 A Macro Monte Carlo method for electron beam dose calculations *Phys. Med. Biol.* **37** 107–25
- Palma B A, Sánchez A U, Salguero F J, Arráns R, Sánchez C M, Zurita A W, Hermida M I R and Leal A 2012 Combined modulated electron and photon beams planned by a Monte-Carlo-based optimization procedure for accelerated partial breast irradiation *Phys. Med. Biol.* **57** 1191–202
- Xiong W, Li J, Chen L, Price R A, Freedman G, Ding M, Qin L, Yang J and Ma C M 2004 Optimization of combined electron and photon beams for breast cancer *Phys. Med. Biol.* **49** 1973–89

2

Electron beam collimation with a photon MLC for standard electron treatments

**S. Mueller¹, M.K. Fix¹, D. Henzen¹, D. Frei¹, D. Frauchiger¹, K. Loessl¹,
M.F.M. Stampanoni² and P. Manser¹**

- 1: Division of Medical Radiation Physics and Department of Radiation Oncology, Inselspital, Bern University Hospital, and University of Bern, Bern, Switzerland
- 2: Institute for Biomedical Engineering, ETH Zürich and PSI, Villigen, Switzerland

published in
Physics in Medicine & Biology

2018, Vol. 63, 025017(14pp)
<https://doi.org/10.1088/1361-6560/aa9fb6>

© Institute of Physics and Engineering in Medicine.
Reproduced with permission. All rights reserved.

Abstract

Standard electron treatments are currently still performed using standard or molded patient-specific cut-outs placed in the electron applicator. Replacing cut-outs and electron applicators with a photon multileaf collimator (pMLC) for electron beam collimation would make standard electron treatments more efficient and would facilitate advanced treatment techniques like modulated electron radiotherapy (MERT) and mixed beam radiotherapy (MBRT). In this work, a multiple source Monte Carlo beam model for pMLC shaped electron beams commissioned at a source-to-surface distance (SSD) of 70 cm is extended for SSDs of up to 100 cm and validated for several Varian treatment units with field sizes typically used for standard electron treatments. Measurements and dose calculations agree generally within 3% of the maximal dose or 2 mm distance to agreement. To evaluate the dosimetric consequences of using pMLC collimated electron beams for standard electron treatments, pMLC-based and cut-out-based treatment plans are created for a left and a right breast boost, a sternum, a testis and a parotid gland case. The treatment plans consist of a single electron field, either alone (1E) or in combination with two 3D conformal tangential photon fields (1E2X). For each case, a pMLC plan with similar treatment plan quality in terms of dose homogeneity to the target and absolute mean dose values to the organs at risk (OARs) compared to a cut-out plan is found. The absolute mean dose to an OAR is slightly increased for pMLC-based compared to cut-out-based 1E plans if the OAR is located laterally close to the target with respect to beam direction, or if a 6 MeV electron beam is used at an extended SSD. In conclusion, treatment plans using cut-out collimation can be replaced by plans of similar treatment plan quality using pMLC collimation with accurately calculated dose distributions.

Keywords: electron therapy, electron beam collimation, multileaf collimator, Monte Carlo

1. Introduction

In the history of photon radiation therapy, a huge effort was made to replace molded patient-specific blocks with the photon multileaf collimator (pMLC), in order to substantially increase treatment safety and efficiency (Brewster *et al* 1995, Boyer *et al* 2001). The introduction of the pMLC was later important in the development and provision of inverse-planning-based advanced treatment techniques like IMRT (Convery and Webb 1992, Bortfeld *et al* 1994) and VMAT (Otto 2008), which have now been important parts of radiotherapy in the clinical routine for many years.

The dose distributions of electron beams, with their sharp distal dose fall-off in tissue, differ fundamentally from those of photon beams. This characteristic makes electron beams in the energy range of 6–22 MeV suitable for treatments of superficial targets with a depth of up to 5 cm. To optimally utilize the electron beam dose characteristics, inverse-planning-based advanced treatment techniques like modulated electron radiotherapy (MERT) (Lee *et al* 2001, Olofsson *et al* 2004, Al-Yahya *et al* 2005, Engel and Gauer 2009, Salguero *et al* 2009, 2010, Alexander *et al* 2010, 2012, Henzen *et al* 2014a), dynamic electron arc radiation therapy (DEAR) (Rodrigues *et al* 2014) and mixed beam radiotherapy (MBRT) (Li *et al* 2000, Mu *et al* 2004, Xiong *et al* 2004, Al-Yahya *et al* 2005, Surucu *et al* 2010, Ge and Faddegon 2011, Alexander *et al* 2012, Palma *et al* 2012, Rosca 2012, Mueller *et al* 2017, Renaud *et al* 2017), using either a few leaf electron collimator (FLEC), an electron multileaf collimator (eMLC) or a pMLC, were developed and investigated. However, standard electron treatments in the clinical routine are currently still performed using the cumbersome and inefficient standard or molded patient-specific cut-outs placed in the electron applicator and using limited planning features.

Just as the pMLC is an appropriate collimation device for 3D conformal photon radiotherapy, FLEC, eMLC and pMLC might also be appropriate collimation devices for standard electron treatments. This was shown in detail for eMLC-based single electron field breast boost treatments (Eldib *et al* 2013). For pMLC collimation, it was shown that a similar treatment plan quality can be achieved compared to cut-out collimation for chest wall treatment plans consisting of multiple electron fields, to be

delivered with a Siemens Primus treatment unit, at a reduced source-to-surface distance (SSD) of 60–70 cm (Salguero *et al* 2009).

Besides facilitating advanced treatment techniques, all of the collimation devices FLEC, eMLC and pMLC offer the following advantages over molded patient-specific cut-outs. Firstly, the time-consuming molding of cut-outs involving toxic materials like cadmium and lead could be avoided. Secondly, the effort required for machine quality assurance (QA) is reduced as each electron beam energy needs to be maintained only once and not for every electron applicator size. Thirdly, treatment errors, caused by accidentally using a cut-out molded for another patient, are avoided.

The FLEC contains only four leaves in total. Hence, an opening conformal to the target shape is not feasible using the FLEC instead of the eMLC or the pMLC. The pMLC offers additionally the advantage that it is already part of the treatment head and thus the necessity to mount and remove the electron applicator during treatment can be avoided. This is valuable for the treatment workflow, especially for any treatment technique combining photon and electron beams. Additionally, machine QA for the positioning accuracy of the pMLC leaves is already performed for the photon beams. Moreover, no heavy weighted electron beam add-on device needs to be lifted up and down by a radiation therapy technologist if the pMLC is used, and thus these electron beam add-on devices can also not fall down accidentally. Lastly, gantry sag due to the weight of an electron beam add-on device is avoided.

The dosimetric characteristics of pMLC shaped electron beams were investigated in detail (du Plessis *et al* 2006, Klein *et al* 2008, 2009, Lloyd *et al* 2015). A disadvantage of pMLC electron beam collimation is the enlarged penumbra for extended distance between the collimation device and the patient surface, due to increased in-air scatter. Hence, the shortest feasible SSD, i.e. 70 cm in case of Varian treatment units, is dosimetrically optimal. However, a reduced SSD of 70 cm could lead to collisions with the patient or the couch for certain beam directions. Moreover, a reduced SSD might be uncomfortable for patients suffering from claustrophobia. Thus, supporting extended SSDs > 70 cm is of great importance if cut-outs should be replaced.

Using a Monte Carlo (MC)-based beam model and dose calculation for predicting electron dose distributions in radiotherapy is necessary to accurately account for tissue

inhomogeneities, particle scattering at the collimation devices and SSDs not used for commissioning measurements (Cygler *et al* 2004, Ding *et al* 2005). MC dose calculations of pMLC shaped electron beams were investigated using full MC simulations (Lee *et al* 2000, Klein *et al* 2008, Salguero *et al* 2009, Mihaljevic *et al* 2011), vendor-provided phase-spaces (Lloyd *et al* 2016) and a multiple source beam model (Henzen *et al* 2014b). The latter offers a commissioning procedure without requiring MC experience and large computation times. To the best of our knowledge, the work of Mihaljevic *et al* (2011) is the only one that includes a validation of their beam model for pMLC collimated electron beams at an SSD > 85 cm. They reported an agreement between measurements and dose calculations generally within 3% of the maximal dose, or with 3 mm distance to agreement (DTA) for several field sizes at an SSD of 80 and 95 cm, for 10, 12 and 15 MeV beams of an Elekta Synergy S treatment unit.

In this work, we suggest the pMLC as an alternative collimation device for standard electron treatments, to overcome the disadvantages in clinical workflow and delivery when using conventional cut-outs. Hence, the feasibility of accurately predicting the dose distributions of pMLC collimated electron beams for the SSD range of 70–100 cm using an MC-based beam model and dose calculation is conducted for Varian treatment units. With the aim of replacing cut-out collimation with pMLC collimation in clinics, the availability of pMLC plans with similar treatment plan quality to that of cut-out plans is investigated for a broad selection of standard electron treatments.

2. Materials and methods

2.1. MC simulations

In this work, in order to predict dose distributions of pMLC shaped electron beams, a multiple source MC beam model (Henzen *et al* 2014b), referred to as ebm70, and an MC dose calculation are used. The ebm70 is connected to the Swiss Monte Carlo plan (SMCP) (Fix *et al* 2007) such that particle transport through the pMLC is performed with the PIN MC algorithm (Terribilini *et al* 2010) and the dose calculation in the patient is performed with the macro MC algorithm (MMC) (Neuenschwander and Born 1992, Neuenschwander *et al* 1995, Fix *et al* 2013). The sources of the ebm70 are a foil and a jaw source, both divided into an electron and a photon part. For a specific treatment unit, the sources of the ebm70 are commissioned using treatment unit specific depth dose and air profile measurements at an SSD of 70 cm, and pre-calculated MC configuration data, which are common for each combination of a treatment head model and secondary collimator jaws settings. Further details about the ebm70 can be found in the reference.

Henzen *et al* (2014b) configured and commissioned the ebm70 for an SSD of 70 cm with a fixed jaw field size of $15 \times 35 \text{ cm}^2$ for all electron beam energies of a Clinac 23EX and a TrueBeam (Varian Medical Systems, Palo Alto, CA), both equipped with a Millennium 120 pMLC (Varian Medical Systems, Palo Alto, CA). They validated the ebm70 at an SSD of 70 cm against diode, film and standalone electronic portal imaging device (EPID) measurements. Dose calculations and measurements agreed within 2% or 2 mm DTA for rectangular field sizes from $2 \times 2 \text{ cm}^2$ to $15 \times 34 \text{ cm}^2$, and within 3% or 3 mm DTA for complex field shapes. Mueller *et al* (2017) further validated the ebm70 for several field sizes of $2 \times 2 \text{ cm}^2$ and larger at an SSD of 80 cm with an agreement of 3% or 2 mm DTA. In this work, the ebm70 is further fine-tuned for its application at extended SSDs in the range of 70–100 cm. This includes adjustments of the parameter values describing the foil sources and the relative weight between the foil and jaw sources.

In order to make the ebm70 suitable for Varian treatment units equipped with a high definition multileaf collimator (HDMLC) (Varian Medical System, Palo Alto, CA) in this work, an existing geometry pMLC model (Fix *et al* 2011) is linked to the ebm70

and simplified to increase efficiency for MC transport through the pMLC. Thereby, the interleaf gaps, the mechanical leaf guides and the screw holes are neglected. To use the ebm70 with the HDMLC, the field size of the jaws in the inplane direction is reduced from 35 cm to 17 cm, because the HDMLC is only 22 cm wide in the inplane direction in comparison to the Millennium 120 pMLC with a width of 40 cm. Moreover, measurements showed that particles can pass between the jaws and the HDMLC, if the field size of the jaws is larger than 17 cm in the inplane direction. Consequently, the pre-calculated MC configuration data for the ebm70 are also calculated for the jaw settings of $15 \times 17 \text{ cm}^2$ for the HDMLC.

For dose calculation of cut-out collimated electron beams, the Eclipse treatment planning system (TPS) integrated generalized electron Monte Carlo (eMC), version 13.6.23 (Varian Medical Systems, Palo Alto, CA), is used, which is based on the work of Fix *et al* (2010, 2013). The eMC includes a multiple source model linked to an MMC dose calculation algorithm. Hence, the dose calculations of the eMC and the ebm70 are both based on the same MMC algorithm.

In this work, ebm70 and eMC are both commissioned for all available beam energies (6, 9, 12, 15, 18 and 22 MeV) of a Clinac 23iX (Varian Medical System, Palo Alto, CA) and a TrueBeam, both equipped with a Millennium 120 pMLC and a Novalis Tx (Varian Medical Systems, Palo Alto, CA) equipped with a HDMLC. All eMC commissionings are performed including optional measured applicator air profiles and the configuration setting for the statistical uncertainty of the involved eMC dose calculation of 0.5% (Varian Medical Systems 2015).

2.2. Validation

To validate the commissioned ebm70 and eMC for standard electron treatments using pMLC and cut-out collimated electron beams, respectively, depth dose curves and dose profiles at a depth of 1 cm and R_{50} of pMLC collimated electron beams at an SSD of 70, 80, 90 and 100 cm, and cut-out collimated electron beams at an SSD of 105 cm, are measured in units of cGy/MU. These measurements are repeated for two field sizes, $9.8 \times 9.8 \text{ cm}^2$ and $4.2 \times 4.2 \text{ cm}^2$ (measured at the SSD plane), using all available beam energies of the treatment units Novalis Tx, Clinac 23iX and TrueBeam. The two field

sizes span the range of most field sizes used for standard electron treatments. In the case of cut-out collimation, the SSD of 105 cm is typically used in the clinical routine. The pMLC field sizes used for the validation are only approximately to the stated dimensions in the inplane direction due to the discrete leaf width resolutions. For pMLC collimation, the jaws are set to $15 \times 35 \text{ cm}^2$ and $15 \times 17 \text{ cm}^2$ for the Millennium 120 pMLC and the HDMLC, respectively. In the case of cut-out collimation, the $15 \times 15 \text{ cm}^2$ and $6 \times 6 \text{ cm}^2$ electron applicators with standard jaw settings are used to hold the $9.8 \times 9.8 \text{ cm}^2$ and $4.2 \times 4.2 \text{ cm}^2$ cut-outs, respectively.

All measurements are performed in an MP3 water tank (PTW, Freiburg, Germany). An EFD^{3G} diode (IBA Dosimetry, Schwarzenbruck, Germany) is used to collect the relative dose measurements and MEPHYSTO mc² 3.0 (PTW, Freiburg, Germany) is used for post-processing purposes. To transform the relative dose measurements into units of cGy/MU, the output is measured with a microDiamond 60019 (PTW, Freiburg, Germany). The reference output of 1 cGy/MU is defined per beam energy and treatment unit at the depth of maximum dose for the $10 \times 10 \text{ cm}^2$ electron applicator at an SSD of 100 cm.

Corresponding dose distributions are calculated in units of cGy/MU in a $30 \times 30 \times 30 \text{ cm}^3$ water phantom using a voxel size of $2 \times 2 \times 2 \text{ mm}^3$ and compared to the measurements in terms of dose difference relative to the maximal dose and DTA. Moreover, the relative output difference between measured (O_{meas}) and calculated (O_{calc}) output, in units of cGy/MU at the location of maximal dose on the central beam axis, is evaluated by

$$Output\ difference(\%) = \frac{O_{calc} - O_{meas}}{O_{meas}} \cdot 100\%. \quad (1)$$

2.3. Clinical cases

Clinical cases of a left and a right breast boost, a sternum, a testis and a parotid gland with prescribed doses of 10, 9, 7, 20 and 49 Gy to the median dose in the target volume, respectively, are selected for the following three purposes:

1. To evaluate the dosimetric consequences for treatment plans consisting of a single electron field (1E), if the electron field is shaped with the pMLC instead of a cut-out.
2. To evaluate the dosimetric consequences for treatment plans consisting of a single electron field and two tangential 3D conformal photon fields (1E2X), if the electron field is shaped with the pMLC instead of a cut-out.
3. To investigate the dosimetric influence of the SSD for 1E and 1E2X treatment plans with pMLC shaped electron fields.

The cases differ in the maximal depth of the target and the geometrical situation between the target and organs at risk (OARs). Thus, the selected cases offer a broad variety of standard electron treatments such that the limits and opportunities of applying pMLC shaped electron beams are explored thoroughly.

Table 1 lists all the treatment plans created for the three purposes mentioned above. Treatment plans are compared in terms of dose distributions, dose-volume histograms (DVHs), dose homogeneity expressed as $HI = V_{95\%} - V_{107\%}$, D_{mean} to the OARs and the low dose bath expressed as $V_{10\%}$ of the normal tissue, which is defined as the body volume minus the volume of any planning target volume (PTV) definition, i.e. also the primary PTV in the breast boost cases. Moreover, the ratio between the volume receiving at least 50% of the median PTV dose of a pMLC collimated ($V_{50\%}^{pMLC}$) and a cut-out collimated ($V_{50\%}^{Cut-out}$) electron field is evaluated by

$$VR_{50\%} = \frac{V_{50\%}^{pMLC}}{V_{50\%}^{Cut-out}}. \quad (2)$$

Table 1. The treatment plans created for clinical treatment plan comparisons and their settings for the single electron fields. The field target distance is given on the plane of the patient's surface.

Clinical case	Plan type	Treatment unit	Electron field			
			Collimation device	Energy (MeV)	SSD (cm)	Field target distance (cm)
Left breast boost	1E	TrueBeam	pMLC	18	70	0.8
	1E	TrueBeam	pMLC	18	80	0.8
	1E	TrueBeam	pMLC	18	90	0.9
	1E	TrueBeam	pMLC	18	100	1.1
	1E	TrueBeam	Cut-out	18	105	0.7
Left breast boost	1E2X	TrueBeam	pMLC	12	70	0.7
	1E2X	TrueBeam	pMLC	12	80	0.8
	1E2X	TrueBeam	pMLC	12	90	0.9
	1E2X	TrueBeam	pMLC	12	100	1
	1E2X	TrueBeam	Cut-out	12	105	0.7
Right breast boost	1E	TrueBeam	pMLC	6	70	2.4
	1E	TrueBeam	pMLC	6	80	2.7
	1E	TrueBeam	pMLC	6	90	2.9
	1E	TrueBeam	pMLC	6	100	3
	1E	TrueBeam	Cut-out	6	105	1
Right breast boost	1E2X	TrueBeam	pMLC	6	70	2.4
	1E2X	TrueBeam	pMLC	6	80	2.7
	1E2X	TrueBeam	pMLC	6	90	2.9
	1E2X	TrueBeam	pMLC	6	100	3
	1E2X	TrueBeam	Cut-out	6	105	1
Sternum	1E	Novalis Tx	pMLC	12	75	1.1
	1E	Novalis Tx	Cut-out	12	105	0.7
Testis	1E	Clinac 23iX	pMLC	12	80	0.9
	1E	Clinac 23iX	Cut-out	12	110	0.8
Parotid gland	1E2X	Novalis Tx	pMLC	15	80	0.4
	1E2X	Novalis Tx	Cut-out	15	105	0.3

For each treatment plan comparison, a cut-out plan is created with typical clinical settings. In addition, deliverable pMLC plans are also created, with the aim of achieving a PTV dose homogeneity similar to the cut-out plan (*HI* difference compared to the cut-out plan within 3%). Beside the collimation device, only the SSD is reduced and the distance between the target contour and the field opening projected to the target plane (field target distance) is adjusted, including adapted collimator rotation with the aim of minimizing the area between pMLC leaves and target contour. In the case of the 1E2X plan comparisons, the monitor units (MUs) of the two photon fields are kept the same for all treatment plans determined for the same clinical case.

For all treatment plans, the dose calculation is performed using a voxel size of $2.5 \times 2.5 \times 2.5 \text{ mm}^3$ and the validated ebm70 and eMC for the pMLC and cut-out shaped electron fields, respectively. Moreover, a clinically commissioned analytical anisotropic algorithm, version 13.6.23 (Varian Medical Systems, Palo Alto, CA) is used for the dose calculation of the photon fields.

3. Results

The mean statistical uncertainty (one standard deviation) of the voxels with dose values higher than 50% of maximum dose, determined with the history by history method (Walters *et al* 2002), is about 0.5% for all ebm70-based dose calculations. The required computation time is between 1 and 4 h using 100 CPU cores, depending on the SSD, and is mainly dominated by the particle transport through the pMLC. The reason for this large dependency of the computation time on the SSD is that for larger SSDs the fraction of the particles scattered to the volume receiving less than 50% of the maximal dose is increasing. Accordingly, more particles need to be simulated for a large SSD to reach the same statistical uncertainty than for a short SSD.

The eMC-based dose calculations are performed with randomly selected seeds, 0.5% statistical uncertainty, 50% dose threshold for uncertainty and without dose smoothing (specified in Eclipse TPS).

3.1. Validation

In the following, agreements between dose measurements and calculations performed by the ebm70 or the eMC are summarized. Figure 1 shows the output differences for all field sizes, beam energies, SSDs and treatment units investigated. Measurements and calculations of some selected depth dose curves and crossplane profiles for the 6 and 22 MeV beams of the Novalis Tx are given in figures 2 and 3, respectively.

Measured and ebm70 calculated depth dose curves and in- and crossplane dose profiles of pMLC collimated electron beams at an SSD of 70 and 80 cm agree within 3% or 2 mm DTA for all three investigated treatment units. In particular, the output differences between measurements and dose calculations shown in figure 1 are within 2%.

The analogous depth dose and dose profile measurements with an SSD of 90 and 100 cm and corresponding ebm70-based dose calculations agree generally within 3% or 2 mm DTA for all investigated treatment units with a few exceptions in the buildup of the depth dose curves with dose differences of up to 4% (always overestimated by the dose calculation). The 6 MeV depth dose curve of the $9.8 \times 9.8 \text{ cm}^2$ field at an SSD of

100 cm for the Novalis Tx is a representative example for these exceptions (figure 2). Furthermore, the output of the same Novalis Tx 6 MeV field is overestimated by 2.2% compared to the measurement (figure 1).

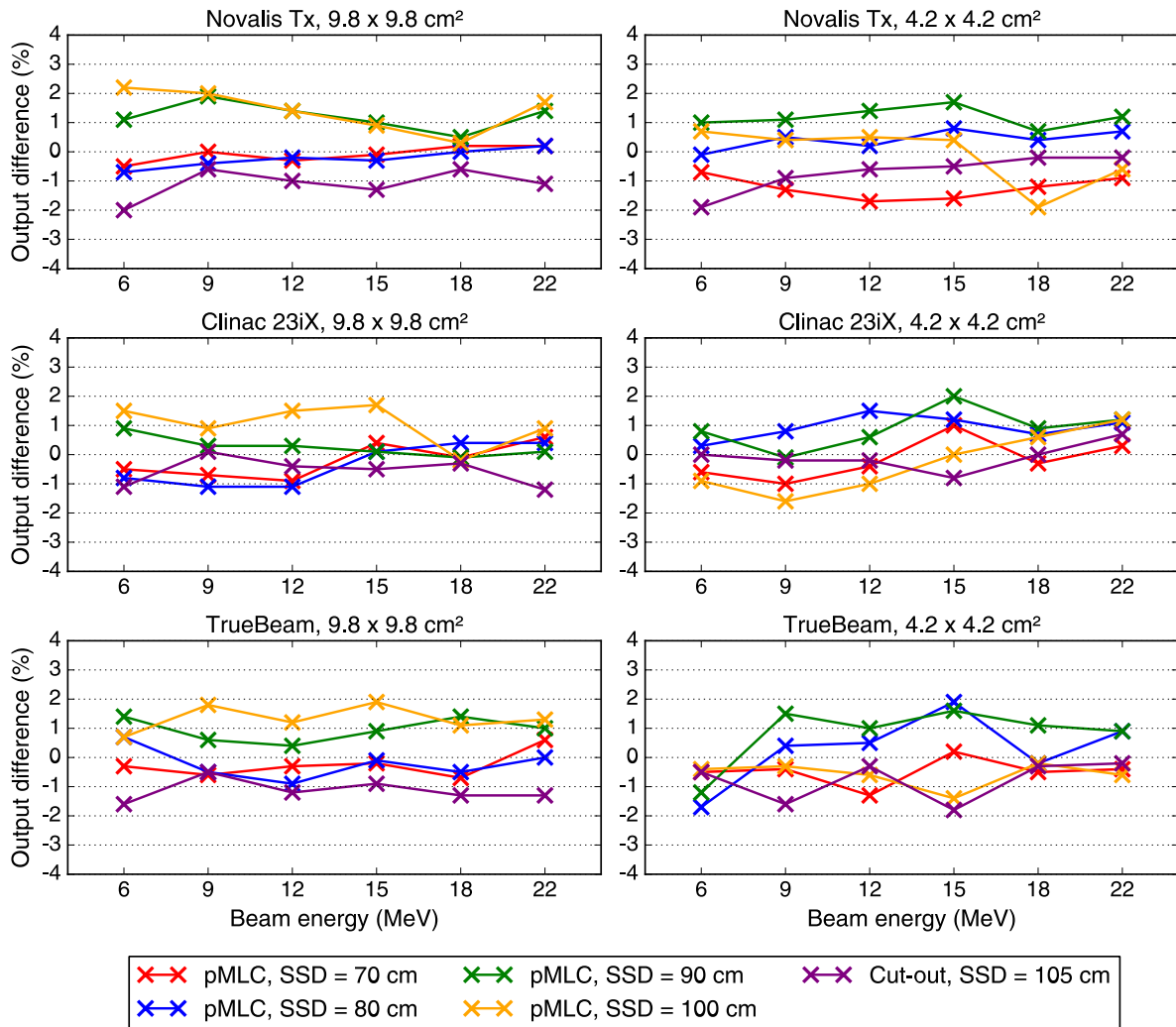


Figure 1. Output difference between measurement and dose calculation in water at the location of maximum dose on the central beam axis for all field sizes, beam energies, SSDs and treatment units investigated. The connecting lines serve only for visual guidance and the legend applies to all subplots.

For the cut-out collimated electron beams with an SSD of 105 cm, the analogous depth dose and dose profile measurements and the corresponding eMC dose calculations also agree generally within 3% or 2 mm DTA. Exceptions are an underestimation of the build-up in the depth dose curves by up to 4% for the $9.8 \times 9.8 \text{ cm}^2$ 22 MeV fields of all investigated treatment units, and out of field dose underestimations of up to 4.5% for

the in- and crossplane profiles at a depth of 1 cm for the 18 and 22 MeV energies of both field sizes and for all investigated treatment units. These exceptions are illustrated in figure 3 for the $9.8 \times 9.8 \text{ cm}^2$ field of the Novalis Tx. Output agreements between measurements and eMC dose calculations are within 2% for all investigated treatment units (figure 1).

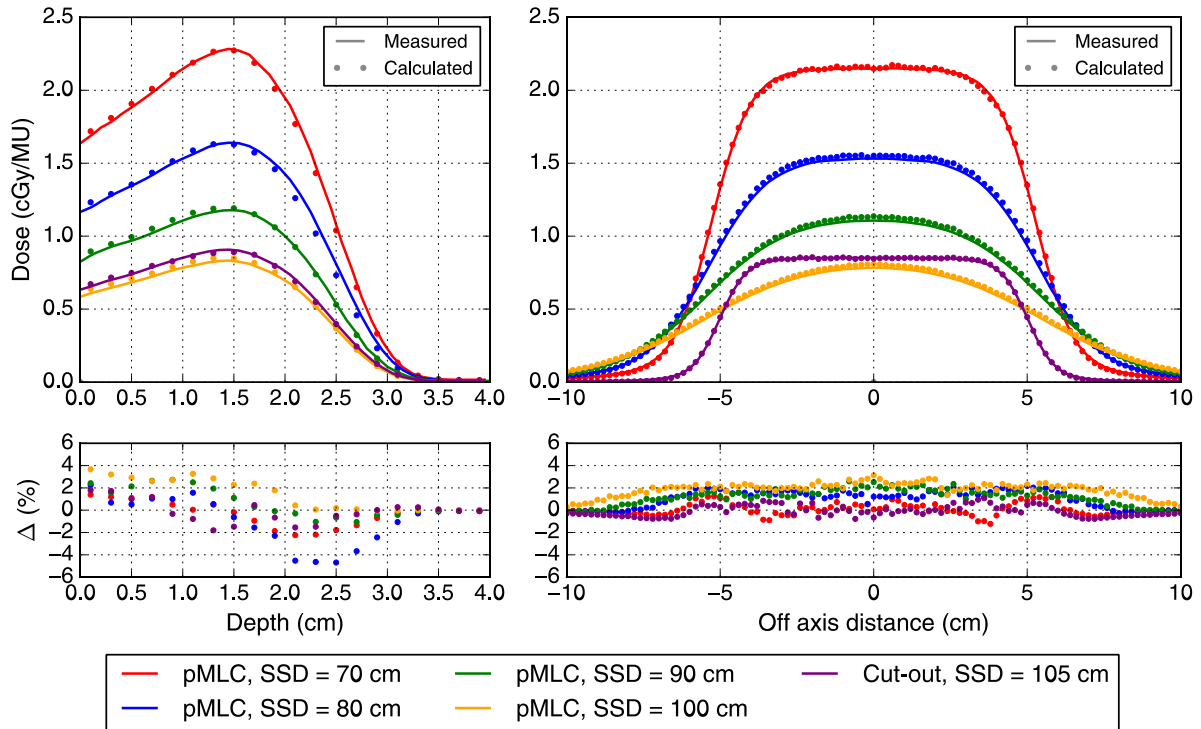


Figure 2. Measured and calculated depth dose curves (left) and crossplane dose profiles at a depth of 1 cm (right) of the field size of $9.8 \times 9.8 \text{ cm}^2$ for the 6 MeV beam of the Novalis Tx for every combination of SSD and collimation device investigated. The dose differences between measurements and calculations are shown below and the legend at the bottom applies to all subplots.

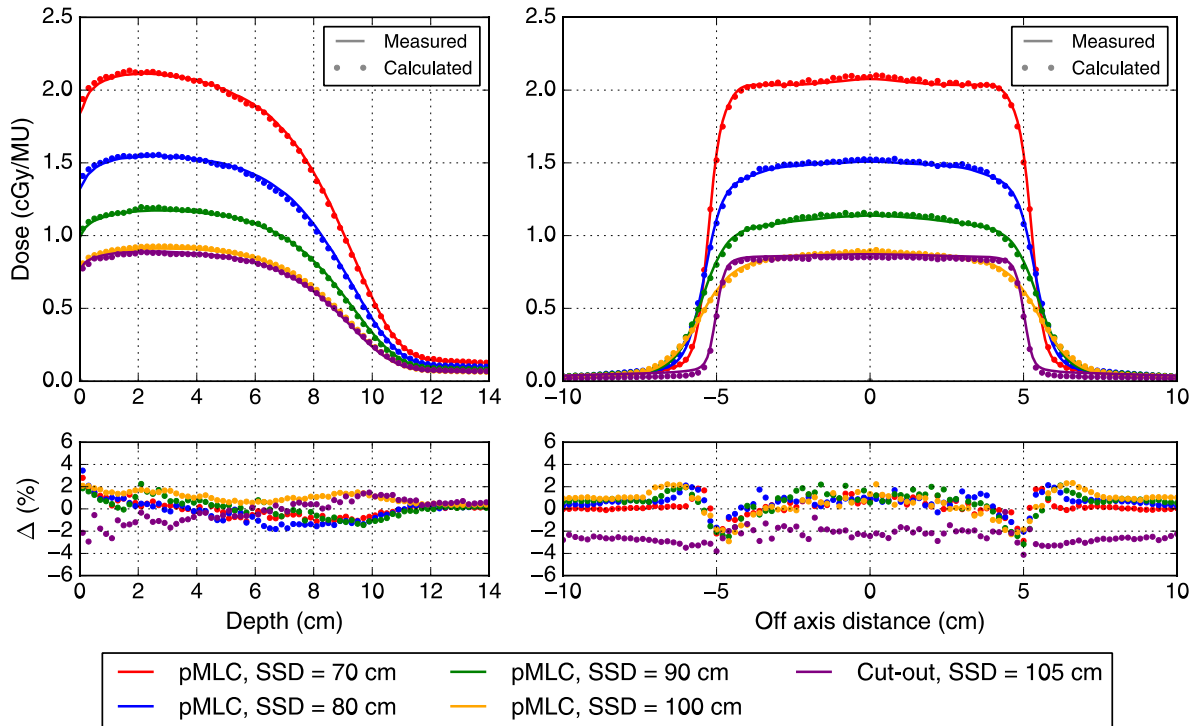


Figure 3. Measured and calculated depth dose curves (left) and crossplane dose profiles at a depth of 1 cm (right) of the field size of $9.8 \times 9.8 \text{ cm}^2$ for the 22 MeV beam of the Novalis Tx for every combination of SSD and collimation device investigated. The dose differences between measurements and calculations are shown below and the legend at the bottom applies to all subplots.

3.2. Left breast boost case

The 1E plans created for the left breast boost case using an 18 MeV electron field are compared in figure 4 and table 2. None of the pMLC plans achieve an HI within 3% of the cut-out plan. However, the dose coverage of the boost PTV for dose values below the prescribed dose is similar for all treatment plans (visible in the DVHs in figure 4). The mean doses to the ipsilateral lung and the heart are similar for the cut-out plan and the pMLC plans at an SSD of 70, 80 and 90 cm, while they are slightly increased for the pMLC plan at an SSD of 100 cm. However, the absolute difference of the mean dose to both OARs is still within 0.3 Gy to the cut-out plan. $V_{10\%}$ of the normal tissue is similar for the pMLC plan at an SSD of 70 cm compared to the cut-out plan and increases as the SSD is extended. A similar behavior is seen for the $VR_{50\%}$ values, as illustrated in one dimension with the dose profile comparison in figure 4.

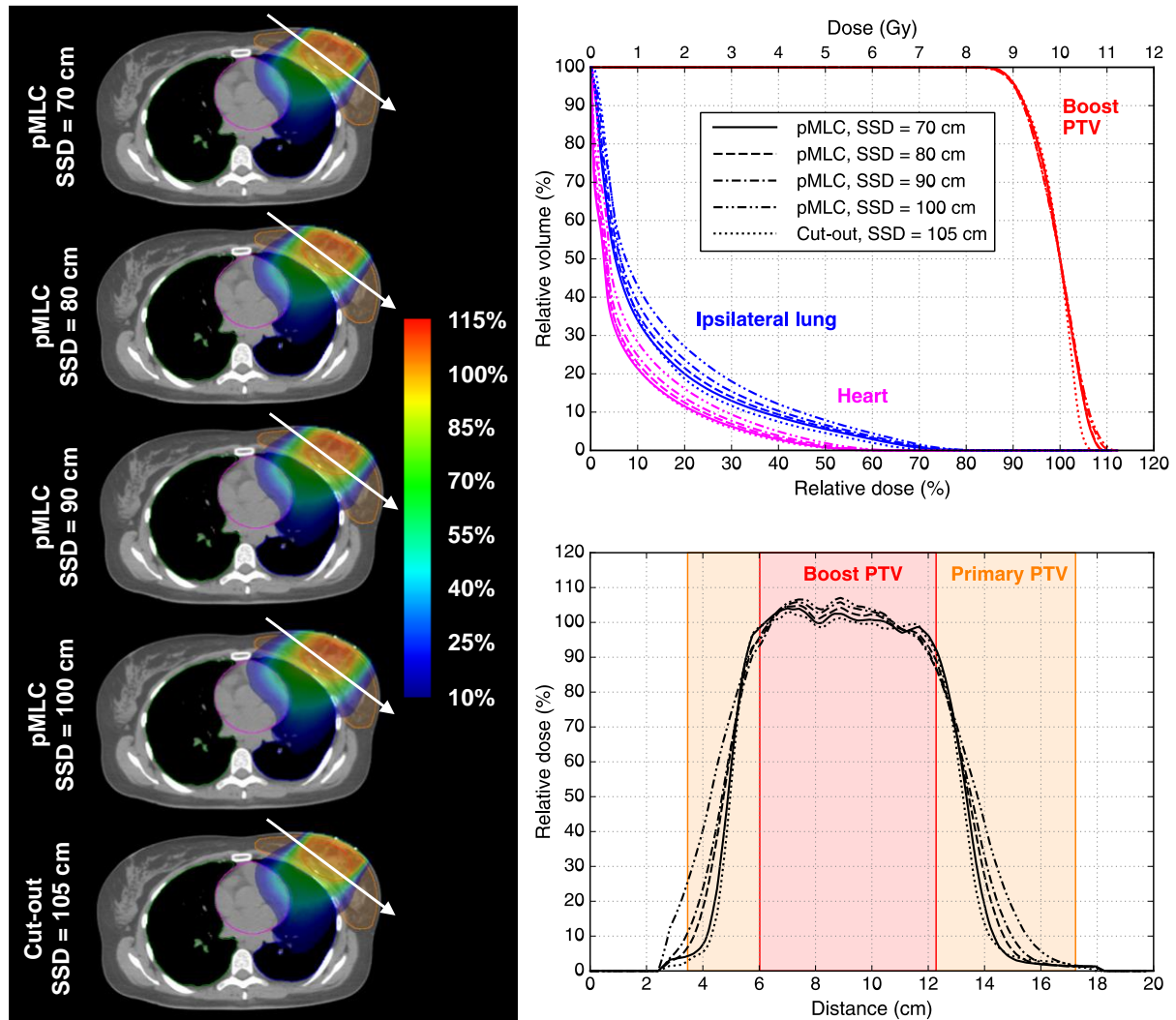


Figure 4. Dose distributions (left) and DVHs (top right) of TrueBeam 18 MeV 1E plans created for the left breast boost case and dose profiles (bottom right) indicated by a white arrow on the dose distributions. The legend of the DVHs also applies to the dose profiles. The contours of the boost PTV (red), primary PTV (orange), ipsilateral lung (blue), contralateral lung (green) and heart (magenta) are visible on the transversal CT images.

Table 2. Dosimetric values of TrueBeam 18 MeV 1E plans created for the left breast boost case.

	pMLC SSD = 70 cm	pMLC SSD = 80 cm	pMLC SSD = 90 cm	pMLC SSD = 100 cm	Cut-out SSD = 105 cm
PTV - HI	77.6%	77.1%	72.7%	71.5%	82.5%
Ipsilateral lung - D_{mean}	1.2 Gy	1.3 Gy	1.4 Gy	1.6 Gy	1.3 Gy
Heart - D_{mean}	0.7 Gy	0.8 Gy	0.8 Gy	1.0 Gy	0.8 Gy
Normal tissue - $V_{10\%}$	717 cm ³	771 cm ³	850 cm ³	990 cm ³	726 cm ³
Electron field - $VR_{50\%}$	1.11	1.17	1.26	1.44	-

The 1E2X plans for the same left breast boost case are compared in figure 5 and table 3. The beam energy of the electron field is now 12 MeV for the 1E2X plans instead of 18 MeV. The fraction of the integral dose in the boost PTV of the electron field (electron boost PTV dose contribution) is about 20% for all treatment plans. The dose homogeneity, the dose values to the OARs and the $V_{10\%}$ to the normal tissue are similar for all treatment plans. $VR_{50\%}$ is close to 1.0 for the pMLC plan at an SSD of 70 cm and increases as the SSD is extended.

Table 3. Dosimetric values of TrueBeam 12 MeV 1E2X plans created for the left breast boost case.

	pMLC SSD = 70 cm	pMLC SSD = 80 cm	pMLC SSD = 90 cm	pMLC SSD = 100 cm	Cut-out SSD = 105 cm
PTV - HI	95.7%	95.6%	95.3%	95.4%	96.1%
Ipsilateral lung - D_{mean}	0.3 Gy	0.3 Gy	0.3 Gy	0.3 Gy	0.3 Gy
Heart - D_{mean}	0.1 Gy	0.1 Gy	0.1 Gy	0.1 Gy	0.1 Gy
Normal tissue - $V_{10\%}$	442 cm ³	445 cm ³	449 cm ³	454 cm ³	442 cm ³
Electron field - $VR_{50\%}$	1.04	1.14	1.23	1.36	-

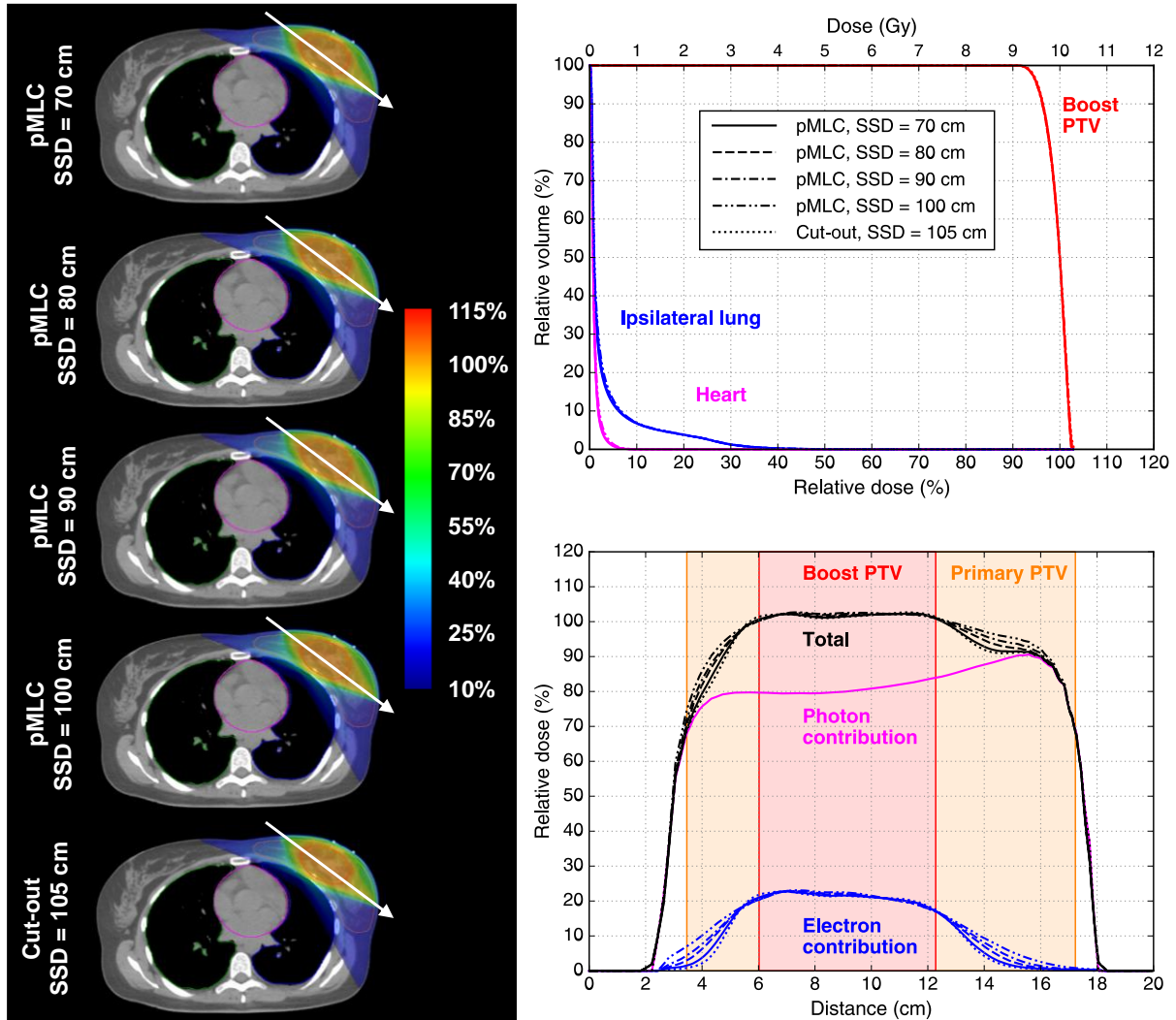


Figure 5. Dose distributions (left) and DVHs (top right) of TrueBeam 12 MeV 1E2X plans created for the left breast boost case and dose profiles (bottom right) indicated by a white arrow on the dose distributions. The legend of the DVHs also applies to the dose profiles. The contours of the boost PTV (red), primary PTV (orange), ipsilateral lung (blue), contralateral lung (green) and heart (magenta) are visible on the transversal CT images.

3.3. Right breast boost case

The 1E treatment plans created for the right breast boost case using a 6 MeV electron field are compared in figure 6 and table 4. Only the pMLC plan at an SSD of 70 cm achieves an *HI* within 3% of the cut-out-based treatment plan. The mean dose to the ipsilateral lung is slightly increased for all the pMLC plans compared to the cut-out-based treatment plan, as shown in table 4. However, the mean dose to the ipsilateral lung is, in absolute values, at most 0.3 Gy higher. Compared to the cut-out plan, $V_{10\%}$ of the normal tissue is 75%, 137%, 212% and 299% higher for the pMLC plans using an SSD of 70, 80, 90 and 100 cm, respectively. The $VR_{50\%}$ values also increase strongly as the

SSD is extended. The mentioned increase of the $V_{10\%}$ and $VR_{50\%}$ values are visible in the dose distributions and dose profiles in figure 6.

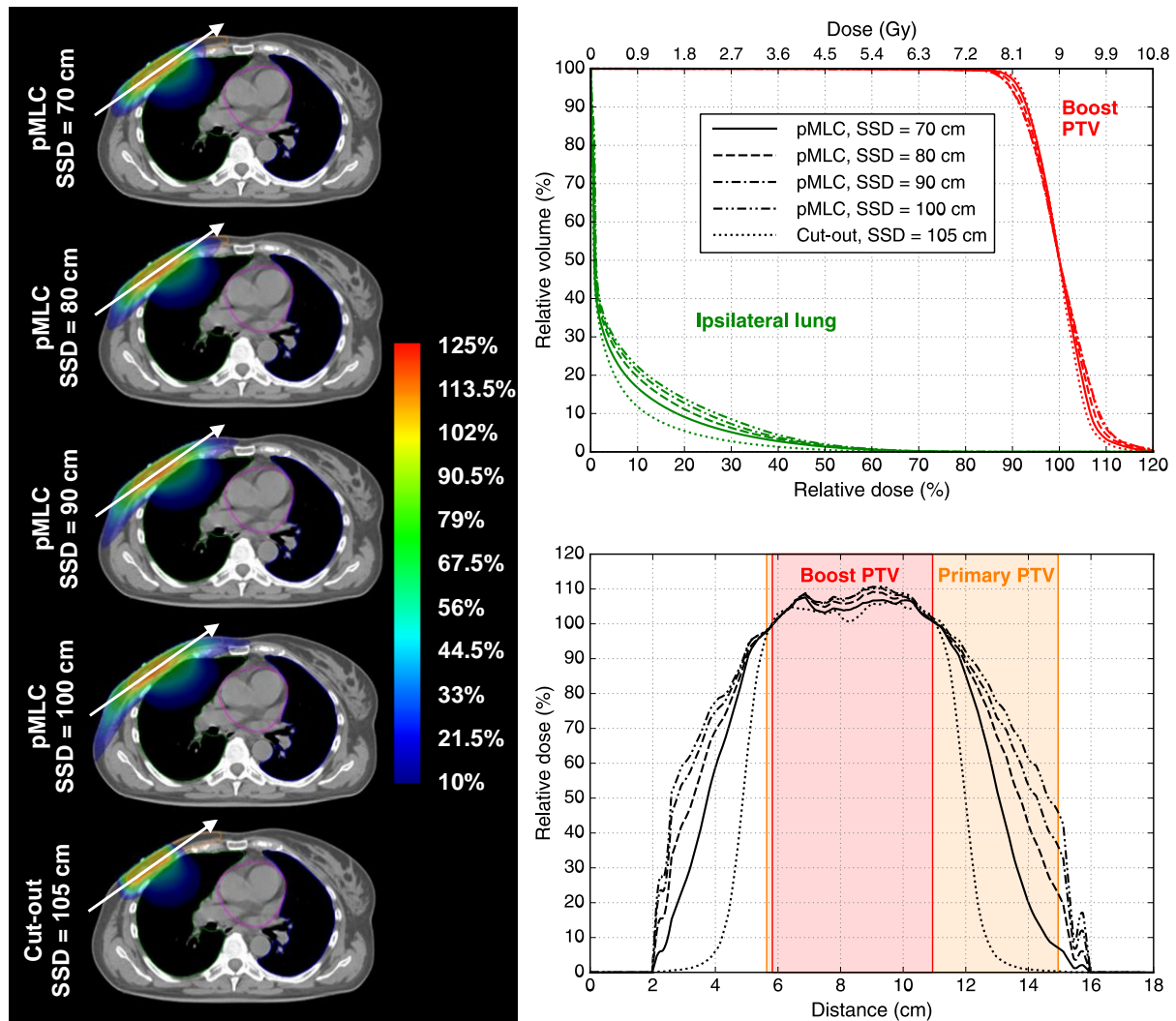


Figure 6. Dose distributions (left) and DVHs (top right) of TrueBeam 6 MeV 1E plans created for the right breast boost case and dose profiles (bottom right) indicated by a white arrow on the dose distributions. The legend of the DVHs also applies to the dose profiles. The contours of the boost PTV (red), primary PTV (orange), ipsilateral lung (green), contralateral lung (blue) and heart (magenta) are visible on the transversal CT images.

Table 4. Dosimetric values of TrueBeam 6 MeV 1E plans created for the right breast boost case.

	pMLC SSD = 70 cm	pMLC SSD = 80 cm	pMLC SSD = 90 cm	pMLC SSD = 100 cm	Cut-out SSD = 105 cm
PTV - HI	73.4%	67.8%	62.9%	62.1%	76.2%
Ipsilateral lung - D_{mean}	0.5 Gy	0.6 Gy	0.6 Gy	0.7 Gy	0.4 Gy
Normal tissue - $V_{10\%}$	451 cm ³	609 cm ³	802 cm ³	1026 cm ³	257 cm ³
Electron field - $VR_{50\%}$	1.69	2.05	2.43	2.87	-

The 1E2X plans for the same right breast boost case are compared in figure 7 and table 5. The electron boost PTV dose contribution is about 36% for all treatment plans. All pMLC plans achieve an HI within 3% of the cut-out plan. Due to the equal contribution of the photon fields for all treatment plans, the $V_{10\%}$ values increase less for the pMLC-based 1E2X plans than for the pMLC-based 1E plans in comparison to the corresponding cut-out plans. The $VR_{50\%}$ values are the same as for the 1E plans, because the same 6 MeV electron fields are used.

Table 5. Dosimetric values of TrueBeam 6 MeV 1E2X plans created for the right breast boost case.

	pMLC SSD = 70 cm	pMLC SSD = 80 cm	pMLC SSD = 90 cm	pMLC SSD = 100 cm	Cut-out SSD = 105 cm
PTV - HI	98.3%	97.5%	96.6%	96.9%	98.9%
Ipsilateral lung - D_{mean}	0.3 Gy	0.3 Gy	0.3 Gy	0.3 Gy	0.2 Gy
Normal tissue - $V_{10\%}$	350 cm ³	407 cm ³	476 cm ³	564 cm ³	276 cm ³
Electron field - $VR_{50\%}$	1.69	2.05	2.43	2.87	-

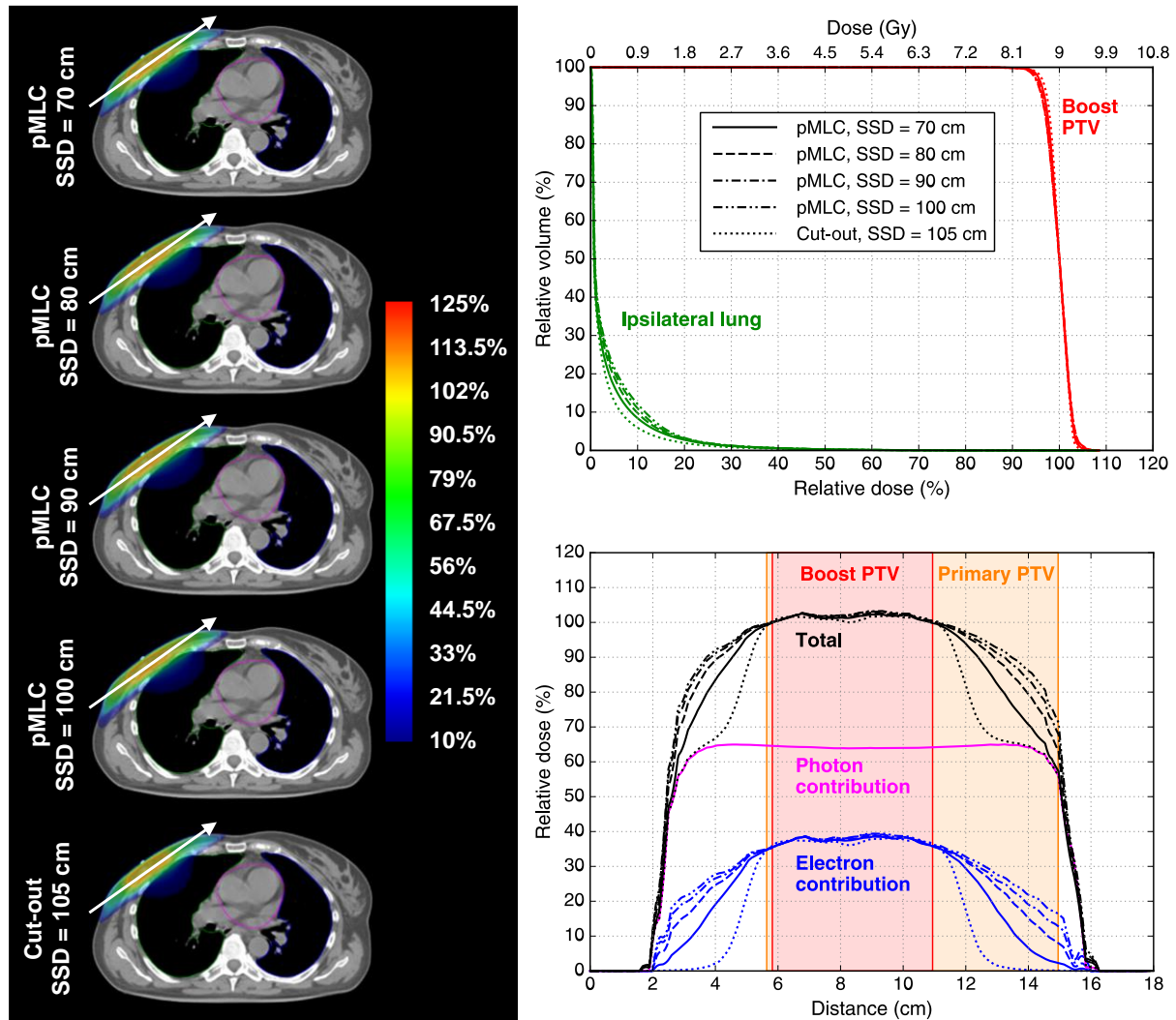


Figure 7. Dose distributions (left) and DVHs (top right) of TrueBeam 6 MeV 1E2X plans created for the right breast boost case and dose profiles (bottom right) indicated by a white arrow on the dose distributions. The legend of the DVHs also applies to the dose profiles. The contours of the boost PTV (red), primary PTV (orange), ipsilateral lung (green), contralateral lung (blue) and heart (magenta) are visible on the transversal CT images.

3.4. Sternum case

The 1E plans for the sternum case using a 12 MeV electron field are compared in figure 8. The pMLC and the cutout plans yield an HI value of 93.8% and 96.1%, respectively, and thus have a difference in the HI smaller than 3%. The dose to the lungs is increased for the pMLC plan compared to the cut-out plan, but the difference in the absolute mean dose is only 0.3 Gy. $V_{10\%}$ of the normal tissue is 1104 cm³ and 677 cm³ for the pMLC and cut-out plans, respectively, and the $VR_{50\%}$ value of the pMLC plan is 1.42.

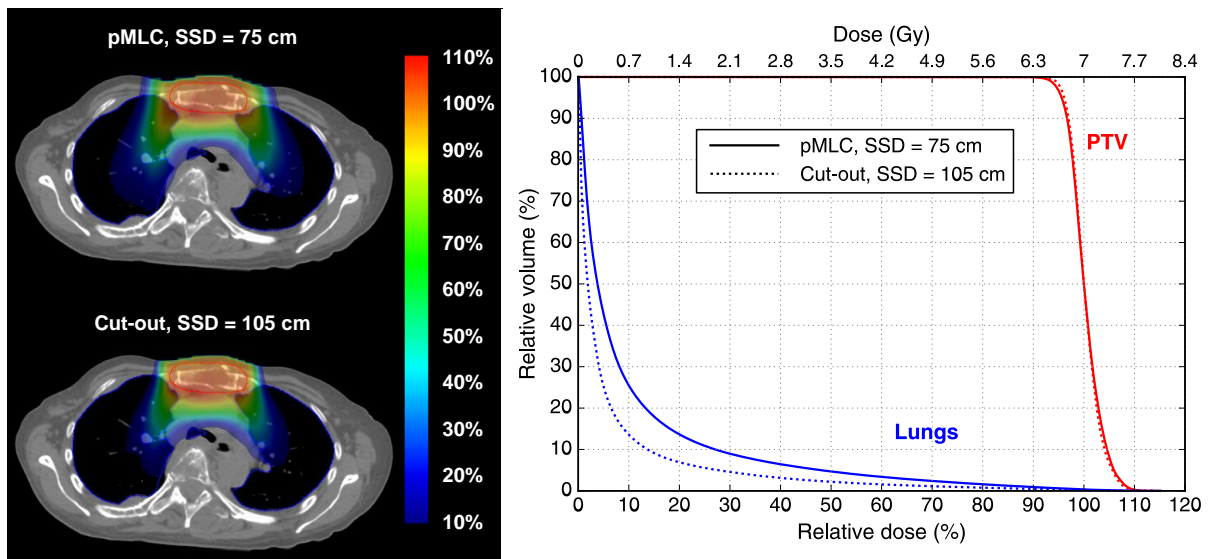


Figure 8. Dose distributions (left) and DVHs (right) of Novalis Tx 12 MeV 1E plans created for the sternum case. The contours of the PTV (red) and the lungs (blue) are visible on the transversal CT images.

3.5. Testis case

The 1E plans for the testis case using a 12 MeV electron field are compared in figure 9. The pMLC and the cut-out plans yield a similar HI value of 83.0% and 83.3%, respectively. $V_{10\%}$ of the normal tissue is 492 cm³ and 385 cm³ for the pMLC and the cut-out plans, respectively, and the $VR_{50\%}$ value of the pMLC plan is 1.20.

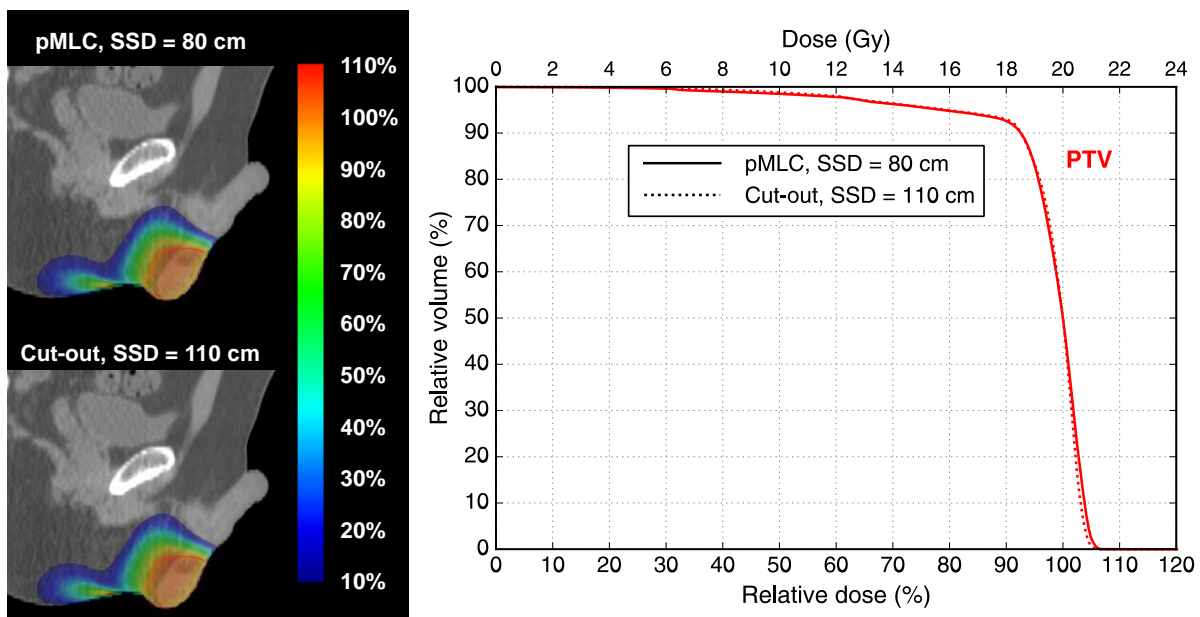


Figure 9. Dose distributions (left) and DVHs (right) of Clinac 23iX 12 MeV 1E plans created for the testis case. The contours of the PTV (red) are visible on the sagittal CT images.

3.6. Parotid gland case

The 1E2X treatment plans for the parotid gland case using a 15 MeV electron field are compared in figure 10. The electron PTV dose contribution is about 25% for both treatment plans. The pMLC and the cut-out plans have a similar *HI* value of 93.7% and 94.2%, respectively. The mean dose to the ipsilateral cochlea and the mandibula and $V_{10\%}$ to the normal tissue are similar for both treatment plans (7.0 Gy, 11.6 Gy and 522 cm³ for the pMLC plan and 6.8 Gy, 11.6 Gy and 502 cm³ for the cut-out plan). The $VR_{50\%}$ value of the pMLC plan is 1.18.

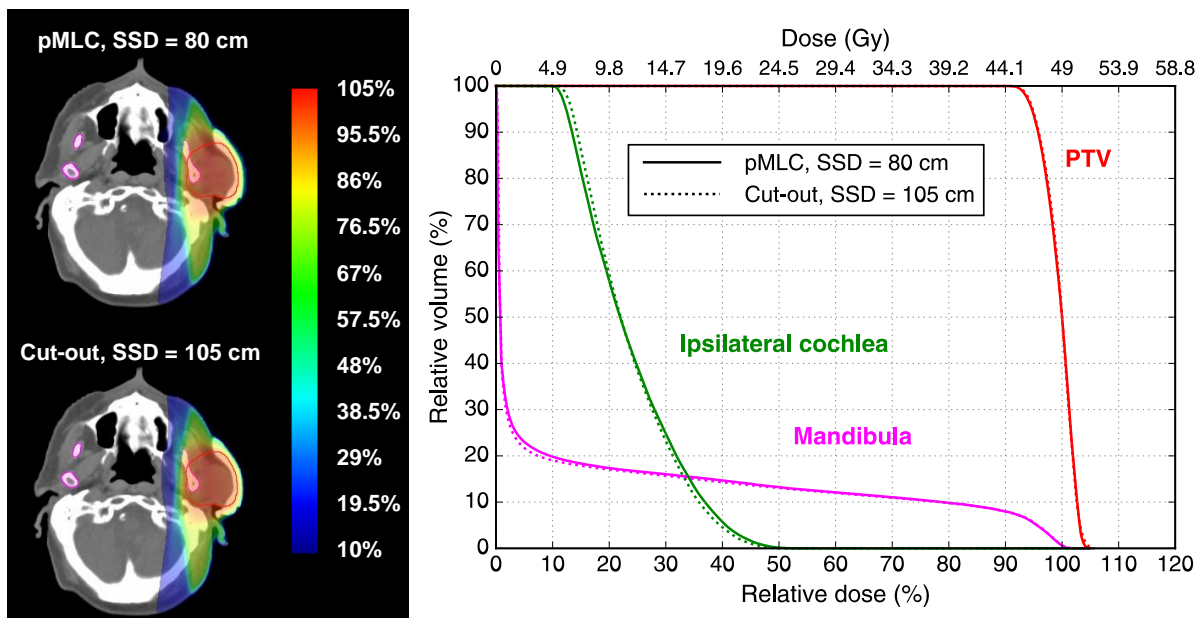


Figure 10. Dose distributions (left) and DVHs (right) of Novalis Tx 15 MeV 1E2X plans created for the parotid gland case. The contours of the PTV (red) and the mandibula (magenta) are visible on the transversal CT images.

4. Discussion

The beam model *ebm70*, originally developed to reconstruct Millennium 120 pMLC shaped electron beams of Clinac 23EX and TrueBeam treatment units at an SSD of 70 cm, is adjusted for accurate dose calculations of extended SSDs up to 100 cm and for usage of the HDMLC model. The accuracy of *ebm70*-based dose calculations of field sizes common for standard electron treatments is investigated for a Clinac 23iX and a TrueBeam, both equipped with a Millennium 120 pMLC and a Novalis Tx equipped with a HDMLC. No substantial difference in the dose calculation accuracy is found among the three tested treatment units and the accuracy is similar to *eMC*, which is a commercial dose calculation for clinical use of cut-out collimated electron beams. Since the *ebm70* is commissioned using measurements collected only at an SSD of 70 cm, these results demonstrate that an MC-based beam model and dose calculation for pMLC shaped electron beams allow us to accurately account for SSDs not used for commissioning measurements.

The pMLC-based 1E plans for the left and right breast boost cases at an SSD of 70 cm, the sternum case at an SSD of 75 cm and the testis case at an SSD of 80 cm have similar treatment plan quality regarding target coverage and absolute dose delivered to the OARs as the corresponding cut-out-based 1E plans. However, if the electron beam energy is 6 MeV as shown for the right breast boost case, the $VR_{50\%}$ value is considerably increased to 1.69. For breast boost irradiations, most of the additional dose is delivered to the primary PTV. In the case of the OARs being located laterally close to the target with respect to beam direction, the dose to the OARs is considerably increased for pMLC plans relative to cut-out plans, as is shown for the sternum case. Nevertheless, the pMLC plan is still a viable alternative to the cut-out plan for this palliative treatment due to the small mean dose to the lungs in absolute values. All the observations of the 1E plans can be explained with the similar depth dose curve and the enlarged penumbra of pMLC compared to cut-out shaped electron beams.

The pMLC-based 1E2X plans for the left and right breast boost cases at an SSD of 70 cm, and the parotid gland case at an SSD of 80 cm, have similar treatment plan quality in all dosimetric aspects compared to the corresponding cut-out-based 1E2X

plans. Reducing the fraction of the electron contribution compared to 1E plans made it possible to achieve similar values for $V_{10\%}$ of normal tissue compared to the cut-out plans. Conclusions of these 1E2X-based results are also expected to be generally valid for combined electron and photon plans using more than two photon fields.

The dosimetric influence of the SSD and the electron beam energy is well determined with the $VR_{50\%}$ values. Firstly, the larger the SSD, the larger the $VR_{50\%}$ value. Secondly, for the 6 MeV electron field used for the right breast boost case, the $VR_{50\%}$ is substantially increased compared to all other electron fields shown with beam energies between 12 and 18 MeV. Both findings can be explained by the increase of in-air scatter with smaller beam energy and larger SSD. It can be concluded that a reduced SSD is of high importance for low beam energy.

As with the sternum and the two breast boost cases investigated in this work, it is estimated that a reduced SSD of 70–75 cm is generally feasible for these treatment sites. However, many clinical cases of other treatment sites, like head and neck, would require an SSD of at least 80 cm and could still be treated with a treatment plan quality similar to that of cut-out plans. The parotid gland case shown is such an example, where a shorter SSD would lead to a collision with the couch. This underlines the necessity of a dose calculation with an acceptable accuracy also for SSDs > 70 cm. Every treatment plan presented in this work is considered to be deliverable regarding collision avoidance with the patient and the couch, based on the CT images. However, a collision detection system, building a 3D model of the patient and the couch during the acquisition of the planning CT (Padilla *et al* 2015, Cardan *et al* 2017), is suggested. The same system could be used in the treatment room to assure that collisions are avoided for every fraction.

From a practical point of view, using pMLC collimation for electron beams would profoundly improve clinical workflow compared to using molded patient-specific cut-outs, because no heavy add-on device is used and no cut-out fabrication is necessary. For clinics which do not have access to any cut-out fabrication and instead use standard cut-outs, pMLC collimation would allow the use of electron beams individually shaped to the target. Furthermore, combined electron and photon treatments would not be interrupted to mount and unmount any add-on device and could even be planned in an

isocentric setup without substantial loss of treatment plan quality. This can be concluded from the 1E2X plans for the left and right breast boost at an SSD of 90 and 100 cm. Moreover, image-guided radiation therapy (IGRT) would be eased using an isocentric setup, e.g. reduced number of image acquisitions. However, planning in an isocentric setup is not necessary for practical reasons, because Míguez *et al* (2017) showed in a clinical trial for MBRT that using a reduced SSD does not generate any additional inconvenience for the patients, neither for the positioning process, nor for the slightly larger treatment time due to the isocenter transition.

5. Conclusions

The feasibility of accurately calculating dose distributions of pMLC collimated electron beams at an SSD of 70–100 cm for standard electron treatments is shown for several Varian treatment units. A multiple source MC beam model linked to an MMC dose calculation, commissioned only at one SSD of 70 cm, is used for this purpose. At this SSD it is likely that certain beam directions lead to collisions with the patient or the couch. However, the results shown in this work suggest using a larger SSD for such fields. For standard electron treatments, similar treatment plan quality can be achieved with pMLC collimation instead of cut-out collimation. In the case of OARs located close to the target in the lateral direction with respect to beam direction, and in the case of using electron beams with 6 MeV beam energy at an extended SSD, OAR dose values are slightly increased. The results of this work support the suggestion of using a pMLC as the collimation device for standard electron treatments such that clinical workflow is profoundly improved and the introduction of advanced treatment techniques like MERT and MBRT is facilitated.

Acknowledgments

This work was partly supported by Varian Medical Systems. Calculations were partly performed on UBELIX (www.id.unibe.ch/hpc), the HPC cluster at the University of Bern.

ORCID iDs

S Mueller <https://orcid.org/0000-0002-9835-4362>

References

- Al-Yahya K, Schwartz M, Shenouda G, Verhaegen F, Freeman C and Seuntjens J 2005 Energy modulated electron therapy using a few leaf electron collimator in combination with IMRT and 3D-CRT: Monte Carlo-based planning and dosimetric evaluation *Med. Phys.* **32** 2976–86
- Alexander A, DeBlois F and Seuntjens J 2010 Toward automatic field selection and planning using Monte Carlo-based direct aperture optimization in modulated electron radiotherapy *Phys. Med. Biol.* **55** 4563–76
- Alexander A, Soisson E, Renaud M-A and Seuntjens J 2012 Direct aperture optimization for FLEC-based MERT and its application in mixed beam radiotherapy *Med. Phys.* **39** 4820–31
- Bortfeld T R, Kahler D L, Waldron T J and Boyer A L 1994 X-ray field compensation with multileaf collimators *Int. J. Radiat. Oncol.* **28** 723–30
- Boyer A L, Biggs P, Galvin J, Klein E, LoSasso T, Low D, Mah K and Yu C 2001 Basic applications of multileaf collimators *Med. Phys. AAPM Report No 72* (Alexandria, VA: AAPM) (https://aapm.org/pubs/reports/RPT_72.pdf)
- Brewster L, Mohan R, Mageras G, Burman C, Leibel S and Fuks Z 1995 Three-dimensional conformal treatment planning with multileaf collimators *Int. J. Radiat. Oncol. Biol. Phys.* **33** 1081–9
- Cardan R A, Popple R A and Fiveash J 2017 A priori patient-specific collision avoidance in radiotherapy using consumer grade depth cameras *Med. Phys.* **44** 3430–6
- Convery D J and Webb S 1992 The generation of intensity-modulated fields for conformal radiotherapy by dynamic collimation *Phys. Med. Biol.* **37** 1359–74
- Cygler J E, Daskalov G M, Chan G H and Ding G X 2004 Evaluation of the first commercial Monte Carlo dose calculation engine for electron beam treatment planning *Med. Phys.* **31** 142
- Ding G X, Cygler J E, Yu C W, Kalach N I and Daskalov G 2005 A comparison of electron beam dose calculation accuracy between treatment planning systems using either a pencil beam or a Monte Carlo algorithm *Int. J. Radiat. Oncol. Biol. Phys.* **63** 622–33

- du Plessis F C P, Leal A, Stathakis S, Xiong W and Ma C-M 2006 Characterization of megavoltage electron beams delivered through a photon multi-leaf collimator (pMLC) *Phys. Med. Biol.* **51** 2113–29
- Eldib A, Jin L H, Li J S and Ma C M C 2013 Feasibility of replacing patient specific cutouts with a computer-controlled electron multileaf collimator *Phys. Med. Biol.* **58** 5653–72
- Engel K and Gauer T 2009 A dose optimization method for electron radiotherapy using randomized aperture beams *Phys. Med. Biol.* **54** 5253–70
- Fix M, Manser P and Frei D 2007 An efficient framework for photon Monte Carlo treatment planning *Phys. Med. Biol.* **52** N425–37
- Fix M K, Cygler J, Frei D, Volken W, Neuenschwander H, Born E J and Manser P 2013 Generalized eMC implementation for Monte Carlo dose calculation of electron beams from different machine types *Phys. Med. Biol.* **58** 2841–59
- Fix M K, Frei D, Volken W, Neuenschwander H, Born E J and Manser P 2010 Monte Carlo dose calculation improvements for low energy electron beams using eMC *Phys. Med. Biol.* **55** 4577–88
- Fix M K, Volken W, Frei D, Frauchiger D, Born E J and Manser P 2011 Monte Carlo implementation, validation, and characterization of a 120 leaf MLC *Med. Phys.* **38** 5311–20
- Ge Y and Faddegon B A 2011 Study of intensity-modulated photon–electron radiation therapy using digital phantoms *Phys. Med. Biol.* **56** 6693–708
- Henzen D *et al* 2014a Beamlet based direct aperture optimization for MERT using a photon MLC *Med. Phys.* **41** 121711
- Henzen D, Manser P, Frei D, Volken W, Neuenschwander H, Born E J, Vetterli D, Chatelain C, Stampanoni M F M and Fix M K 2014b Monte Carlo based beam model using a photon MLC for modulated electron radiotherapy *Med. Phys.* **41** 21714
- Klein E E, Mamalui-Hunter M and Low D A 2009 Delivery of modulated electron beams with conventional photon multi-leaf collimators *Phys. Med. Biol.* **54** 327–39

- Klein E E, Vicic M, Ma C-M, Low D A and Drzymala R E 2008 Validation of calculations for electrons modulated with conventional photon multileaf collimators *Phys. Med. Biol.* **53** 1183–208
- Lee M C, Deng J, Li J, Jiang S B and Ma C 2001 Monte Carlo based treatment planning for modulated electron beam radiation therapy *Phys. Med. Biol.* **46** 2177–99
- Lee M C, Jiang S B and Ma C M 2000 Monte Carlo and experimental investigations of multileaf collimated electron beams for modulated electron radiation therapy *Med. Phys.* **27** 2708–18
- Li J G, Williams S S, Goffinet D R, Boyer A L and Xing L 2000 Breast-conserving radiation therapy using combined electron and intensity modulated radiotherapy technique *Radiother. Oncol.* **56** 65–71
- Lloyd S A M, Gagne I M, Bazalova-carter M and Zavgorodni S 2016 Validation of Varian TrueBeam electron phase—spaces for Monte Carlo simulation of MLC-shaped fields *Med. Phys.* **43** 2894–903
- Lloyd S A M, Zavgorodni S and Gagne I M 2015 Comparison of measured Varian Clinac 21EX and TrueBeam accelerator electron field characteristics *J. Appl. Clin. Med. Phys.* **16** 193–201
- Míguez C, Jiménez-Ortega E, Palma B A, Miras H, Ureba A, Arráns R, Carrasco-Peña F, Illescas-Vacas A and Leal A 2017 Clinical implementation of combined modulated electron and photon beams with conventional MLC for accelerated partial breast irradiation *Radiother. Oncol.* **124** 124–9
- Mihaljevic J, Soukup M, Dohm O and Alber M 2011 Monte Carlo simulation of small electron fields collimated by the integrated photon MLC *Phys. Med. Biol.* **56** 829–43
- Mu X, Olofsson L, Karlsson M, Sjögren R and Zackrisson B 2004 Can photon IMRT be improved by combination with mixed electron and photon techniques? *Acta Oncol.* **43** 727–35
- Mueller S, Fix M, Joosten A, Henzen D, Frei D, Volken W, Kueng R, Aebersold D, Stampanoni M and Manser P 2017 Simultaneous optimization of photons and electrons for mixed beam radiotherapy *Phys. Med. Biol.* **62** 5840–60
- Neuenschwander H and Born E J 1992 A Macro Monte Carlo method for electron beam dose calculations *Phys. Med. Biol.* **37** 107–25

- Neuenschwander H, Mackie T R and Reckwerdt P J 1995 MMC—a high-performance Monte Carlo code for electron beam treatment planning *Phys. Med. Biol.* **40** 543–74
- Olofsson L, Mu X, Nill S, Oelfke U, Zackrisson B and Karlsson M 2004 Intensity modulated radiation therapy with electrons using algorithm based energy/range selection methods *Radiother. Oncol.* **73** 223–31
- Otto K 2008 Volumetric modulated arc therapy: IMRT in a single gantry arc *Med. Phys.* **35** 310–7
- Padilla L, Pearson E A, Pelizzari C A and Francisco S 2015 Collision prediction software for radiotherapy treatments *Med. Phys.* **42** 6448–56
- Palma B A, Sánchez A U, Salguero F J, Arráns R, Sánchez C M, Zurita A W, Hermida M I R and Leal A 2012 Combined modulated electron and photon beams planned by a Monte-Carlo-based optimization procedure for accelerated partial breast irradiation *Phys. Med. Biol.* **57** 1191–202
- Renaud M-A, Serban M and Seuntjens J 2017 On mixed electron–photon radiation therapy optimization using the column generation approach *Med. Phys.* **44** 4287–98
- Rodrigues A, Yin F-F and Wu Q 2014 Dynamic electron arc radiotherapy (DEAR): a feasibility study *Phys. Med. Biol.* **59** 327–45
- Rosca F 2012 A hybrid electron and photon IMRT planning technique that lowers normal tissue integral patient dose using standard hardware *Med. Phys.* **39** 2964–71
- Salguero F J, Arráns R, Palma B A and Leal A 2010 Intensity- and energy-modulated electron radiotherapy by means of an xMLC for head and neck shallow tumors *Phys. Med. Biol.* **55** 1413–27
- Salguero F J, Palma B, Arrans R, Rosello J and Leal A 2009 Modulated electron radiotherapy treatment planning using a photon multileaf collimator for post-mastectomized chest walls *Radiother. Oncol.* **93** 625–32
- Surucu M, Klein E E, Mamalui-Hunter M, Mansur D B and Low D A 2010 Planning tools for modulated electron radiotherapy *Med. Phys.* **37** 2215–24
- Terribilini D, Fix M K, Frei D, Volken W and Manser P 2010 VMC++ validation for photon beams in the energy range of 20–1000 keV *Med. Phys.* **37** 5218–27
- Varian Medical Systems 2015 Eclipse photon and electron algorithms reference guide version 13.6 Online: <https://www.varian.com>

Walters B R B, Kawrakow I and Rogers D W O 2002 History by history statistical estimators in the BEAM code system *Med. Phys.* **29** 2745–52

Xiong W, Li J, Chen L, Price R A, Freedman G, Ding M, Qin L, Yang J and Ma C M 2004 Optimization of combined electron and photon beams for breast cancer *Phys. Med. Biol.* **49** 1973–89

3**A dosimetric evaluation of different levels
of energy and intensity modulation
for inversely planned multi-field MERT**

**A. Joosten, S. Mueller, D. Henzen, W. Volken, D. Frei, D.M. Aebersold,
P. Manser and M.K. Fix**

Division of Medical Radiation Physics and Department of Radiation Oncology,
Inselspital, Bern University Hospital, and University of Bern, Bern, Switzerland

published in

Biomedical Physics & Engineering Express

2018, Vol. 4, 045003(10pp)

<https://doi.org/10.1088/2057-1976/aabe40>

© IOP Publishing.

Reproduced with permission. All rights reserved.

Abstract

For inversely planned multi-field modulated electron radiation therapy (MERT), the impact of different levels of energy and intensity modulation on the dosimetric characteristics of MERT plans was investigated. Four cases (breast, skin, larynx, parotid) were selected for this study. One to four different energies and one to four different intensity levels per energy were considered resulting in sixty optimized plans. The optimized plans with the best combinations of one, two, three and four energies considering all intensity levels were selected for final dose calculation. The influence of energy and intensity levels on the homogeneity index (HI) in the planning target volume (PTV) and on organs at risk (OAR) sparing was investigated. Additionally, the difference in the HI between final and optimized plans ΔHI was studied. Energy and intensity modulation both improved the HI in the PTV for the final plans. While intensity modulation had negligible influence on OAR sparing, energy modulation could also improve OAR sparing depending on the selected energies. To achieve a HI > 90% in the PTV, the minimal number of energies required were four for the breast case, three for the parotid and skin cases and one for the larynx case. ΔHI decreased with increasing number of apertures. Overall, energy modulation had a larger impact on the dosimetric characteristics of MERT plans than intensity modulation.

Keywords: MERT, Monte Carlo, electron radiotherapy, energy modulation, intensity modulation

1. Introduction

Electron beams are particularly well-suited to treat shallow tumors and spare distally located organs at risk (OAR) due to the limited range of electrons in tissue. In sharp contrast with photon radiotherapy and the recent developments of intensity modulated radiation therapy (IMRT) and volumetric modulated arc therapy (VMAT), electron radiotherapy has not evolved much over the last decades due to greater challenges in dose calculation and specific collimation device requirements. Modulated electron radiation therapy (MERT) using both energy and intensity modulation has the potential to substantially improve the dose distribution compared to conventional electron radiotherapy (Salguero *et al* 2009). In recent years, some research groups developed forward as well as inverse planning strategies for MERT using either a specific add-on collimation device (Lee *et al* 2001, Ma *et al* 2003, Gauer *et al* 2006, Al-Yahya *et al* 2005a, 2005b, 2007, Gauer *et al* 2010, Alexander *et al* 2010, 2011, 2012) or the photon MLC (pMLC) at a shorter source-to-skin distance (SSD) (Klein, 1998, du Plessis *et al* 2006, Jin *et al* 2008, Klein *et al* 2008, 2009, Salguero *et al* 2009, Salguero *et al* 2010, Surucu *et al* 2010, Palma *et al* 2012, Henzen *et al* 2014a, 2014b, 2014c) for electron beam collimation. While many of them showed the planning capabilities of these tools applied to selected clinical cases, none of them investigated thoroughly the impact of different levels of energy and intensity modulation on the dosimetric characteristics of the final plan. Additionally, the majority of the planned clinical cases employed only 1 or 2 fields covering the target (Klein 1998, Lee *et al* 2001, Ma *et al* 2000, 2003, Olofsson *et al* 2004, Jin *et al* 2008, Klein *et al* 2009, Salguero *et al* 2009, 2010, Surucu *et al* 2010, Alexander *et al* 2011, 2012), while inverse planning systems should be able to handle multiple overlapping fields similarly to inversely planned photon IMRT. It had already been shown for conformal electron therapy that multiple gantry angles or an arc could substantially improve the dose homogeneity to the target compared to a single field setup (Zackrisson and Karlsson 1996, Rodrigues *et al* 2014). While it had been suggested that the target coverage achieved with MERT could be improved with multiple beams or a limited arc (Alexander *et al* 2012), the available published data on this subject is currently lacking. The aim of the current study was to investigate field setups consisting

of multiple overlapping fields forming a pseudo-arc employing a previously developed direct aperture optimization (DAO) algorithm for pMLC-based MERT (Henzen *et al* 2014a, 2014c). More specifically, the impact of different levels of energy and intensity modulation on the dosimetric characteristics of the MERT plans was thoroughly investigated. Finally, the degradation of the plan quality between the optimized and the final deliverable plans was investigated.

2. Materials and method

2.1. Patient selection

Four clinical cases already treated with either photons (conventional or VMAT) or conventional electron beam techniques were selected for MERT planning. The maximum distal depth of the PTV for all selected cases was inferior to 5–6 cm in order to be able to cover the most distal part of the PTV with the highest electron energy available (20 MeV). The sites selected represented a variety of tumors, which could benefit from MERT, and were as follows with the respective prescribed doses given in parentheses: a right-sided breast tumor (50 Gy), a skin carcinoma of the back (55 Gy), a larynx tumor (66 Gy) and a parotid tumor (50 Gy).

2.2. Field setup, energy selection and beamlet dose calculation

In our MERT model, all fields will be delivered with the photon MLC without any additional accessories. A short source-to-skin distance (SSD) between 70 and 75 cm was used for all cases to limit in-air scattering of electrons. The jaws were set to define a field of $15 \times 35 \text{ cm}^2$ as the Monte Carlo (MC) beam model for pMLC-delivered electron beams was previously validated only for a fixed jaws opening of $15 \times 35 \text{ cm}^2$ (defined at isocenter) (Henzen *et al* 2014c). Hence, defining multiple field entries using a single isocenter to cover the planning target volume (PTV) appropriately was challenging and not always feasible: indeed with the isocenter far removed from the PTV, a relatively small change in the gantry angle might leave the PTV out of the projected maximal field size, which also became smaller at short SSD. For the larynx and parotid tumors five and seven fields were setup with a different isocenter for each field, respectively (see figure 1). With this setup, the whole PTVs could be covered from each beam's eye view. For the breast and the skin cases, six equally spaced fields sharing a single isocenter were setup to cover the PTV with a limited arc (see figure 1). None of the single fields could completely cover the PTVs due to their large sizes relative to the jaws opening and the short SSD used.

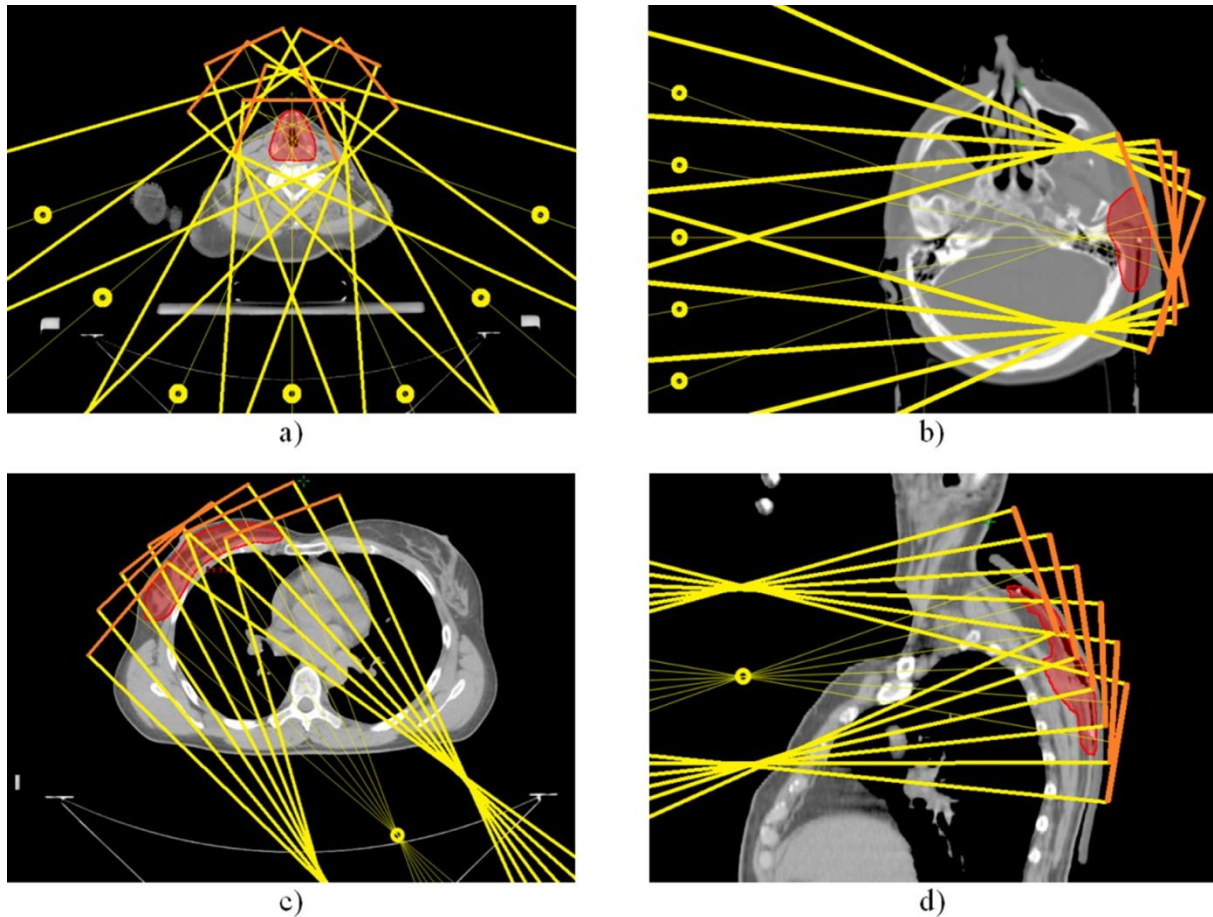


Figure 1. Field setup for the (a) larynx case (b) parotid case (c) breast case (d) skin case. The PTV is displayed in red.

The MC beam model of the Varian Clinac 23EX (Varian Medical Systems, Inc., Palo Alto, CA) was used (Henzen *et al* 2014c) with the following available energies: 4, 6, 9, 12, 16 and 20 MeV. For each case, the highest energy required to cover the deepest part of the target was user-determined by trial-and-error using open fields. This energy and the three successive lower available energies were then selected for beamlet dose calculation resulting in four available energies per case. The beamlet size at isocenter varied between $0.4 \times 0.5 \text{ cm}^2$ and $0.6 \times 1.0 \text{ cm}^2$ depending on the size of the target. For each field, beamlet dose distributions were calculated for all four energies in the voxelised CT phantom (Kawrakow and Walters 2006) using the Macro Monte Carlo (MMC) dose calculation algorithm (Neuenschwander *et al* 1995, Fix *et al* 2013). The size of the dose grid varied between 2.5 and 3 mm depending on the volumes of the PTVs and OARs. For each beamlet, the statistical uncertainty of the dose was lower than 3% for all voxels receiving more than 50% of the maximum dose.

2.3. Plan definition

With the DAO algorithm (Henzen *et al* 2014a), the initial apertures per beam energy and fields from which they were delivered needed to be defined. With four available energies per case for all fields, fifteen different energy combinations of one, two, three or four energies could be investigated to study the effect of different levels of energy modulation on the dose characteristics of the treatment plan. For a given plan, the same combination of energies was selected for all fields. For a given field and beam energy, a number of initial apertures was defined. We refer to this number as the intensity level; if one initial aperture per field and per energy was defined we had an intensity level of one. Different levels of intensity modulation varying between one and four were investigated. Considering all energy and intensity levels combinations, a total of sixty treatment plans per case were considered for DAO. The largest number of initial apertures to be optimized for a single plan was 112 for the larynx case considering all four energies and four intensity levels for each of the seven fields.

2.4. Inverse optimization and cost function analysis

Each plan was optimized with a recently developed DAO employing a simulated annealing algorithm (Henzen *et al* 2014a) based on Shepard *et al*'s work (Shepard *et al* 2002). The original python code was rewritten in C++ to improve computational efficiency. The initial apertures were shaped to match the PTV projections and all initial weights were set equal to each other. More details about the simulated annealing algorithm used in this work can be found in the supplementary data is available online at stacks.iop.org/BPEX/4/045003/mmedia. The dose-volume constraints used for optimization are defined in the supplementary data. Two million iterations were carried out for each plan. For each case, the final cost function values corresponding to the 15 different energy combinations were plotted as a function of intensity level.

2.5. Plan selection for final dose calculation and dosimetric analysis

From the cost function plots (figure 2), the best combinations (i.e. the one with lowest cost function values) of one, two, three and four energies were selected for final dose calculation in order to determine the best achievable dosimetry using one, two, three or

four different energies. For each energy combination, all intensity levels from one to four were considered resulting into sixteen plans per case selected for final dose calculation. The pMLC openings were set to match the beamlet patterns for each aperture and the dose distributions for pMLC-collimated electron apertures were recalculated with MC. The weights of the pMLC-collimated apertures were then reoptimized to obtain the final plans. All plans were normalized such that the median dose in the PTV corresponded to the prescribed dose. For each case, the final plans were compared with respect to energy modulation and intensity modulation using dose volume histograms (DVH) and relevant dosimetric parameters. The latter included the homogeneity index (HI) in the PTV defined as $V_{95\%}-V_{107\%}$, as well as mean dose, max dose and other relevant dose volume parameters in OAR. Finally, the difference in the cost function values between final and optimized plans ΔCF was investigated as a function of number of initial apertures and the degradation of the dose homogeneity ΔHI taken as the absolute difference between the HI found for the optimal and the final plans was derived and investigated as a function of ΔCF .

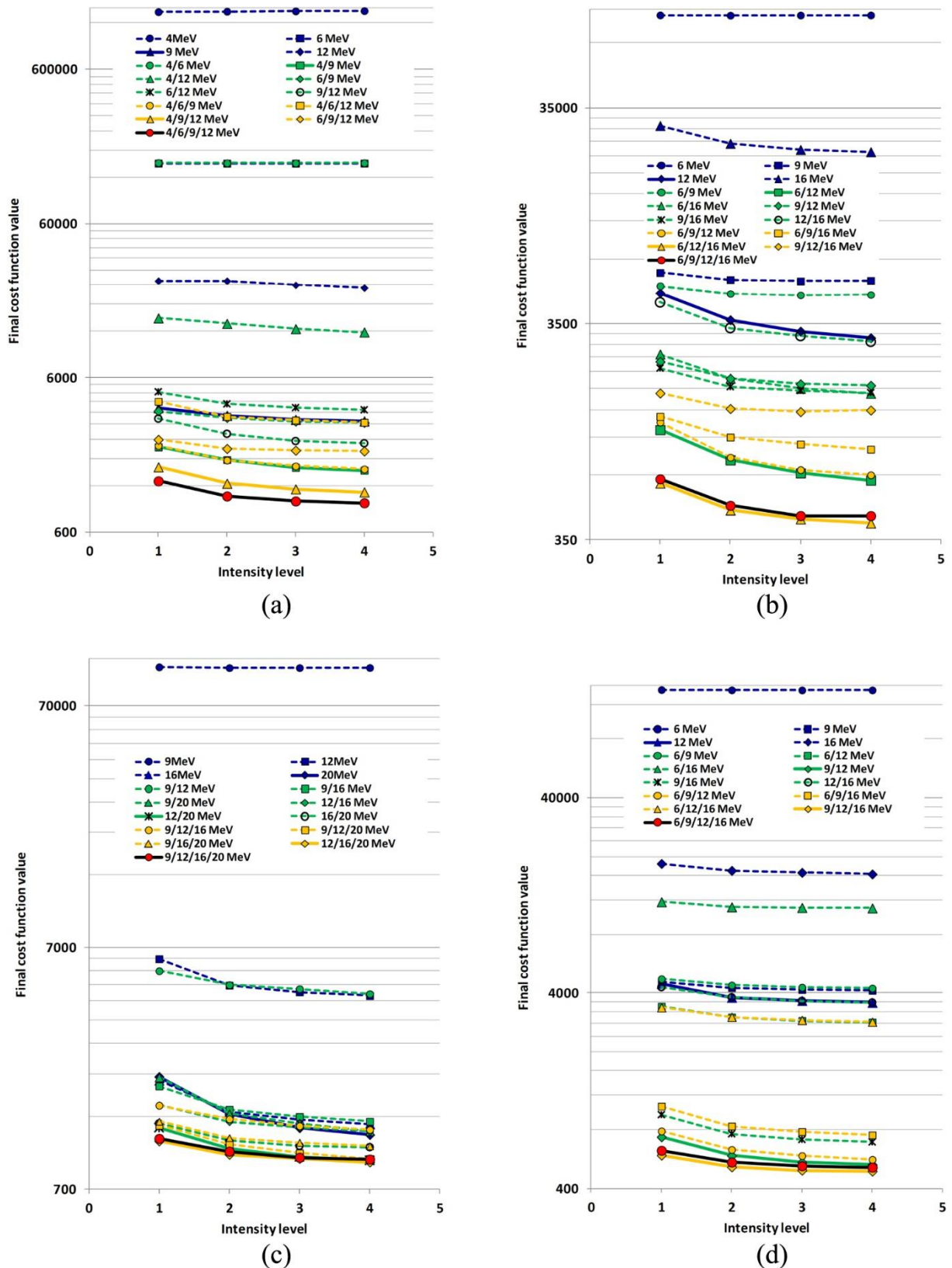


Figure 2. Final cost function plots of all possible energy combinations as a function of intensity level for the following cases: (a) breast (b) skin (c) larynx (d) parotid. For a given number of selected energies, the best energy combination is shown in full lines while other combinations are shown in dotted lines.

3. Results

The energies selected were as follows: 12/9/6/4 MeV for the breast case, 16/12/9/6 MeV for the skin case, 20/16/12/9 MeV for the larynx case and 16/12/9/6 MeV for the parotid case. The optimization time for a given plan using two million iterations varied between 10 min and 1 h (CPU time). Using more iterations lowered the cost function value only marginally. Figure 2 shows the final cost function values after two million iterations for each energy combination as a function of intensity level for all cases.

Table 1. Comparison of the dose homogeneity in the PTV between optimal and final plans for all cases and all energy/intensity levels. The worsening of the PTV dose homogeneity in the final plan is given by $\Delta HI = HI(\text{optimal plan}) - HI(\text{final plan})$.

Energies [MeV]	HI (optimal plan)				HI (final plan)				ΔHI			
	Intensity level				Intensity level				Intensity level			
	1	2	3	4	1	2	3	4	1	2	3	4
<i>Breast</i>												
9	72.7	74.5	74.8	75.6	68.3	71.9	73.2	73.5	4.3	2.6	1.6	2.0
4/9	86.0	88.3	89.1	90.0	78.9	80.9	83.4	84.9	7.1	7.5	5.8	5.0
4/9/12	89.4	90.7	92.0	92.5	84.1	87.9	88.5	89.4	5.3	2.8	3.5	3.1
4/6/9/12	90.1	92.2	92.6	92.6	86.6	89.7	89.1	91.1	3.5	2.5	3.5	1.5
<i>Skin</i>												
12	72.8	78.6	80.2	81.2	56.8	57.0	65.7	64.4	16.0	21.6	14.6	16.8
6/12	88.2	91.1	92.0	92.6	67.1	73.2	82.4	86.3	21.1	17.9	9.5	6.3
6/12/16	93.2	94.6	95.3	95.6	77.4	89.2	88.1	91.3	15.8	5.4	7.1	4.2
6/9/12/16	93.0	94.3	94.9	95.1	80.5	89.0	90.9	92.0	12.5	5.3	4.0	3.1
<i>Larynx</i>												
20	89.1	93.3	94.4	94.8	82.7	89.8	92.8	90.8	6.4	3.4	1.6	4.1
12/20	93.7	94.8	95.2	95.5	92.4	94.2	95.2	94.7	1.3	0.6	0.0	0.8
12/16/20	94.7	95.6	95.3	95.7	92.7	93.8	94.7	94.9	2.0	1.8	0.6	0.9
9/12/16/20	94.8	95.6	95.5	95.7	87.7	93.7	94.4	94.0	7.0	1.8	1.1	1.8
<i>Parotid</i>												
12	85.2	94.3	95.8	95.1	57.8	77.3	74.4	81.3	27.3	16.9	21.4	13.9
9/12	88.3	95.4	96.0	95.6	80.9	86.4	85.8	89.3	7.4	9.0	10.3	6.3
9/12/16	88.4	95.7	96.2	96.1	84.1	91.2	91.1	91.9	4.3	4.5	5.1	4.2
6/9/12/16	88.4	95.9	96.4	96.2	83.0	88.5	89.1	91.6	5.4	7.4	7.3	4.6

Table 2. For each case, relevant dosimetric parameters to the relevant OAR are shown for the final plans considering all intensity/energy levels.

Energies [MeV]	Intensity level				Intensity level				Intensity level				
	1	2	3	4	1	2	3	4	1	2	3	4	
Breast	Lungs				Lungs				Lungs				
	V5 Gy [%]				V20 Gy [%]				V30 Gy [%]				
	9	25.1	25.1	25.2	25.3	14.1	14.0	14.0	14.1	6.9	6.6	6.6	6.6
	4/9	25.3	25.4	25.5	25.4	14.0	14.3	14.3	14.2	6.6	6.9	6.9	6.9
	4/9/12	29.8	29.8	29.3	29.0	15.9	15.7	15.8	15.6	7.9	7.8	7.8	7.9
4/6/9/12	30.6	30.3	30.0	30.0	14.8	15.2	14.8	14.9	6.9	7.2	7.1	7.1	
Skin	Lungs				Spinal cord								
	V5 Gy [%]				Max dose [Gy]								
	12	1.1	1.0	1.1	1.1	1.5	1.5	1.5	1.5				
	6/12	0.4	0.5	0.5	0.5	2.3	2.1	2.3	2.3				
	6/12/16	4.5	4.4	4.7	4.8	6.6	6.3	7.0	7.5				
6/9/12/16	4.5	4.6	4.0	4.3	7.5	6.8	6.6	6.8					
Larynx	Spinal cord				Submandibular glands				Pharynx				
	Max dose [Gy]				Mean dose [Gy]				Mean dose [Gy]				
	20	29.1	26.4	27.0	27.5	5.4	5.4	5.3	5.1	4.2	4.1	4.0	4.0
	12/20	24.2	23.7	24.4	24.5	5.1	4.9	4.9	4.9	4.4	4.4	4.2	4.2
	12/16/20	25.0	25.4	25.5	25.4	5.0	4.9	4.9	4.8	4.4	4.3	4.3	4.3
9/12/16/20	25.3	25.7	24.9	25.0	5.0	4.8	4.9	4.8	4.4	4.3	4.3	4.3	
Parotid	Spinal cord				Inner ear				Brain				
	Max dose [Gy]				Mean dose [Gy]				Mean dose [Gy]				
	12	4.0	4.0	4.0	4.0	19.7	18.9	19.4	19.2	2.8	2.8	2.8	2.7
	9/12	3.2	3.4	3.1	3.5	15.3	15.6	16.1	16.1	2.2	2.4	2.3	2.3
	9/12/16	4.3	4.0	3.9	4.1	16.6	15.9	15.7	15.4	2.9	2.8	2.7	2.8
6/9/12/16	4.3	4.2	4.1	3.9	14.8	16.5	16.0	16.1	2.8	2.9	2.8	2.7	

For different levels of energy modulation, the optimal energy combinations for each case according to figure 2 were: 9 MeV, 4/9 MeV, 4/9/12 MeV, 4/6/9/12 MeV for the breast case, 12 MeV, 6/12 MeV, 6/12/16 MeV, 6/9/12/16 MeV for the skin case, 20 MeV, 12/20 MeV, 12/16/20 MeV, 9/12/16/20 MeV for the larynx case and 12 MeV, 9/12 MeV, 9/12/16 MeV, 6/9/12/16 MeV for the parotid case. For each optimal energy combination, final plans were calculated for all four different intensity levels. Dosimetric quantities for the PTV and relevant OAR are shown in tables 1 and 2.

Figure 3 shows the effect of intensity modulation on the DVH for monoenergetic plans (no energy modulation) and the effect of energy modulation on the DVH for single intensity plans (no intensity modulation). Figure 4 shows the DVH of the best plan for each case determined by the highest HI in the PTV.

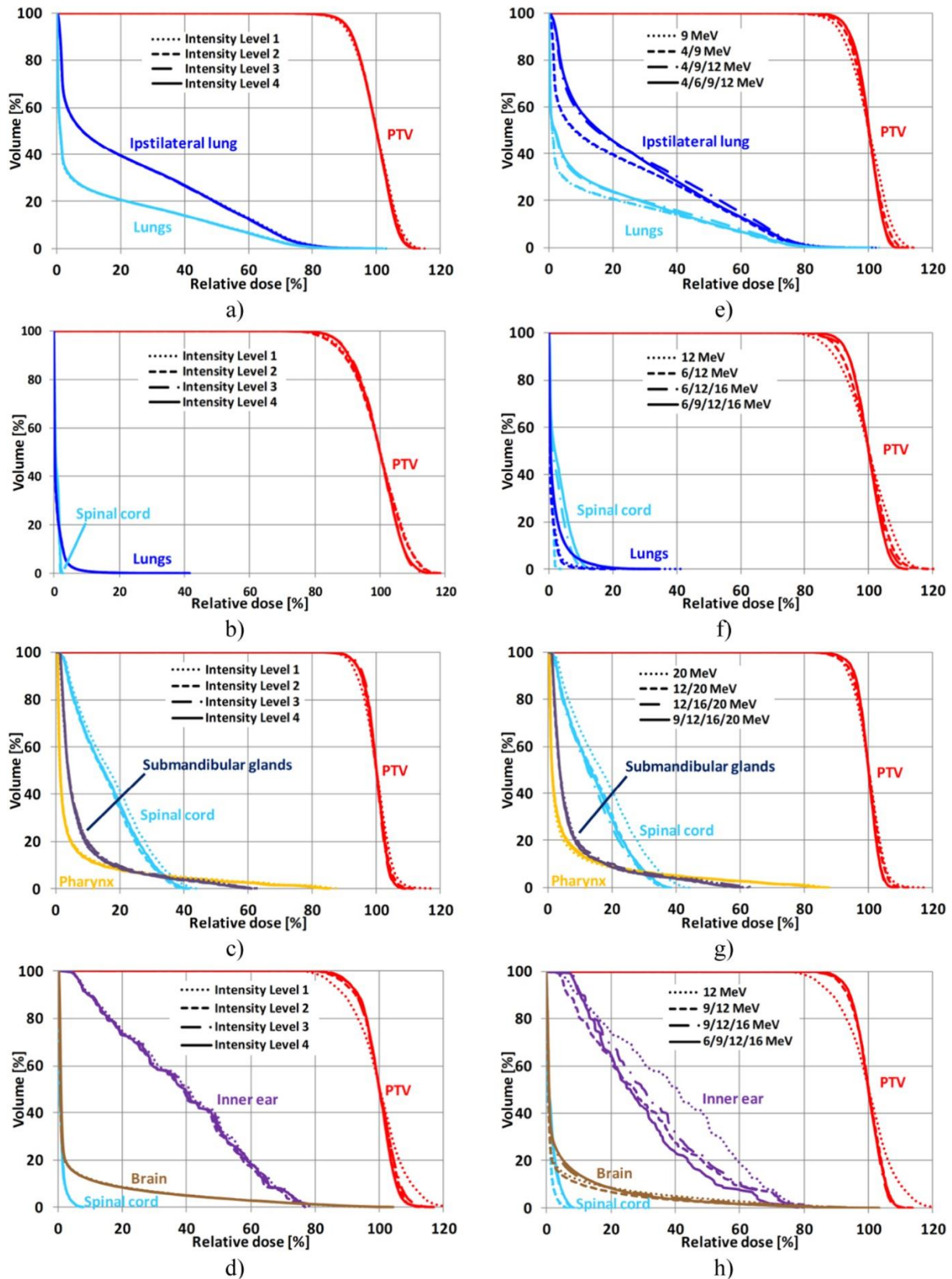


Figure 3. DVH comparison of different intensity levels for monoenergetic plans of the (a) breast with 9 MeV (b) skin with 12 MeV (c) larynx with 20 MeV (d) parotid with 12 MeV and different levels of energy modulation for a single intensity level for the (e) breast (f) skin (g) larynx (h) parotid cases.

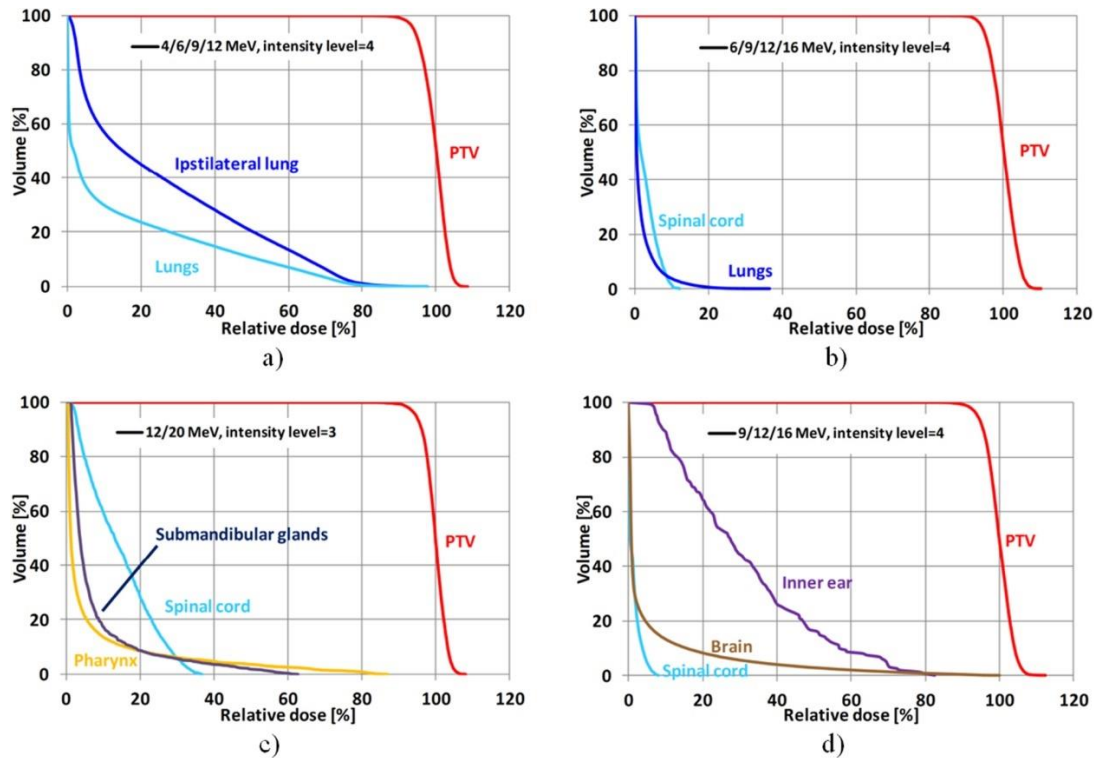


Figure 4. DVH of the best plans for the following cases: (a) breast (b) skin (c) larynx (d) parotid.

As can be seen from table 2 and figures 3(a)–(d), intensity modulation had overall negligible influence on the dose distribution in OAR. In contrast, energy modulation had a bigger influence on the dose distributions in OAR: using more than a single energy, the mean dose to the inner ear for the parotid case and the max dose to the spinal cord for the larynx case could be decreased by 3–5 Gy. Conversely, the inclusion of higher energies such as the 12 MeV for the breast case and the 16 MeV for the skin case resulted in higher doses to the lungs (and spinal cord for the skin case as well) compared to the plans using only one or two energies. This was however not visible in the total cost function value as the increase of the cost function values associated to these OAR was counterbalanced by the decrease of the cost function value associated to the PTV resulting in a higher HI in the PTV (see table 1). Both energy and intensity modulation improved the dose homogeneity in the PTV for the final plans overall (table 1). The improvement of the HI in the PTV with different levels of energy and intensity modulation was less emphasized for the optimal plans as it was for the final plans. This was due to the more pronounced degradation of the dose homogeneity in the PTV for the final plan compared to the optimal plan when few levels of energy and intensity

modulation were considered (table 1). The worsening of the dose homogeneity in the PTV for the final plan was particularly pronounced for the parotid case using only one energy and one intensity level ($\Delta\text{HI} = 27.3\%$) or for the skin case using only one or two energies resulting with ΔHI as high as 21.6%. Figure 5(a) shows for each case that ΔCF decreased with more initial apertures and therefore with more energy and intensity levels. The analysis of ΔCF into its various components shows that this difference was strongly dominated by the difference in cost function values associated to the PTV constraints between optimal and final plans (data not shown). Using at least 40 initial apertures for a plan, we found for all cases ΔCF to be inferior to 1000, which resulted into a ΔHI inferior to 7.5%. Figure 5(b) shows a strong correlation between ΔCF and ΔHI . The two largest values of ΔCF were found for monoenergetic plans of the parotid and skin using one and two intensity levels, respectively. For both cases, a comparison of the hot and cold spot areas in the PTV for the optimal and final plans is displayed in figures 5(c)–(f).

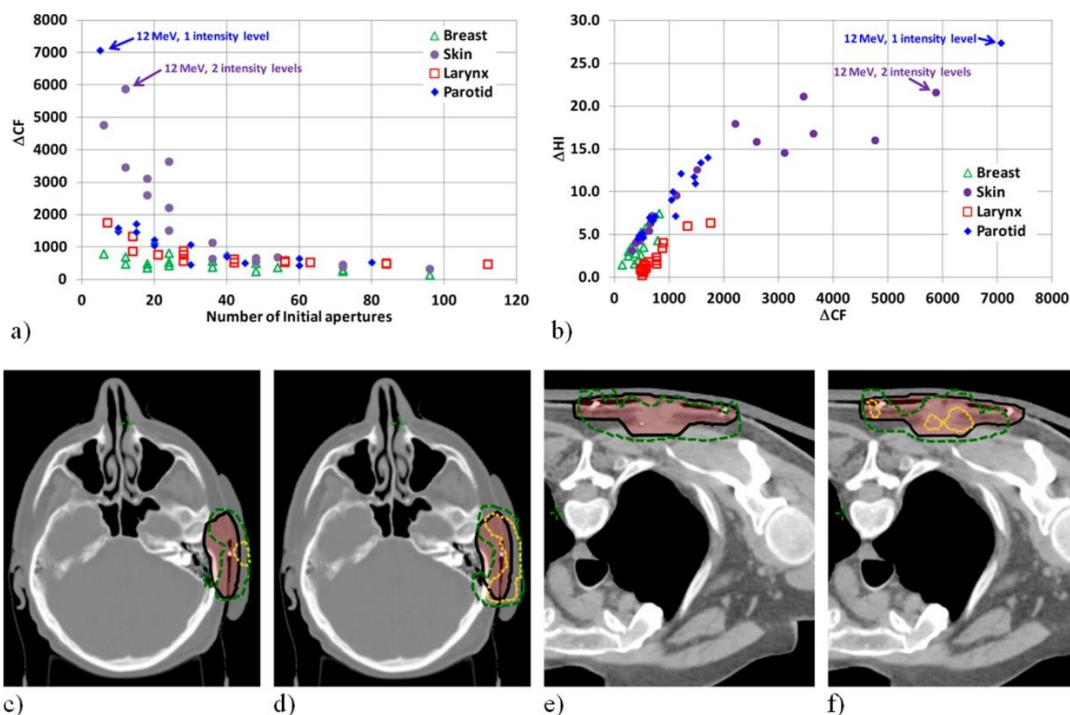


Figure 5. (a) ΔCF is shown as function of number of initial apertures for all cases (b) ΔHI is shown as a function of ΔCF . For the parotid plan showing the largest ΔCF marked by an arrow on (a), the 95% (green dashed lines) and 107% (orange dotted lines) isodoses are shown for the (c) optimal plan (d) final plan. The corresponding DVH for the final plan can be seen in either figures 3(d) or (h). Similarly for the largest ΔCF of the skin plan, the isodose contours are compared for the (e) optimal plan (f) final plan. The corresponding DVH for the final plan can be seen in figure 3(b).

4. Discussion

In this study, we investigated the effect of different levels of energy and intensity modulation of multi-field MERT on the dosimetric characterization for breast, skin, larynx and parotid tumors.

Considering four different energies for each case, we determined the best combinations of one, two, three and four different energies resulting in the lowest final cost function values. For the following discussion, we will call the selected energy resulting into the best monoenergetic plan for each case the primary energy. For all cases, we found that the best combination of two energies consisted of the primary energy and a lower energy which we will call the secondary energy. The best combination of three energies consisted of the primary and secondary energies and a third energy higher than the primary energy (if available). For the cases investigated in this work, energy modulation improved the dose homogeneity in the PTV and could either decrease or increase the dose to OAR depending on the energy selection. The dose increase in OAR was observed when an additional higher energy was included compared to the energies selected for the monoenergetic or dual energies plans. The best sparing of OAR overall was found for the dual energies plans consisting of the primary energy and a lower secondary energy. To achieve a HI of at least 90% in the PTV for the final plans, the minimal number of different energies required was four for the breast case, three for the skin and parotid cases and one for the larynx case. Finding the most suitable energy combination without trial-and-error is challenging. As some previous investigators selected energies according to the 90% isodose depth R90 of a beam matching the distal depth of the PTV (Klein 1998, Olofsson *et al* 2004), we looked if the primary energy corresponded to the energy required to cover the median distal depth of the PTV using the R90 of the different fields assuming a 5×5 cm² field size, but we didn't find a clear correlation. As already mentioned by Olofsson *et al* (Olofsson *et al* 2004), the range of electrons varies with field size, which is unknown at the time of optimization. Additionally, in our case we had multiple overlapping fields and therefore different parts of the distal fall-off of the electron fields might be used to cover the PTV appropriately. This was particularly obvious for the larynx case, where some of the fields

were nearly opposing and therefore the 50% isodose depth of these fields could be used to cover the PTV appropriately.

In contrast to energy modulation, intensity modulation had negligible effects on the dose distributions in OAR. However, for a given combination of energies, increased intensity modulation improved the HI in the PTV for the final plans. The effect of different intensity levels on the HI for the optimized plans was not as pronounced as for the final plans and using more than two intensity levels did not lead to a substantial improvement of the HI in the PTV. These results are in accordance with previous research showing that two intensity levels per energy were sufficient (Jin *et al* 2008). The apparent inconsistent influence of varying intensity levels on the HI of the PTV for optimized and final plans could be attributed to the differential worsening of the final plan (compared to the optimized plan) as a function of number of apertures. In sharp contrast with Jin *et al*'s study, who found improved dose uniformity in the PTV for the final plans compared to the optimal plans (Jin *et al* 2008), in our study the final plans were always worse than the optimized plans and the magnitude of the worsening was inversely correlated with the number of initial apertures and therefore the number of intensity levels. For plans consisting of many apertures, the differences between optimized and final plans could be reduced to a reasonable level as the many available MLC-delivered apertures allow for more degrees of freedom to satisfy the dose constraints during weight reoptimization for the final plans. Using at least 40 initial apertures, the absolute difference in the HI between optimized and final plans was always less than 7.5%. When three energies were selected, an intensity level of two or three was then sufficient to achieve a good plan.

One limitation of the study was that only one case per treatment site was studied. However, as the results from different sites show the same patterns with increasing level of energy and intensity modulation, it can be reasonably assumed that the same patterns apply for different cases of a specific treatment site. Another limitation of this study is that the results were based on the DAO algorithm. Other optimization algorithms might give slightly different results, however we expect to see the same overall trends with energy and intensity modulation.

5. Conclusion

In this work, we investigated the impact of different levels of energy and intensity modulation on the dosimetric characteristics of MERT plans of the breast, skin, parotid and larynx. Energy modulation had overall a larger impact on dosimetric characteristics of the final plans regarding dose homogeneity in the PTV and OAR sparing compared to intensity modulation. For most cases, at least three energies were required to obtain adequate dose homogeneity in the PTV and OAR sparing. Intensity modulation had negligible effects on OAR sparing for both optimal and final plans and dose homogeneity in the PTV for the optimal plans; however, for the final plan the dose homogeneity in the PTV improved with more intensity levels due to decreasing discrepancies between optimized and final plans using more apertures.

Acknowledgments

This work was supported by the Swiss Cancer League & Foundation Cancer Research Switzerland grant KFS-3279-08-2013.

ORCID iDs

A Joosten <https://orcid.org/0000-0002-7641-0044>

References

- Al-Yahya K, Hristov D, Verhaegen F and Seuntjens J 2005a Monte Carlo based modulated electron beam treatment planning using a few-leaf electron collimator—feasibility study *Phys. Med. Biol.* **50** 847–57
- Al-Yahya K, Schwartz M, Shenouda G, Verhaegen F, Freeman C and Seuntjens J 2005b Energy modulated electron therapy using a few leaf electron collimator in combination with IMRT and 3D-CRT: Monte Carlo-based planning and dosimetric evaluation *Med. Phys.* **32** 2976–86
- Al-Yahya K, Verhaegen F and Seuntjens J 2007 Design and dosimetry of a few leaf electron collimator for energy modulated electron therapy *Med. Phys.* **34** 4782–91
- Alexander A, DeBlois F and Seuntjens J 2010 Toward automatic field selection and planning using Monte Carlo-based direct aperture optimization in modulated electron radiotherapy *Phys. Med. Biol.* **55** 4563–76
- Alexander A, Soisson E, Hijal T, Sarfehnia A and Seuntjens J 2011 Comparison of modulated electron radiotherapy to conventional electron boost irradiation and volumetric modulated photon arc therapy for treatment of tumour bed boost in breast cancer *Radiother. Oncol.* **100** 253–8
- Alexander A, Soisson E, Renaud M A and Seuntjens J 2012 Direct aperture optimization for FLEC-based MERT and its application in mixed beam radiotherapy *Med. Phys.* **39** 4820–31
- du Plessis F C, Leal A, Stathakis S, Xiong W and Ma C M 2006 Characterization of megavoltage electron beams delivered through a photon multi-leaf collimator (pMLC) *Phys. Med. Biol.* **51** 2113–29
- Fix M K, Cygler J, Frei D, Volken W, Neuenschwander H, Born E J and Manser P 2013 Generalized eMC implementation for Monte Carlo dose calculation of electron beams from different machine types *Phys. Med. Biol.* **58** 2841–59
- Gauer T, Albers D, Cremers F, Harmansa R, Pellegrini R and Schmidt R 2006 Design of a computer-controlled multileaf collimator for advanced electron radiotherapy *Phys. Med. Biol.* **51** 5987–6003

- Gauer T, Engel K, Kiesel A, Albers D and Rades D 2010 Comparison of electron IMRT to helical photon IMRT and conventional photon irradiation for treatment of breast and chest wall tumours *Radiother. Oncol.* **94** 313–8
- Henzen D *et al* 2014a Beamlet based direct aperture optimization for MERT using a photon MLC *Med. Phys.* **41** 121711
- Henzen D, Manser P, Frei D, Volken W, Neuenschwander H, Born E J, Lossl K, Aebbersold D M, Stampanoni M F and Fix M K 2014b Forward treatment planning for modulated electron radiotherapy (MERT) employing Monte Carlo methods *Med. Phys.* **41** 031712
- Henzen D, Manser P, Frei D, Volken W, Neuenschwander H, Born E J, Vetterli D, Chatelain C, Stampanoni M F and Fix M K 2014c Monte Carlo based beam model using a photon MLC for modulated electron radiotherapy *Med. Phys.* **41** 021714
- Jin L *et al* 2008 Dosimetric verification of modulated electron radiotherapy delivered using a photon multileaf collimator for intact breasts *Phys. Med. Biol.* **53** 6009–25
- Kawrakow I and Walters B R 2006 Efficient photon beam dose calculations using DOSXYZnrc with BEAMnrc *Med. Phys.* **33** 3046–56
- Klein E E 1998 Modulated electron beams using multi-segmented multileaf collimation *Radiother. Oncol.* **48** 307–11
- Klein E E, Vicic M, Ma C M, Low D A and Drzymala R E 2008 Validation of calculations for electrons modulated with conventional photon multileaf collimators *Phys. Med. Biol.* **53** 1183–208
- Klein E E, Mamalui-Hunter M and Low D A 2009 Delivery of modulated electron beams with conventional photon multileaf collimators *Phys. Med. Biol.* **54** 327–39
- Lee M C, Deng J, Li J, Jiang S B and Ma C M 2001 Monte Carlo based treatment planning for modulated electron beam radiation therapy *Phys. Med. Biol.* **46** 2177-99
- Ma C M, Pawlicki T, Lee M C, Jiang S B, Li J S, Deng J, Yi B, Mok E and Boyer A L 2000 Energy- and intensity-modulated electron beams for radiotherapy *Phys. Med. Biol.* **45** 2293–311
- Ma C M, Ding M, Li J S, Lee M C, Pawlicki T and Deng J 2003 A comparative dosimetric study on tangential photon beams, intensity-modulated radiation therapy

- (IMRT) and modulated electron radiotherapy (MERT) for breast cancer treatment *Phys. Med. Biol.* **48** 909–24
- Neuenschwander H, Mackie T R and Reckwerdt P J 1995 MMC—a high-performance Monte Carlo code for electron beam treatment planning *Phys. Med. Biol.* **40** 543–74
- Olofsson L, Mu X, Nill S, Oelfke U, Zackrisson B and Karlsson M 2004 Intensity modulated radiation therapy with electrons using algorithm based energy/range selection methods *Radiother. Oncol.* **73** 223–31
- Palma B A, Sanchez A U, Salguero F J, Arrans R, Sanchez C M, Zurita A W, Hermida M I and Leal A 2012 Combined modulated electron and photon beams planned by a Monte-Carlo-based optimization procedure for accelerated partial breast irradiation *Phys. Med. Biol.* **57** 1191–202
- Rodrigues A, Yin F F and Wu Q 2014 Dynamic electron arc radiotherapy (DEAR): a feasibility study *Phys. Med. Biol.* **59** 327–45
- Salguero F J, Palma B, Arrans R, Rosello J and Leal A 2009 Modulated electron radiotherapy treatment planning using a photon multileaf collimator for post-mastectomized chest walls *Radiother. Oncol.* **93** 625–32
- Salguero F J, Arrans R, Palma B A and Leal A 2010 Intensity- and energy-modulated electron radiotherapy by means of an xMLC for head and neck shallow tumors *Phys. Med. Biol.* **55** 1413–27
- Shepard D M, Earl M A, Li X A, Naqvi S and Yu C 2002 Direct aperture optimization: a turnkey solution for step-and-shoot IMRT *Med. Phys.* **29** 1007–18
- Surucu M, Klein E E, Mamalui-Hunter M, Mansur D B and Low D A 2010 Planning tools for modulated electron radiotherapy *Med. Phys.* **37** 2215–24
- Zackrisson B and Karlsson M 1996 Matching of electron beams for conformal therapy of target volumes at moderate depths *Radiother. Oncol.* **39** 261–70

Supplementary data

Simulated annealing algorithm and dose-volume constraints

The optimizer randomly selects an aperture and then selects whether to change the weight or the shape of the aperture with a 90% probability to select a shape change. Weight and shape changes are sampled from Gaussian distributions and are accepted if they lower the cost function value. The width of the Gaussians decreases with each accepted iteration based on schedules defined by Shephard *et al.* (Shepard *et al.*, 2002). The width of the Gaussian for shape changes σ_S decreases with each accepted iteration according to the following formula:

$$\sigma_S = 1 + (\sigma_{S0} - 1) \cdot e^{-\frac{\log(\frac{n_S}{N_L} + 1)}{T_S}}$$

where σ_{S0} is the initial aperture change in units of number of beamlets, n_S is the number of accepted shape changes leading to a lower cost function value, N_L is the total number of leaf pairs over all apertures and T_S is the cooling rate for σ_S .

Similarly, for weight changes we have used:

$$\sigma_W = 0.01 + (\sigma_{W0} - 0.01) \cdot e^{-\frac{\log(\frac{n_W}{N_A} + 1)}{T_W}}$$

where σ_{W0} is the initial weight change, n_W is the number of accepted weight changes leading to a lower cost function value, N_A is the total number of apertures and T_W is the cooling rate for σ_W .

Finally, some changes resulting in a higher cost function value are accepted with a probability P , which decreases with the total number of accepted iterations according to:

$$P = 2 \cdot P_0 \cdot \frac{1}{1 + e^{\frac{\log(\frac{n_W + n_S}{N_A} + 1)}{T_P}}}$$

where P_0 is the initial probability to accept a change resulting in a higher cost function value and T_P is the cooling rate of P . In contrast to the cooling schemes used in the original DAO version (Henzen *et al.*, 2014) and in Shephard *et al.*'s work (Shepard *et*

al., 2002), the cooling rates now depend on the number of apertures or leaf pairs of the plan to be optimized; these modifications allow to select the parameters independently of the number of initial apertures and the number of leaf pairs per aperture. The following sets of parameters were used for all optimizations: $\sigma_{S0}=40$, $T_S=2$, $\sigma_{W0}=0.5$, $T_W=3$, $P_0=3.5\%$, $T_P=3$.

The structures used for the optimization were the PTV, the relevant OARs as well as avoidance structures. Avoidance structures were placed laterally, distally or cranially/caudally from the PTV edge to avoid the opening of leaves outside of the PTV projection. The following table lists all dose-volume constraints used for the DAO optimization of each plan:

Case	Organ	Type of limit	Priority	Dose [%]	Volume [%]
Breast	PTV	Upper	150	102	0
	PTV	Lower	250	98	100
	Lung (ipsilateral)	Upper	100	80	0
	Lung (ipsilateral)	Upper	100	60	10
	Lung (ipsilateral)	Upper	100	40	25
	Lung (ipsilateral)	Upper	100	10	50
	Avoidance	Upper	150	85	0
Skin	PTV	Upper	150	102	0
	PTV	Lower	250	98	100
	Spinal cord	Upper	150	10	0
	Lung (subvolume)	Upper	150	30	0
	Lung (subvolume)	Upper	150	10	40
	Avoidance 1	Upper	150	90	10
	Avoidance 1	Upper	150	80	30
Larynx	Avoidance 2	Upper	150	10	5
	PTV	Upper	150	102	0
	PTV	Lower	250	98	100
	Spinal cord	Upper	100	30	0
	Spinal cord	Upper	100	10	50
	Pharynx	Upper	50	60	0
	Pharynx	Upper	100	10	10
Parotid	Submandibular (left)	Upper	50	50	0
	Submandibular (left)	Upper	100	10	10
	Submandibular (right)	Upper	50	50	0
	Submandibular (right)	Upper	100	10	10
	Avoidance	Upper	50	90	0
	PTV	Upper	150	102	0
	PTV	Lower	250	98	100
Parotid	Inner ear	Upper	150	70	10
	Inner ear	Upper	100	40	30
	Inner ear	Upper	100	20	60
	Spinal cord	Upper	150	5	0
	Eye (ipsilateral)	Upper	150	5	0
	Avoidance 1	Upper	150	105	0
	Avoidance 1	Upper	150	80	30
	Avoidance 2	Upper	150	80	0
	Avoidance 2	Upper	150	10	50
	Avoidance 3	Upper	150	80	0
	Avoidance 3	Upper	150	10	50

References

- Henzen D, Manser P, Frei D, Volken W, Neuenschwander H, Born E J, Joosten A, Lossl K, Aebbersold D M, Chatelain C, Stampanoni M F and Fix M K 2014 Beamlet based direct aperture optimization for MERT using a photon MLC *Med. Phys.* **41** 121711
- Shepard D M, Earl M A, Li X A, Naqvi S and Yu C 2002 Direct aperture optimization: a turnkey solution for step-and-shoot IMRT *Med. Phys.* **29** 1007-18

4

Simultaneous optimization of photons and electrons for mixed beam radiotherapy

**S. Mueller¹, M.K. Fix¹, A. Joosten¹, D. Henzen¹, D. Frei¹, W. Volken¹,
R. Kueng¹, D.M. Aebersold¹, M.F.M. Stampanoni² and P. Manser¹**

- 1: Division of Medical Radiation Physics and Department of Radiation Oncology, Inselspital, Bern University Hospital, and University of Bern, Bern, Switzerland
- 2: Institute for Biomedical Engineering, ETH Zürich and PSI, Villigen, Switzerland

published in

Physics in Medicine & Biology

2017, Vol. 62, 5840–5860

<https://doi.org/10.1088/1361-6560/aa70c5>

© Institute of Physics and Engineering in Medicine.
Reproduced with permission. All rights reserved.

Abstract

The aim of this work is to develop and investigate an inverse treatment planning process (TPP) for mixed beam radiotherapy (MBRT) capable of performing simultaneous optimization of photon and electron apertures.

A simulated annealing based direct aperture optimization (DAO) is implemented to perform simultaneous optimization of photon and electron apertures, both shaped with the photon multileaf collimator (pMLC). Validated beam models are used as input for Monte Carlo dose calculations. Consideration of photon pMLC transmission during DAO and a weight re-optimization of the apertures after deliverable dose calculation are utilized to efficiently reduce the differences between optimized and deliverable dose distributions. The TPP for MBRT is evaluated for an academic situation with a superficial and an enlarged PTV in the depth, a left chest wall case including the internal mammary chain and a squamous cell carcinoma case. Deliverable dose distributions of MBRT plans are compared to those of modulated electron radiotherapy (MERT), photon IMRT and if available to those of clinical VMAT plans.

The generated MBRT plans dosimetrically outperform the MERT, photon IMRT and VMAT plans for all investigated situations. For the clinical cases of the left chest wall and the squamous cell carcinoma, the MBRT plans cover the PTV similarly or more homogeneously than the VMAT plans, while OARs are spared considerably better with average reductions of the mean dose to parallel OARs and $D_{2\%}$ to serial OARs by 54% and 26%, respectively. Moreover, the low dose bath expressed as $V_{10\%}$ to normal tissue is substantially reduced by up to 45% compared to the VMAT plans.

A TPP for MBRT including simultaneous optimization is successfully implemented and the dosimetric superiority of MBRT plans over MERT, photon IMRT and VMAT plans is demonstrated for academic and clinical situations including superficial targets with and without deep-seated part.

Keywords: mixed beam radiotherapy, simultaneous optimization, direct aperture optimization, Monte Carlo

1. Introduction

Electron beams are well suited to treat superficial targets, while sparing organs at risk (OARs) due to their sharp distal dose fall-off in tissue. Nowadays, electron radiotherapy is still based on cumbersome and inefficient delivery methods, where patient-individually molded cut-outs are needed in order to shape the dose to the target. To overcome this limitation and to exploit intensity and energy modulation for improved plan quality, some research groups investigated several approaches for modulated electron radiotherapy (MERT) using different motorized multileaf collimators. The collimation devices applied were a few leaf electron collimator (FLEC) (Al-Yahya *et al* 2005, 2007, Alexander *et al* 2010, 2012), an electron multileaf collimator (eMLC) (Gauer *et al* 2008, Vatanen *et al* 2009, Jin *et al* 2014) or a photon multileaf collimator (pMLC) (du Plessis *et al* 2006, Jin *et al* 2008, Klein *et al* 2009, Salguero *et al* 2009, 2010, Surucu *et al* 2010, Henzen *et al* 2014a, 2014b). However, there are some dosimetric limitations of applying MERT: Firstly, due to the broad penumbra of electron beams, OARs located nearby to the target in lateral direction with respect to beam direction cannot be spared adequately. Secondly, the dose cannot be delivered homogeneously to targets with a part located deeper than 5 cm from the surface (called deep-seated part), because the range delivering 95% of the maximal dose of the beam with highest energy supported by conventional treatment units (typically 22 MeV) is insufficient, especially for smaller field sizes.

Photon beams have a completely different characteristics than electron beams with their steep penumbra and exponential dose fall-off. With the most advanced techniques like photon intensity modulated radiation therapy (IMRT) (Bortfeld 2006) and volumetric modulated arc therapy (VMAT) (Otto 2008), photon beams can be delivered conformal to the target and thus nearby OARs are spared efficiently. However, in contrast to electron beams, low doses are delivered over a large volume of normal tissue, also known as the low dose bath.

Given the different characteristics of photons and electrons, mixed beam radiotherapy (MBRT) promises high potential by combining the advantageous properties of both particle types for treating superficial tumor sites possibly with a deep-

seated part. Finding the optimal contribution of photon and electron dose distributions during the treatment planning process (TPP) and delivering both types of beams in a convenient manner for the same treatment are two of the major challenges for MBRT. Optimizing photon and electron apertures simultaneously is desirable compared to sequentially, because then the freedom of exploiting intensity and energy modulation and the choice between different beam directions and particle types is given within one single process.

Several approaches for optimization and delivery were already investigated for MBRT (Li *et al* 2000, Mu *et al* 2004, Xiong *et al* 2004, Al-Yahya *et al* 2005, Surucu *et al* 2010, Ge and Faddegon 2011, Rosca 2012, Alexander *et al* 2012, Palma *et al* 2012). To our best knowledge, only Xiong *et al* (2004), Alexander *et al* (2012) and Palma *et al* (2012) utilized some kind of simultaneous optimization. For whole breast treatments including boost, Xiong *et al* (2004) compared five different MBRT techniques. In the most sophisticated technique, two intensity modulated photon beams were combined with an intensity modulated electron beam. The eMLC shaped electron beam is set up with the intention to deliver the dose to the boost volume. A fluence map optimization (FMO) was used to simultaneously optimize the intensity maps of the photon and electron beams using a gradient search method. Subsequently, a leaf sequencing algorithm was used to translate the intensity maps into deliverable segments. With the comparison of five different techniques for MBRT, it was underlined that simultaneously optimized MBRT plans achieved improved plan quality compared to sequentially optimized MBRT plans. Alexander *et al* (2012) developed a TPP for MERT using a FLEC for collimation. A direct aperture optimization (DAO) (Shepard *et al* 2002) was used to obtain a MERT plan for a squamous case with a superficial target. Subsequently, a gradient optimization algorithm further simultaneously optimized the weights of the electron FLEC apertures of the MERT plan with the weights of $1 \times 1 \text{ cm}^2$ photon beamlets to obtain an MBRT plan. The MBRT plan was superior to a photon IMRT plan in terms of dose homogeneity in the PTV and sparing of OARs. However, a post processing fluence map segmentation was not performed for the MBRT plan in their study and the electron FLEC apertures were fixed in their shape during FMO. For three cases of partial breast irradiations, Palma *et al* (2012) simultaneously optimized

photon and electron beamlets with an FMO. The fluence maps were subsequently sequenced to deliverable pMLC segments for the use on a Siemens Primus. The MBRT plans showed similar dose homogeneity and improved sparing of OARs compared to photon IMRT plans.

The pMLC is already part of conventional accelerator treatment heads, while FLEC and eMLC devices have to be mounted and unmounted from the applicator. Hence, the approach used by Palma *et al* (2012) is the most convenient regarding delivery and treatment workflow, because both beam types are collimated with the pMLC without applicator. However, their work focuses only on MBRT plans determined for partial breast irradiations in comparison to photon IMRT plans. Thus, the potential of MBRT with simultaneous optimization of pMLC shaped apertures determined for other treatment sites, especially to targets with a deep-seated part remains unknown. Moreover, using a FMO and subsequent leaf sequencing leads to a degradation of the optimized fluence map dose distributions. The alternative DAO directly optimizes the apertures and their weights under consideration of mechanical pMLC constraints and possibly pMLC transmission (Shepard *et al* 2002, Bergman *et al* 2006). Furthermore, DAO leads to fewer pMLC segments and less monitor units (MUs) and thus to shorter treatment times.

The aim of this work is to develop an MC beamlet based inverse TPP for MBRT performing simultaneous optimization of photon and electron apertures with a simulated annealing based DAO. The apertures are determined to be delivered in a segmented manner and collimated with the pMLC for both photon and electron beams. We demonstrate the dosimetric superiority of MBRT plans compared to MERT, photon IMRT and VMAT plans for academic and clinical situations including superficial targets with and without deep-seated part.

2. Materials and methods

An MC beamlet based inverse TPP for MERT previously developed by Henzen *et al* (2014a) is extended to generate treatment plans for MBRT. The extension is accompanied by the idea to handle the photon beams analogously to the electron beams in all aspects of the TPP. In the following subchapters, the TPP for MBRT, the MC simulations, the simultaneous optimization and the performed evaluations with an academic and two clinical situations are presented.

2.1. Treatment planning process for MBRT

The TPP for MBRT starts with the import of the CT images into a research version of the Eclipse treatment planning system (TPS) (Varian Medical Systems, Palo Alto, CA) and the contouring of the planning target volume (PTV) and the OARs. Next, the photon and electron fields are manually defined by the beam energy and direction and isocenter position. Preferentially, the isocenter of the photon fields is located in the PTV while for the electron fields the isocenter is positioned such that the source to surface distance (SSD) is reduced leading to a smaller penumbra (du Plessis *et al* 2006, Klein *et al* 2009). The settings of the secondary collimator jaws for the photon fields correspond to the respective PTV projection in the beams eye view with a margin of 0.6 cm. For the electron fields, the positions of the secondary collimator jaws are fixed to $15 \times 35 \text{ cm}^2$. Beamlet dose distributions are then calculated in the Eclipse TPS interfaced framework of the Swiss Monte Carlo Plan (SMCP) (Fix *et al* 2007) for every field based on pre patient phase spaces. To create these pre patient phase spaces, a beamlet grid is positioned on the mid-plane of the pMLC. Particles are transported through the treatment head and stored in the corresponding beamlet pre patient phase space. Once all beamlet dose distributions are calculated the following input needs to be defined to perform a simultaneous optimization of photon and electron apertures: the number of apertures per field and dose-volume objectives prioritized with factors. The output of the optimization are the optimized dose distribution, the aperture shapes and their absolute weights in MUs. Because the previous beamlet based optimization did not consider the pMLC impact like tongue- and groove effects and pMLC particle scattering

except pMLC transmission of photon beams, a dose prediction error (DPE) is present (Jeraj 2002). Hence, an MC deliverable dose calculation is then performed for every aperture in the SMCP framework considering the impact of the pMLC. The weights of the apertures are then re-optimized based on their deliverable dose distributions to reduce the DPE caused optimization convergence error (OCE) (Jeraj 2002, Dogan *et al* 2006, Mihaylov and Siebers 2008). Finally, the deliverable weight re-optimized dose distribution of the total plan is loaded back into the Eclipse TPS for plan evaluation.

2.2. Monte Carlo simulations

In this work, all MC dose calculations are performed for a TrueBeam (Varian Medical Systems, Palo Alto, CA) equipped with a Millennium 120 pMLC (Varian Medical Systems, Palo Alto, CA) using the VMC++ (Kawrakow and Fippel 2000) and the MMC (Neuenschwander and Born 1992, Neuenschwander *et al* 1995, Fix *et al* 2013) algorithms for photon and electron beams, respectively. For the inner leaf pairs of the pMLC, a beamlet grid resolution of $0.3 \times 0.5 \text{ cm}^2$ and $0.5 \times 0.5 \text{ cm}^2$ is used for the photon and electron fields, respectively. For the outer leaf pairs, the beamlet size perpendicular to leaf travel direction is 1 cm for both photon and electron fields corresponding to the doubled leaf width compared to the inner leaf pairs.

The beam model used as input for the MC simulation of a 6 MV photon beam is a phase space located above the secondary collimator jaws (Magaddino *et al* 2011). For validating the photon beam model for a TrueBeam accelerator, depth dose curves and dose profiles are measured with a microDiamond (PTW, Freiburg, Germany) detector in a MP3 water tank (PTW, Freiburg, Germany) in units of cGy/MU for several pMLC collimated field sizes of $1 \times 1 \text{ cm}^2$ and larger applied with an SSD of 100 cm. Corresponding dose calculations agree within 2% of the maximal dose value or 1 mm distance to agreement.

The input used for MC simulations of 6, 9, 12, 15, 18 and 22 MeV electron beams as available on the TrueBeam is a multiple source model consisting of foil and jaw sources for every beam energy (Henzen *et al* 2014c). The electron beam model is commissioned with microDiamond measurements for a TrueBeam accelerator. Calculated and measured depth dose curves and dose profiles in units of cGy/MU of

several pMLC collimated field sizes of $2 \times 2 \text{ cm}^2$ and larger collected with an SSD of 70 and 80 cm agree within 3% of the maximal dose value or 2 mm distance to agreement for all available beam energies. Supporting an SSD of up to 80 cm is highly appreciated to overcome field setups leading to patient or couch collisions with an SSD of 70 cm.

2.3. MBRT optimization

The optimization of photon and electron apertures is performed by a simulated annealing based DAO (Shepard *et al* 2002). Our object oriented C++ implementation of the DAO optimizes plans for MBRT, MERT and photon IMRT without any adjustment of the algorithm. The focus of the implementation is to guarantee smooth extendibility for future investigations like supporting other types of objectives, to support optimizations performed in parallel differing in the number of apertures per field and objective definitions and not primarily on minimal computation time.

pMLC transmission is considered during DAO for photon beams based on the work of Bergman *et al* (2006) but further extended with transmission factors increasing gradationally towards the leaf tip in direction of leaf travel. Transmission factors of 25.5%, 4.7% and 1.6% are used for the range of 0–0.3 cm, 0.3–0.9 cm and > 0.9 cm from the leaf tip (measured in the isocenter plane). The dose distributions of photon beamlets blocked by leafs are weighted according to these factors. These transmission factors are determined by comparing beamlet and deliverable dose distributions of a set of rectangular pMLC segments.

The DAO minimizes the value of an objective function iteratively by changing the shape or weights of the apertures according to a cooling schedule. The objective function used is a sum of squared differences between achieved and desired dose voxel deposits (Wu and Mohan 2000) given by

$$f = \sum_{k=1}^M p_k \sum_{i=1}^{N_k} \frac{\Theta(a_k(D_i - D_k)) \cdot \Theta(a_k(D(V_k) - D_i)) \cdot (D_i - D_k)^2}{N_k} \quad (1)$$

where D_i is the dose value in the i th voxel of the structure considered (PTV or an OAR), θ is the Heaviside function, p_k is the priority factor, D_k is the desired dose, $D(V_k)$ is the dose received by at least the tolerated volume V_k and N_k is the number of voxels to be

considered for the k th of in total M dose-volume objectives. a_k equals 1 for objectives penalizing dose values higher than D_k , otherwise -1 .

The number of apertures per field are user defined and can be determined by running several DAOs using different number of apertures per field until no more substantial improvements are achieved anymore. The initial shape of an aperture corresponds to the PTV projection in the beams eye view in the resolution of the beamlet grid of the corresponding field. The initial weight of an aperture, given in MUs, is set in two steps. First, each aperture weight is initialized with the inverse of the average of its ten largest dose voxel values in the PTV. This initial value guarantees equal initial conditions for apertures of different beam types and distances from the patient surface to the PTV and is less sensitive to statistical noise of the MC calculated dose distribution as compared to using the maximal dose. Afterwards all aperture weights of the plan are normalized such that 50% of the PTV receives a dose value of at least the prescribed dose.

In every DAO iteration of in total N iterations, an aperture gets selected randomly and with a probability of P_S its shape is changed, otherwise its weight. A change is always accepted if the objective function value decreases. If the objective function increases, the change is accepted with a probability of

$$P = 2 \cdot P_0 \cdot \frac{1}{1 + e^{\frac{\log\left(\frac{n_S+n_W}{N_A}+1\right)}{T_P}}} \quad (2)$$

where n_S and n_W are the previous total accepted shape and weight change iterations, respectively, N_A is the number of apertures and T_P and P_0 are the cooling rate and the initial value of P , respectively. In case of a shape change, a leaf is randomly selected and its position is randomly changed according to a normal distribution around the current leaf position and a width of

$$\sigma_S = 1 + (\sigma_{S0} - 1) \cdot e^{-\frac{\log\left(\frac{n_S}{N_L}+1\right)}{T_S}} \quad (3)$$

where N_L is the total number of leaf pairs of all apertures and T_S and σ_{S0} are the cooling rate and the initial width of the normal distribution, respectively. Both σ_S and σ_{S0} are given in discretized units of number of beamlets. Similar for a weight change, the weight is changed according to a normal distribution around the current aperture weight w and a width of

$$\sigma_W = 0.01 + (\sigma_{W0} - 0.01) \cdot e^{-\frac{\log\left(\frac{n_W}{N_A} + 1\right)}{T_W}} \quad (4)$$

where T_W and σ_{W0} are the cooling rate and the initial width of the normal distribution, respectively. Both σ_W and σ_{W0} are given in relative units of w . Adjusting the cooling formulas of Shepard *et al* (2002) to be dependent on N_A and N_L allows a more flexible usage for arbitrary number of apertures. In this work, the following parameter set is used: $N = 1000\ 000$, $P_S = 90\%$, $T_P = 3$, $P_O = 3.5\%$, $T_S = 2$, $\sigma_{S0} = 40$, $T_W = 3$, $\sigma_{W0} = 50\%$. To only perform a weight re-optimization, P_S is set to 0.

2.4. Academic situation

To systematically evaluate the TPP for MBRT in a simplified setup, an academic situation is defined with the following purposes:

1. To demonstrate that MBRT is not like MERT limited to deliver the dose homogenously to targets with a deep-seated part.
2. To evaluate whether the benefit of MBRT over photon IMRT decreases for a target with a deep-seated part compared to a target without.
3. To analyze the photon and electron contributions of MBRT plans.
4. To evaluate the reduction of the DPE after deliverable dose calculation and the reduction of the OCE after performing the weight re-optimization due to considering photon pMLC transmission.
5. To evaluate whether the drawback of photon IMRT compared to MBRT could be fully compensated by utilizing more photon apertures.

The academic situation consists of a cylindrical, homogenous water phantom with a radius of 10 cm and a length of 40 cm and includes contours of two PTVs (PTV-Superficial and PTV-Enlarged), two OARs (OAR-Distal and OAR-Lateral) and two Avoidance structures (figure 1 on the left). All mentioned structures have an extension of 7.4 cm in the direction perpendicular to the transversal plane. The PTV-Enlarged is an enlargement of the PTV-Superficial from a maximal depth from the surface of 5 cm to 7.5 cm. The Avoidance structures are 0.5 cm thick shells with a margin of 0.5 cm

around the PTV-Superficial and PTV-Enlarged, respectively. Their purpose is to avoid hot spots close to the corresponding PTV.

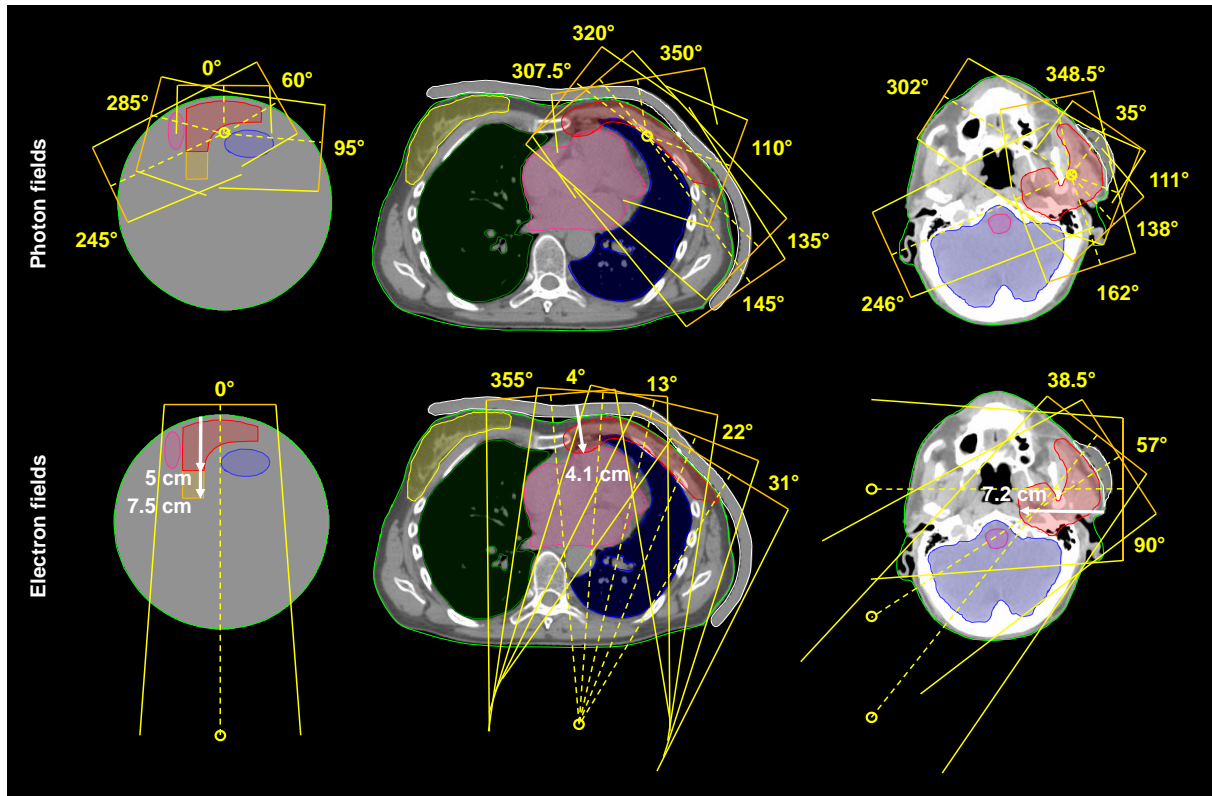


Figure 1. Photon (top) and electron (bottom) fields with their beam direction (dashed line), position of the isocenter (circle) and secondary collimator jaws (field width) displayed on transversal views for the academic situation (left), the chest wall case (center) and the squamous cell carcinoma case (right). The contours of the following structures are visible: PTV-Superficial (red), PTV-Enlarged (red and orange), OAR-Distal (blue), OAR-Lateral (magenta) and body (light green) for the academic situation, PTV (red), ipsilateral lung (blue), contralateral lung (green), contralateral breast (yellow), heart (magenta), body (light green) and bolus (white) for the chest wall case and PTV (red), brain (blue), brain stem (magenta), body (light green) and bolus (white) for the squamous cell carcinoma case. For each PTV, the deepest part with respect to all electron field directions is indicated with a white arrow.

For the first three purposes, plans for MBRT, MERT and photon IMRT, each with 40 apertures are generated using the presented TPP for both PTV contours. The photon and electron fields and the number of apertures per field of the created plans for MBRT, MERT and photon IMRT are listed in table 1 and visualized in figure 1 (left). The plans are compared by means of isodose lines, DVHs and the objective function value. For purpose four, the DVH differences between optimized, deliverable and deliverable weight re-optimized dose distributions of the MBRT plan are examined and compared

to another MBRT plan with the same number of apertures per field but optimized without consideration of photon pMLC transmission. The fractional DPE and OCE reductions achieved by considering the photon pMLC transmission during optimization are quantified by

$$\text{rDPE} = 1 - \text{DPE}^c / \text{DPE}^n = 1 - \frac{f_d^c - f_o^c}{f_d^n - f_o^n} \quad (5)$$

and

$$\text{rOCE} = 1 - \text{OCE}^c / \text{OCE}^n = 1 - \frac{f_w^c - f_o^c}{f_w^n - f_o^n} \quad (6)$$

where the superscripts *c* and *n* refer to as transmission considered and not considered during optimization, respectively and the subscripts *o*, *d* and *w* refer to as optimized, deliverable and deliverable weight re-optimized dose distributions, respectively. *f* is given by equation (1). Note that both rDPE and rOCE are only estimates assuming that a deliverable MC dose calculation is an accurate estimate for the actual dose delivered to the patient and that the objective function value of the truly optimal dose distribution optimized based on the most accurate dose calculation can be estimated with f_o^c . For purpose five, several MBRT and photon IMRT plans targeting the PTV-Enlarged are created with a number of apertures in the range of 15-75. In case of the MBRT plans, the number of electron apertures is thereby kept constant at 10. For all five purposes, every optimization of plans for MBRT, MERT and photon IMRT is performed using the same objectives listed in table 2. Thus, the objective function value is a useful quantity to compare the quality of plans for MBRT, MERT and photon IMRT.

Table 1. Photon and electron fields and the number of apertures per field used to create the coplanar MBRT, MERT and photon IMRT plans for the academic situation. The number of apertures per field is the same independent whether the plan is targeting the PTV-Superficial or the PTV-Enlarged.

Gantry		Number of apertures			
angle (°)	Beam	SSD (cm)	MERT	Photon IMRT	MBRT
0	6 MV	96.5	-	8	6
60	6 MV	95.0	-	8	6
95	6 MV	91.7	-	8	6
245	6 MV	89.3	-	8	6
285	6 MV	94.0	-	8	6
0	6, 9, 15, 18, 22 MeV	70.0	8, 8, 8, 8, 8	-	2, 2, 2, 2, 2

Table 2. The dose-volume objectives used for generating the MBRT, MERT and photon IMRT plans for the academic situation. The first two objectives listed are either applied to the PTV-Superficial or the PTV-Enlarged.

Structure	Objective			
	type	Priority factor	Dose (%)	Volume (%)
PTV-Superficial & PTV-Enlarged	Lower	35	98	100
	Upper	39	102	0
OAR-Distal	Upper	3	20	30
	Upper	6	60	0
OAR-Lateral	Upper	2	20	40
	Upper	4	35	25
	Upper	4	55	10
	Upper	4	75	0
Avoidance	Upper	4	90	0

2.5. Chest wall case

To evaluate the presented TPP for MBRT for a clinical case with a superficial target, an MBRT plan with 50 apertures is created for a left chest wall case including the internal mammary chain with a prescribed dose of 50 Gy determined to be delivered in 25 fractions. The MBRT plan is compared to plans for MERT and photon IMRT generated with the same TPP and the same number of apertures and its photon and electron

contributions are analyzed. The photon and electron fields and the number of apertures per field of the created plans for MBRT, MERT and photon IMRT are listed in table 3 and visualized in figure 1 (center). A clinical coplanar two-arc VMAT plan is also used for comparisons. The dose distribution of the VMAT plan is recalculated using VMC++ for comparison with the MC based MBRT, MERT and photon IMRT plans. Plan comparisons are performed by means of isodose lines, DVHs, the dose homogeneity in the PTV expressed as $HI = V_{95\%} - V_{107\%}$, D_{mean} to the OARs and the extent of the low dose bath expressed as $V_{10\%}$ of the normal tissue.

To evaluate whether MBRT can also be applied without using a bolus while keeping the treatment plan quality, another MBRT plan is created (MBRT-WOB) for the chest wall case. The resulting DVHs are compared to the MBRT plan created with bolus. Due to the change in the geometrical situation in the case without using a bolus, different number of apertures per field are used for the MBRT-WOB plan, however the total number of apertures is maintained (table 3).

Table 3. Photon and electron fields and the number of apertures per field used to create the coplanar MBRT, MERT and photon IMRT plans for the chest wall case.

Gantry angle (°)	Beam	SSD (cm)	Number of apertures			
			MERT	Photon IMRT	MBRT	MBRT-WOB
110	6 MV	93.7	-	9	5	5
135	6 MV	88	-	8	5	5
145	6 MV	86.1	-	8	5	5
307.5	6 MV	93.4	-	9	5	5
320	6 MV	94.7	-	8	5	5
350	6 MV	96.2	-	8	5	5
355	12, 15 MeV	73.4	4, 4	-	2, 2	2, 2
4	6, 9, 12, 15 MeV	73.3	0, 4, 4, 4	-	0, 0, 2, 2	1, 2, 1, 1
13	6, 9, 12, 15 MeV	73.3	0, 4, 4, 5	-	0, 2, 2, 2	2, 2, 2, 0
22	6, 9, 12 MeV	75.1	0, 4, 4	-	2, 2, 0	1, 1, 0
31	6, 9, 12 MeV	76.6	0, 5, 4	-	0, 2, 0	2, 1, 0

2.6. Squamous cell carcinoma case

An MBRT plan with 60 apertures is created for a squamous cell carcinoma case with a prescribed dose of 66 Gy determined to be delivered in 33 fractions to evaluate the presented TPP for MBRT for a clinical case with a superficial target including a deep-seated part. The MBRT plan is compared to plans for MERT and photon IMRT generated with the same TPP and the same number of apertures and its photon and electron contributions are analyzed. The photon and electron fields and the number of apertures per field of the created plans for MBRT, MERT and photon IMRT are listed in table 4 and visualized in figure 1 (right). A clinical non-coplanar five-arc VMAT plan is also used for comparisons. The dose distribution of the VMAT plan is recalculated using VMC++. The plan comparisons are performed by means of isodose lines, DVHs, HI in the PTV, D_{mean} and $D_{2\%}$ to parallel and serial OARs, respectively and $V_{10\%}$ of the normal tissue. $D_{2\%}$ is reported instead of the maximum dose as $D_{2\%}$ is clinically more relevant and less dependent on the statistical uncertainty of MC dose calculations (Gregoire and Mackie 2011).

Table 4. Photon and electron fields and the number of apertures per field used to create the coplanar MBRT, MERT and photon IMRT plans for the squamous cell carcinoma case.

Gantry		Number of apertures			
		Beam	SSD (cm)	Photon	
angle (°)	MERT			IMRT	MBRT
35	6 MV	95.9	-	10	6
111	6 MV	96.5	-	8	6
138	6 MV	95.6	-	8	6
162	6 MV	93.2	-	8	6
246	6 MV	84.7	-	8	6
302	6 MV	88.5	-	9	6
348.5	6 MV	94.5	-	9	6
38.5	6, 9, 12, 15, 18, 22 MeV	71	5, 1, 1, 1, 5, 6	-	0, 0, 3, 4, 4, 4
57	6, 9, 12, 15, 18, 22 MeV	76.6	1, 1, 1, 1, 5, 5	-	0, 0, 1, 0, 0, 0
90	6, 9, 12, 15, 18, 22 MeV	80.1	5, 5, 1, 5, 5, 6	-	1, 1, 0, 0, 0, 0

3. Results

The dose distributions of the MBRT, MERT and photon IMRT plans presented in this section are deliverable weight re-optimized if not stated otherwise. All treatment plans are normalized such that 50% of the PTV receives a dose value of at least the prescribed dose. A voxel size of $2.5 \times 2.5 \times 2.5 \text{ mm}^3$ is used for the dose calculations and dose values are reported to medium. All dose calculations in this work are performed in parallel on a Linux high-performance-computing cluster using 100 cores of Intel Xeon CPUs of type E5-2650 v2—2.60 GHz or similar. The computation time to generate the beamlet dose distributions of the field setups for the presented MBRT plans takes 2–6 h depending on the number of fields. The statistical uncertainty (expressed as one standard deviation) of a single beamlet dose distribution is thereby about 2%. A history by history method considering only dose values above 50% of the maximal dose value is used to determine the statistical uncertainty (Walters *et al* 2002). Deliverable dose calculation of the presented MBRT plans with a statistical uncertainty of about 1.5% needs < 1 h depending on the number of apertures. The optimizations are performed with a computation time of < 1 h depending on the number of voxels to be considered.

3.1. Academic situation

Isodose lines and DVHs of treatment plans for MBRT, MERT and photon IMRT targeting the PTV-Superficial and the PTV-Enlarged are compared in figures 2 and 3, respectively. The MBRT plans outperform the MERT and the photon IMRT plans in terms of objective function value (233.7 compared to 826.8 and 402.8 for the PTV-Superficial and 268.6 compared to 4526.2 and 701.2 for the PTV-Enlarged). The improved dose homogeneity in the PTV and the better sparing of the OARs are visible in the DVHs and isodose lines. Only the sparing of the OAR-Lateral is slightly better for dose values above 32% for the photon IMRT plan targeting the PTV-Superficial and the sparing of both OARs for dose values below 20% is partially better for both MERT plans compared to the MBRT plans. The low dose bath is slightly reduced for the MBRT plans compared to the photon IMRT plans, but increased with respect to the MERT

plans as expected. The MERT plan targeting the PTV-Enlarged would fail to cover the PTV-Enlarged homogeneously due to the enlarged depth.

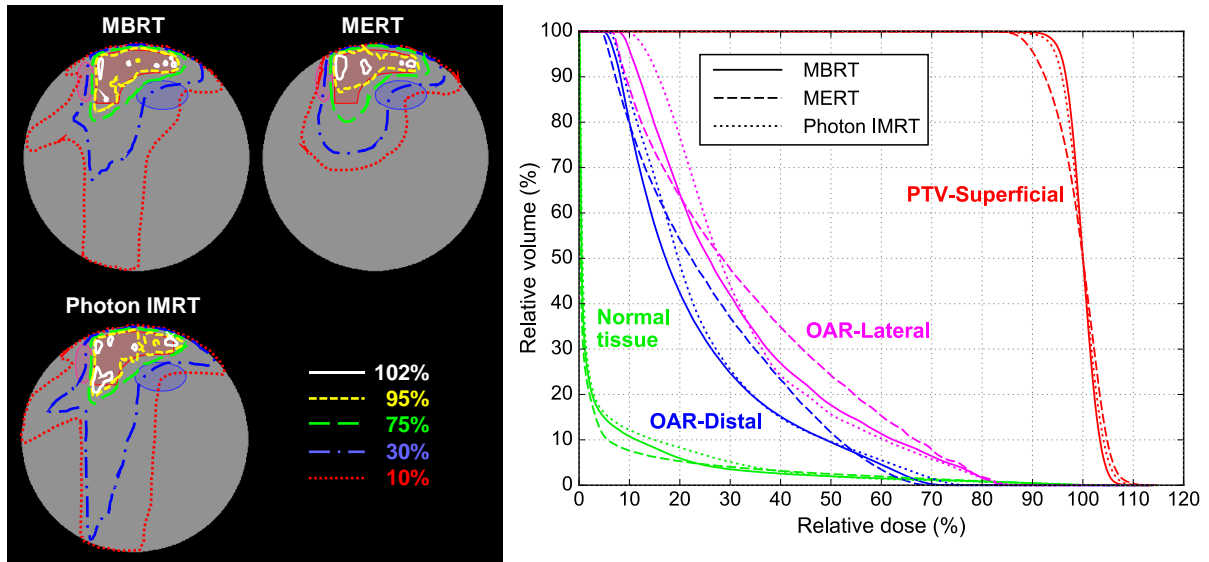


Figure 2. Isodose lines (left) and DVHs (right) of the MBRT, MERT and photon IMRT plans targeting the PTV-Superficial.

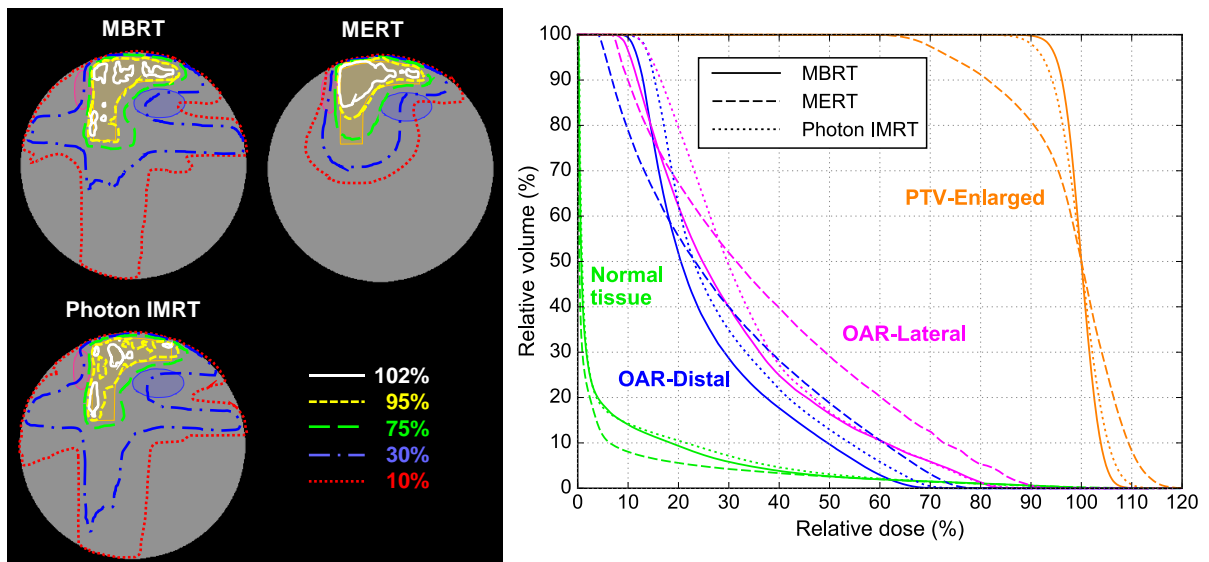


Figure 3. Isodose lines (left) and DVHs (right) of the MBRT, MERT and photon IMRT plans targeting the PTV-Enlarged.

The dose distributions and dose profiles of the photon and electron contributions of the MBRT plans targeting the PTV-Superficial and the PTV-Enlarged are presented in figure 4. Note that for both plans the electron beams dominantly cover the region between the surface and the OAR-Distal, while the photon beams cover the main part

of the deepest part of the PTV. Neither in the electron nor in the photon contribution steep dose gradients are visible except at the border of the PTV. The fraction of the integral dose in the PTV (PTV dose contribution) of the photon apertures is 44.3% and 53.3% for the MBRT plans targeting the PTV-Superficial and PTV-Enlarged, respectively. The difference is explained with the enlarged part of the PTV-Enlarged only sufficiently coverable with photon beams.

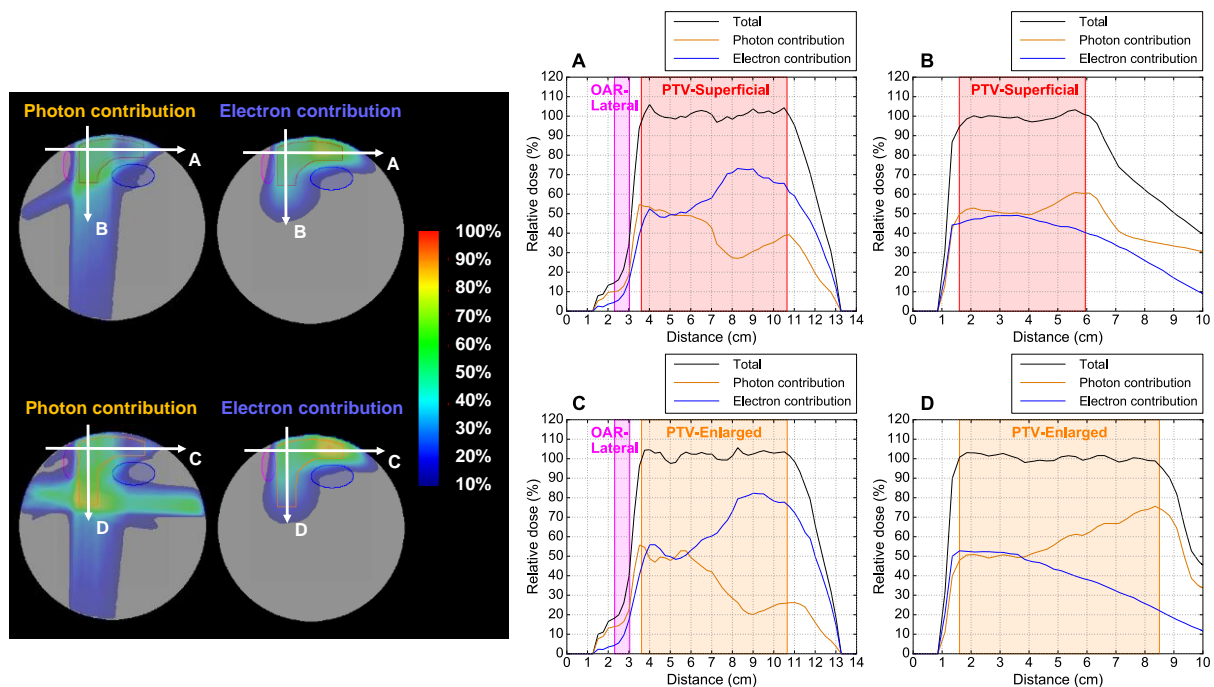


Figure 4. Dose distributions (left) and dose profiles (right) indicated with (A), (B), (C) and (D) of the photon and electron contributions of the MBRT plans targeting the PTV-Superficial (top) and the PTV-Enlarged (bottom).

Figure 5 compares the optimized, deliverable and deliverable weight re-optimized dose distributions of two MBRT plans targeting the PTV-Enlarged (either optimized with or without consideration of photon pMLC transmission) in terms of the objective function value and the DVHs. The rDPE is 28% and the rOCE is 49%. Hence, a DPE caused by not considering photon pMLC transmission could not be compensated by applying the weight re-optimization. Comparing the deliverable weight re-optimized dose distributions shows that not considering photon pMLC transmission leads to increased dose values to both OARs. There is still a remaining OCE even if photon pMLC transmission is considered during optimization. However, the DVHs of the

deliverable weight re-optimized dose distribution are similar to those of the optimized dose distribution, which is used as the estimate for the truly optimal objective function value in this work (both optimized considering photon pMLC transmission). Only the dose homogeneity in the PTV and the dose values delivered to the OAR-Lateral below 30% are marginally reduced and increased, respectively.

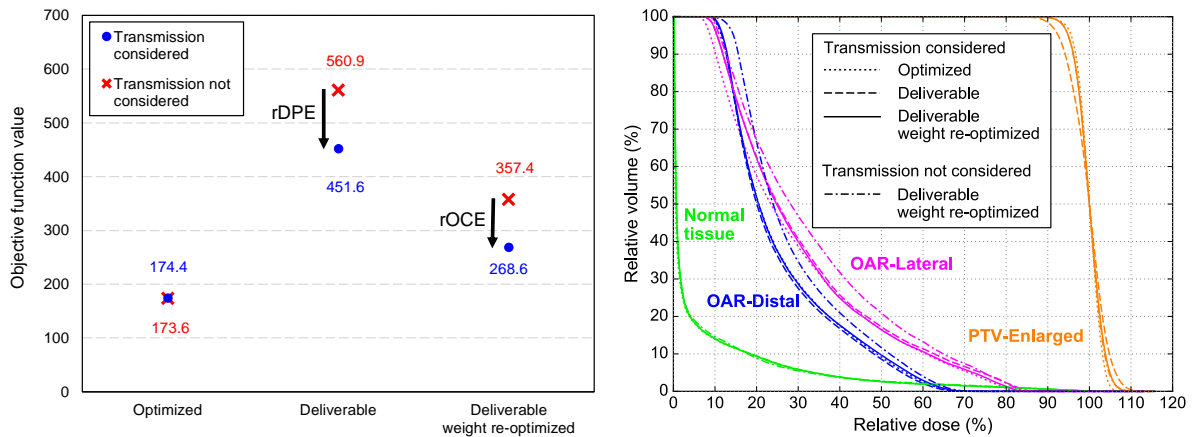


Figure 5. Objective function value (left) and DVH (right) comparisons of optimized, deliverable and deliverable weight re-optimized dose distributions of two MBRT plans targeting the PTV-Enlarged either optimized with or without consideration of photon pMLC transmission. For better visibility, the DVHs of the optimized and deliverable dose distributions without weight re-optimization are not displayed in case of the plan optimized without consideration of photon pMLC transmission.

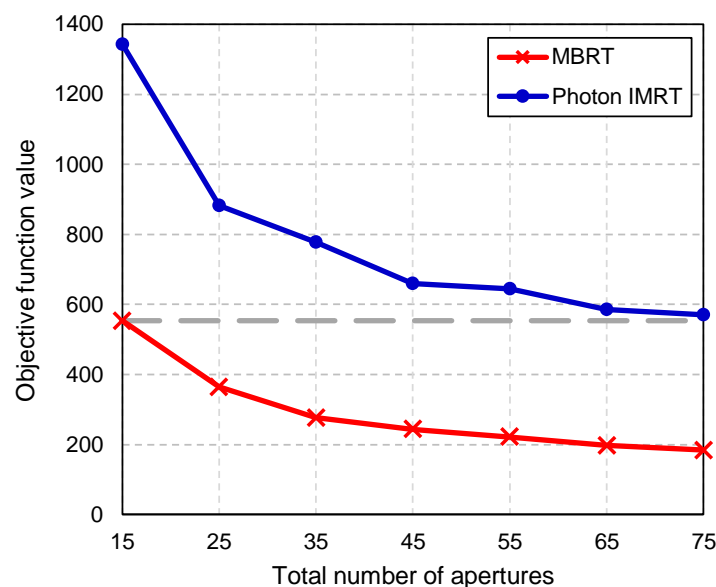


Figure 6. Dependency of the final objective function value on the number of apertures used for creating MBRT and photon IMRT plans targeting the PTV-Enlarged. In case of the MBRT plans, the number of electron apertures is kept constant at 10.

Figure 6 illustrates the dependency of MBRT and photon IMRT plans targeting the PTV-Enlarged on the number of apertures utilized. An MBRT plan consisting of only 5 photon and 10 electron apertures has a 3% lower objective function value than a photon IMRT plan with 75 photon apertures.

3.2. Chest wall case

The treatment plans for MBRT, MERT, photon IMRT and VMAT determined for the chest wall case are compared in figure 7 and table 5. The HI in the PTV for the MBRT plan is similar than for the VMAT plan and 5% higher than for the MERT and photon IMRT plans. The MBRT plan outperforms the VMAT plan in terms of OAR sparing and the volume of the low dose bath (visible in the isodose line comparison). The mean dose delivered to the ipsilateral lung, heart, contralateral lung and breast and the $V_{10\%}$ of normal tissue are lower by 11%, 31%, 83%, 77% and 45%. For the MERT plan, the low dose bath is even more reduced and the sparing of the OARs is similar to the MBRT plan except for the ipsilateral lung, while for the photon IMRT plan only the sparing of the contralateral lung is similar to the MBRT plan.

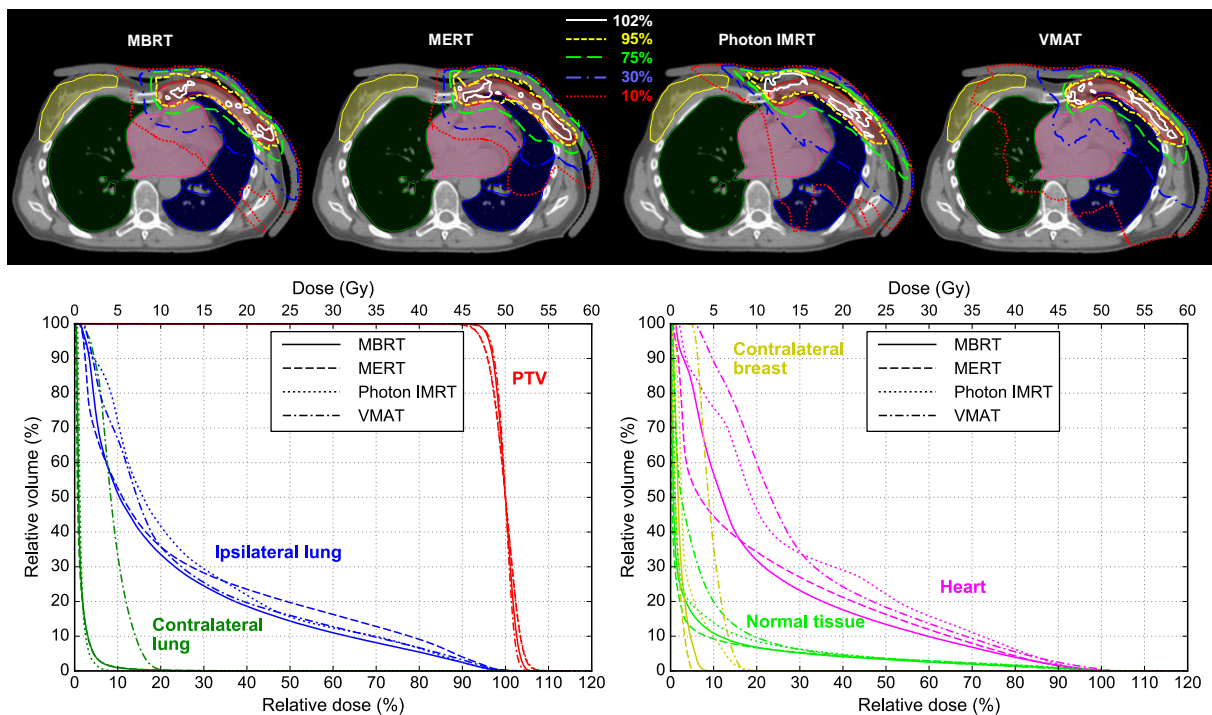


Figure 7. Isodose lines (top) and DVHs (bottom) of the MBRT, MERT, photon IMRT and VMAT plans determined for the chest wall case.

Table 5. Comparison between the MBRT, MERT, photon IMRT and VMAT plans determined for the chest wall case. For every evaluated dosimetric quantity, the best, second best and third best values are marked bold, underlined and italic, respectively.

	MBRT	MERT	Photon IMRT	VMAT
PTV - HI	<u>98.3%</u>	93.3%	93.3%	98.5%
Ipsilateral lung - D_{mean}	10.9 Gy	<i>12.4 Gy</i>	13 Gy	<u>12.3 Gy</u>
Contralateral lung - D_{mean}	<u>0.8 Gy</u>	0.7 Gy	<u>0.8 Gy</u>	4.5 Gy
Heart - D_{mean}	<u>10.7 Gy</u>	10.5 Gy	<i>14.6 Gy</i>	15.5 Gy
Contralateral breast - D_{mean}	<u>1.1 Gy</u>	0.8 Gy	<i>2 Gy</i>	4.7 Gy
Normal tissue - $V_{10\%}$	<u>1917 cm³</u>	1624 cm³	<i>2438 cm³</i>	3508 cm ³
Total MU	740.7	658.5	673.9	563
Photon MU fraction	48.5%	-	-	-
Photon PTV dose contribution	34.7%	-	-	-

MBRT plan outperforms the VMAT plan in terms of OAR sparing and the volume of the low dose bath (visible in the isodose line comparison). The mean dose delivered to the ipsilateral lung, heart, contralateral lung and breast and the $V_{10\%}$ of normal tissue are lower by 11%, 31%, 83%, 77% and 45%. For the MERT plan, the low dose bath is even more reduced and the sparing of the OARs is similar to the MBRT plan except for the ipsilateral lung, while for the photon IMRT plan only the sparing of the contralateral lung is similar to the MBRT plan.

Figure 8 compares the dose distributions of the photon and electron contributions of the MBRT plan. The electron beams dominantly cover the region of the internal mammary chain and the shallower part of the chest wall, while the photon beams cover the major part of the deeper located part of the chest wall adjacent to the ipsilateral lung. For this case, the PTV dose contribution of the photon apertures is with 38.7% considerably smaller than of the electron apertures.

Figure 9 compares the DVHs of the MBRT and MBRT-WOB plans. While the dose homogeneity in the PTV and the sparing of the heart for dose values above 10 Gy are marginally worsened, the sparing of the ipsilateral lung, the heart and normal tissue for dose values below 10 Gy is marginally improved for the MBRT-WOB plan compared to the MBRT plan.

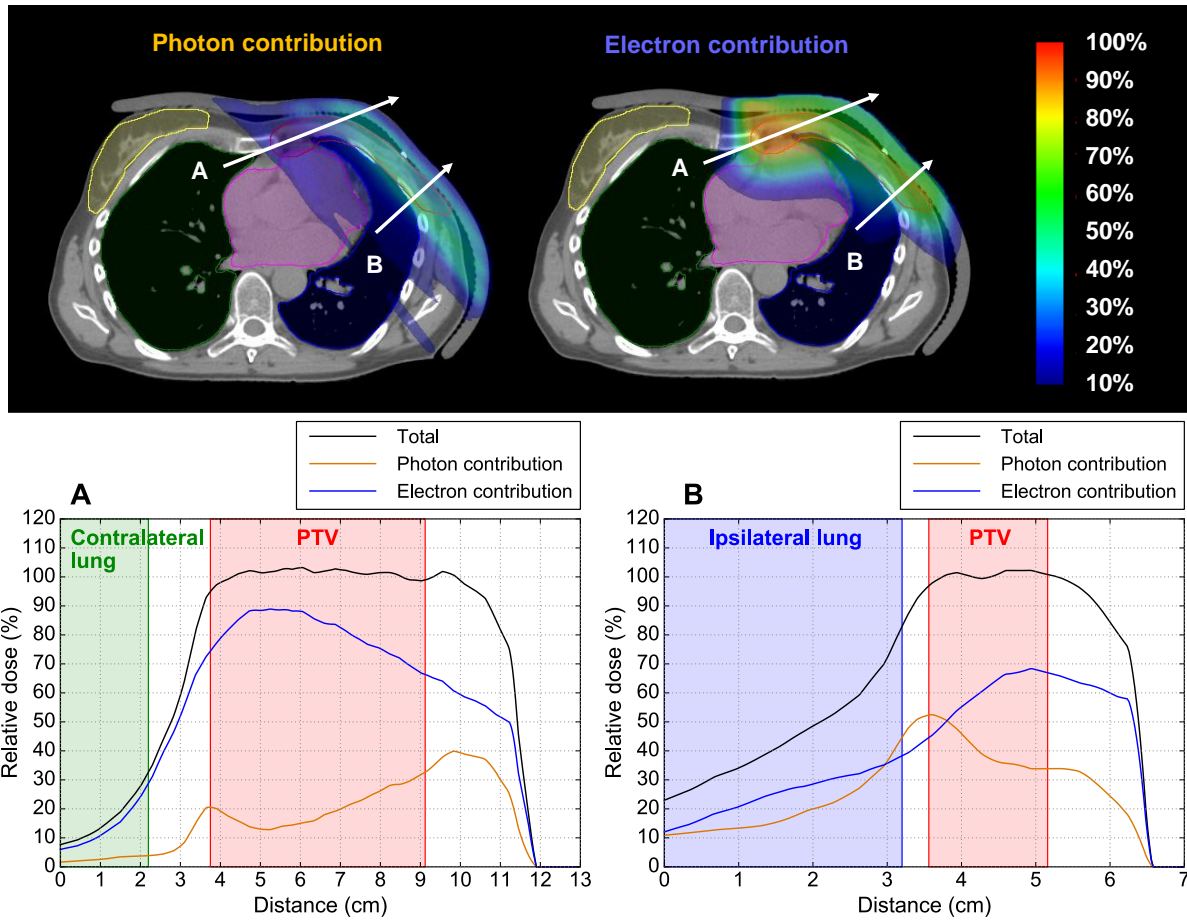


Figure 8. Dose distributions (top) and dose profiles (bottom) indicated with (A) and (B) of the photon and electron contributions of the MBRT plan determined for the chest wall case.

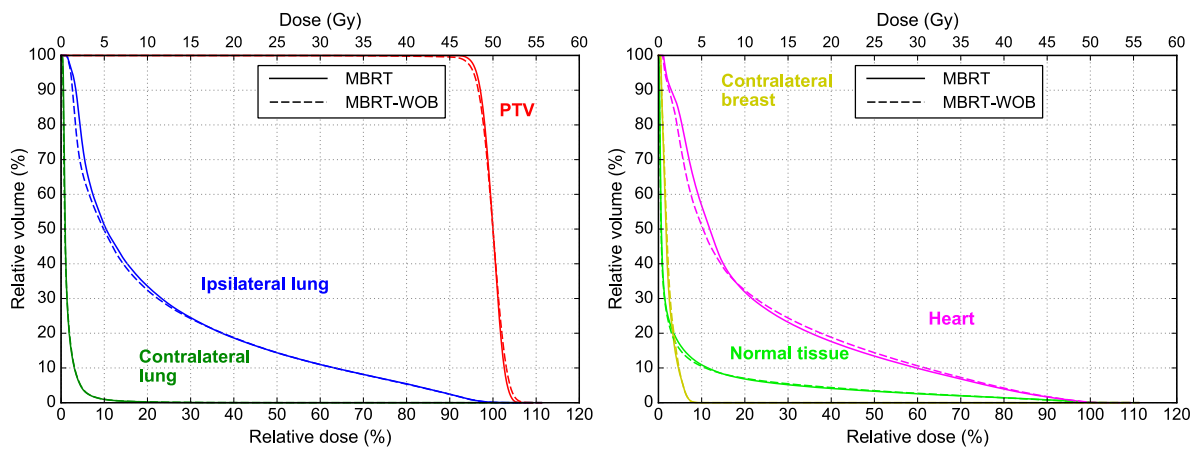


Figure 9. DVHs (bottom) of the MBRT and the MBRT-WOB plans determined for the chest wall case.

3.3. Squamous cell carcinoma case

The treatment plans for MBRT, MERT, photon IMRT and VMAT determined for the squamous cell carcinoma case are compared in figure 10 and table 6. The HI in the PTV for the MBRT plan is 2.2% higher than for the VMAT plan and 8.2% higher than for the MERT plan. Only the photon IMRT plan has a similar HI in the PTV. The MBRT plan outperforms the VMAT plan in terms of OAR sparing and extent of the low dose bath except for the high dose values in the brain ($D_{2\%}$ is 5% higher for the MBRT plan). D_{mean} or $D_{2\%}$ to all other OARs are 5%–62% lower and the $V_{10\%}$ of normal tissue is 28% lower for the MBRT plan compared to the VMAT plan. The mentioned quantities for the contralateral eye, lens and parotid glands and the normal tissue are even more reduced by the MERT plan. However, all other OARs, especially the brain, ipsilateral cochlea and the spinal cord are spared considerably less. In case of the photon IMRT plan, all OARs are spared less or similar to the MBRT plan. In contrast to the VMAT plan, the photon IMRT plan has an increased $D_{2\%}$ value in the brain compared to the MBRT plan.

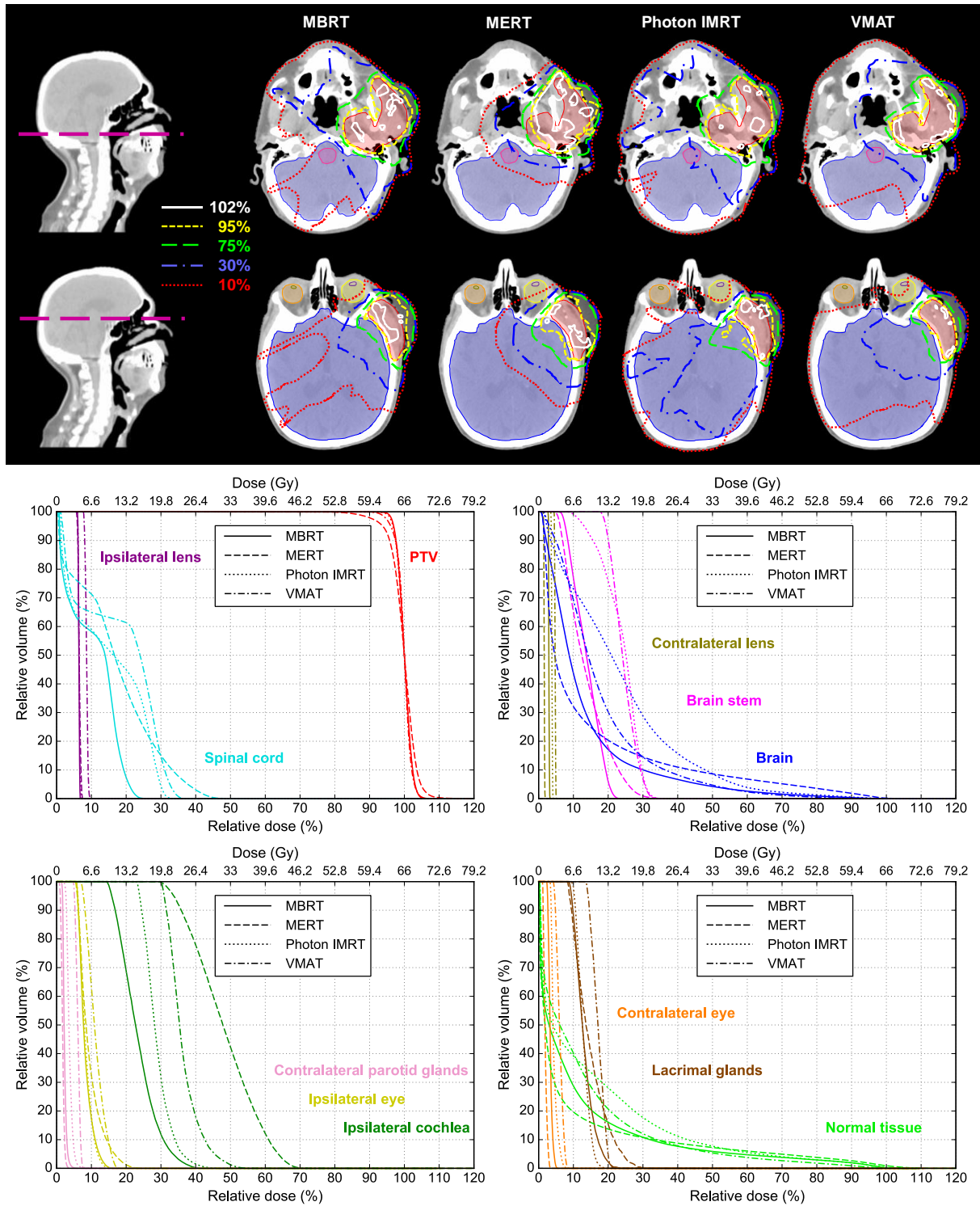


Figure 10. Isodose lines for two different transversal views (top) and DVHs (bottom) of the MBRT, MERT, photon IMRT and VMAT plans determined for the squamous cell carcinoma case.

Table 6. Comparison between the MBRT, MERT, photon IMRT and VMAT plans determined for the squamous cell carcinoma case. For every evaluated dosimetric quantity, the best, second best and third best values are marked bold, underlined and italic, respectively.

	MBRT	MERT	Photon IMRT	VMAT
PTV - HI	99.5%	91.3%	<u>99.2%</u>	<i>97.3</i>
Ipsilateral cochlea - D_{mean}	15.4 Gy	31.8 Gy	<u>19.1 Gy</u>	<i>24 Gy</i>
Lacrimal glands - D_{mean}	<u>8.6 Gy</u>	9.7 Gy	8.4 Gy	11.3 Gy
Contralateral parotid glands - D_{mean}	<u>1.5 Gy</u>	1.1 Gy	2.4 Gy	4 Gy
Brain – $D_{2\%}$	<u>43 Gy</u>	58.9 Gy	47.5 Gy	41.1 Gy
Brain stem – $D_{2\%}$	14 Gy	<u>18.5 Gy</u>	20.9 Gy	20.8 Gy
Spinal cord – $D_{2\%}$	14.6 Gy	27.4 Gy	<u>20.4 Gy</u>	22.4 Gy
Ipsilateral eye – $D_{2\%}$	<u>8.9 Gy</u>	12.6 Gy	8.5 Gy	<i>10.9 Gy</i>
Contralateral eye – $D_{2\%}$	<u>3.1 Gy</u>	2 Gy	4.5 Gy	5.2 Gy
Ipsilateral lens – $D_{2\%}$	4.4 Gy	4.8 Gy	<u>4.6 Gy</u>	6.2 Gy
Contralateral lens – $D_{2\%}$	<u>2.1 Gy</u>	1.2 Gy	2.7 Gy	3.3 Gy
Normal tissue - $V_{10\%}$	<u>1932 cm³</u>	1321 cm³	2632 cm ³	2700 cm ³
Total MU	598.1	556	647.6	603
Photon MU fraction	66%	-	-	-
Photon PTV dose contribution	46.9%	-	-	-

Figure 11 compares the dose distributions of the photon and electron contributions of the MBRT plan. The superior transversal view shows that the electron contribution covers the whole PTV dominantly on this slice. Only the part of the PTV adjacent to the left eye has a photon contribution higher than 30%. On the inferior slice, the electron apertures cover only the shallow part dominantly, while the central region and especially the deep-seated part adjacent to the brain, brain stem and ipsilateral cochlea (located superiorly to the slice shown) is covered dominantly by the photon apertures. Also for this clinical case, the PTV dose contribution of the photon apertures is with 46.9% smaller than of the electron apertures.

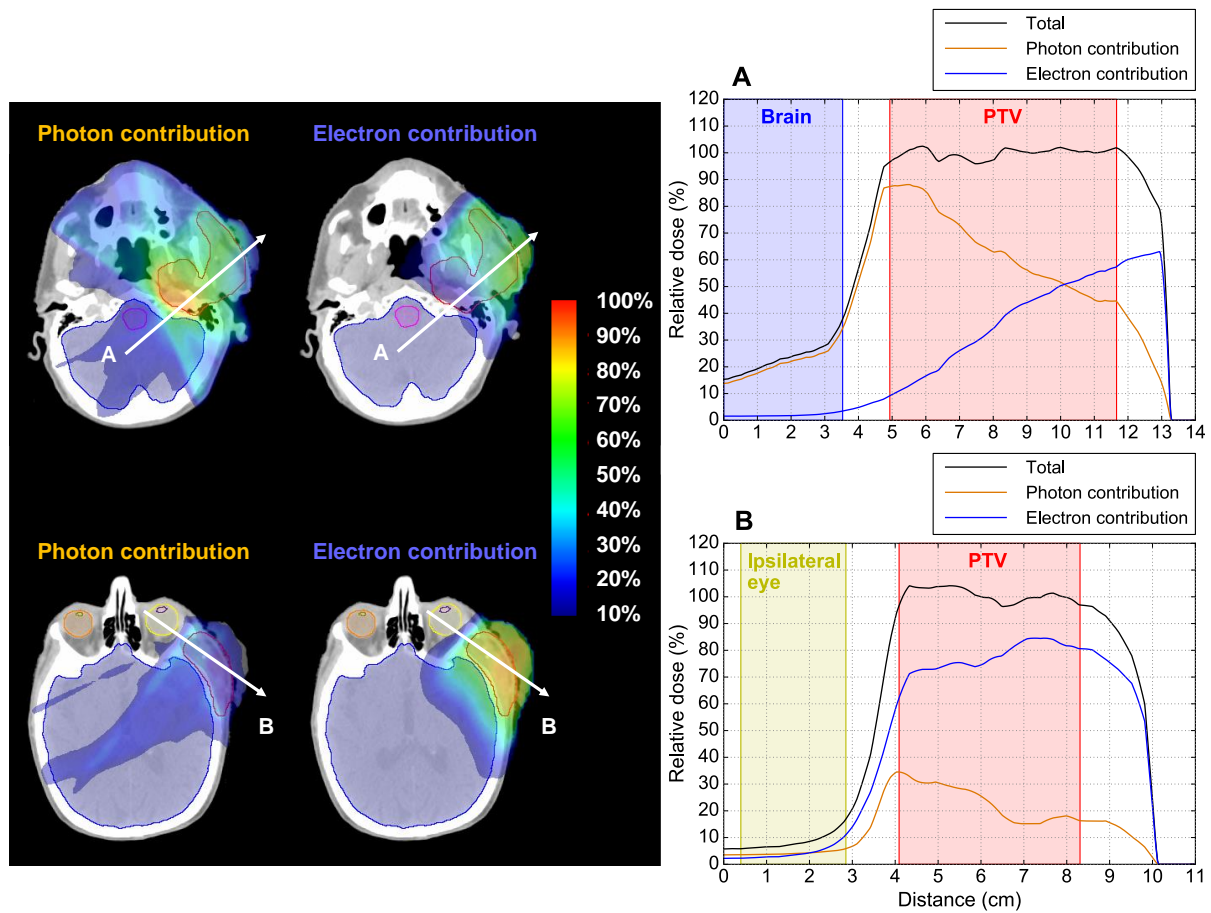


Figure 11. Dose distributions (left) and dose profiles (right) indicated with (A) and (B) of the photon and electron contributions of the MBRT plan determined for the squamous cell carcinoma case.

4. Discussion

A simulated annealing based DAO is implemented to create MBRT plans with pMLC shaped photon and electron apertures. It is demonstrated for the MBRT plan targeting the PTV-Enlarged in the academic situation that the differences between optimized and deliverable weight re-optimized dose distributions are efficiently minimized. Consideration of photon pMLC transmission factors during DAO and performing a weight re-optimization of the deliverable dose distributions are utilized for this purpose. Compared to DAO, a fluence-based approach could not account for transmission until leaf-sequencing. A downside of the simulated annealing based DAO is the requirement to predefine the number of apertures per field. Thus, several optimizations with different number of apertures per field have to be executed until the desired plan is found. The presented TPP for MBRT partially circumvents this issue as it allows executing optimizations differing in the number of apertures per field and the objectives in parallel. An alternative solution would be to use a column generation based DAO, because of the included pricing mechanism used to add apertures to the plan (Romeijn *et al* 2005). However, the algorithm is confronted with other limitations, e.g. the fixed shape of added apertures.

The evaluations of the TPP with the academic situation show for both PTVs that the objective function is clearly further minimized for optimizations of MBRT plans than of MERT and photon IMRT plans. In case of targeting the PTV-Enlarged, the benefit of using MBRT is even more pronounced. This is not expected with respect to photon IMRT, as the electron beams cover even a smaller fraction of the PTV-Enlarged. Moreover, this underlines that MBRT is not like MERT limited to deliver the dose homogeneously to targets with a deep-seated part. For photon IMRT plans targeting the PTV-Enlarged, even a higher number of photon apertures cannot reach the benefit of electron apertures.

The plan comparisons for the clinical situations indicate that MBRT plans are well suited to treat chest wall and squamous cell carcinoma cases. The comparisons of the photon and electron contributions demonstrate that the DAO efficiently exploits the dosimetric characteristics of photon and electron beams. However further investigations

for these treatment sites are required to make treatment site specific conclusions. Basically every target with at least a superficial part can be considered to be investigated for MBRT, because it is shown for the squamous cell carcinoma case and the academic situation that MBRT is ideally suited to treat superficial targets with a deep-seated part. The results of the MBRT-WOB plan for the chest wall case further indicate that MBRT can be applied to targets closely located to the patient surface without using the bolus but still with a similar treatment plan quality. The clinical workflow is improved without bolus as the risk to accidentally miss to place the bolus before delivery is not present.

Regarding applicability of the presented MBRT plans for the clinical cases: they can already be delivered in the developer mode of a TrueBeam with XML files. Moreover, all dose distributions presented are based on deliverable weight re-optimized dose distributions, calculated with validated beam models and MC dose calculation algorithms. The SSD of the electron fields is chosen between 70 and 80 cm with a margin of at least 5 cm to the patient and the couch such that no collision is expected under consideration of the CT data set. Building a complete 3D model of the patient and the couch could be implemented to certainly prevent collisions. For both clinical cases, the isocenter positions of the electron fields differ from the isocenter position of the photon beams. For the chest wall case, the electron fields share the same isocenter position, while for the squamous cell carcinoma case, the isocenter position of the electron fields differ in vertical direction. Thus, couch movements are required every time another isocenter position is needed and, as in stereotactic treatments, appropriate image guidance techniques combined with six degree of freedom couches will play an important role (Schmidhalter *et al* 2014). For performing a patient specific QA of an MBRT plan, it is suggested to compare 2D calculated dose distributions in a water phantom to measurements with the TrueBeam built-in electronic portal imaging device (EPID) positioned at $SSD = 100$ cm. The EPID is well established for dosimetric verification of photon IMRT plans and on the other side Chatelain *et al* (2013) showed the feasibility to use a standalone EPID positioned with an $SSD = 70$ cm as an efficient verification tool for MERT plans. Moreover, using the built-in EPID at $SSD = 100$ cm for dose verification of electron beams is already explored (Henzen *et al* 2014d).

5. Conclusions

An MC beamlet based inverse TPP for MBRT including a simulated annealing based DAO capable of performing simultaneous optimization of pMLC shaped photon and electron beams is successfully implemented and tested for an academic situation with two PTV definitions and two clinical cases. MBRT plans dosimetrically outperformed MERT, photon IMRT and VMAT plans for all investigated academic and clinical situations. MBRT is a possible solution to known limitations and downsides of treatments using only photons or only electron beams: Compared to photon only plans, the low dose bath delivered to distal OARs and normal tissue is considerably reduced. Compared to electron only plans, MBRT is not limited due to the depth of the target and the sparing of OARs located nearby to the target is substantially improved. The results indicate that MBRT has the potential to become an alternative modality for treating superficial targets with and without deep-seated part.

Acknowledgments

This work was supported by Varian Medical Systems and partly by the Swiss Cancer League & Foundation Cancer Research Switzerland grant KFS-3279-08-2013. Calculations were performed on UBELIX (www.id.unibe.ch/hpc), the HPC cluster at the University of Bern.

References

- Al-Yahya K, Schwartz M, Shenouda G, Verhaegen F, Freeman C and Seuntjens J 2005 Energy modulated electron therapy using a few leaf electron collimator in combination with IMRT and 3D-CRT: Monte Carlo-based planning and dosimetric evaluation *Med. Phys.* **32** 2976–86
- Al-Yahya K, Verhaegen F and Seuntjens J 2007 Design and dosimetry of a few leaf electron collimator for energy modulated electron therapy *Med. Phys.* **34** 4782–91
- Alexander A, DeBlois F and Seuntjens J 2010 Toward automatic field selection and planning using Monte Carlo-based direct aperture optimization in modulated electron radiotherapy *Phys. Med. Biol.* **55** 4563–76
- Alexander A, Soisson E, Renaud M-A and Seuntjens J 2012 Direct aperture optimization for FLEC based MERT and its application in mixed beam radiotherapy *Med. Phys.* **39** 4820–31
- Bergman A M, Bush K, Milete M-P, Popescu I A, Otto K and Duzenli C 2006 Direct aperture optimization for IMRT using Monte Carlo generated beamlets *Med. Phys.* **33** 3666–79
- Bortfeld T 2006 IMRT: a review and preview *Phys. Med. Biol.* **51** R363–79
- Chatelain C, Vetterli D, Henzen D, Favre P, Morf D, Scheib S, Fix M K and Manser P 2013 Dosimetric properties of an amorphous silicon EPID for verification of modulated electron radiotherapy *Med. Phys.* **40** 61710
- Dogan N, Siebers J V, Keall P J, Lerma F, Wu Y, Fatyga M, Williamson J F and Schmidt-ullrich R K 2006 Improving IMRT dose accuracy via deliverable Monte Carlo optimization for the treatment of head and neck cancer patients *Med. Phys.* **33** 4033–43
- du Plessis F C P, Leal A, Stathakis S, Xiong W and Ma C-M 2006 Characterization of megavoltage electron beams delivered through a photon multi-leaf collimator (pMLC) *Phys. Med. Biol.* **51** 2113–29
- Fix M K, Cygler J, Frei D, Volken W, Neuenschwander H, Born E J and Manser P 2013 Generalized eMC implementation for Monte Carlo dose calculation of electron beams from different machine types *Phys. Med. Biol.* **58** 2841–59

- Fix M K, Manser P, D Frei, Volken W, Mini R and Born E J 2007 Efficient photon treatment planning by the use of Swiss Monte Carlo Plan *J. Phys.: Conf. Ser.* **74** 12004
- Gauer T, Sokoll J, Cremers F, Harmansa R, Luzzara M and Schmidt R 2008 Characterization of an add-on multileaf collimator for electron beam therapy *Phys. Med. Biol.* **53** 1071–85
- Ge Y and Faddegon B A 2011 Study of intensity-modulated photon–electron radiation therapy using digital phantoms *Phys. Med. Biol.* **56** 6693–708
- Gregoire V and Mackie T R 2011 Dose prescription, reporting and recording in intensity-modulated radiation therapy: a digest of the ICRU Report 83 *Imaging Med.* **3** 367–73
- Henzen D *et al* 2014a Beamlet based direct aperture optimization for MERT using a photon MLC *Med. Phys.* **41** 121711
- Henzen D, Manser P, Frei D, Volken W, Neuenschwander H, Born E J, Lössl K, Aebbersold D M, Stampanoni M F M and Fix M K 2014b Forward treatment planning for modulated electron radiotherapy (MERT) employing Monte Carlo methods *Med. Phys.* **41** 31712
- Henzen D, Manser P, Frei D, Volken W, Neuenschwander H, Born E J, Vetterli D, Chatelain C, Stampanoni M F M and Fix M K 2014c Monte Carlo based beam model using a photon MLC for modulated electron radiotherapy *Med. Phys.* **41** 21714
- Henzen D *et al* 2014d On the accuracy and efficiency of different verification methods for modulated electron radiotherapy treatment plans *Joint Conf. of the SSRMP, DGMP, ÖGMP* p 251
- Jeraj R 2002 The effect of dose calculation accuracy on inverse treatment planning *Phys. Med. Biol.* **47** 391–407
- Jin L, Eldib A, Li J, Emam I, Fan J, Wang L and Ma C M 2014 Measurement and Monte Carlo simulation for energy- and intensity-modulated electron radiotherapy delivered by a computer-controlled electron multileaf collimator *J. Appl. Clin. Med. Phys.* **15** 177–86

- Jin L *et al* 2008 Dosimetric verification of modulated electron radiotherapy delivered using a photon multileaf collimator for intact breasts *Phys. Med. Biol.* **53** 6009–25
- Kawrakow I and Fippel M 2000 VMC++, a fast MC algorithm for radiation treatment planning *The Use of Computers in Radiotherapy, 8th Int. Conf. (Heidelberg, Germany)* ed W Schlegel and T Bortfeld (Heidelberg: Springer) (<https://doi.org/10.1007/978-3-642-59758-9>)
- Klein E E, Mamalui-Hunter M and Low D A 2009 Delivery of modulated electron beams with conventional photon multi-leaf collimators *Phys. Med. Biol.* **54** 327–39
- Li J G, Williams S S, Goffinet D R, Boyer A L and Xing L 2000 Breast-conserving radiation therapy using combined electron and intensity-modulated radiotherapy technique *Radiother. Oncol.* **56** 65–71
- Magaddino V, Manser P, Frei D, Volken W, Schmidhalter D, Hirschi L and Fix M K 2011 Validation of the Swiss Monte Carlo Plan for a static and dynamic 6 MV photon beam *Z. Med. Phys.* **21** 124–34
- Mihaylov I B and Siebers J V 2008 Evaluation of dose prediction errors and optimization convergence errors of deliverable-based head-and-neck IMRT plans computed with a superposition/convolution dose algorithm *Med. Phys.* **35** 3722–7
- Mu X, Olofsson L, Karlsson M, Sjögren R and Zackrisson B 2004 Can photon IMRT be improved by combination with mixed electron and photon techniques? *Acta Oncol.* **43** 727–35
- Neuenschwander H and Born E J 1992 A Macro Monte Carlo method for electron beam dose calculations *Phys. Med. Biol.* **37** 107–25
- Neuenschwander H, Mackie T R and Reckwerdt P J 1995 MMC—a high-performance Monte Carlo code for electron beam treatment planning *Phys. Med. Biol.* **40** 543–74
- Otto K 2008 Volumetric modulated arc therapy: IMRT in a single gantry arc *Med. Phys.* **35** 310–7
- Palma B A, Sánchez A U, Salguero F J, Arráns R, Sánchez C M, Zurita A W, Hermida M I R and Leal A 2012 Combined modulated electron and photon beams planned by a Monte-Carlo-based optimization procedure for accelerated partial breast irradiation *Phys. Med. Biol.* **57** 1191–202

- Romeijn H, Ahuja R, Dempsey J and Kumar A 2005 A column generation approach to radiation therapy treatment planning using aperture modulation *SIAM J. Optim.* **15** 838–62
- Rosca F 2012 A hybrid electron and photon IMRT planning technique that lowers normal tissue integral patient dose using standard hardware *Med. Phys.* **39** 2964–71
- Salguero F J, Arráns R, Palma B A and Leal A 2010 Intensity- and energy-modulated electron radiotherapy by means of an xMLC for head and neck shallow tumors *Phys. Med. Biol.* **55** 1413–27
- Salguero F J, Palma B, Arrans R, Rosello J and Leal A 2009 Modulated electron radiotherapy treatment planning using a photon multileaf collimator for post-mastectomized chest walls *Radiother. Oncol.* **93** 625–32
- Schmidhalter D, Malthaner M, Born E J, Pica A, Schmuecking M, Aebersold D M, Fix M K and Manser P 2014 Assessment of patient setup errors in IGRT in combination with a six degrees of freedom couch *Z. Med. Phys.* **24** 112–22
- Shepard D M, Earl M A, Li X A, Naqvi S and Yu C 2002 Direct aperture optimization: a turnkey solution for step-and-shoot IMRT *Med. Phys.* **29** 1007–18
- Surucu M, Klein E E, Mamalui-Hunter M, Mansur D B and Low D A 2010 Planning tools for modulated electron radiotherapy *Med. Phys.* **37** 2215–24
- Vatanen T, Traneus E and Lahtinen T 2009 Comparison of conventional inserts and an add-on electron MLC for chest wall irradiation of left-sided breast cancer *Acta Oncol.* **48** 446–51
- Walters B R B, Kawrakow I and Rogers D W O 2002 History by history statistical estimators in the BEAM code system *Med. Phys.* **29** 2745–52
- Wu Q and Mohan R 2000 Algorithms and functionality of an intensity modulated radiotherapy optimization system *Med. Phys.* **27** 701–11
- Xiong W, Li J, Chen L, Price R A, Freedman G, Ding M, Qin L, Yang J and Ma C M 2004 Optimization of combined electron and photon beams for breast cancer *Phys. Med. Biol.* **49** 1973–89

5

Part 1: Optimization and evaluation of dynamic trajectory radiotherapy

**M.K. Fix, D. Frei, W. Volken, D. Terribilini, S. Mueller, O. Elicin,
H. Hemmatzad, D.M. Aebbersold and P. Manser**

Division of Medical Radiation Physics and Department of Radiation Oncology,
Inselspital, Bern University Hospital, and University of Bern, Bern, Switzerland

published in
Medical Physics

2018, Vol. 45, 4201-4212

<https://doi.org/10.1002/mp.13086>

© American Association of Physicists in Medicine.
Reproduced with permission. All rights reserved.

Abstract

Purpose: Although volumetric modulated arc therapy (VMAT) is a well-accepted treatment technique in radiotherapy using a coplanar delivery approach, VMAT might be further improved by including dynamic table and collimator rotations leading to dynamic trajectory radiotherapy (DTRT). In this work, an optimization procedure for DTRT was developed and the potential benefit of DTRT was investigated for different treatment sites.

Methods: For this purpose, a dedicated optimization framework for DTRT was developed using the Eclipse Scripting Research Application Programming Interface (ESRAPI). The contours of the target and organs at risk (OARs) structures were exported by applying the ESRAPI and were used to determine the fractional volume-overlap of the OARs with the target from several potential beam directions. Thereby, an additional weighting was applied taking into account the relative position of the OAR with respect to the target and radiation beam, that is, penalizing directions where the OAR is proximal to the target. The resulting two-dimensional gantry-table map was used as input for an A* path finding algorithm returning an optimized gantry-table path. Thereby, the process is also taking into account CT scan length and collision restrictions. The A* algorithm was used again to determine the dynamic collimator angle path by optimizing the area between the MLC leaves and the target contour for each gantry-table path leading to gantry-collimator paths. The resulting gantry-table and gantry-collimator paths are combined and serve as input for the intensity modulation optimization using a research VMAT optimizer and the ESRAPI resulting in dynamic trajectories. This procedure was evaluated for five clinically motivated cases: two head and neck, one lung, one esophagus, and one prostate. Final dose calculations were performed using the Swiss Monte Carlo Plan (SMCP). Resulting dose distributions for the DTRT treatment plans and for the standard VMAT plans were compared based on dose distributions and dose volume histogram (DVH) parameters. For this comparison, the dose distribution for the VMAT plans were recalculated using the SMCP. In addition, the suitability of the delivery of a DTRT treatment plan was demonstrated by means of gafchromic film measurements on a TrueBeam linear accelerator.

Results: DVHs for the target volumes showed similar or improved coverage and dose homogeneity for DTRT compared with VMAT using equal or less number of dynamic trajectories for DTRT than arcs for VMAT for all cases studied. Depending on the case, improvements in mean and maximum dose for the DTRT plans were achieved for almost all OARs compared with the VMAT plans. Improvements in DTRT treatment plans for mean and maximum dose compared to VMAT plans were up to 16% and 38% relative to the prescribed dose, respectively. The measured and calculated dose values resulted in a passing rate of more than 99.5% for the two-dimensional gamma analysis using 2% and 2 mm criteria and a threshold of 10%.

Conclusions: DTRT plans for different treatment sites were generated and compared with VMAT plans. The delivery is suitable and dose comparisons demonstrate a high potential of DTRT to reduce dose to OARs using less dynamic trajectories than arcs, while target coverage is preserved.

Key words: dynamic trajectory, intensity modulation, Monte Carlo, trajectory optimization

1. Introduction

Since several years, intensity modulated radiotherapy (IMRT) and more recently volumetric modulated arc therapy (VMAT) are well-established treatment techniques in radiotherapy.¹⁻³ During the VMAT delivery technique, the gantry rotation, the position of the leaves of the multi leaf collimator (MLC) as well as the dose rate change dynamically throughout the treatment application leading to a highly efficient and conformal dose delivery to the patient. The availability of appropriate treatment planning options together with quality assurance (QA) procedures and suitable linear accelerator hardware led to the successful introduction of VMAT into clinical routine.⁴ However, the application of VMAT is mainly limited to coplanar arcs and further improvements in the dose distribution could be achieved using non-coplanar beam arrangement, that is, increase the degrees of freedom.

The impact of non-coplanar beam arrangements was investigated in several previous studies using different approaches outlined in the following. One approach is using many non-coplanar IMRT fields leading to 4π radiotherapy, which demonstrated substantial reduction in dose to organs at risk (OARs) for several different treatment sites.⁵⁻⁸ Alternatively, a set of partial arcs each at another static table rotation angle can be used.⁹ Another approach is including table rotation in the beam arrangements either at different static gantry angles¹⁰⁻¹³ or with a dynamic gantry rotation.¹⁴⁻¹⁹ Instead of including the table rotation also the collimator rotation can be taken into account to additionally increase the number of degrees of freedom.^{20,21} A further step, which is also the aim of this work, is to include both collimator and table rotation during beam delivery.²²

Typically, these non-coplanar techniques are implemented as a two-step procedure. In the first step the beam path is determined. For this purpose either a user-defined input,^{10,12,13,18,19} a geometrically based approach^{9,11,15,20,22} or a method including fluence optimization^{5-8,14,16} is utilized. While the user-based input is manual, the geometrically based approach can be automated and is typically faster than those using fluence optimization to determine the path, as the latter includes dose calculations. Recently, a fluence optimization based method to determine paths that additionally determines the

connectedness of the target structure to avoid contentious issues of the VMAT optimization was developed.²³ In the second step of this procedure, the optimization of the dose distribution for a treatment plan along the determined path is performed leading to dynamic trajectories. In this step, different optimization algorithms were used. Thereby, the used optimization algorithm might not support all dynamic components that have been applied to determine the path in the first step. Consequently, approximations were applied including for example the approximation of a continuous dynamic trajectory by a set of static fields^{9,12,13,19} or to omit certain dynamic components.²³

The final dose calculation of the optimized dynamic trajectory based treatment plans generally discretize the dynamic components based on the underlying DICOM control point description of the plan. Alternatively Monte Carlo (MC) dose calculation algorithms provide the possibility to model the continuous application of dynamic components.²⁴⁻²⁸ It is worth mentioning that the efficiency of MC dose calculations is only weakly dependent on the number of dynamic components involved.

This work aims in efficiently generating dynamic trajectory radiotherapy (DTRT) treatment plans using dynamic, that is, continuously moving, MLC leaves as well as gantry, table and collimator rotations while beam is on. The dynamic paths are determined not only by geometrical information, but also include dosimetric input in contrast to the study of Yang *et al.* in which only geometrical information was used.²² While the dynamic collimator rotation in previous studies was steered by considering a dedicated OAR,^{20,22} in this work the collimator angle is optimized based on the conformity assessment of MLC apertures with respect to the target structure. The resulting dose distribution of DTRT treatment plans for five clinically motivated cases of different treatment sites were compared with those using conventional clinical VMAT treatment plans. Thereby, for all plans the Swiss Monte Carlo Plan (SMCP) was applied for final MC dose calculations taking the continuous delivery into account, that is, no discretization of dynamic components is applied.^{24,27,28} Finally, not only the treatment planning procedure but also the suitability of the dose delivery of a DTRT treatment plan is demonstrated for one clinically motivated case utilizing the developer mode on a TrueBeam linear accelerator (Varian Medical Systems, Palo Alto, CA, USA)

for which the measured film dose is compared with the corresponding MC calculated dose distribution.

2. Materials and methods

The basic concept for the optimization of DTRT treatment plans is illustrated in Fig. 1 and is outlined in detail in the following sections by means of an example for a clinically motivated head and neck cancer patient. The framework is based on the optimization of dynamic paths and a research version of the Eclipse VMAT photon optimizer using the Eclipse Scripting Research Application Programming Interface (ESRAPI; Varian Medical Systems). The dynamic paths including the intensity modulation by the dynamic MLC are referred to as dynamic trajectories. Currently, the framework supports all dynamic components used for VMAT as well as collimator and table rotations. Thereby, the dynamics of these components are handled by means of DICOM control points,²⁷ that is, for each DICOM control point not only the position of the gantry and the MLC leaves but also the collimator and table angles are specified. In between two DICOM control points, a linear interpolation is performed. In this work gantry, table and collimator angles are provided in the ICE coordinate system.

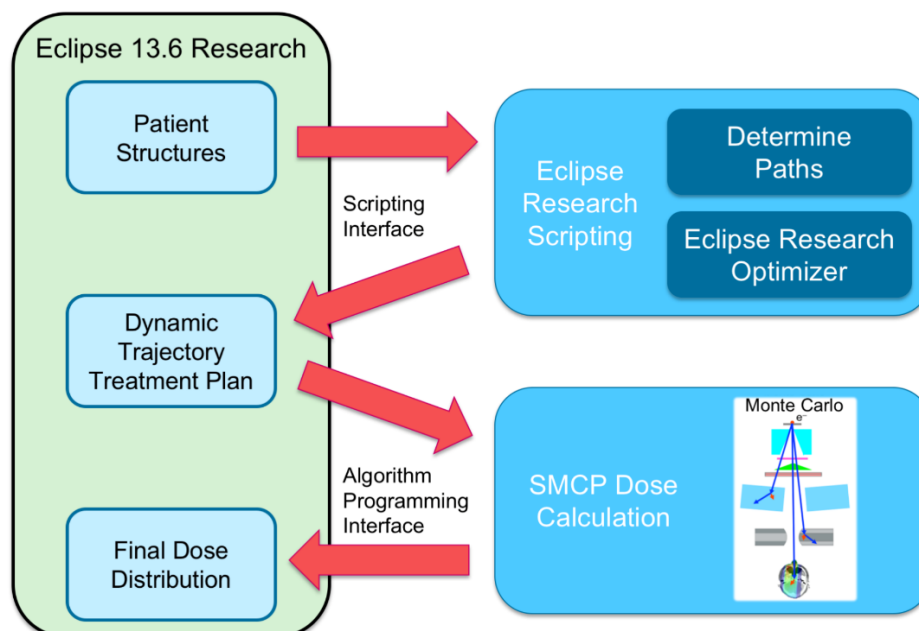


Fig. 1. Schematic view of the basic concept for dynamic trajectory radiotherapy. Patient structures are exported using the Eclipse scripting interface. The script handles the determination of the dynamic paths as well as the optimization using the Eclipse research VMAT optimizer. The optimized plan is loaded back into Eclipse and the final dose calculation is performed using the Swiss Monte Carlo Plan (SMCP) by means of the algorithm programming interface. Details about each step are provided in the text.

2.A. Dynamic trajectory optimization

The DTRT optimization starts with a previously imported CT data set of a cancer patient including the outline of the target as well as OAR structures. The first step of this optimization is the determination of the dynamic paths, that is, the gantry-table and the gantry-collimator paths. These paths are not independent and first the gantry-table path is determined followed by the determination of the gantry-collimator path.

2.A.1. Gantry-table path

For the generation of the gantry-table path, the structure set of the patient in Eclipse is exported as triangular meshes using the ESRAPI. Sampling potential beam directions, regularly distributed on a sphere using a Fibonacci lattice with its center at the predefined plan iso-center for efficiency, the fractional volume-overlap of each individual OAR and the target structure is determined. In case where no iso-center is defined, the center of the Fibonacci lattice is placed in the center of mass of the target structure. The fractional volume-overlap is determined for 2000 different beam directions and is then weighted based on the relative distance between the OAR and the target structure along the central axis. The dosimetrically based weighting basically accounts for the depth dose characteristics, as for example, the volume overlap is the same for beam directions that are 180° apart, however, the direction for which the OAR is distal to the target structure should be generally preferred due to the lower dose deposition in the OAR. This effect is more pronounced for larger distances between the target structure and the structure of the OAR considered. Overall the procedure leads to a gantry-table map for each OAR. An example of such a gantry-table map for the spinal cord of a head and neck cancer patient is provided in Fig. 2. Such a gantry-table map is created for each OAR that is considered in the DTRT optimization. The summation of all these OAR specific gantry-table maps determines the total gantry-table map. In this summation, different user-defined relative weights of the OAR specific gantry-table maps can be applied. Increasing the weight for an OAR specific gantry-table map leads to dynamic paths with increasingly sparing that OAR. In this work, all the OAR specific gantry-table maps use a relative weight of one, which is the default setting.

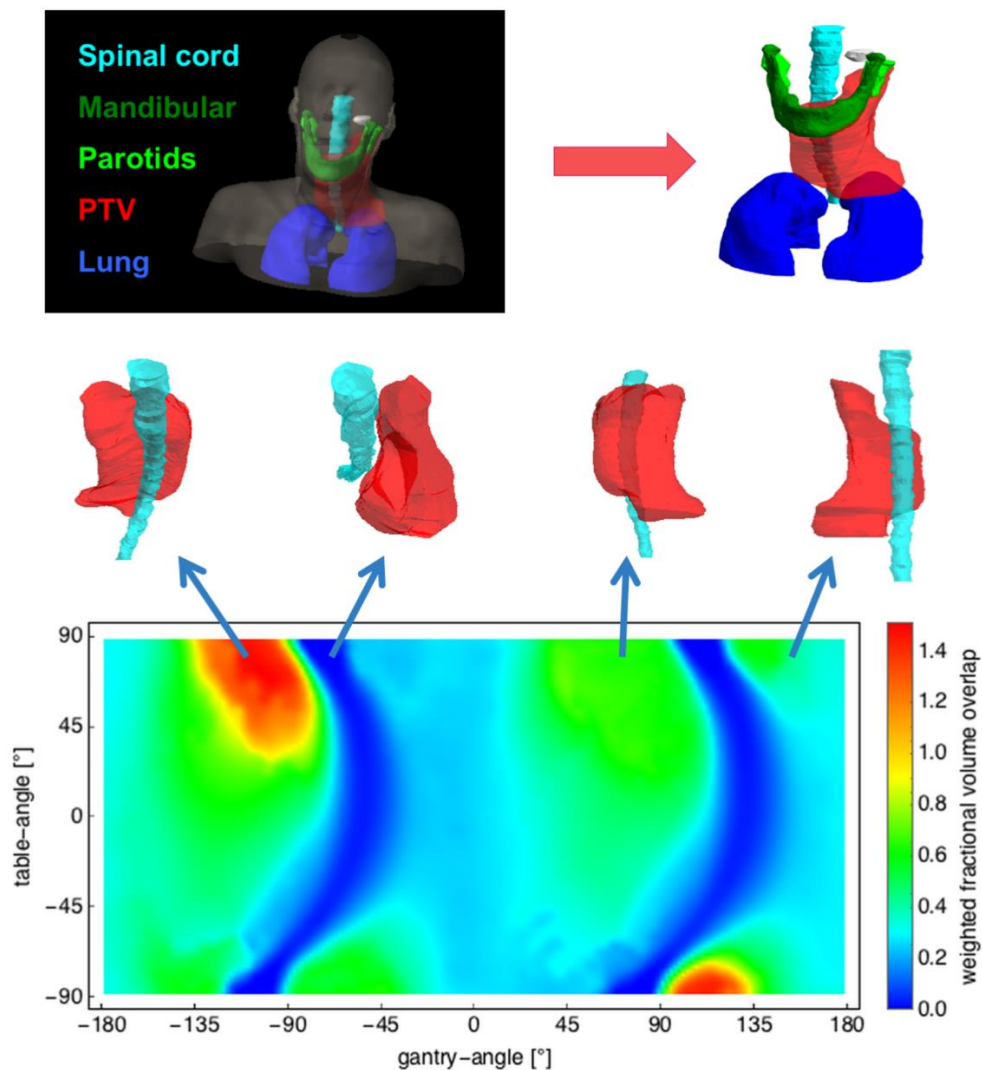


Fig. 2. The structures considered for the dynamic path optimization are shown at the top. For each of the structures, the gantry-table map is generated by determining the weighted fractional volume overlap for the different gantry-table angle combinations as shown for four examples in the middle row. At the bottom, the total gantry-table map is depicted. The color code indicates gantry-table combinations that should be avoided due to a high weighted overlap, while a low weighted overlap indicates regions of favorable angle settings.

The search space for an optimized path in the gantry-table map is restricted due to the limited CT scan length. Certain gantry-table angle combinations in the map lead to directions for which the incoming beam directs through an end slice of the CT data set, which is not allowed. Since the CT data set is known, the segments in the gantry-table map that are not possible due to the limited CT scan length can be determined and excluded from the path search. Another limitation includes potential collisions between the treatment machine and the patient. For this purpose two additional segments, one for head and neck another one for patients with cancer of the trunk, for example, prostate,

are empirically determined using a phantom placed on the table of the linear accelerator. Several beam directions were applied and possible gantry-table angle combinations were determined for a head and neck cancer patient and for a patient with cancer of the trunk, thus leading to segments that are not allowed for the gantry-table path. Although the collision segment is determined for a certain reasonable standard situation, the paths determined for a specific treatment plan have to be checked for collisions in an appropriate pre-treatment QA procedure.

Based on the total gantry-table map a dynamic path, that is, a gantry-table path, is determined using an A* algorithm.²⁹ The A* algorithm searches for the path between a starting and an end point receiving the lowest cost, where the cost is determined by adding the values along the path, that is, the algorithm searches for a path following minimal pixel values. This A* algorithm was adjusted when applied to the gantry-table map to find an optimized dynamic path. First, the gantry is not able to change the direction of rotation, that is, the dynamic path is either from left to right or from right to left. Second, Eclipse does also not support a gantry angle range below 30°. Thus, the A* algorithm was modified in that no specific end point has to be defined, however, a specific gantry angle range is assigned with 360° being the default. The starting gantry angle and the angle range are user defined, but need to cover at least a gantry angle range of 30°. The A* algorithm is forced to follow a path strictly from left to right, while the maximal gradient from step to step, that is, the change in the table angle per gantry angle increment, can be steered by a user-defined value using a value of one in this work. All the dynamic paths determined in this work utilizing the A* algorithm use a starting gantry angle of -180° and a gantry angle range of 360°.

2.A.2. Gantry-collimator path

Based on the gantry-table path determined using the A* algorithm in the gantry-table map, a gantry-collimator map is generated. For this purpose, the area between the MLC leaf ends and the target structure in the beam's eye view is determined similar to the work of MacDonald *et al.*²¹ The area was calculated for 180 × 180 different gantry-collimator angle combinations taking the gantry and table angle values from the determined gantry-table path. Plotting the values of the determined areas leads to a gantry-collimator map. As these values are the same for collimator angles 180° apart,

the gantry-collimator map for collimator angles ranging from -180° to 0° and 0° to 180° are identical. Using the gantry-collimator map as input, the A* algorithm was applied to determine the gantry-collimator path similar as for the gantry-table path, leading to an optimized dynamic path.

2.A.3. DTRT treatment plan

The determined dynamic path was duplicated to either increase the possibility of modulation for the optimizer or to split the field size defined by the secondary collimator jaws in two sub-fields, both following experiences made for VMAT plans with two arcs, as this approach showed improved treatment plans. Such a procedure basically eases the limitations of the optimizer with respect to the connectedness of the target structure in the beam's eye view.

Then, the optimization is automatically started within the ESRAPI using a research version of the Eclipse VMAT photon optimizer supporting dynamic table and collimator rotation settings and which is based on the commercially available VMAT photon optimizer version 13.6 (Varian Medical Systems). The format of priorities and dose objectives in the research version of the VMAT optimizer are the same as in the commercial version of the VMAT optimizer. User-defined dose objectives could be either automatically exported from Eclipse or were provided in a specific input file. For all cases considered in this work, the intermediate dose option was turned on. The final optimized treatment plan was then loaded into Eclipse in a newly created treatment plan using the ESRAPI (see Fig. 1). All these steps are performed fully automatically in the developed framework.

The last step included the final dose distribution of the optimized DTRT treatment plan. For this purpose the SMCP was used,²⁴ which is registered as a dose calculation algorithm in Eclipse using the Algorithm Programming Interface (API; Varian Medical Systems), and was recently extended to calculate dose distributions for dynamic trajectories.²⁸ For all dose calculations in the SMCP, the MC transport code VMC++ was selected.³⁰

2.B. Evaluation

The optimization procedure of DTRT treatment plans as described above was applied to clinically motivated cases for different treatment sites including two head and neck, one lung, one esophagus and one prostate case with prescribed doses of 54, 40, 54, 45, and 39 Gy, respectively. Each DTRT treatment plan contains two dynamic trajectories. The resulting final dose distributions were compared with those for the corresponding clinically applied VMAT treatment plan using two arcs (head and neck), three partial arcs (head and neck), four arcs (lung), three arcs (esophagus), and two arcs (prostate). The dosimetric comparison is performed in terms of dose distributions and dose volume histogram (DVH) parameters for the target as well as for OAR structures. Thereby, the homogeneity index for the target (planning target volume, PTV) is evaluated as determined by $HI = V_{95\%} - V_{105\%}$. For this comparison, the dose distribution for all VMAT plans was recalculated using SMCP. The voxel size for all dose distributions were $0.25 \times 0.25 \times 0.25 \text{ cm}^3$ and the statistical uncertainty of the MC calculated dose distribution was better than 1.5% (one standard deviation). Thereby, the statistical uncertainty associated with the MC dose calculations was determined as the sum in quadrature of the fractional statistical uncertainties of all dose values higher than 50% of the maximum dose calculated. All treatment plans were normalized with the prescribed dose (100%) to the median dose of the target structure.

Finally, to verify the deliverability and to demonstrate the suitability of a DTRT treatment plan, pre-treatment QA was performed utilizing the developer mode at a TrueBeam linear accelerator. For this purpose, an in-house developed xml-converter tool was used to directly convert the DTRT treatment plan for the second head and neck case into an xml file. Gafchromic EBT3 film (Ashland, Wayne, NJ, USA) measurements in a homogeneous cubic solid water phantom were then performed. The film was placed in the iso-center plane in a depth of 5 cm and the measured data were compared with the corresponding MC calculated dose distribution. A two-dimensional gamma analysis was performed using 2% (100% equals maximum dose of the reference) and 2 mm as criteria together with a gamma evaluation threshold of 10%. The film measurement was used as reference.

3. Results

In Fig. 3, the gantry-table maps for the different OARs are shown for the head and neck case shown in Fig. 2 together with the total gantry-table map. The color code corresponds to the total weighted fractional volume overlap using an equal contribution of the OAR specific gantry-table maps in this case.

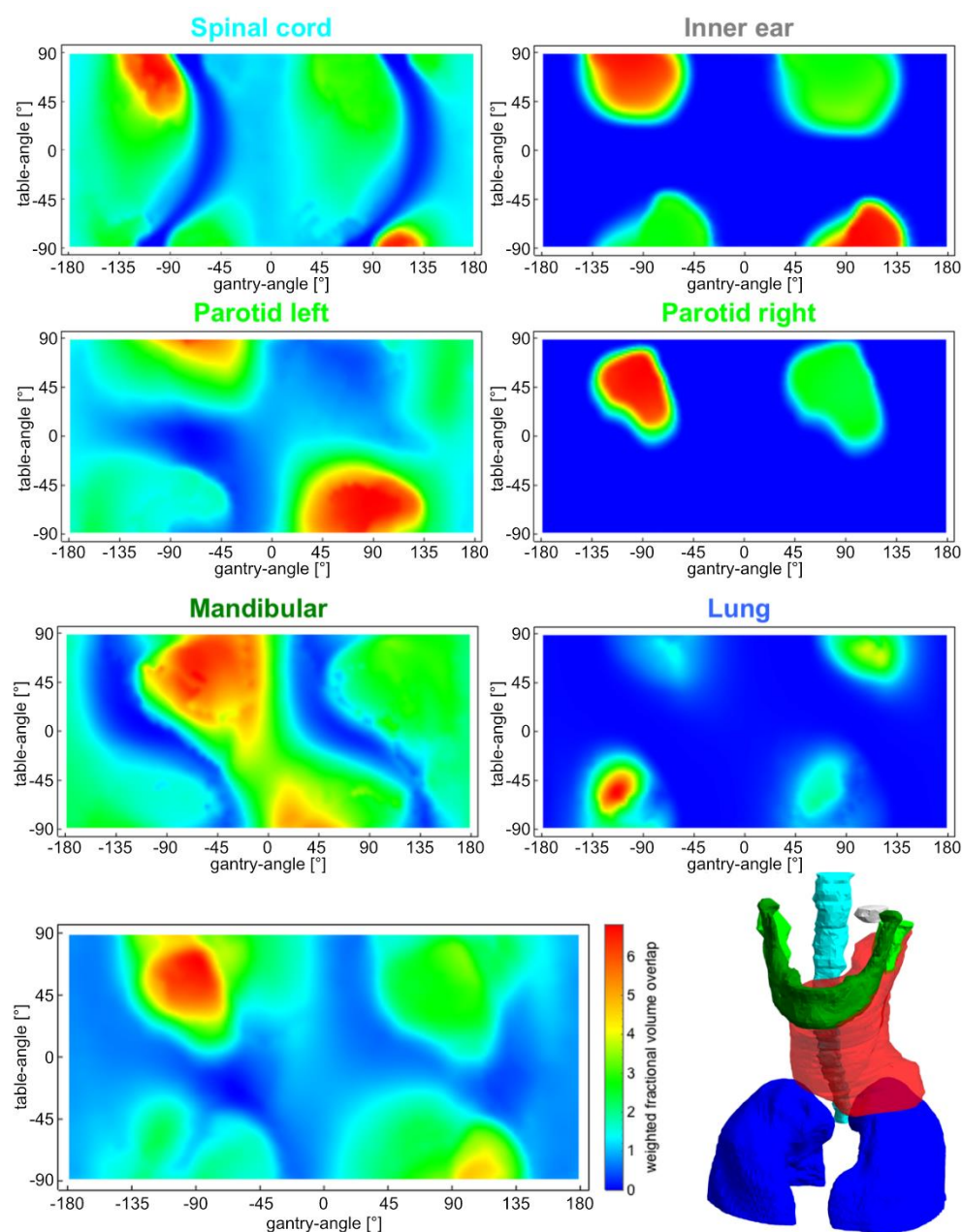


Fig. 3. The gantry-table maps for all structures considered for the first head and neck case (top three rows) together with the total gantry-table map generated as the sum of the individual gantry-table maps (bottom left). The associated structures are shown at the bottom right. The total gantry-table map is used to determine the dynamic path.

The segments that are impossible due to the limited CT scan length as well as potential collisions are illustrated in Fig. 4 for the same case as shown in Fig. 3. In this case, these segments are mainly overlapping with the larger segment due to the limited CT scan length.

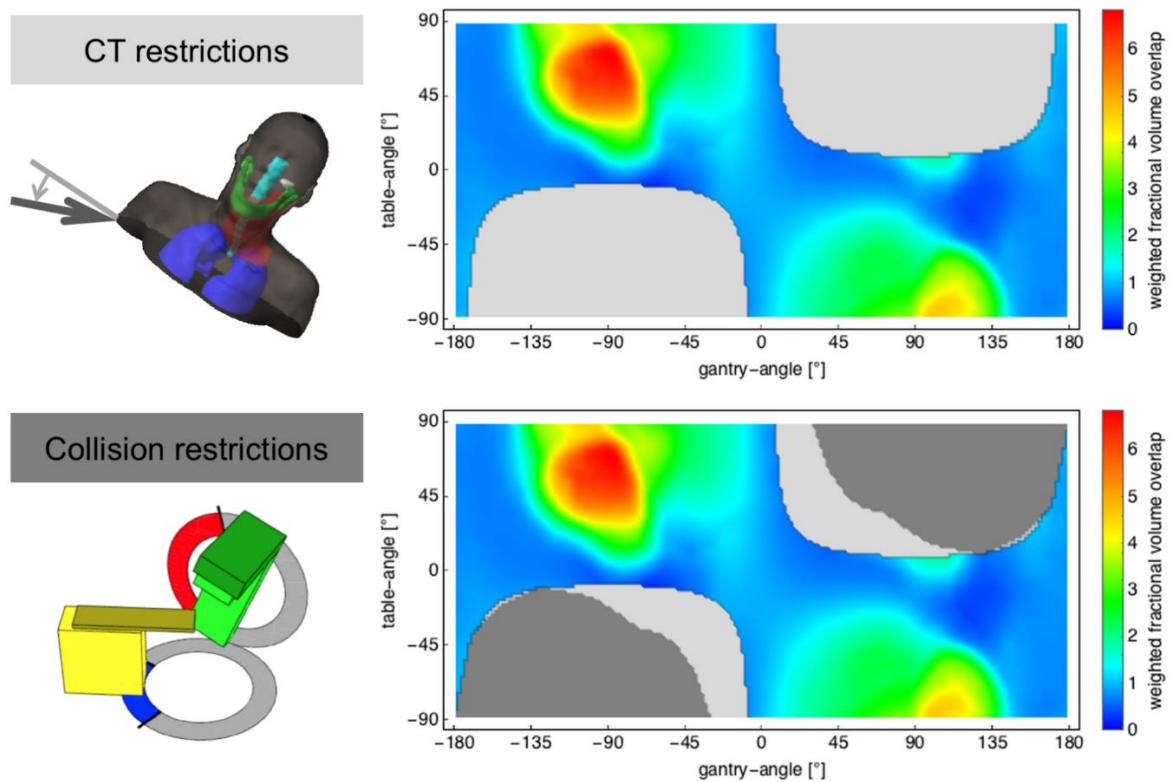


Fig. 4. Gantry-table combinations that have to be avoided due to CT scan length restrictions (top) and collision restrictions (bottom) are illustrated as gray areas.

The dynamic path with the lowest cost and covering a full gantry rotation is determined using the A* algorithm. The result is depicted in Fig. 5 as red line demonstrating that the dynamic path is strictly directed from left to right and through low value areas. The starting values of the path are at gantry angle of -180° and table rotation angle of 45° and the corresponding ending values are 180° and -30° . This optimized path is very close to disallowed segments and considering Fig. 3, it becomes clear that a path passing through these segments would have had an even lower cost. However, for this, a CT scan with an increased scan length would be necessary.

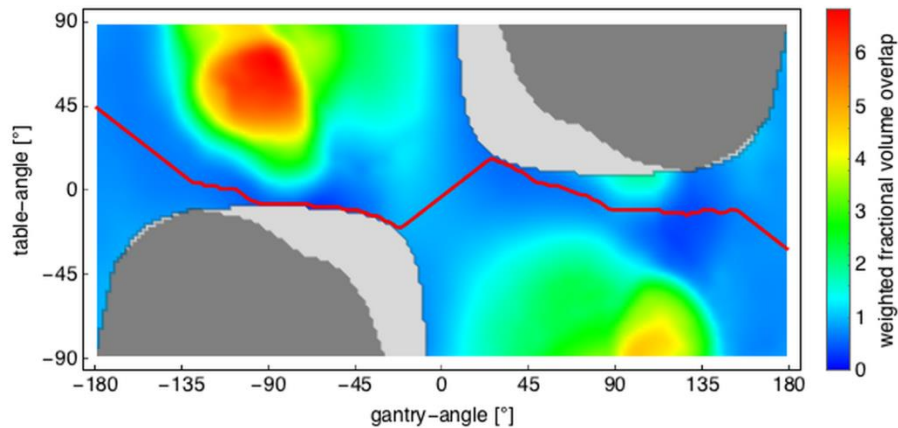


Fig. 5. Resulting dynamic path for the considered head and neck case. Based on the total gantry-table map including the restricted areas shown in Fig. 4, the gantry-table angles shown as red line are determined by the A* path search algorithm.

Based on these gantry and table rotation angles, the gantry-collimator map can be created, which is shown in Fig. 6 for the previously shown head and neck cancer case. Different collimator angle settings are illustrated for a specific gantry and table rotation angle combination. These settings result in different areas between the projected target structure and the leaf tips visible as the white areas in the plots on the left side in Fig. 6, thus leading to different values in the gantry-collimator map. It can also be seen that the gantry-collimator map for collimator angles from -180° to 0° is the same as for 0° to 180° , as a collimator rotation of 180° leads to the same area between the leaves and the projected target structure. The application of the A* algorithm with the lowest cost in the gantry-collimator map is shown as red line in the lower right plot in Fig. 6. This results in a dynamic path for the head and neck case considered, that is, dynamic settings for the gantry, table and collimator rotation angles per DICOM control point.

Applying the research version of the Eclipse VMAT photon optimizer and performing the final dose calculation using SMCP, results in a dose distribution for the DTRT treatment plan illustrated in Fig. 7 for the previously shown head and neck cancer case. The two dynamic trajectories clearly show the non-coplanar characteristics for the gantry-table settings.

The comparison with the dose distributions achieved for the two full arc conventional VMAT treatment plan is depicted in Fig. 8. There is a substantial benefit for several OARs as well as a slight improvement in the target dose homogeneity when

using DTRT compared to VMAT. The largest improvement was achieved for the spinal cord for which the $D_{2\%}$ is reduced by about 38%. The provided percentage values for the differences in the DVH parameters are provided relative to the prescribed dose if not stated otherwise. While the mean dose of the right parotid could be reduced by about 9.5%, the reduction is 3.7% for the left parotid. Moreover, for this case, all DVH curves for DTRT are improved compared with the corresponding DVH curves for the VMAT treatment plan.

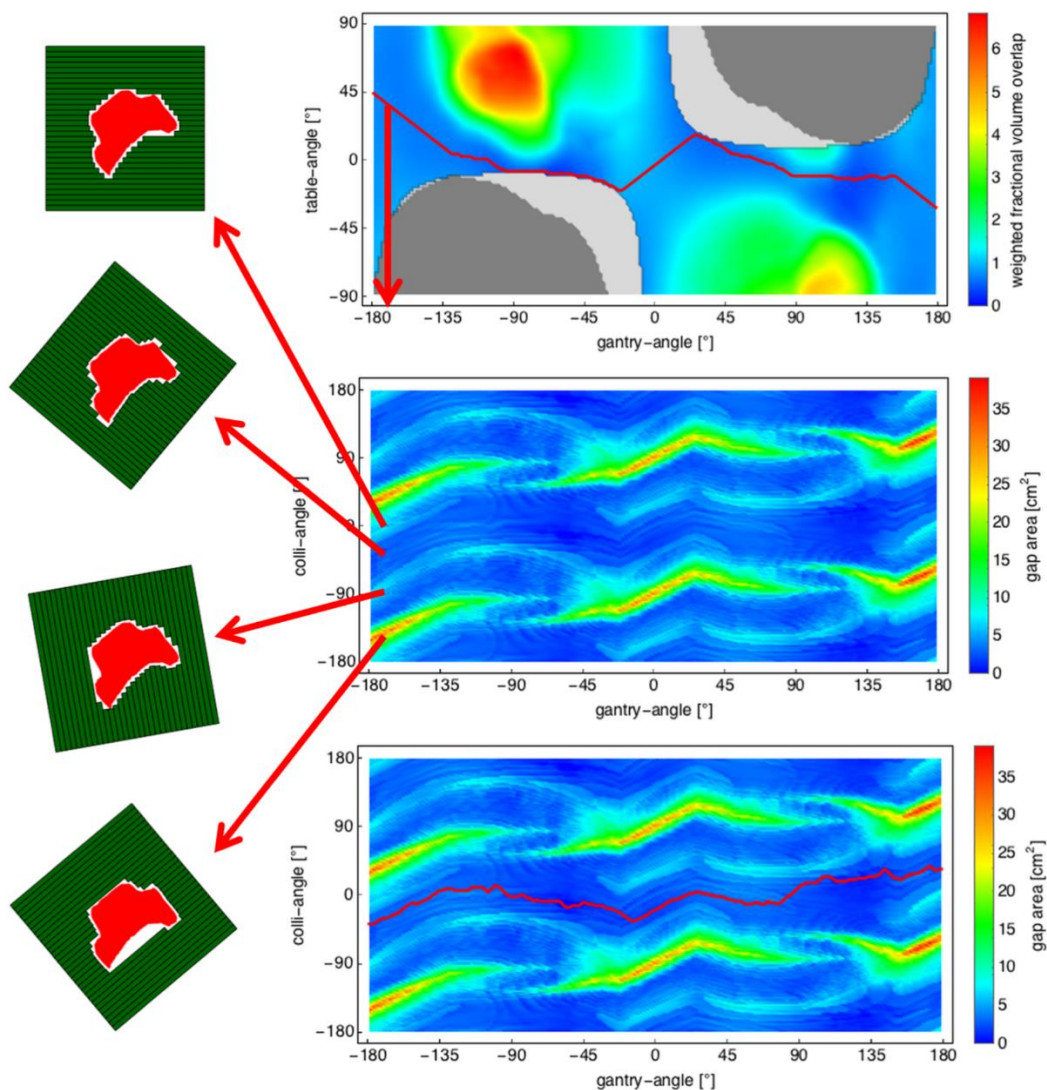


Fig. 6. For each gantry-table angle setting of the previously determined dynamic path (cf. Fig. 5), the gap area for all collimator angles are determined as indicated on the left. This leads to the gantry-collimator map as shown in the middle. Applying the A* path search algorithm for the gantry-collimator map resulted in the dynamic path depicted as red line in the gantry-collimator map at the bottom.

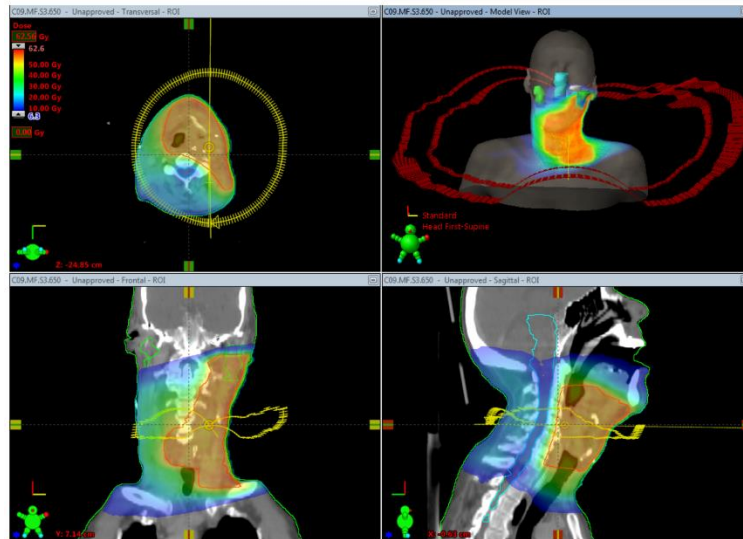


Fig. 7. Dynamic trajectories showing non-coplanar arcs are loaded into Eclipse (top right) together with the optimized leaf sequence. The final dose distribution calculated using the Swiss Monte Carlo Plan (SMCP) by means of the algorithm programming interface is illustrated in color wash.

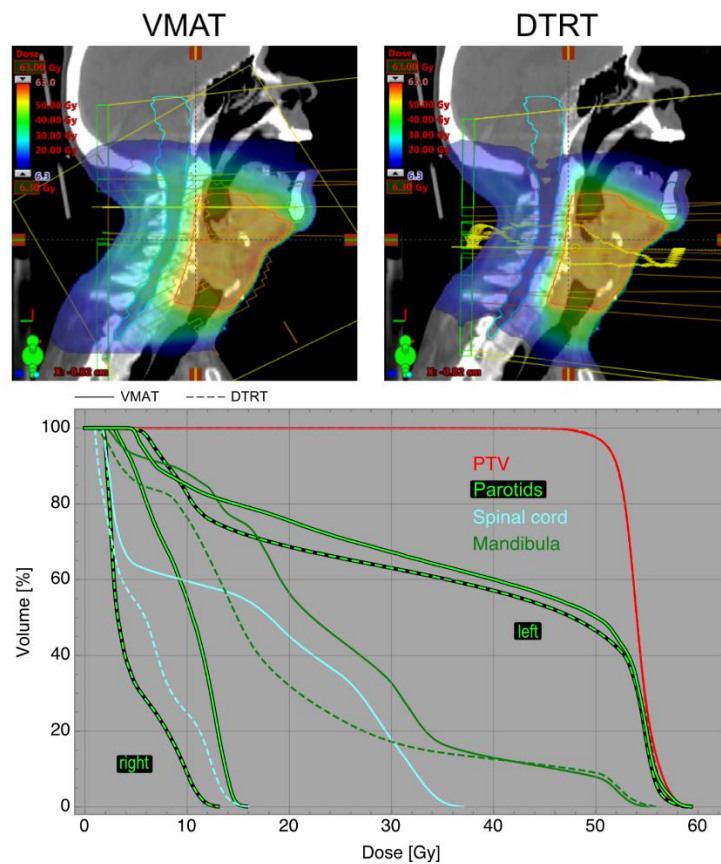


Fig. 8. The comparison of the dose distribution in a sagittal plane together with the dose volume histograms for several structures of the clinically motivated head and neck case (cf. Fig. 7). While the dose coverage and the dose homogeneity to the target structure are preserved, substantial improvements for OAR structures were achieved for the DTRT treatment plan when compared with the VMAT plan.

The two dynamic trajectories for the second head and neck case show a highly non-coplanar path as illustrated in Fig. 9. Also for this case substantial improvements were achieved when compared with a three arc VMAT plan. The target coverage was slightly improved and DVH parameters for the OARs show reductions ranging from 2.5% to 16.3% except for the mandibular, for which virtually the same $D_{2\%}$ was found. However, for this OAR a substantial benefit is reached in the low dose region. For both head and neck cases, $V_{10\%}$ of the normal tissue is reduced by about 790 cm^3 (19%) and 180 cm^3 (6%) when using the DTRT. Table I summarizes the parameters for the two head and neck cases.

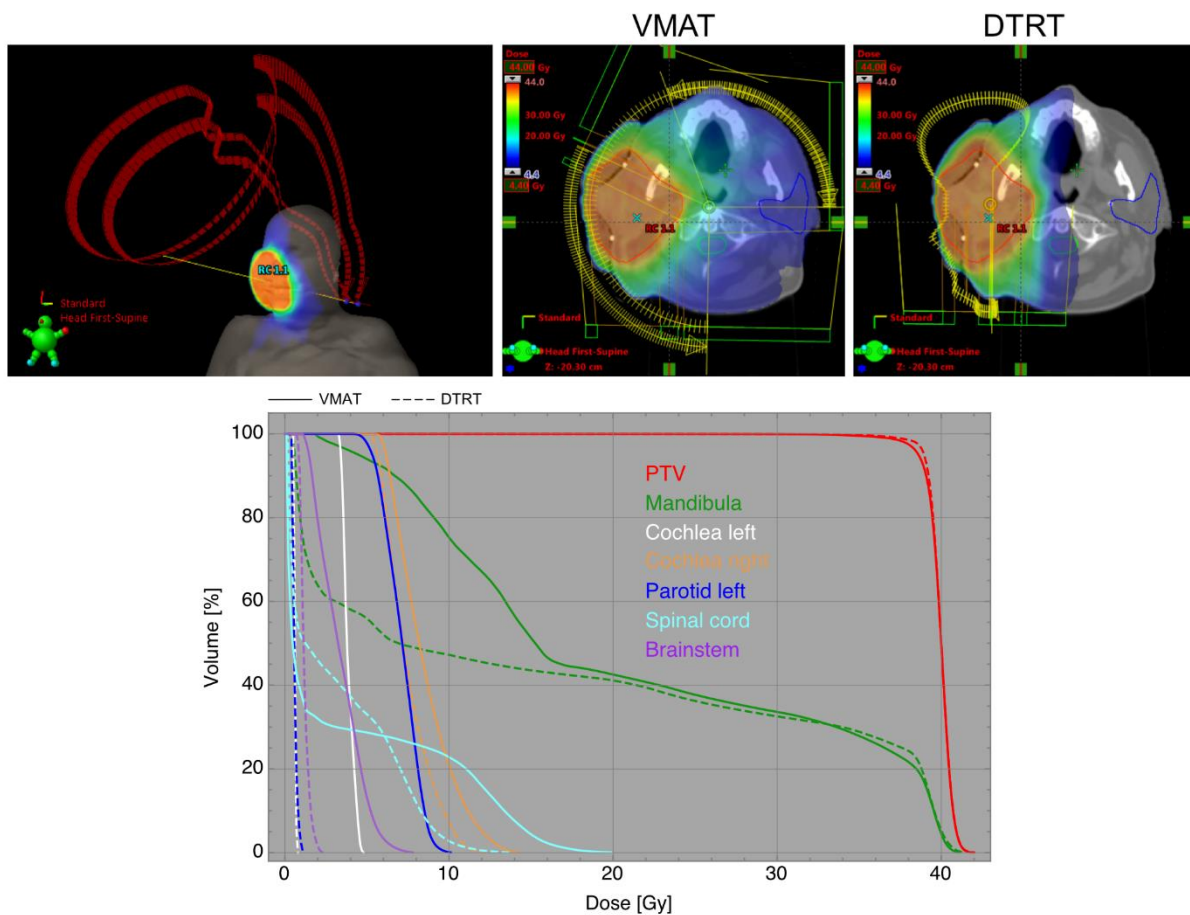


Fig. 9. The dynamic trajectories determined for the second head and neck case are shown on the top left. The comparison of the dose distribution in a transversal plane is depicted for VMAT (top middle) and DTRT (top right). The corresponding dose volume histograms for several structures are shown at the bottom. While the dose coverage and the dose homogeneity to the target structure are slightly improved, substantial improvements for OAR structures were achieved for the DTRT treatment plan when compared with the VMAT plan.

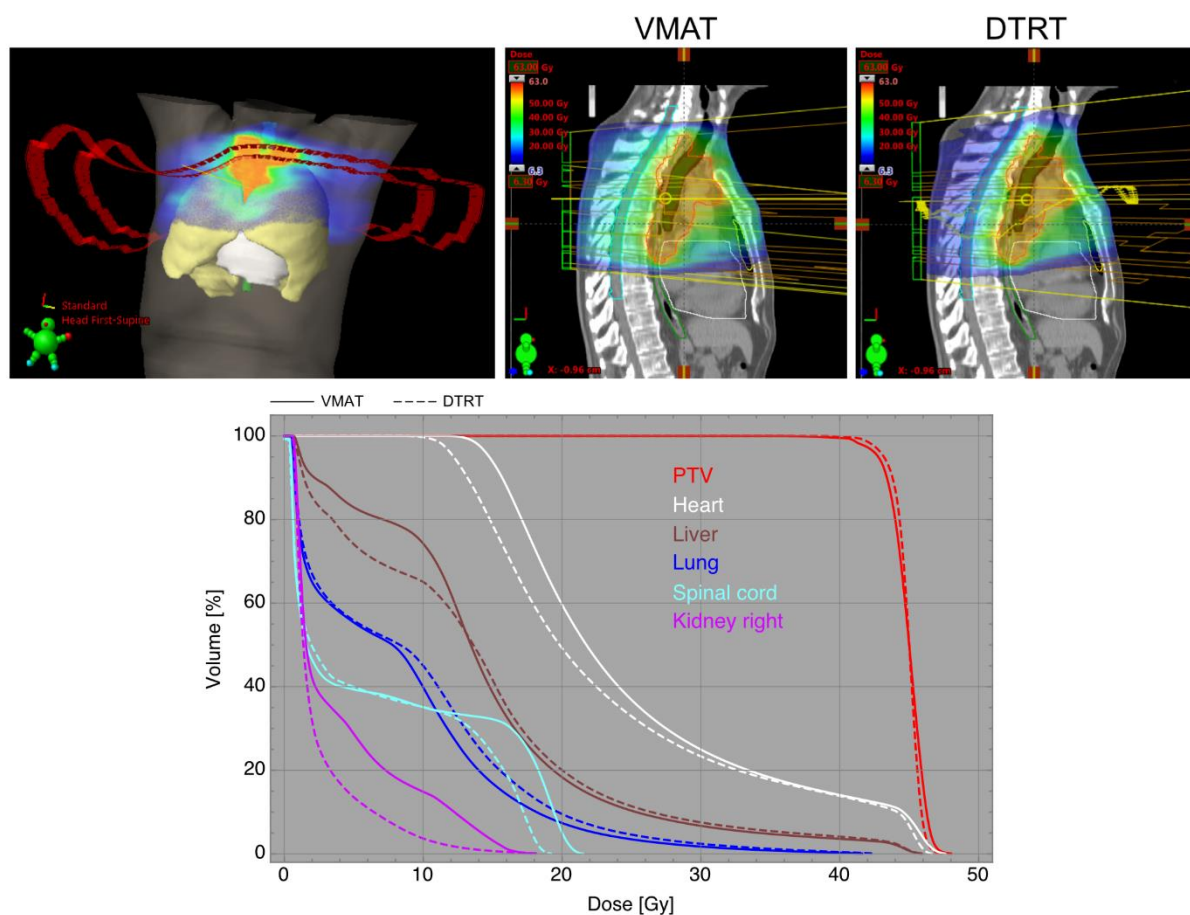
Table I. Comparison of the dose volume histogram parameters for the DTRT and the VMAT treatment plan of the two clinically motivated head and neck cases.

Parameter	Head and neck 1		Head and neck 2	
	DTRT	VMAT	DTRT	VMAT
PTV, HI (%)	89.9	86.5	98.5	97.5
Spinal cord, $D_{2\%}$ (Gy)	14.1	34.5	10.4	16.2
Parotid left, D_{mean} (Gy)	36.8	38.8	0.6	7.1
Parotid right, D_{mean} (Gy)	4.7	9.8		
Mandibula, $D_{2\%}$ (Gy)	53.2	55.1	40.5	40.4
Brain, $D_{2\%}$ (Gy)			10.4	12.0
Brainstem, $D_{2\%}$ (Gy)			1.9	6.4
Cochlea left, D_{mean} (Gy)			0.6	3.9
Cochlea right, D_{mean} (Gy)			7.5	8.5
Lips, D_{mean} (Gy)			5.1	11.5
Normal tissue, $V_{10\%}$ (cm ³)	3468	4257	2702	2882

The analogous results for the lung and the esophagus case, that is, the two thorax cases, are provided in Figs. 10 and 11 as well as in Table II. While for the DTRT two dynamic trajectories were used the VMAT treatment plans had four arcs for the lung and three arcs for the esophagus case. Also for these cases substantial improvements for the $D_{2\%}$ of the spinal cord of 22.6% and 5% for the lung and esophagus case, respectively, were achieved when using the DTRT treatment plan. Some benefits for D_{mean} between 2% and 3.6% to the heart for the two cases as well as for the esophagus in the lung case (2.4%) and the liver in the esophagus case (1.3%) were observed. The mean dose to the lung for both cases is slightly worse in the DTRT plans. The target homogeneity in the DTRT treatment plans was improved by below 1% in the lung and 3.3% in the esophagus case compared to VMAT plans. While the $V_{10\%}$ of the normal tissue is about 250 cm³ lower (2%) for DTRT in the lung case, it is slightly increased by about 80 cm³ (below 1%) for the esophagus case.

Table II. Comparison of the dose volume histogram parameters for the DTRT and the VMAT treatment plan of the clinically motivated lung and esophagus case.

Parameter	Lung		Esophagus	
	DTRT	VMAT	DTRT	VMAT
PTV, HI (%)	94.9	94.1	96.8	93.8
Spinal cord, $D_{2\%}$ (Gy)	21.0	33.2	18.3	20.6
Lung, D_{mean} (Gy)	15.8	15.7	9.6	8.9
Heart, D_{mean} (Gy)	7.4	8.5	23.6	25.2
Esophagus, D_{mean} (Gy)	28.1	29.4		
Liver, D_{mean} (Gy)			13.9	14.4
Normal tissue, $V_{10\%}$ (cm ³)	10,474	10,718	11,493	11,415

**Fig. 10.** The dynamic trajectories determined for the lung case are shown on the top left. The comparison of the dose distribution in a sagittal plane is depicted for VMAT (top middle) and DTRT (top right). The corresponding dose volume histograms for several structures are shown at the bottom. While the dose coverage and the dose homogeneity to the target structure are slightly improved, substantial improvements for OAR structures were achieved for the DTRT treatment plan when compared with the VMAT plan.

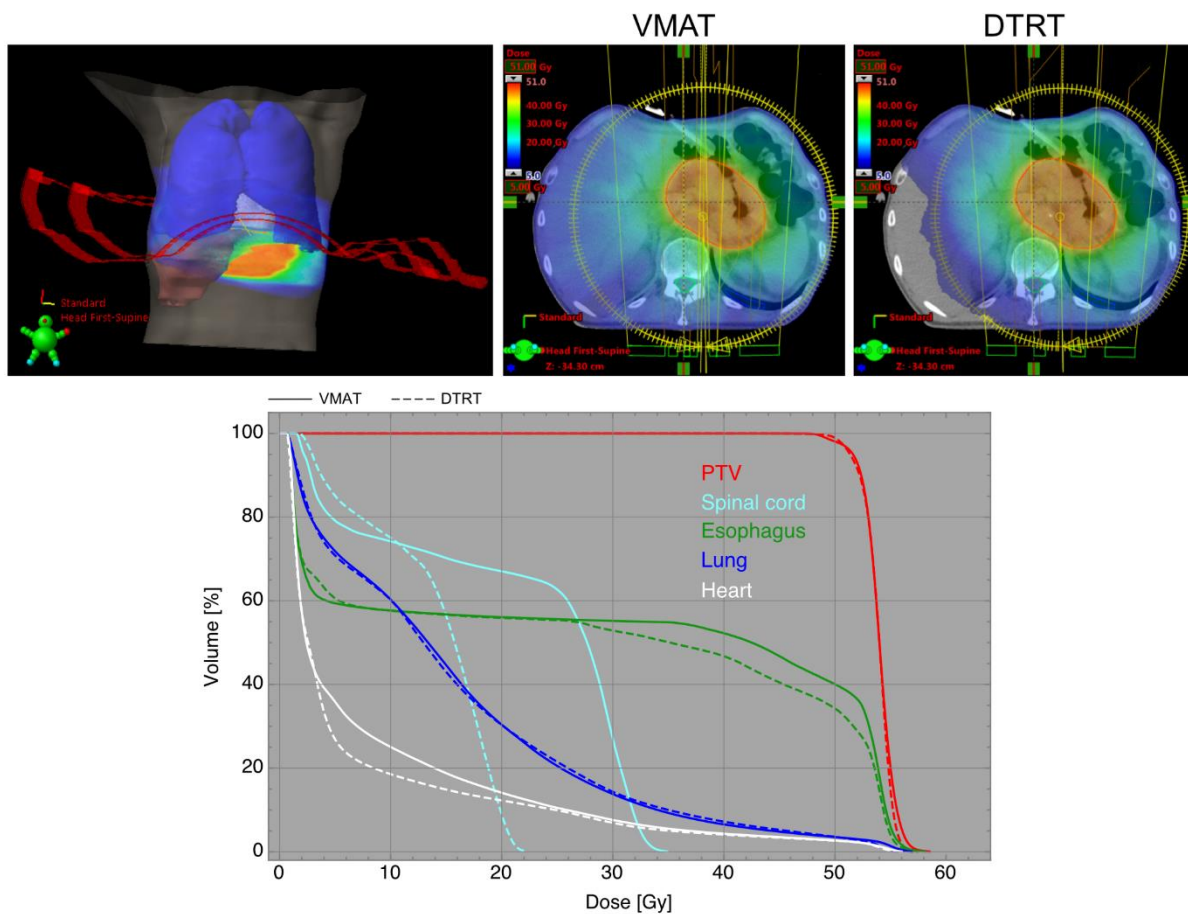


Fig. 11. The dynamic trajectories determined for the esophagus case are shown on the top left. The comparison of the dose distribution in a transversal plane is depicted for VMAT (top middle) and DTRT (top right). The corresponding dose volume histograms for several structures are shown at the bottom. While the dose coverage and the dose homogeneity to the target structure are slightly improved, improvements for OAR structures were achieved for the DTRT treatment plan when compared with the VMAT plan.

The final comparison was performed for the prostate case using two dynamic trajectories for the DTRT treatment plan and two full arcs for the VMAT plan. The corresponding results are presented in Fig. 12 and Table III. While the target homogeneity is almost the same for both techniques, improvements in DVH parameters range from below 1% for D_{mean} to the right femoral head up to about 5% for D_{mean} of the bladder as well as to about 8% and 5% for the $V_{50\%}$ to the bladder and rectum, respectively. The value achieved for $V_{10\%}$ of the normal tissue for the DTRT plan was slightly increased by about 25 cm³ (below 1%) compared to the VMAT plan.

To deliver DTRT treatment plan of the second head and neck case on the TrueBeam linear accelerator, the treatment plan data were converted in an xml file suitable as input for the developer mode of the TrueBeam. The resulting dose distribution from the film

measurements was compared with the corresponding calculated dose distribution as shown in Fig. 13. The agreement between measured and calculated dose values is generally within 2% of the prescribed dose. The two-dimensional gamma analysis using 2% and 2 mm criteria and a threshold of 10% resulted in a passing rate of more than 99.5%.

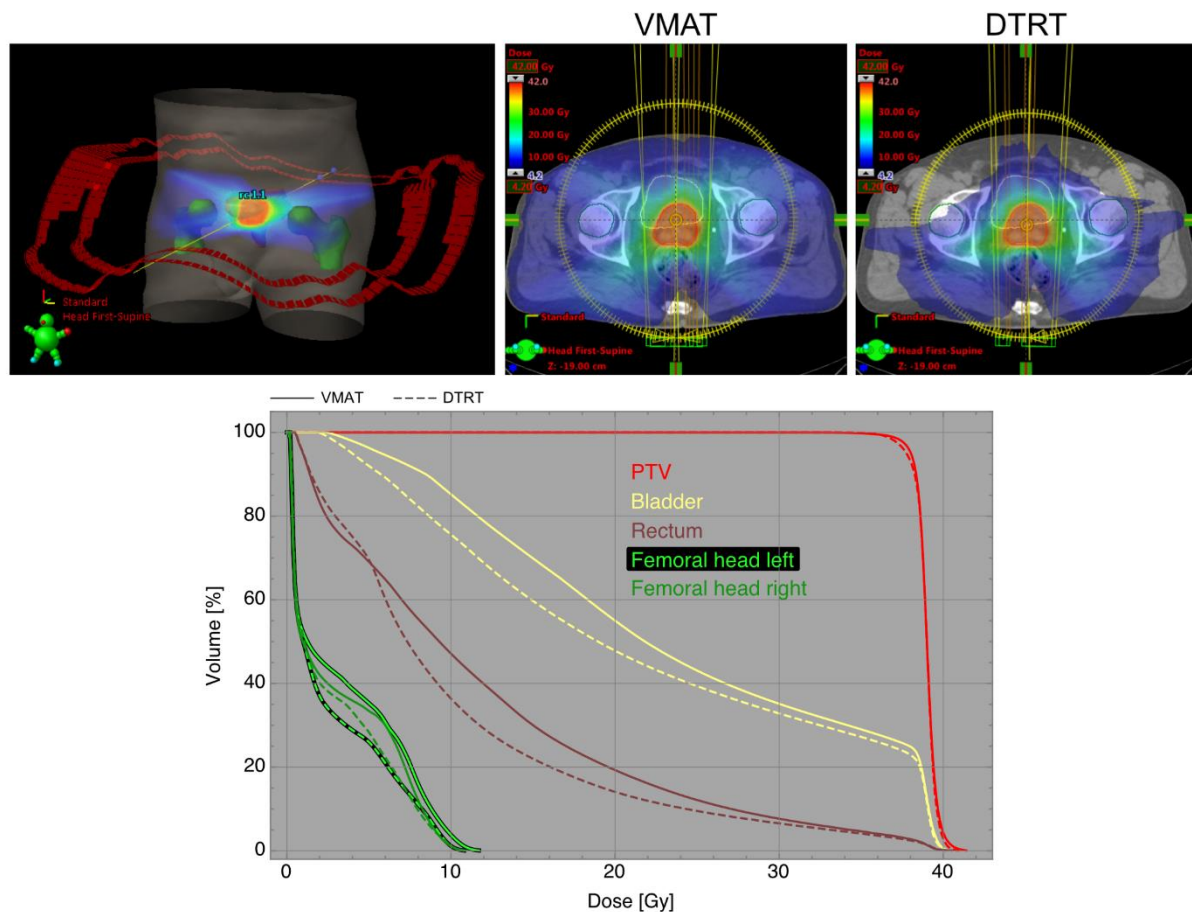
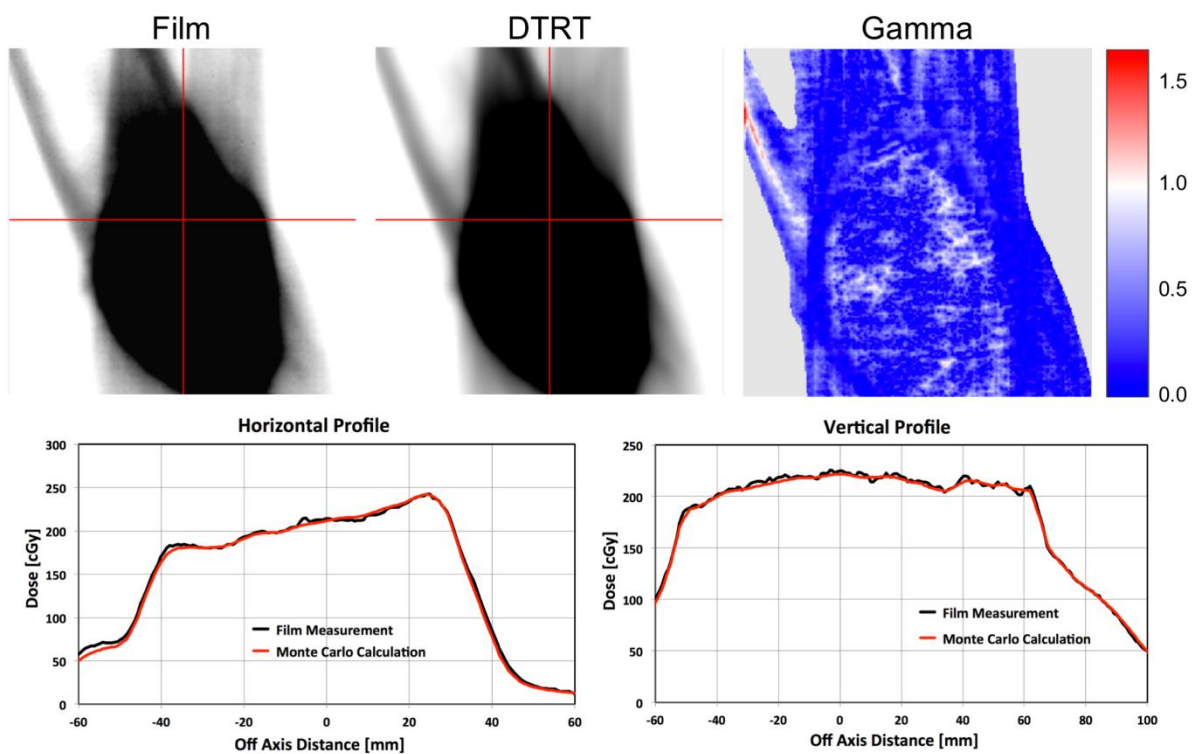


Fig. 12. The dynamic trajectories determined for the prostate case are shown on the top left. The comparison of the dose distribution in a transversal plane is depicted for VMAT (top middle) and DTRT (top right). The corresponding dose volume histograms for several structures are shown at the bottom. While the dose coverage and the dose homogeneity to the target structure is slightly worse, improvements for OAR structures were achieved for the DTRT treatment plan when compared with the VMAT plan.

Table III. Comparison of the dose volume histogram parameters for the DTRT and the VMAT treatment plan of the clinically motivated prostate case.

Parameter	Prostate	
	DTRT	VMAT
PTV, HI	97.9	98.3
Bladder, D_{mean} (Gy)	21.6	23.6
Bladder, $V_{50\%}$ (%)	48.9	56.5
Bladder, $V_{70\%}$ (%)	36.2	39.1
Rectum, D_{mean} (Gy)	10.4	11.9
Rectum, $V_{50\%}$ (%)	14.7	20.2
Rectum, $V_{70\%}$ (%)	8.0	9.8
Femoral head left, D_{mean} (Gy)	2.7	3.4
Femoral head right, D_{mean} (Gy)	2.9	3.1
Normal tissue, $V_{10\%}$ (cm ³)	3028	3002

**Fig. 13.** Comparison of film measured (top left) with calculated dose values (top middle) of the DTRT treatment plan for the second head and neck case. Gamma value distribution (top right) using 2% and 2 mm criteria results in a passing rate of more than 99.5% (gray area show data falling below the threshold of 10%). The bottom row shows the horizontal and vertical dose profile comparisons along the lines indicated in the top row.

4. Discussion and conclusions

In this work, treatment plans for DTRT showed substantial improvements for DVH parameters of OARs, while at least preserving the dose coverage and dose homogeneity to the target structure when compared to the corresponding parameters for VMAT treatment plans of several different treatment sites. Improvements in OARs for non-coplanar treatment techniques are in agreement with findings from other studies, although the level of improvement is spread over a large range.^{5–10,13,15,16,22} This might depend on the specific and different patient cohort considered in the various studies.

It is worth mentioning that the number of dynamic trajectories in the DTRT treatment plan is less or equal to the number of arcs in the corresponding VMAT plan. Thereby, the number of Monitor Units (MU) is lower for the DTRT plan in four of the five cases. The decrease ranges from 1.5% for the second head and neck case up to 47% for the esophagus case. However, the number of MUs increased by 12% for the prostate case. This confirms similar results found in other studies.^{12,20,22} Aside from the numbers of MUs the treatment delivery time is of importance. On average, the beam on time increased for DTRT treatment plans by about 20% when compared with the VMAT plans, which is mainly due to the lower maximum table rotation speed of 3°/s in comparison with the gantry rotation speed of 6°/s.

While the achieved benefits for the DTRT are substantial for the head and neck cases, they are less emphasized for targets of the trunk. One reason is that for targets in the body region the range of suitable table angles is restricted due to collisions. Another reason encountered especially in the lung and esophagus case is that the target structure is virtually completely surrounded by OARs, thus, even the enlarged degrees of freedom do only provide beam directions that have fewer benefits when compared to head and neck cases.

To efficiently perform the DTRT optimization the major part of the dynamic trajectory optimization is written in C++. Furthermore, the entire generation of the DTRT treatment plan is fully automated given the user-specific information such as which OAR to be considered or the starting gantry angle and the range of the gantry rotation. In this mode also, the final MC dose calculation is performed automatically

before the result is loaded back into Eclipse. The computation time needed to generate the gantry-table maps is about 1 min, while the determination of the dynamic paths takes only a few seconds. The time for optimization using the research VMAT optimizer is the same as for conventional VMAT optimizations (on the order of several minutes). The computation time needed for the final dose calculation using SMCP achieving a statistical uncertainty of 1.5% was between about 10 and 15 min on a Linux cluster using 40 cores of Intel Xeon CPUs (type E5-2650 or similar) depending on the case.

In this study, CT data acquired for conventional treatments were used for DTRT. However, due to the increased range of beam directions, CT data with an increased scan length could further exploit the potential of DTRT, which was not in the scope of the current investigation, but will be studied in more detail in future work.

The DTRT optimization applied in this work benefits from the additional degrees of freedom by means of including dynamic table and collimator rotation in the optimization, which are currently supported by the research VMAT photon optimizer. Thereby, these additional dynamic components were described by DICOM control points analogous to the position of the gantry and the MLC leaves. In contrast to other studies in which the additional dynamic components were approximated as a series of static positions, in this work, the components are dynamically moving during beam delivery. This continuously irradiation is also taken into account in the dose calculation using the SMCP.

In this work, the determination of the gantry-collimator map is based on geometry aiming to guide the intensity-modulation optimizer. There are alternative approaches that might lead to more optimal collimator angles, for example, selecting the collimator angle leading to the smallest travelling distance. This is part of further investigations.

The results for the DTRT treatment plans presented in this work take all OAR specific gantry-table maps into account using the same weight. However, the procedure also works when different gantry-table map weights are applied for different OARs. This would lead to a different total gantry-table map with an increased emphasize on dose sparing to higher weighted OAR gantry-table maps. These weights can also indirectly influence the impact of the dose objectives on the optimized dynamic path, as these are not independent from each other. Thus, to further optimize the DTRT treatment

plans an iterative process can be defined. For a DTRT treatment plan the optimizer also returns cost function values for all structures. Those values can be analyzed to determine the structure with the highest cost. In the next iteration, the weight of this structure map in the total gantry-table map can be increased. Alternatively, however not automatically, the user can increase the weight of an OAR gantry-table map for which the dose distribution should be improved. The search of a new dynamic path in the modified total gantry-table map by means of the A* algorithm might improve the sparing of the structure in this iteration step, which takes only a calculation time of a few seconds. Then, for the new determined dynamic path the optimization and final dose calculation can be performed again. Currently, the number of iterations is one as was also used in this work. However, the performance of such an iterative procedure will be explored in future studies.

In conclusion, the results presented for DTRT treatments suggest a high potential to efficiently improve treatment plans compared to conventional VMAT plans.

Acknowledgments

This work was supported by Varian Medical Systems. The MC dose calculations were performed on UBELIX (www.id.unibe.ch/hpc), the high-performance-computing cluster at the University of Bern.

References

1. Yu CX. Intensity-modulated arc therapy with dynamic multileaf collimation: an alternative to tomotherapy. *Phys Med Biol.* 1995;40:1435–1449.
2. Spirou SV, Chui CS. Generation of arbitrary intensity profiles by dynamic jaws or multileaf collimators. *Med Phys.* 1994;21:1031–1041.
3. Otto K. Volumetric modulated arc therapy: IMRT in a single gantry arc. *Med Phys.* 2008;35:310–317.
4. Verbakel WF, Cuijpers JP, Hoffmans D, Bieker M, Slotman BJ, Senan S. Volumetric intensity-modulated arc therapy vs. conventional IMRT in head-and-neck cancer: a comparative planning and dosimetric study. *Int J Radiat Oncol Biol Phys.* 2009;74:252–259.
5. Rwigema JC, Nguyen D, Heron DE, *et al.* 4pi noncoplanar stereotactic body radiation therapy for head-and-neck cancer: potential to improve tumor control and late toxicity. *Int J Radiat Oncol Biol Phys.* 2015;91:401–409.
6. Dong P, Lee P, Ruan D, *et al.* 4pi noncoplanar stereotactic body radiation therapy for centrally located or larger lung tumors. *Int J Radiat Oncol Biol Phys.* 2013;86:407–413.
7. Dong P, Lee P, Ruan D, *et al.* 4pi non-coplanar liver SBRT: a novel delivery technique. *Int J Radiat Oncol Biol Phys.* 2013;85:1360–1366.
8. Nguyen D, Rwigema JC, Yu VY, *et al.* Feasibility of extreme dose escalation for glioblastoma multiforme using 4pi radiotherapy. *Radiat Oncol.* 2014;9:239.
9. MacDonald RL, Thomas CG. Dynamic trajectory-based couch motion for improvement of radiation therapy trajectories in cranial SRT. *Med Phys.* 2015;42:2317–2325.
10. Liang J, Atwood T, von Eyben R, *et al.* Trajectory modulated arc therapy: a fully dynamic delivery with synchronized couch and gantry motion significantly improves dosimetric indices correlated with poor cosmesis in accelerated partial breast irradiation. *Int J Radiat Oncol Biol Phys.* 2015;92:1148–1156.

11. Fahimian B, Yu V, Horst K, Xing L, Hristov D. Trajectory modulated prone breast irradiation: a LINAC-based technique combining intensity modulated delivery and motion of the couch. *Radiother Oncol.* 2013;109:475–481.
12. Shaitelman SF, Kim LH, Yan D, Martinez AA, Vicini FA, Grills IS. Continuous arc rotation of the couch therapy for the delivery of accelerated partial breast irradiation: a treatment planning analysis. *Int J Radiat Oncol Biol Phys.* 2011;80:771–778.
13. Krayenbuehl J, Davis JB, Ciernik IF. Dynamic intensity-modulated noncoplanar arc radiotherapy (INCA) for head and neck cancer. *Radiother Oncol.* 2006;81:151–157.
14. Papp D, Bortfeld T, Unkelbach J. A modular approach to intensity modulated arc therapy optimization with noncoplanar trajectories. *Phys Med Biol.* 2015;60:5179–5198.
15. Smyth G, Bamber JC, Evans PM, Bedford JL. Trajectory optimization for dynamic couch rotation during volumetric modulated arc radiotherapy. *Phys Med Biol.* 2013;58:8163–8177.
16. Smyth G, Evans PM, Bamber JC, *et al.* Non-coplanar trajectories to improve organ at risk sparing in volumetric modulated arc therapy for primary brain tumors. *Radiother Oncol.* 2016;121:124–131.
17. Wild E, Bangert M, Nill S, Oelfke U. Noncoplanar VMAT for nasopharyngeal tumors: plan quality versus treatment time. *Med Phys.* 2015;42:2157–2168.
18. Podgorsak EB, Olivier A, Pla M, Lefebvre PY, Hazel J. Dynamic stereotactic radiosurgery. *Int J Radiat Oncol Biol Phys.* 1988;14:115–126.
19. Popescu CC, Beckham WA, Patenaude VV, Olivotto IA, Vlachaki MT. Simultaneous couch and gantry dynamic arc rotation (CG-Darc) in the treatment of breast cancer with accelerated partial breast irradiation (APBI): a feasibility study. *J Appl Clin Med Phys.* 2013;14:4035.
20. Zhang P, Happersett L, Yang Y, Yamada Y, Mageras G, Hunt M. Optimization of collimator trajectory in volumetric modulated arc therapy: development and evaluation for paraspinal SBRT. *Int J Radiat Oncol Biol Phys.* 2010;77:591–599.
21. MacDonald RL, Thomas CG, Syme A. Dynamic collimator trajectory algorithm for multiple metastases dynamic conformal arc treatment planning. *Med Phys.* 2018;45:5–17.

22. Yang Y, Zhang P, Happersett L, *et al.* Choreographing couch and collimator in volumetric modulated arc therapy. *Int J Radiat Oncol Biol Phys.* 2011;80:1238–1247.
23. Locke CB, Bush KK. Trajectory optimization in radiotherapy using sectioning (TORUS). *Med Phys.* 2017;44:3375–3392.
24. Fix MK, Manser P, Frei D, Volken W, Mini R, Born EJ. An efficient framework for photon Monte Carlo treatment planning. *Phys Med Biol.* 2007;52:N425–N437.
25. Bush K, Townson R, Zavgorodni S. Monte Carlo simulation of RapidArc radiotherapy delivery. *Phys Med Biol.* 2008;53:N359–N370.
26. Magaddino V, Manser P, Frei D, *et al.* Validation of the Swiss Monte Carlo Plan for a static and dynamic 6 MV photon beam. *Z Med Phys.* 2011;21:124–134.
27. Fix MK, Frauchiger D, Henrich L, *et al.* OC-0277: a Monte Carlo verification tool for dynamic trajectory radiotherapy. *Radiother Oncol.* 2014;111:S107.
28. Manser P, Frauchiger D, Frei D, Volken W, Terribilini D, Fix MK. Dose calculation of dynamic trajectory radiotherapy using Monte Carlo. *Z Med Phys.* 2018. <https://doi.org/10.1016/j.zemedi.2018.03.002>.
29. Hart PE, Nilsson NJ, Raphael B. A formal basis for the heuristic determination of minimum cost paths. *EEE Trans Syst Sci Cybern.* 1968;4:100–107.
30. Kawrakow I, Fippel M. VMC++, a MC algorithm optimized for electron and photon beam dose calculations for RTP. In: *Proceedings of the 22nd Annual International Conference of the IEEE.* Piscataway, NJ: Engineering in Medicine and Biology Society; 2000.

6**Part 2: Dynamic mixed beam radiotherapy
(DYMBER): Photon dynamic trajectories
combined with modulated electron beams**

**S. Mueller¹, P. Manser¹, W. Volken¹, D. Frei¹, R. Kueng¹, E. Herrmann¹,
O. Elicin¹, D.M. Aebersold¹, M.F.M. Stampanoni² and M.K. Fix¹**

- 1: Division of Medical Radiation Physics and Department of Radiation Oncology, Inselspital, Bern University Hospital, and University of Bern, Bern, Switzerland
- 2: Institute for Biomedical Engineering, ETH Zürich and PSI, Villigen, Switzerland

published in
Medical Physics

2018, Vol. 45, 4213-4226

<https://doi.org/10.1002/mp.13085>

Abstract

Purpose: The purpose of this study was to develop a treatment technique for dynamic mixed beam radiotherapy (DYMBER) utilizing increased degrees of freedom (DoF) of a conventional treatment unit including different particle types (photons and electrons), intensity and energy modulation and dynamic gantry, table, and collimator rotations.

Methods: A treatment planning process has been developed to create DYMBER plans combining photon dynamic trajectories (DTs) and step and shoot electron apertures collimated with the photon multileaf collimator (pMLC). A gantry-table path is determined for the photon DTs with minimized overlap of the organs at risk (OARs) with the target. In addition, an associated dynamic collimator rotation is established with minimized area between the pMLC leaves and the target contour. pMLC sequences of photon DTs and electron pMLC apertures are then simultaneously optimized using direct aperture optimization (DAO). Subsequently, the final dose distribution of the electron pMLC apertures is calculated using the Swiss Monte Carlo Plan (SMCP). The pMLC sequences of the photon DTs are then re-optimized with a finer control point resolution and with the final electron dose distribution taken into account. Afterwards, the final photon dose distribution is calculated also using the SMCP and summed together with the one of the electrons. This process is applied for a brain and two head and neck cases. The resulting DYMBER dose distributions are compared to those of dynamic trajectory radiotherapy (DTRT) plans consisting only of photon DTs and clinically applied VMAT plans. Furthermore, the deliverability of the DYMBER plans is verified in terms of dosimetric accuracy, delivery time and collision avoidance. For this purpose, The DYMBER plans are delivered to Gafchromic EBT3 films placed in an anthropomorphic head phantom on a Varian TrueBeam linear accelerator.

Results: For each case, the dose homogeneity in the target is similar or better for DYMBER compared to DTRT and VMAT. Averaged over all three cases, the mean dose to the parallel OARs is 16% and 28% lower, $D_{2\%}$ to the serial OARs is 17% and 37% lower and $V_{10\%}$ to normal tissue is 12% and 4% lower for the DYMBER plans compared to the DTRT and VMAT plans, respectively. The DYMBER plans are delivered without collision and with a 4–5 min longer delivery time than the VMAT

plans. The absolute dose measurements are compared to calculation by gamma analysis using 2% (global)/2 mm criteria with passing rates of at least 99%.

Conclusions: A treatment technique for DYMBER has been successfully developed and verified for its deliverability. The dosimetric superiority of DYMBER over DTRT and VMAT indicates utilizing increased DoF to be the key to improve brain and head and neck radiation treatments in future.

Key words: dynamic trajectory, mixed beam radiotherapy, Monte Carlo, treatment planning

1. Introduction

Generally, improvements in treatment quality accomplished by novel photon and electron treatment techniques are usually due to accessing previously unexploited degrees of freedom (DoF). With the introduction of intensity modulated radiation therapy (IMRT)¹ for instance, intensity modulation enabled by the photon multileaf collimator (pMLC) was applied to photon beams. The result is a higher dose conformity to the target compared to 3D conformal radiotherapy.¹ The plan quality of IMRT could be maintained using volumetric modulated arc therapy (VMAT) with the additional advantage of improved efficiency.^{2,3} The key for this improvement is to dynamically rotate the gantry during beam on and still allow intensity modulation. Nowadays, IMRT and VMAT are state-of-the-art treatment techniques in clinical routine, also due to the availability of appropriate quality assurance procedures.

More recently, additional treatment techniques like 4π radiotherapy⁴ and dynamic trajectory radiotherapy (DTRT)^{5–12} have been studied in research. Both use table rotations to allow noncoplanar beam setups leading to improved plan quality. In contrast to 4π radiotherapy, which uses static field directions, DTRT approaches rotate gantry and table dynamically along a predetermined path leading to improved efficiency.⁹ Dynamic collimator rotation was additionally added to VMAT¹³ and DTRT,^{6,12} yielding increased freedom for the pMLC optimization.

The DoF have also been extended for electron therapy, for example, modulated electron radiotherapy (MERT)^{14–22} combines intensity and energy modulation. The typically available electron beam energies of 6–22 MeV offer a large variety of different particle ranges. Superficial targets up to a depth of 5 cm could be treated with a homogeneous dose coverage. If photon beams are added to electron beams, called mixed beam radiotherapy (MBRT),^{16,23–33} then this restriction in the target depth is removed. It was shown for targets with at least some superficial part that treatment plan quality of coplanar step and shoot MBRT plans with simultaneously optimized photon and electron beams is substantially improved compared to IMRT and VMAT plans, because of the additional DoF of two different particle types.^{28,29,32,33} At the same time, clinical workflow could be maintained, because photon and electron beams are usually both

available on the same conventional treatment unit and using the pMLC also for electron beam collimation means that no accessory is required to be attached to the treatment unit. Miguez *et al.* demonstrated this for accelerated partial breast irradiations with promising clinical results.³¹ In the research field of MBRT, photon beams are neither applied with any dynamic gantry, table, or collimator rotations nor in a noncoplanar field setup. Thus, there is still unexplored potential to improve treatment plan quality and efficiency of MBRT. Integrating all of the mentioned dynamic rotations in MBRT would even result in a treatment technique that utilizes more DoF of a conventional treatment unit than any other treatment technique presented before.

The aim of this work is to develop a treatment technique for dynamic mixed beam radiotherapy (DYMBER) utilizing increased DoF of a conventional treatment unit including the different particle types, intensity and energy modulation and dynamic gantry, table, and collimator rotations. For this purpose, a treatment planning process (TPP) is developed to create treatment plans combining photon dynamic trajectories (DTs) and step and shoot pMLC collimated electron apertures. We demonstrate the dosimetric superiority of DYMBER over DTRT and VMAT for several clinical cases and verify its deliverability in terms of dosimetric accuracy, delivery time and collision avoidance.

2. Materials and methods

In this work, a TPP to create DYMBER plans consisting of photon DTs and electron pMLC apertures is developed. For clarification, the dynamic components of a photon DT are described by a gantry-table and a gantry-collimator path and a pMLC sequence. For each control point, these three parts define the gantry, table, and collimator rotation angles, the position of each pMLC leaf and the cumulated monitor units (MUs). In this definition, the direction of the gantry rotation is never changed. Moreover, secondary collimator jaw positions are fixed such that the conformal openings to the target are encompassed for each control point. The photon DTs presented in this work have always a beam energy of 6 MV assigned.

The mentioned TPP and the Monte Carlo (MC) simulations included in this TPP are described in more detail in the first two subchapters. The third subchapter describes the investigations of the potential of DYMBER. There, the TPP is applied to a TrueBeam linear accelerator (Varian Medical Systems, Palo Alto, CA) equipped with a Millennium 120 pMLC (Varian Medical Systems).

2.A. Treatment planning process

The TPP illustrated in Fig. 1 starts by defining the electron fields, which are later used to generate electron pMLC apertures to be delivered in a step and shoot manner. An electron field definition requires the specification of gantry and collimator angles, isocenter position and beam energy. Typically, a field definition is duplicated for all available electron beam energies. For pMLC collimated electron beams, it is suggested to use a reduced source-to-surface distance (SSD) to yield a shorter penumbra, because of reduced particle in-air scatter.^{17,34,35} Therefore, the isocenter position is chosen such that the SSD is as short as possible, but still large enough to avoid collisions between the gantry and the patient and table. The resulting SSD is typically in the range of 70-82.5 cm. The opening of the secondary collimator jaws is set fixed to $15 \times 35 \text{ cm}^2$ for each electron field as required by the utilized beam model for dose calculation.³⁶ In this work, the gantry angles are chosen such that each part of the PTV could be covered by at least one electron field with a perpendicular incidence angle. However, the

maximal number of electron beam directions is currently limited to three such that delivery time is not inappropriately prolonged due to the corresponding isocenter changes.

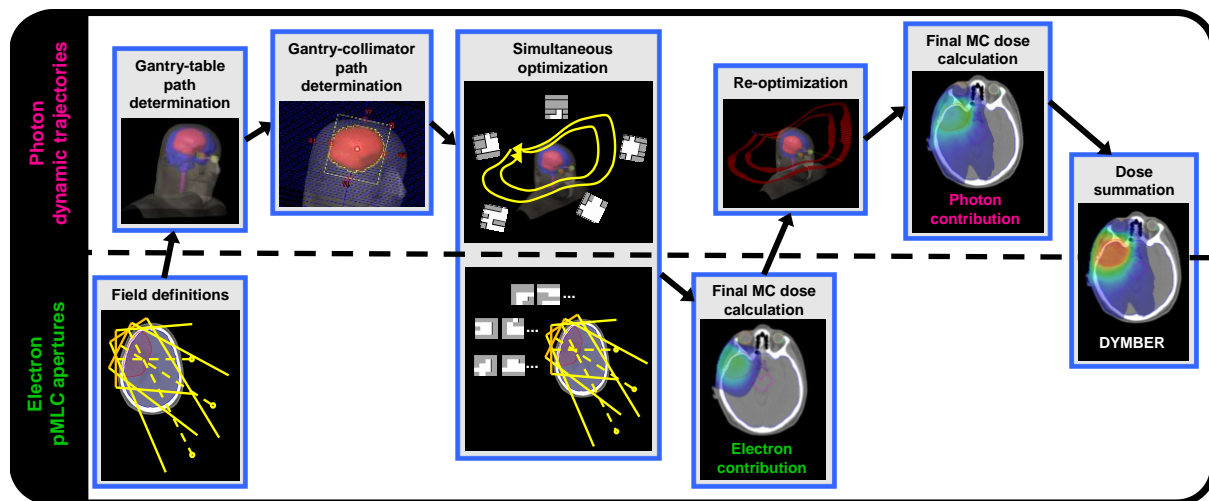


Fig. 1. The treatment planning process used to create DYMBER plans. All sub processes (boxes with blue border) displayed in the upper, the lower, or over both halves of the illustration deal with the photon DTs, electron pMLC apertures or both, respectively.

Next, the gantry-table path of a photon DT is determined using the framework presented in the work of Fix *et al.*¹² There, the fractional volume-overlaps of organs at risk (OARs) with the target are calculated based on beams eye view and summed together as a function of gantry and table angles. In this work, equal OAR weightings are used for the summation. Next, an implementation of the A* pathfinding algorithm is used to find a gantry-table path with minimized summed OAR target overlaps. Regions leading to collisions or a beam entering the CT end are avoided.

The gantry-collimator path is subsequently determined using the same framework.¹² For this purpose, the area between the target and a conformal pMLC opening around the target is first determined based on beams eye view along the gantry-table path defined before. This is done as a function of gantry and collimator angles. Afterwards, an A* pathfinding is performed resulting in a gantry-collimator path with minimized area between the pMLC leaves and the target contour. The DYMBER plans created in this work always contain two photon DTs such that freedom for intensity modulation is increased compared to using only one photon DT. The two photon DTs consist of the

same gantry-table and gantry-collimator paths except that the collimator rotation of one photon DT has a constant offset of 90° to the other photon DT, again to increase freedom for intensity modulation.

The pMLC sequences of the photon DTs and the electron pMLC apertures with their associated MUs are then simultaneously optimized using an in-house developed simulated annealing based direct aperture optimization (DAO).^{32,37} This simultaneous optimization is the key element of the entire TPP, because it allows to merge the advantageous properties of photons and electrons. The required beamlet dose distributions are pre-calculated using the Eclipse (Varian Medical System) interfaced Swiss Monte Carlo Plan (SMCP).³⁸ For this DAO, the pMLC sequence of a photon DT is represented by 12 photon apertures distributed equally along the gantry rotation range. The number of pMLC apertures per electron field is predetermined in an iterative approach. The goal of this approach is to reduce delivery time without compromising plan quality. For this, the number of electron apertures is reduced to 15 for the total DYMBER plan. In this approach, the DYMBER plan optimization starts with five electron apertures per electron field and iteratively restarts the optimization without the electron apertures with low MU contribution of the previous optimization until 15 electron apertures are reached.

The DAO changes in each iteration out of $N = 500,000$ iterations in total either a pMLC leaf position or the weight (in terms of MUs) of a randomly selected aperture with a certain probability. The magnitude of the change is randomly sampled according to a cooling schedule with separate parameter values for pMLC leaf position and weight changes. A change is accepted if the objective function value is reduced. A change leading to an increased objective function value is accepted with a probability, which also follows a cooling schedule. Hence, the optimizer converges potentially to the global minimum of the objective function. Independent of the clinical case, the same parameter values describing the cooling schedules are used as described in a previous work.³² The objective function given by

$$f = \sum_{k=1}^{N_{DV}} w_k \cdot f_k^{DV} + \sum_{j=1}^{N_{gEUD}} w_j \cdot f_j^{gEUD}$$

is a weighted sum of N_{DV} dose-volume³⁹ and N_{gEUD} generalized equivalent uniform dose (gEUD)⁴⁰ objectives, where w_k is the weight of the k th dose-volume objective with its objective function given by

$$f_k^{DV} = \sum_{i=1}^{M_k} \frac{\theta(a_k \cdot (D_i - D_k)) \cdot \theta(a_k \cdot (D(V_k) - D_i)) \cdot (D_i - D_k)^2}{N_i}$$

and w_j is the weight of the j th gEUD objective with its objective function given by

$$f_j^{gEUD} = \theta(gEUD(t, j) - gEUD_j) \cdot (gEUD(t, j) - gEUD_j)^2$$

D_i is the dose in the i th voxel of in total M_k voxels of the structure (PTV or OAR) to be considered, θ is the Heaviside function, D_k is the objective dose and $D(V_k)$ is the dose received by at least the tolerated volume V_k . a_k is equal to 1 and -1 for upper and lower dose-volume objectives, respectively. Upper and lower means that dose values higher or lower than D_k , respectively, are desired to be penalized. Regarding the gEUD objectives, $gEUD_j$ is the gEUD objective value and

$$gEUD(t, j) = \left(\frac{1}{M_j}\right) \cdot \sum_{i=1}^{M_j} (D_i)^t$$

where t is a tissue-specific parameter and D_i is the dose in the i th voxel of in total M_j voxels of the OAR structure to be considered. The necessary computation time per optimization is about 30 min on a single Intel Xeon CPU core of type E5-2650.

After the optimization, the final dose distribution of all electron pMLC apertures with at least 1 MU is calculated, again using the SMCP. All other electron pMLC apertures are rejected before by the optimizer. Upon this, the pMLC sequences of the photon DTs are re-optimized with a finer control point resolution and with the final electron dose distribution taken into account. For this purpose, a research version of the Eclipse VMAT photon optimizer is used, which is based on the commercially available VMAT photon optimizer version 13.6 (Varian Medical Systems). This optimizer uses the multi-resolution approach.³ The final dose distribution of the photon DTs is subsequently calculated with the SMCP.⁴¹ Ultimately, the final dose distributions of the photon DTs and the electron pMLC apertures are summed together.

2.B. Monte Carlo simulations

The final and beamlet dose distributions are calculated using SMCP integrated beam models^{36,42} and dose calculation algorithms VMC++⁴³ (photon beams) and macro MC⁴⁴⁻⁴⁶ (electron beams). Measured and calculated dose distributions of single fields generally agree within 2% dose difference (global) or 1 mm distance to agreement for photon beams and 3% dose difference (global) or 2 mm distance to agreement for electron beams.³² A voxel size of $2.5 \times 2.5 \times 2.5 \text{ mm}^3$ is used for all final dose calculations in this work. The mean statistical uncertainty (one standard deviation) of the voxels with dose values higher than 50% and 10% of the maximal dose is below 1% and 2% for all presented dose distributions, respectively. A history by history method is used for this determination.⁴⁷ The necessary computation time to calculate the final photon and electron dose distributions of a DYMBER plan with such settings is about 15 and 30 min, respectively, using 100 cores of Intel Xeon CPUs of type E5-2650 connected on a Linux cluster. About 6 h using 100 CPU cores of the same type as mentioned above are needed to calculate the beamlet dose distributions, which are used as input for the simultaneous optimization sub process.

2.C. Clinical cases

One brain and two head and neck cases with prescribed doses of 60, 45, and 40 Gy to the median dose in the planning target volume (PTV) and fractional doses of 2, 2.5, and 2 Gy, respectively, are selected. The PTVs of these cases all have some superficial part and their deepest part is 6.8, 6.3, and 6.8 cm away from the body surface, respectively. In this work, these three cases serve for the following purposes:

1. To evaluate the dosimetric suitability of DYMBER for treatments in the brain and head and neck region compared to DTRT and VMAT.
2. To verify the deliverability of DYMBER plans in terms of dosimetric accuracy, delivery time and collision avoidance.
3. To analyze the contribution of photon and electron beams to DYMBER plans.

For the first purpose, a DYMBER plan is created for each of the three clinical cases using the presented TPP. The photon DTs and electron fields are illustrated in Fig. 2 and specifications of the electron fields and the number of electron pMLC apertures per field are given in Table I. DTRT plans are created using the same two photon DTs regarding gantry-table and gantry-collimator paths as the DYMBER plans. However, the pMLC sequences and associated MUs are different after optimization compared to the DYMBER plans as no electron pMLC apertures are included in the plan. The VMAT plans are the clinically applied plans but the dose distributions are recalculated using the SMCP such that all plans compared have MC calculated dose distributions. The VMAT plans consist of two (brain case), two (first head and neck case) and three (second head and neck case) arcs. These DYMBER, DTRT, and VMAT plans are compared in terms of dose distributions, dose-volume histograms (DVHs), dose homogeneity in the PTV expressed as $HI = V_{95\%} - V_{107\%}$, D_{mean} to parallel OARs, $D_{2\%}$ to serial OARs and the low dose bath expressed as $V_{10\%}$ of normal tissue (body minus PTV).

Table I. Electron fields and number of apertures per field used to create the DYMBER plans. Every electron field is defined with a collimator rotation of 0° . In case of aperture removals due to the threshold of 1 MU, the corrected number of apertures is given in brackets.

Clinical case	Gantry angle ($^\circ$)	SSD (cm)	Beam energy (MeV)	Number of apertures per beam energy
Brain	330	70	6, 9, 12, 15, 18, 22	0, 0, 0, 1(0), 2, 2
	300	75	6, 9, 12, 15, 18, 22	0, 0, 0, 2, 2, 1
	270	82.5	6, 9, 12, 15, 18, 22	0, 0, 0, 2, 2(1), 1(0)
First head and neck	30	70	6, 9, 12, 15, 18, 22	0, 0, 2(0), 5(4), 2(1), 2(1)
	90	82.5	6, 9, 12, 15, 18, 22	2, 2(1), 0, 0, 0, 0
Second head and neck	0	77.5	6, 9, 12, 15, 18, 22	1, 0, 0, 0, 2(1), 2(1)
	310	77.5	6, 9, 12, 15, 18, 22	0, 0, 2(1), 2(1), 0, 1
	270	82.5	6, 9, 12, 15, 18, 22	0, 0, 0, 2(1), 1, 2(1)

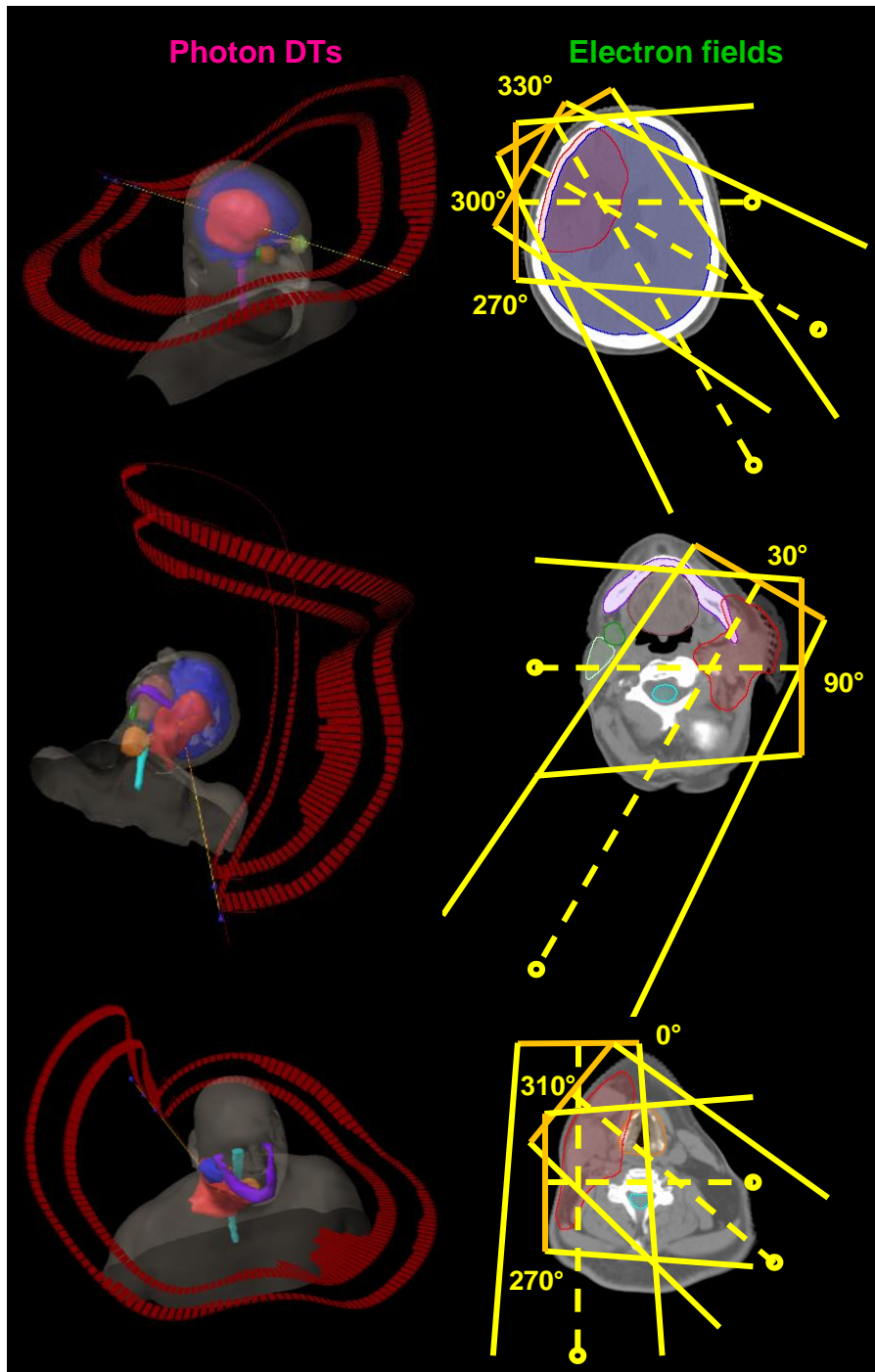


Fig. 2. Photon DTs (left) and electron fields (right) of the DYMBER plans determined for the brain case (top row) and the first (middle row) and second (bottom row) head and neck case. For each electron field defined, beam direction (dashed lines), isocenter position (small circles) and secondary collimator field size (pairs of diverging lines) are displayed.

For the second purpose, each DYMBER plan is delivered to a Gafchromic EBT3 film (Ashland Advanced Materials, Bridgewater, NJ) in the developer mode of a TrueBeam linear accelerator with the MUs of one fraction. The delivery of a DYMBER plan is exemplary illustrated in Fig. 3 for the brain case. The film is placed between two

slabs of an anthropomorphic Alderson head phantom (Alderson Research Labs, Stanford, CA) as illustrated in Fig. 4. The film is scanned 1 week after dose delivery using an Epson expression 10000 XL flatbed scanner (Epson America, Inc., Long Beach, CA). The red color values are transformed to absolute dose with a calibration, which is re-scaled in FilmQA Pro 2014 (Ashland Advanced Materials) using two additional film strips according to the one-scan protocol.⁴⁸ The DYMBER plans are re-calculated for the Alderson phantom using dose to water instead of dose to medium. Measured dose values are compared to calculated dose values in FilmQA Pro 2014 by 2D gamma analysis using 2% dose difference (global) and 2 mm distance to agreement criteria and a global 10% dose threshold. The global reference dose (=100%) is the maximal calculated dose on the 2D dose plane. Regions covering air cavities or the supporting sticks of the phantom are not considered for comparison, because the films have two holes to fit the supporting sticks. The delivery times of all treatment plans are determined starting from the delivery of the first MU until the last MU of the whole treatment plan delivery. This includes all actions for preparing the next beam, for example, table translations to change the isocenter position. Except for the initial positioning of the patient on the table before any beam delivery, no entering of the treatment room is necessary. The required time to position the patient on the table is assumed to be the same for all three treatment techniques investigated and are thus not considered.

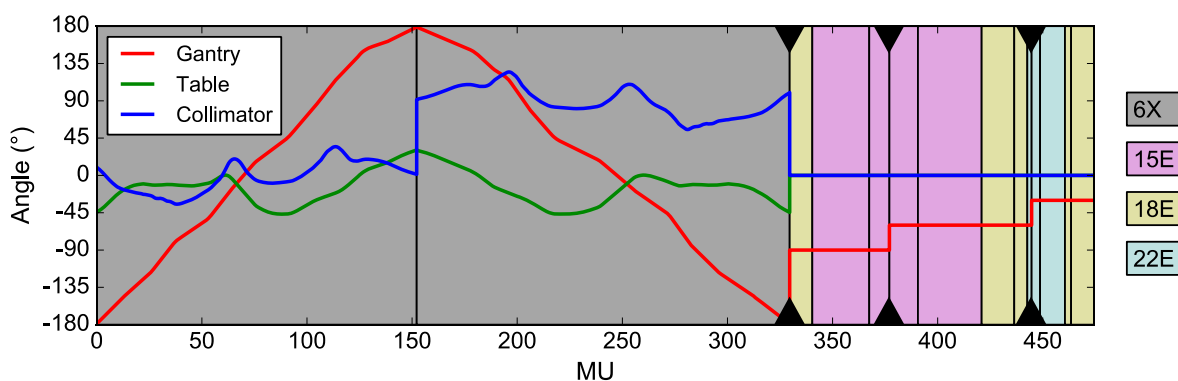


Fig. 3. Illustration of the delivery of the DYMBER plan for the brain case. The gantry, table and collimator angles are provided in the IEC co-ordinate system. The vertical black lines separate the MU ranges of the single photon DTs and electron pMLC apertures, while the black triangles indicate isocenter changes.

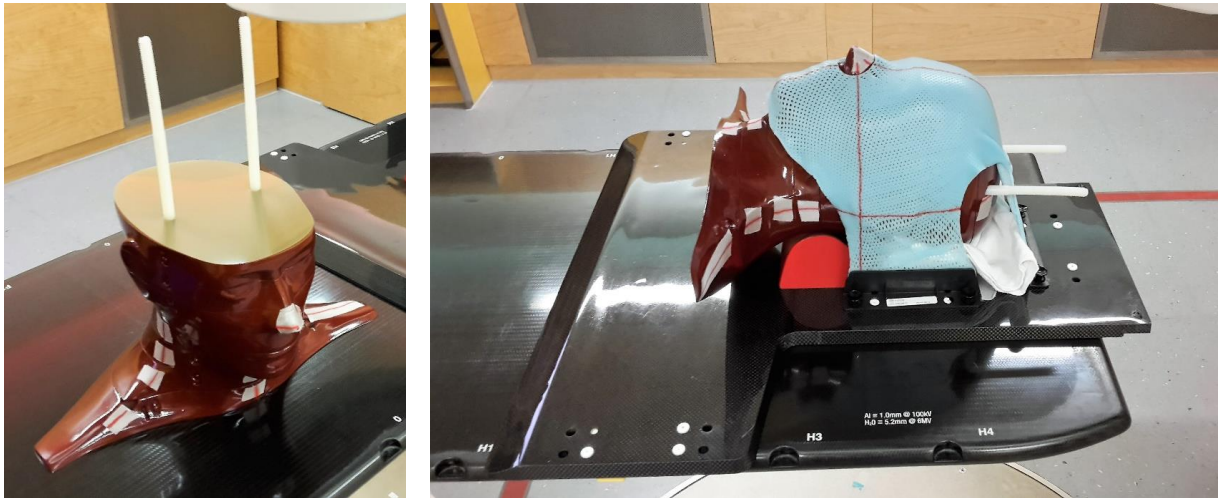


Fig. 4. The measurement setup used for dosimetric verification of DYMBER plans: A film is placed between two slabs of an Alderson head phantom (left), which is afterwards positioned on the table with a holding plate, a cushion, a cloth, and a mask (right). The cloth is used to place the Alderson phantom such that the slabs are parallel to the CT slices.

For the third purpose, the fractional amounts of the electron beams to the MUs, delivery time and integral dose to the PTV (PTV dose contribution) of the corresponding total DYMBER plan are evaluated. The corresponding fractions of the photons are simply the difference from the electron fractions to 100%. Furthermore, the DYMBER dose distributions are split into their photon and electron contributions to analyze the spatial contribution of photon and electron beams.

3. Results

3.A. Brain case

Table II. Results of the DYMBER, DTRT, and VMAT plans determined for the brain case. For every evaluated dosimetric quantity, the best and the second-best values are marked bold and italics, respectively.

		DYMBER	DTRT	VMAT
PTV	HI	99.0%	<i>98.5%</i>	96.5
Ipsilateral lacrimal gland	D_{mean} (Gy)	11.0	<i>15.4</i>	17.0
Contralateral lacrimal gland	D_{mean} (Gy)	1.4	<i>1.9</i>	10.1
Brain	D_{mean} (Gy)	23.1	<i>24.5</i>	26.7
	$D_{2\%}$ (Gy)	61.1	61.1	61.1
Brainstem	$D_{2\%}$ (Gy)	31.1	<i>34.0</i>	33.9
Chiasm	$D_{2\%}$ (Gy)	31.5	<i>34.7</i>	38.0
Ipsilateral optical nerve	$D_{2\%}$ (Gy)	33.5	<i>38.2</i>	45.1
Contralateral optical nerve	$D_{2\%}$ (Gy)	<i>6.4</i>	6.1	23.3
Ipsilateral eye	$D_{2\%}$ (Gy)	13.7	<i>17.5</i>	19.7
Contralateral eye	$D_{2\%}$ (Gy)	3.0	<i>5.9</i>	18.2
Normal tissue	$V_{10\%}$ (cm ³)	1697	<i>1839</i>	1810
Delivery time (min)		6.1	<i>3.1</i>	2.1
Electron delivery time fraction		49%	-	-
Total MU		474.4	<i>477.5</i>	411.1
Electron MU fraction		31%	-	-
Electron PTV dose contribution		44%	-	-

The DYMBER, DTRT, and VMAT plans for the brain case are compared in Table II (dosimetric and delivery values), Fig. 5 (DVHs) and Fig. 6 (dose distributions). The dose homogeneity of the DYMBER and DTRT plans are similar and slightly worse for the VMAT plan. $V_{10\%}$ of normal tissue and all D_{mean} and $D_{2\%}$ values to the OARs are lowest for the DYMBER plan except for $D_{2\%}$ to the contralateral optical nerve, which is 0.3 Gy lower for DTRT. Largest dose reductions for DYMBER compared to VMAT are

observed for the contralateral OARs (D_{mean} to the lacrimal gland, $D_{2\%}$ to the optical nerve and $D_{2\%}$ to the eye are relatively reduced by 86%, 73% and 83%, respectively). DTRT achieved similar dose reductions for the mentioned contralateral OARs. Advantages of DYMBER compared to DTRT are present for the OARs located closer to the PTV as illustrated with the dose profiles in Fig. 6 for the ipsilateral eye and the brain. The same figure also demonstrates that the photons predominantly cover distal parts of the PTV. The dose fall-off of the electron beams starts clearly within the PTV. Overall, a notable electron PTV dose contribution of 44% is found.

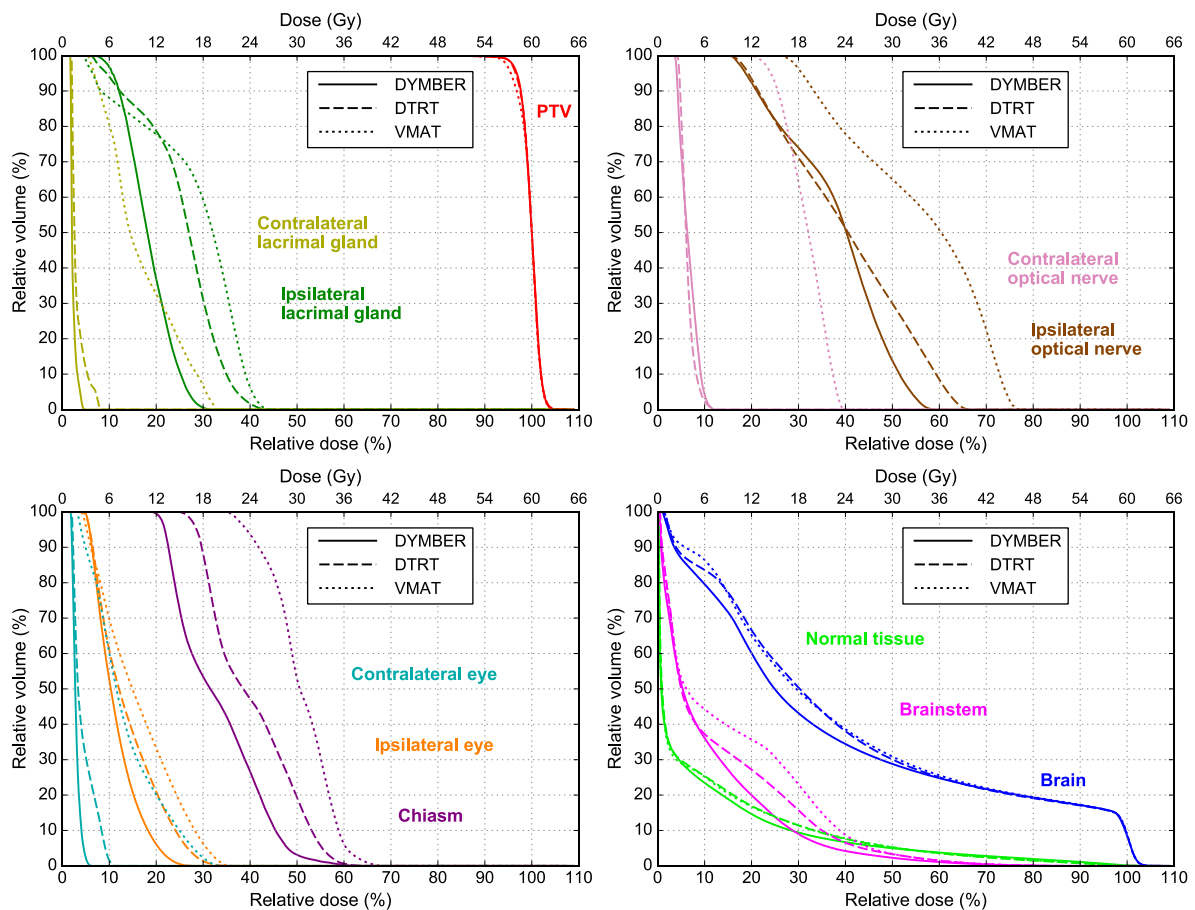


Fig. 5. DVH comparison between the DYMBER, DTRT and VMAT plans determined for the brain case.

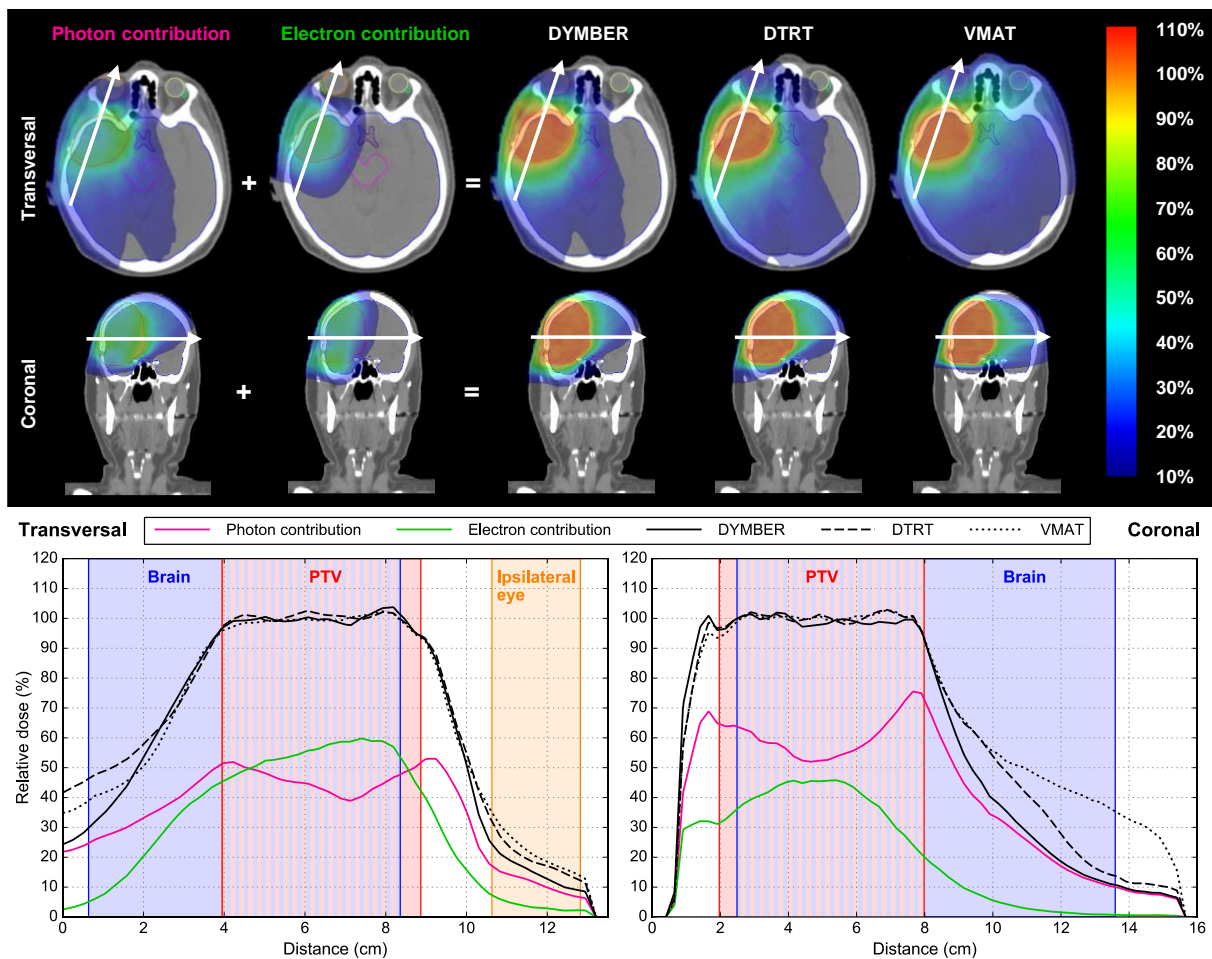


Fig. 6. Dose color wash comparisons (top) between the DYMBER, DTRT and VMAT plans and the photon and electron contributions of the DYMBER plan on a transversal and a coronal plane of the brain case. Dose profiles along the white arrows visible on the transversal and coronal planes are shown on the bottom left and right, respectively.

The results of the comparison between film measurement and dose calculation for the brain case are presented in Fig. 7. The passing rate of the 2%/2 mm gamma analysis is 99.9%. During delivery of the DYMBER plan, collisions are avoided, and the delivery time is 3 and 4 min longer than for the DTRT and VMAT plans, respectively.

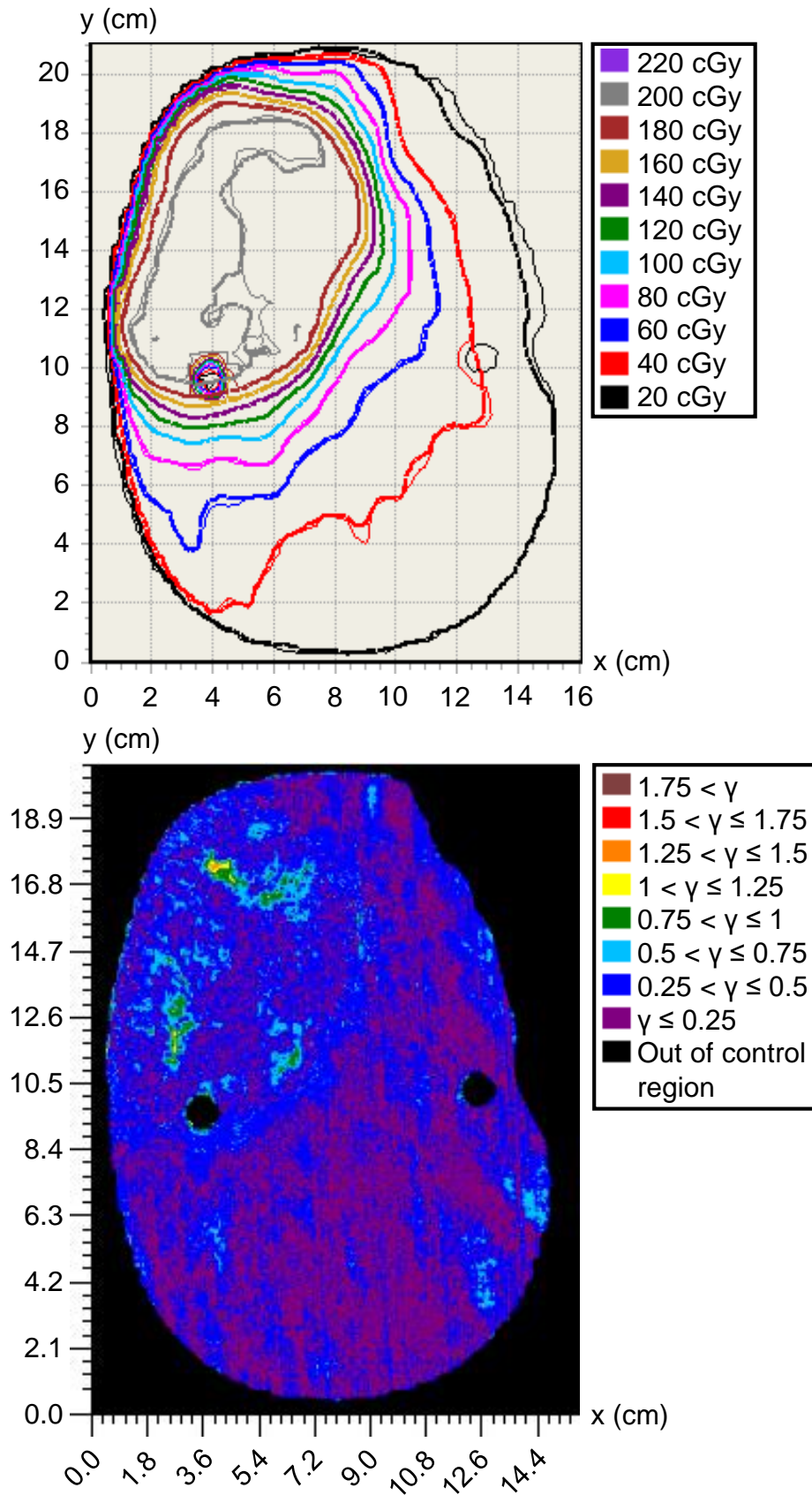


Fig. 7. Isodose comparison (top) between the measured (thin lines) and calculated (thick lines) dose distributions of the DYMBER plan for the brain case. The gamma map of the corresponding 2%/2 mm gamma analysis is shown on the bottom.

3.B. First head and neck case

Table III. Results of the DYMBER, DTRT, and VMAT plans determined for the first head and neck case. For every evaluated dosimetric quantity, the best and the second-best values are marked bold and italics, respectively.

		DYMBER	DTRT	VMAT
PTV	HI	98.0%	<i>97.5%</i>	<i>97.0%</i>
Ipsilateral cochlea	D _{mean} (Gy)	6.8	<i>7.9</i>	<i>7.7</i>
Contralateral parotid gland	D _{mean} (Gy)	0.8	<i>1.0</i>	<i>7.3</i>
Contralateral submandibular gland	D _{mean} (Gy)	1.6	<i>2.0</i>	<i>11.7</i>
Oral cavity	D _{mean} (Gy)	8.2	<i>10.0</i>	<i>12.2</i>
Mandible	D _{mean} (Gy)	16.4	<i>17.7</i>	<i>20.3</i>
Larynx	D _{mean} (Gy)	5.8	<i>8.5</i>	<i>6.2</i>
Brain	D _{mean} (Gy)	<i>3.2</i>	<i>3.3</i>	2.0
	D _{2%} (Gy)	<i>19.1</i>	<i>20.1</i>	14.1
Brainstem	D _{2%} (Gy)	11.5	<i>14.3</i>	<i>20.8</i>
Spinal cord	D _{2%} (Gy)	12.2	<i>15.1</i>	<i>17.8</i>
Normal tissue	V _{10%} (cm ³)	1545	<i>1807</i>	<i>1730</i>
Delivery time (min)		<i>6.3</i>	<i>3.6</i>	<i>2.0</i>
Electron delivery time fraction		<i>43%</i>	-	-
Total MU		<i>590.9</i>	<i>473.2</i>	<i>540.2</i>
Electron MU fraction		<i>33%</i>	-	-
Electron PTV dose contribution		<i>45%</i>	-	-

The DYMBER, DTRT, and VMAT plans for the first head and neck case are compared in Table III (dosimetric and delivery values), Fig. 8 (DVHs) and Fig. 9 (dose distributions). The dose homogeneity is similar for all three plans and V_{10%} of the normal tissue is lowest for DYMBER. Except for the brain, where VMAT yields the lowest dose values, every other OAR receives lower values for D_{mean} to parallel OARs and D_{2%} to serial OARs by the DYMBER plan than for the DTRT and VMAT plans. Largest dose reductions with DYMBER compared to VMAT are reported again for the contralateral OARs (the parotid and the submandibular gland have a 90% and 87% lower D_{mean}, respectively) and DTRT yields again similar reductions for these contralateral

OARs. The benefit of DYMBER compared to DTRT is also for this case larger for OARs located closer to the PTV like this is illustrated for the brainstem in the bottom left dose profile comparison in Fig. 9. In contrast to the ipsilateral eye of the brain case, the brainstem is not located laterally but distally with respect to electron field directions. The profile comparison on the bottom right in Fig. 9 shows that the OARs, which are spared worse (brain) or only slightly better (larynx) with DYMBER compared to VMAT, are in cranial or caudal direction to the PTV. The photon and electron contributions displayed in Fig. 9 on the transversal and coronal view illustrate that the deepest PTV parts are mainly covered by the photons (up to 80% local dose contribution). Superficial parts of the PTV and especially the part close to the larynx is nearly equally covered by photons and electrons. The electron PTV dose contribution is 45% and thus similar as for the DYMBER plan of the brain case.

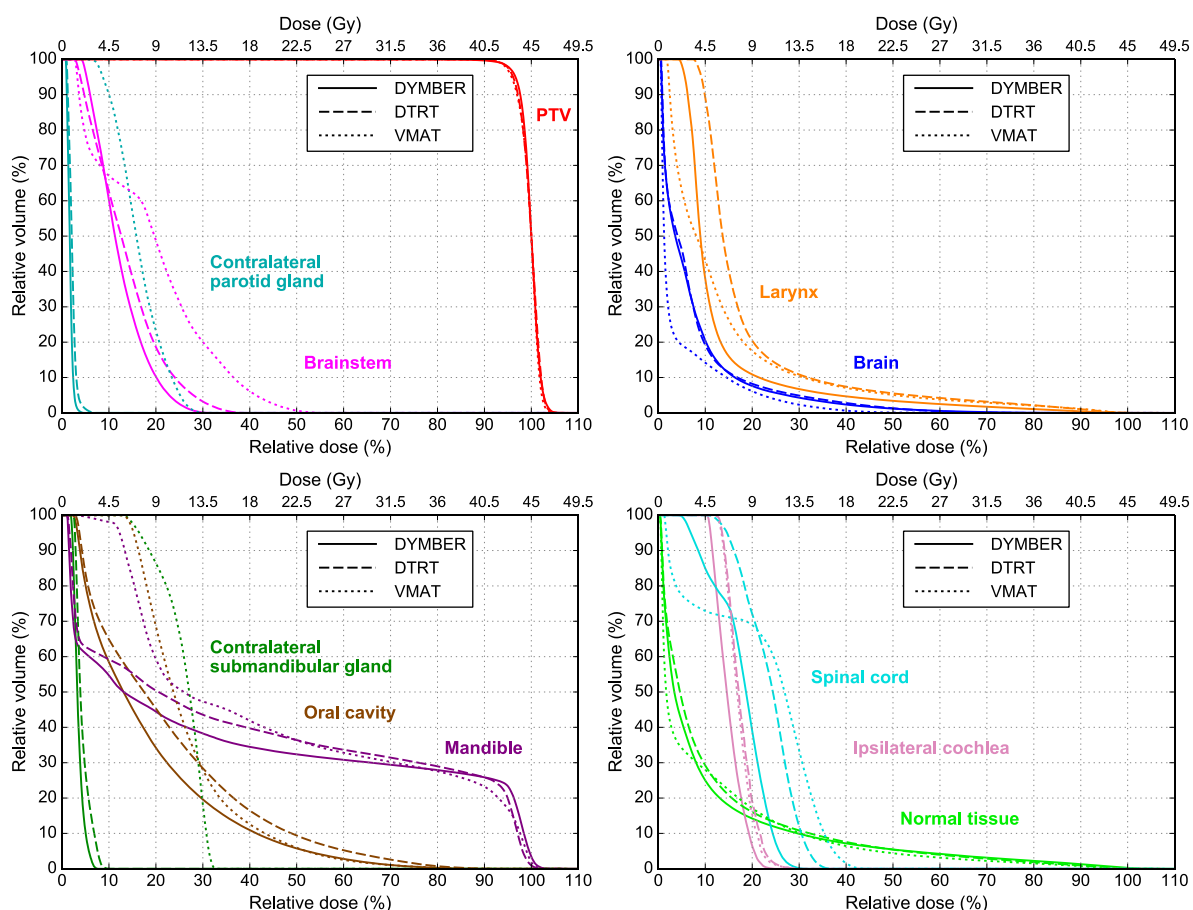


Fig. 8. DVH comparison between the DYMBER, DTRT and VMAT plans determined for the first head and neck case.

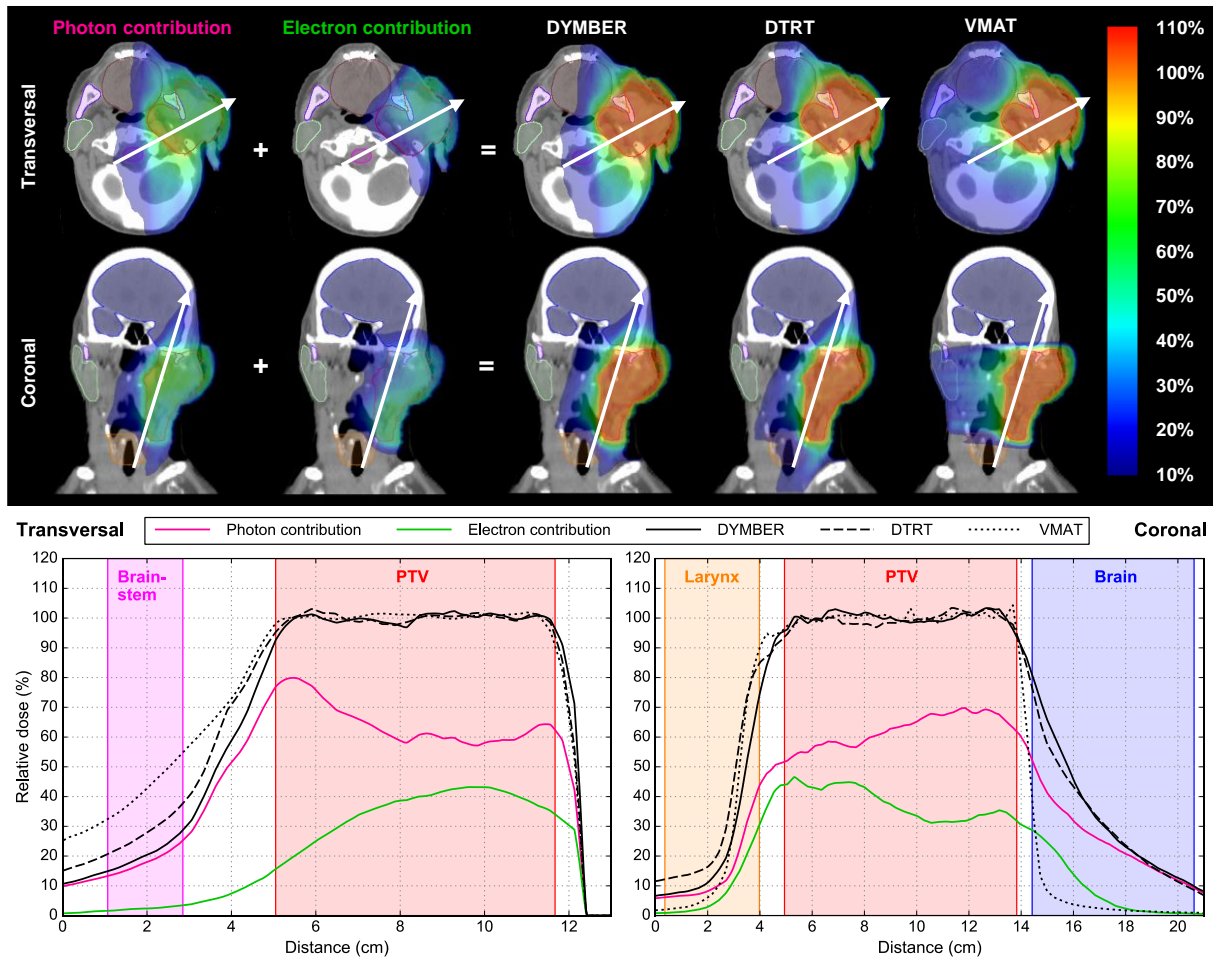


Fig. 9. Dose color wash comparisons (top) between the DYMBER, DTRT and VMAT plans and the photon and electron contributions of the DYMBER plan on a transversal and a coronal plane of the first head and neck case. Dose profiles along the white arrows visible on the transversal and coronal planes are shown on the bottom left and right, respectively.

The results of the comparison between film measurement and dose calculation for the first head and neck case are presented in Fig. 10. The passing rate of the 2%/2 mm gamma analysis is 99.2%. During delivery of the DYMBER plan, collisions are avoided, and the delivery time is 2.7 and 4.3 min longer than for the DTRT and VMAT plans, respectively.

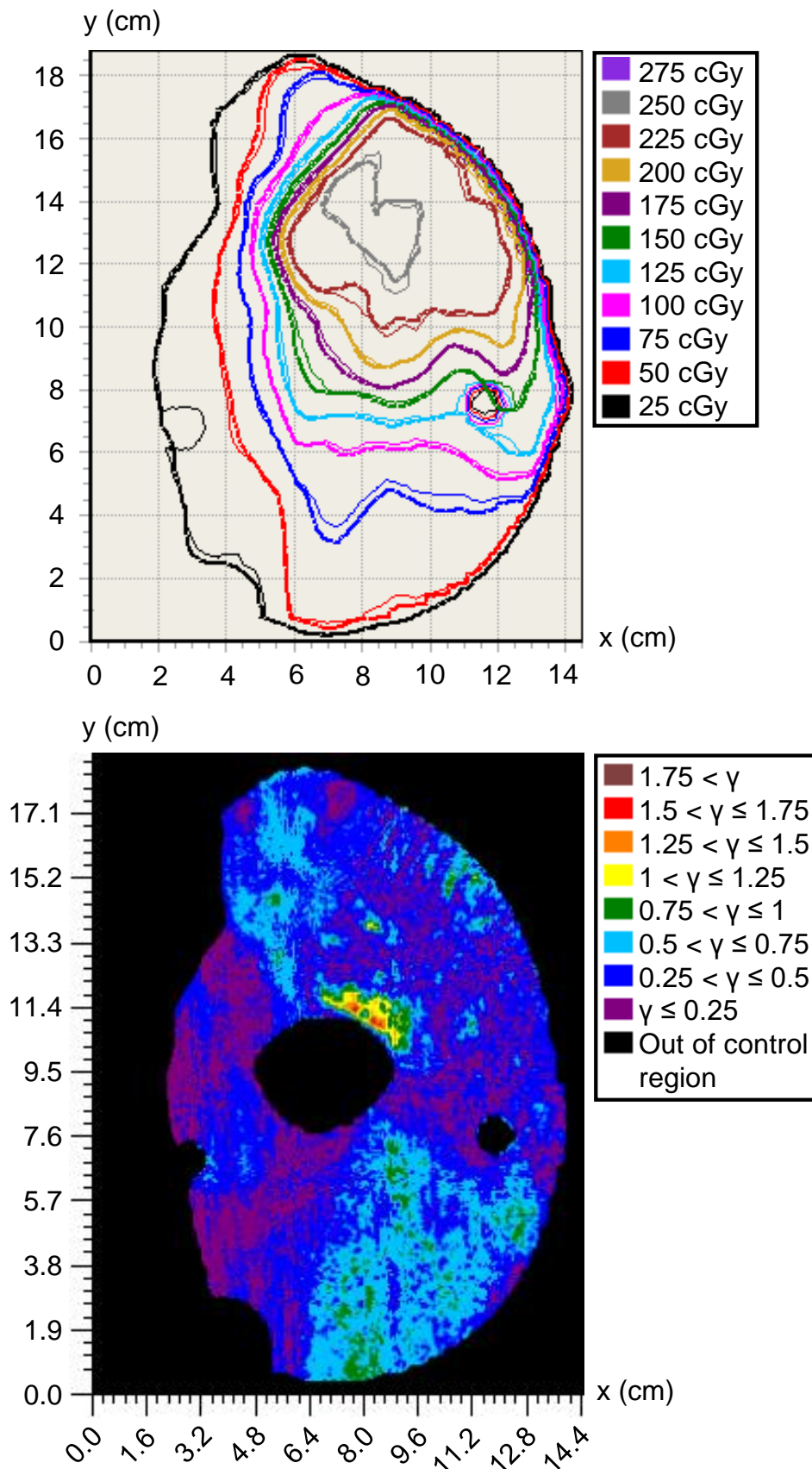


Fig. 10. Isodose comparison (top) between the measured (thin lines) and calculated (thick lines) dose distributions of the DYMBER plan for the first head and neck case. The gamma map of the corresponding 2%/2 mm gamma analysis is shown on the bottom.

3.C. Second head and neck case

The DYMBER, DTRT and VMAT plans for the second head and neck case are compared in Table IV (dosimetric and delivery values), Fig. 11 (DVHs) and Fig. 12 (dose distributions). The dose homogeneity of the three plans is similar and $V_{10\%}$ of the normal tissue is lowest for VMAT followed by DYMBER. Except for the ipsilateral parotid gland, where DTRT delivers the lowest D_{mean} value, all other OARs are spared best by DYMBER. The ipsilateral parotid gland is in cranial-caudal direction to the PTV, similarly as the larynx in the first head and neck case (see Fig. 12). Most benefit with DYMBER is given for the sparing of the larynx (25% smaller D_{mean} compared to VMAT). In contrast to the first head and neck case, the larynx is now on the same cranial-caudal level as the PTV. Even though the electron PTV dose contribution of the DYMBER plan is not more than 23%, an advantage in sparing of the larynx is apparent and is demonstrated in the dose profile comparison on the bottom left in Fig. 12. The DTRT plan without electrons clearly delivers higher dose values to the larynx.

Table IV. Results of the DYMBER, DTRT, and VMAT plans determined for the second head and neck case. For every evaluated dosimetric quantity, the best and the second-best values are marked bold and italics, respectively.

		DYMBER	DTRT	VMAT
PTV	HI	99.0%	98.0%	99.0%
Ipsilateral parotid gland	D_{mean} (Gy)	14.0	13.6	<i>13.9</i>
Mandible	D_{mean} (Gy)	8.2	8.9	9.9
Larynx	D_{mean} (Gy)	13.7	<i>16.8</i>	18.2
Spinal cord	$D_{2\%}$ (Gy)	11	<i>13.1</i>	14.2
Normal tissue	$V_{10\%}$ (cm ³)	3938	4552	3720
Delivery time (min)		7.0	3.3	2.4
Electron delivery time fraction		53%	-	-
Total MU		648.9	443.1	587.4
Electron MU fraction		26%	-	-
Electron PTV dose contribution		23%	-	-

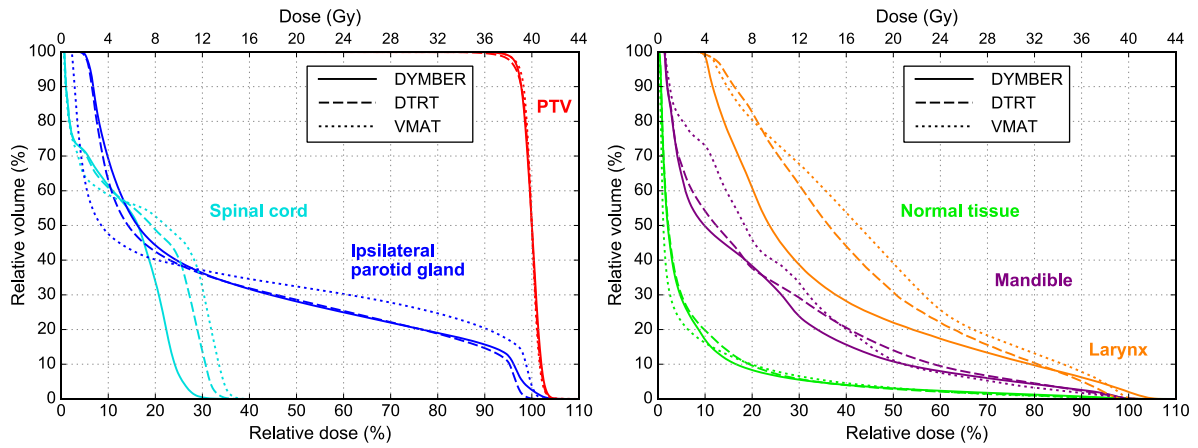


Fig. 11. DVH comparison between the DYMBER, DTRT and VMAT plans determined for the second head and neck case.

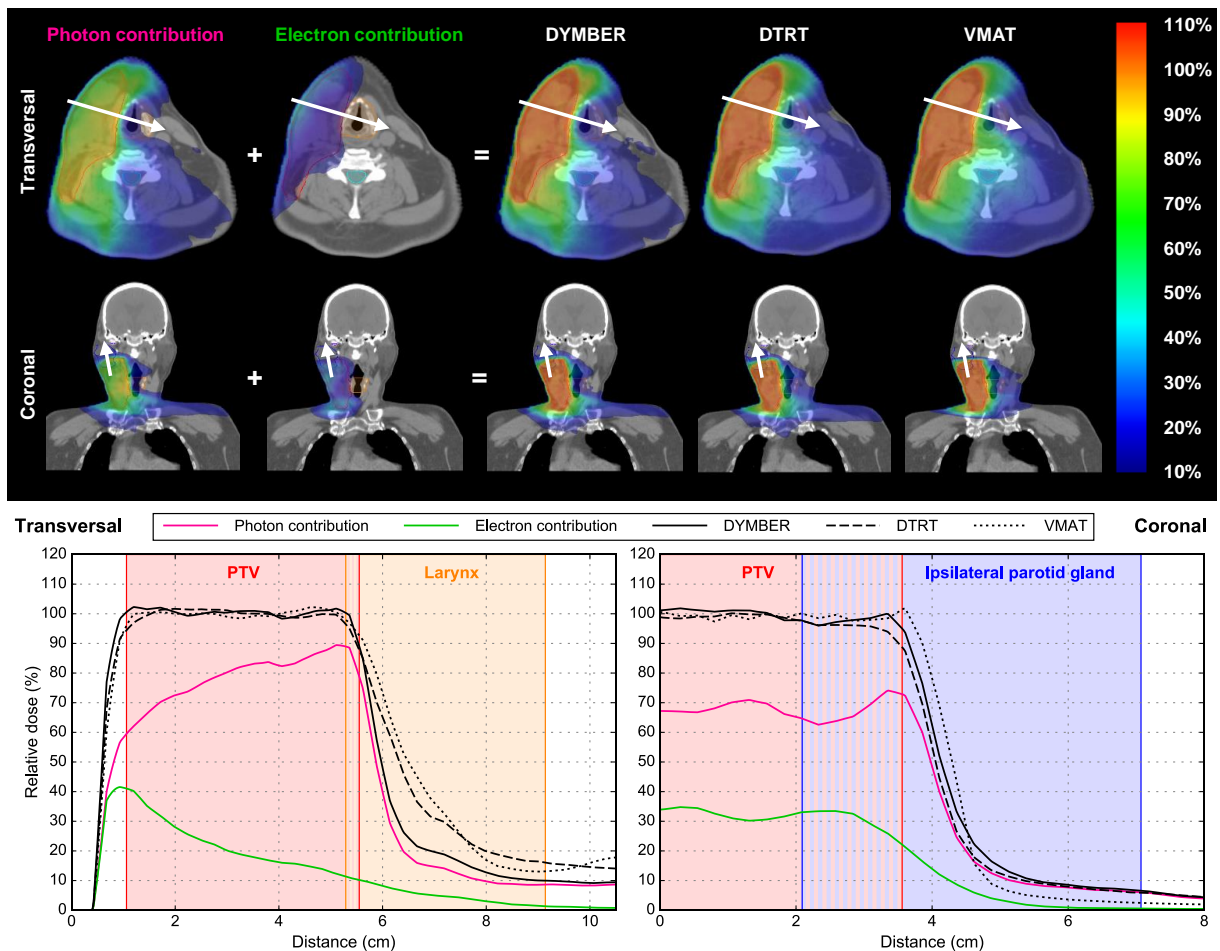


Fig. 12. Dose color wash comparisons (top) between the DYMBER, DTRT and VMAT plans and the photon and electron contributions of the DYMBER plan on a transversal and a coronal plane of the second head and neck case. Dose profiles along the white arrows visible on the transversal and coronal planes are shown on the bottom left and right, respectively.

The results of the comparison between film measurement and dose calculation for the second head and neck case are presented in Fig. 13. The passing rate of the 2%/2 mm gamma analysis is 99.6%. During delivery of the DYMBER plan, collisions are avoided, and the delivery time is 3.7 and 4.6 min longer than for the DTRT and VMAT plans, respectively.

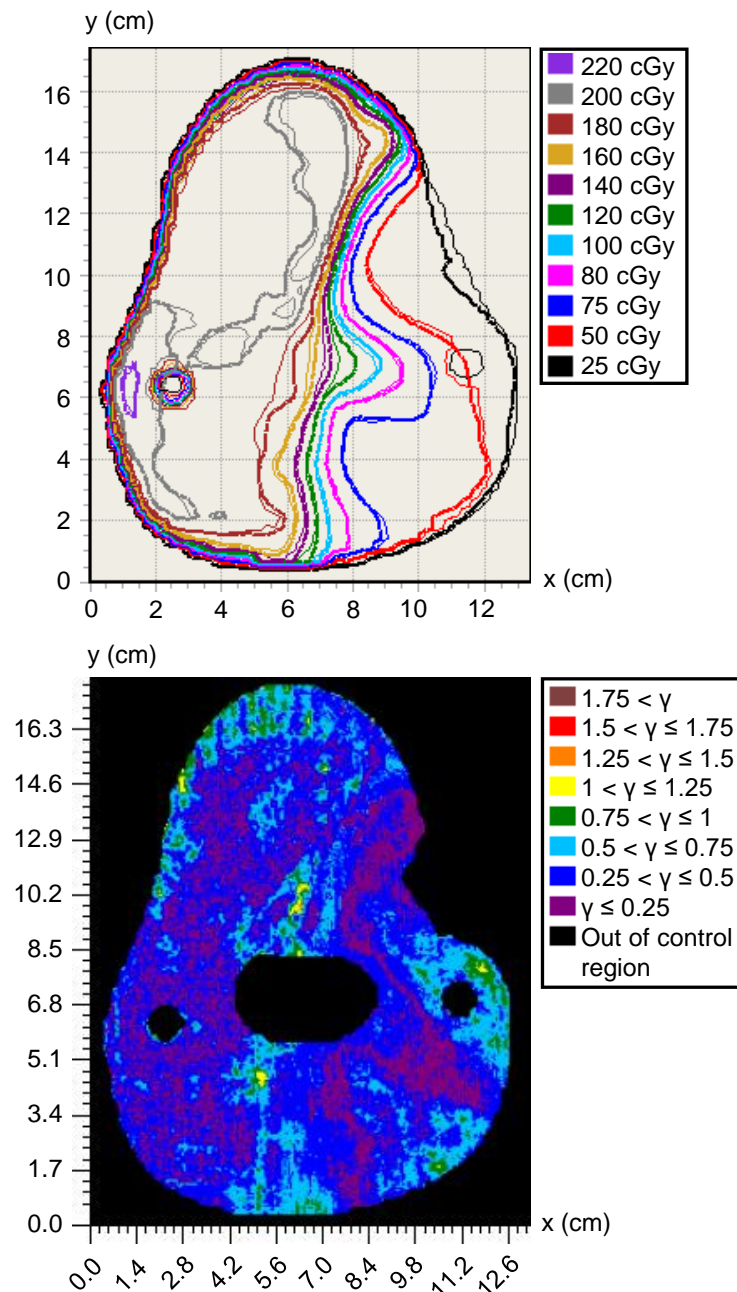


Fig. 13. Isodose comparison (top) between the measured (thin lines) and calculated (thick lines) dose distributions of the DYMBER plan for the second head and neck case. The gamma map of the corresponding 2%/2 mm gamma analysis is shown on the bottom.

4. Discussion

An MC based TPP for DYMBER has been successfully developed. The generated DYMBER plans keep the dose homogeneity in the PTV at least as good as for the clinically applied VMAT plans and provide better OAR sparing. Only one of 22 OARs (brain in the first head and neck case) is spared better with VMAT and just one is similar spared (ipsilateral parotid gland in the second head and neck case). Both DYMBER and DTRT achieve substantial dose reductions in the contralateral OARs compared to VMAT. Probable reasons for this are that beam directions directly facing these contralateral OARs are usually avoided for photon DTs and that the electron beams deliver only dose due to the bremsstrahlung tail to these contralateral OARs. OARs located close to the PTV on the same cranial-caudal level are spared best by DYMBER, followed by DTRT. The limited range of electron beams is of advantage for sparing these OARs. On the other side, the sparing of OARs located further in cranial or caudal direction to the PTV is similar for DYMBER compared to VMAT, except for one organ worse (as mentioned above). This might be a limitation of the noncoplanar photon DTs, because the presented DTRT plans also do not yield better dose values for such OARs.

It is expected that the benefits of DYMBER compared to DTRT and VMAT could not be compensated using more photon DTs or arcs for DTRT and VMAT, respectively. To indicate this, we created an additional DTRT plan with four photon DTs for the brain case. Only for the ipsilateral optical nerve a clear improvement is visible for DTRT with four photon DTs compared to two photon DTs. The resulting $D_{2\%}$ value to the ipsilateral optical nerve is similar to the one of DYMBER. All other OARs are spared similarly for the DTRT plans with two and four photon DTs.

Regarding normal tissue sparing, DYMBER yields the lowest $V_{10\%}$ values for two of three clinical cases and DTRT always the highest value. For these cases, this can be explained by the lower dose spread over normal tissue by the electron compared to the photon contributions. The clinical case with lowest $V_{10\%}$ value for VMAT is also the case for which DYMBER has the lowest electron PTV dose contribution. On the other side, the presented DYMBER plans deliver more dose to normal tissue regions proximal to the PTV for the electron beams. If it is of clinical relevance, these dose values could

be minimized during optimization. For PTVs including skin like for the first head and neck case, the higher entrance dose of electrons compared to photons is of advantage. However, this advantage is not apparent for this case, because a bolus is applied such that photon only plans achieve a sufficient PTV dose homogeneity. The plan quality of DYMBER is expected to be less dependent on using a bolus than photon only techniques, as already indicated for MBRT.³² On the other hand, the risk for skin toxicity on cases, where the skin is not a part of the target, should be clinically evaluated.

Although the presented clinical cases are all in the brain and head and neck region, DYMBER could be used for every treatment site, where targets have some superficial part. However, benefits of DYMBER are assumed to be largest for these treatment sites, because of the large collision free space for gantry-table angle combinations.

The presented DYMBER plans are deliverable without collisions and with a 4–5 min longer delivery time than the VMAT plans. Thus, delivery times of these DYMBER plans are similar to IMRT plans, which are nowadays well-integrated into clinical routine. On a TrueBeam linear accelerator, it takes about 20 s to switch beam energy. Hence, delivery time could be further reduced by up to 2 min for the presented DYMBER plans if beam energy switch required less time.

The dose distributions of the DYMBER plans are verified in a realistic situation with passing rates of at least 99% for 2%/2 mm gamma analysis. It is noteworthy, that the output of the electron beams must be well predicted for the whole utilized SSD range of 70–82.5 cm. Even though the utilized electron beam model is commissioned using measurements collected only at one SSD of 70 cm, MC simulations are still capable to accurately predict dose distributions for other SSDs.^{35,49,50} A further important deliverability aspect of DYMBER is the plan robustness associated to patient movements and body variations. This is not yet studied and thus, robustness needs to be investigated in future studies and solutions to improve the robustness like robust optimization are desirable to be used for DYMBER.

For delivery of DYMBER and DTRT, it needs to be ensured that table rotations do not induce movements of the patient leading to unfavorable changes in the dose distribution. An option to address this concern would be to define an appropriate threshold for rotational table acceleration values, especially at the beginning and at the

end of delivering a photon DT. For DYMBER in particular, the necessary isocenter changes due to the reduced SSD defined for the electron fields could also induce patient movements. However, this depends also on the table performance.⁵¹ An appropriate image guided radiotherapy (IGRT) solution is favorable to assure that the patient position is correct. IGRT solutions such as room-fixed imaging systems and 3D patient-surface guidance for the whole DYMBER delivery and MV imaging followed to isocenter changes could play important roles for this purpose.

The electron PTV dose contributions of the DYMBER plans are substantial and the spatial dose distributions indicate that the advantages of photons and electrons are synergistically merged, demonstrating the dosimetric value of combining different particle types. In addition, even further extensions to DYMBER are possible. For instance, potential benefits of electron beams could already be taken into account during determination of the gantry-table path of the photon DTs. Another extension would be to deliver the electron beams with arcs or dynamic trajectories to possibly reduce delivery time. For this purpose, a technique similar to dynamic electron arc radiotherapy (DEAR)⁵² could be utilized, but with pMLC collimation instead of applicator based collimation to maintain clinical workflow. Finally, energy modulation could also be used for photon beams as conventional treatment units usually support multiple photon beam energies.⁵³ Such possible improvements will be investigated in future work.

5. Conclusions

A treatment technique for DYMBER utilizing the different particle types, intensity, and energy modulation and dynamic gantry, table, and collimator rotations has been successfully developed. The deliverability of DYMBER plans is verified in terms of dosimetric accuracy, delivery time and collision avoidance for three clinical cases. These DYMBER plans dosimetrically outperformed DTRT and VMAT plans. Thus, it is demonstrated that the capabilities of conventional treatment units in terms of plan quality for treatments of targets with at least some superficial part are not fully exploited neither with today's state of the art VMAT nor with DTRT. The substantial contribution of electron beams to DYMBER plans underlines the dosimetric value of different particle types. This work indicates utilizing increased DoF to be the key to improve brain and head and neck radiation treatments in future.

Acknowledgments

This work was supported by Varian Medical Systems and partly by the Swiss Cancer League & Foundation Cancer Research Switzerland grant KFS-3279-08-2013. Calculations were performed on UBELIX (<http://www.id.unibe.ch/hpc>), the HPC cluster at the University of Bern.

Conflicts of interest

The authors have no relevant conflicts of interest to disclose.

References

1. Bortfeld T. IMRT: a review and preview. *Phys Med Biol.* 2006;51:R363– R379.
2. Yu CX. Intensity-modulated arc therapy with dynamic multileaf collimation: an alternative to tomotherapy. *Phys Med Biol.* 1995;40:1435–1449.
3. Otto K. Volumetric modulated arc therapy: IMRT in a single gantry arc. *Med Phys.* 2008;35:310–317.
4. Dong P, Lee P, Ruan D, *et al.* 4p non-coplanar liver SBRT: a novel delivery technique. *Int J Radiat Oncol Biol Phys.* 2013;85:1360–1366.
5. Podgorsak EB, Olivier A, Pla M, Lefebvre P, Hazel J. Dynamic stereotactic radiosurgery. *Int J Radiat Oncol Biol Phys.* 1988;14:115–126.
6. Yang Y, Zhang P, Happersett L, *et al.* Choreographing couch and collimator in volumetric modulated arc therapy. *Med Phys.* 2010;37:3369.
7. Popescu C, Beckham W, Patenaude VV, Olivetto I, Vlachaki MT. Simultaneous couch and gantry dynamic arc rotation (C-G Darc) in the treatment of breast cancer with accelerated partial breast radiation therapy (APBRT). *J Appl Clin Med Phys.* 2012;14:161–175.
8. Smyth G, Bamber JC, Evans PM, Bedford JL. Trajectory optimization for dynamic couch rotation during volumetric modulated arc radiotherapy. *Phys Med Biol.* 2013;58:8163–8177.
9. Wild E, Bangert M, Nill S, Oelfke U. Noncoplanar VMAT for nasopharyngeal tumors: plan quality versus treatment time. *Med Phys.* 2015;42:2157–2168.
10. Papp D, Bortfeld T, Unkelbach J. A modular approach to intensity modulated arc therapy optimization with noncoplanar trajectories. *Phys Med Biol.* 2015;60:5179–5198.
11. Smyth G, Evans PM, Bamber JC, *et al.* Non-coplanar trajectories to improve organ at risk sparing in volumetric modulated arc therapy for primary brain tumors. *Radiother Oncol.* 2016;121:124–131.
12. Fix MK, Frei D, Volken W, *et al.* Part 1: optimization and evaluation of dynamic trajectory radiotherapy. *Med Phys.* 2018 <https://doi.org/10.1002/mp.13086>

13. Zhang P, Happersett L, Yang Y, Mageras G, Hunt M. Optimization of collimator trajectory in volumetric modulated arc therapy: development and evaluation for paraspinal SBRT. *Med Phys.* 2009;36:2784–2785.
14. Lee MC, Deng J, Li J, Jiang SB, Ma C. Monte Carlo based treatment planning for modulated electron beam radiation therapy. *Phys Med Biol.* 2001;46:2177–2199.
15. Olofsson L, Mu X, Nill S, Oelfke U, Zackrisson B, Karlsson M. Intensity modulated radiation therapy with electrons using algorithm based energy/range selection methods. *Radiother Oncol.* 2004;73:223–231.
16. Al-Yahya K, Schwartz M, Shenouda G, Verhaegen F, Freeman C, Seuntjens J. Energy modulated electron therapy using a few leaf electron collimator in combination with IMRT and 3D-CRT: Monte Carlo-based planning and dosimetric evaluation. *Med Phys.* 2005;32:2976–2986.
17. Klein EE, Mamalui-Hunter M, Low DA. Delivery of modulated electron beams with conventional photon multi-leaf collimators. *Phys Med Biol.* 2009;54:327–339.
18. Engel K, Gauer T. A dose optimization method for electron radiotherapy using randomized aperture beams. *Phys Med Biol.* 2009;54:5253–5270.
19. Salguero FJ, Palma B, Arrans R, Rosello J, Leal A. Modulated electron radiotherapy treatment planning using a photon multileaf collimator for post-mastectomized chest walls. *Radiother Oncol.* 2009;93:625–632.
20. Salguero FJ, Arrans R, Palma BA, Leal A. Intensity- and energy-modulated electron radiotherapy by means of an xMLC for head and neck shallow tumors. *Phys Med Biol.* 2010;55:1413–1427.
21. Alexander A, DeBlois F, Seuntjens J. Toward automatic field selection and planning using Monte Carlo-based direct aperture optimization in modulated electron radiotherapy. *Phys Med Biol.* 2010;55:4563–4576.
22. Henzen D, Manser P, Frei D, *et al.* Beamlet based direct aperture optimization for MERT using a photon MLC. *Med Phys.* 2014;41:121711.
23. Li JG, Williams SS, Goffinet DR, Boyer AL, Xing L. Breast-conserving radiation therapy using combined electron and intensity-modulated radiotherapy technique. *Radiother Oncol.* 2000;56:65–71.

24. Mu X, Olofsson L, Karlsson M, Sjögren R, Zackrisson B. Can photon IMRT be improved by combination with mixed electron and photon techniques? *Acta Oncol.* 2004;43:727–735.
25. Xiong W, Li J, Chen L, *et al.* Optimization of combined electron and photon beams for breast cancer. *Phys Med Biol.* 2004;49:1973–1989.
26. Surucu M, Klein EE, Mamalui-Hunter M, Mansur DB, Low DA. Planning tools for modulated electron radiotherapy. *Med Phys.* 2010;37:2215–2224.
27. Ge Y, Faddegon BA. Study of intensity-modulated photon–electron radiation therapy using digital phantoms. *Phys Med Biol.* 2011;56:6693–6708.
28. Alexander A, Soisson E, Renaud M-A, Seuntjens J. Direct aperture optimization for FLEC-based MERT and its application in mixed beam radiotherapy. *Med Phys.* 2012;39:4820–4831.
29. Palma BA, Sanchez AU, Salguero FJ, *et al.* Combined modulated electron and photon beams planned by a Monte-Carlo-based optimization procedure for accelerated partial breast irradiation. *Phys Med Biol.* 2012;57:1191–1202.
30. Rosca F. A hybrid electron and photon IMRT planning technique that lowers normal tissue integral patient dose using standard hardware. *Med Phys.* 2012;39:2964–2971.
31. Miguez C, Jimenez-Ortega E, Palma BA, *et al.* Clinical implementation of combined modulated electron and photon beams with conventional MLC for accelerated partial breast irradiation. *Radiother Oncol.* 2017;124:124–129.
32. Mueller S, Fix MK, Joosten A, *et al.* Simultaneous optimization of photons and electrons for mixed beam radiotherapy. *Phys Med Biol.* 2017;62:5840–5860.
33. Renaud M-A, Serban M, Seuntjens J. On mixed electron–photon radiation therapy optimization using the column generation approach. *Med Phys.* 2017;44:4287–4298.
34. du Plessis FCP, Leal A, Stathakis S, Xiong W, Ma C-M. Characterization of megavoltage electron beams delivered through a photon multileaf collimator (pMLC). *Phys Med Biol.* 2006;51:2113–2129.
35. Mueller S, Fix MK, Henzen D, *et al.* Electron beam collimation with the photon MLC for standard electron treatments. *Phys Med Biol.* 2018;63:025017.

36. Henzen D, Manser P, Frei D, *et al.* Monte Carlo based beam model using a photon MLC for modulated electron radiotherapy. *Med Phys.* 2014;41:21714.
37. Shepard DM, Ferris MC, Olivera GH, Mackie TR. Optimizing the delivery of radiation therapy to cancer patients. *SIAM Rev.* 1999;41:721–744.
38. Fix MK, Manser P, Frei D, Volken W, Mini R, Born EJ. An efficient framework for photon Monte Carlo treatment planning. *Phys Med Biol.* 2007;52:N425–N437.
39. Wu Q, Mohan R. Algorithms and functionality of an intensity modulated radiotherapy optimization system. *Med Phys.* 2000;27:701–711.
40. Niemierko A. A generalized concept of equivalent uniform dose (EUD). *Med Phys.* 1999;26:1100.
41. Manser P, Frauchiger D, Frei D, Volken W, Terribilini D, Fix MK. Dose calculation of dynamic trajectory radiotherapy using Monte Carlo. *Z Med Phys.* 2018. <https://doi.org/10.1016/j.zemedi.2018.03.002>
42. Magaddino V, Manser P, Frei D, *et al.* Validation of the Swiss Monte Carlo Plan for a static and dynamic 6 MV photon beam. *Z Med Phys.* 2011;21:124–134.
43. Kawrakow I, Fippel M. VMC++, a fast MC algorithm for radiation treatment planning. *Use Comput Radiat Ther 8th Int Conf (Heidelberg, Gered W Schlegel T Bortfeld (heidelb Springer));* 2000:126–128. <https://doi.org/10.1007/978-3-642-59758-9>
44. Neuenschwander H, Born EJ. A Macro Monte Carlo method for electron beam dose calculations. *Phys Med Biol.* 1992;37:107–125.
45. Neuenschwander H, Mackie TR, Reckwerdt PJ. MMC – a high-performance Monte Carlo code for electron beam treatment planning. *Phys Med Biol.* 1995;40:543–574.
46. Fix MK, Cygler J, Frei D, *et al.* Generalized eMC implementation for Monte Carlo dose calculation of electron beams from different machine types. *Phys Med Biol.* 2013;58:2841–2859.
47. Walters BRB, Kawrakow I, Rogers DWO. History by history statistical estimators in the BEAM code system. *Med Phys.* 2002;29:2745–2752.
48. Lewis D, Micke A, Yu X, Chan MF. An efficient protocol for radiochromic film dosimetry. *Med Phys.* 2012;39:6339.

49. Cygler JE, Daskalov GM, Chan GH, Ding GX. Evaluation of the first commercial Monte Carlo dose calculation engine for electron beam treatment planning. *Med Phys.* 2004;31:142.
50. Ding GX, Cygler JE, Yu CW, Kalach NI, Daskalov G. A comparison of electron beam dose calculation accuracy between treatment planning systems using either a pencil beam or a Monte Carlo algorithm. *Int J Radiat Oncol Biol Phys.* 2005;63:622–633.
51. Schmidhalter D, Malthaner M, Born EJ, *et al.* Assessment of patient setup errors in IGRT in combination with a six degrees of freedom couch. *Z Med Phys.* 2014;24:112–122.
52. Rodrigues A, Yin F-F, Wu Q. Dynamic electron arc radiotherapy (DEAR): a feasibility study. *Phys Med Biol.* 2014;59:327–345.
53. Mcgeachy P, Villarreal-barajas JE. Modulated photon radiotherapy (XMRT): an algorithm for the simultaneous optimization of photon beamlet energy and intensity in external beam radiotherapy (EBRT) planning. *Phys Med Biol.* 2016;61:1476-1498.

7

Discussion

In the following subchapters, several aspects of the developed treatment techniques for MBRT are discussed.

7.1. Dosimetric suitability for clinical applications

In chapter 4, deliverable ssMBRT plans were compared to MERT, photon IMRT and VMAT plans for a left chest wall case and a squamous cell carcinoma case in the head and neck region, while in chapter 6, deliverable DYMBER plans were compared to DTRT and VMAT for a brain and two head and neck cases. For all investigated cases, the MBRT plans (either ssMBRT or DYMBER) dosimetrically outperformed the plans of all other treatment techniques under comparison. Dose homogeneity is basically at least as good as for photon-only techniques and improved compared to MERT, while the sparing of serial and parallel OARs is substantially improved compared to each treatment technique investigated. Moreover, the low dose bath delivered to normal tissue is reduced compared to photon-only techniques but increased compared to MERT. The skin dose is potentially increased for MBRT compared to photon-only treatment techniques, because of the higher entrance dose of electron beams compared to photon beams. However, the MC simulations used are not validated against surface dose measurements and thus, the calculated dose values are not suited for quantitative skin dose investigations. Specific methods such as surface dose measurements (Devic *et al* 2006) or experimental animal irradiations could quantify the dose values delivered at submillimeter depths or estimate skin toxicities compared to photon-only deliveries, respectively.

Each of the cases investigated for MBRT plans except of the left chest wall case have a target with parts deeper than 5 cm. Thus, the dosimetric results underline that MBRT can deliver the dose homogeneously to targets with deep-seated parts in contrast to MERT. As long as there are any superficial parts in the target, MBRT benefits from

electron beams compared to photon-only treatment techniques. The investigations with the superficial and enlarged target of the academic situation in chapter 4 also shows that the benefit of MBRT does not necessarily decrease with the depth of the deepest part of the target. Based on these dosimetric observations, clinical cases of many treatment sites could profit from MBRT such as the following:

- Brain (chapter 6 of this thesis)
- Head and neck (chapter 4 and 6 of this thesis)
- Breast (Palma *et al* 2012, Míguez *et al* 2017)
- Chest wall (Renaud *et al* 2017, chapter 4 of this thesis)
- Sternum (Mueller *et al* 2018a)
- Lung (Mueller *et al* 2018a)
- Bladder (Mueller *et al* 2018b)
- Extremity (Renaud *et al* 2017)
- Skin
- Liver

Other studies about simultaneously optimized pMLC based MBRT plans showed similar convincing dosimetric results also for other treatment sites as those investigated in this thesis (references are given in the list of treatment sites above). In summary, MBRT is dosimetrically well suited for broad clinical applications to improve treatment plan quality over photon-only treatments.

7.2. Simultaneous optimization

The TPP used to generate ssMBRT plans optimizes photons and electrons simultaneously in one process, while the TPP used to generate DYMBER plans uses an optimization which is split in two parts. In the first part of the DYMBER optimization, the pMLC sequence of the photon DTs and the electron pMLC apertures are simultaneously optimized and in the second part, the photon DTs are reoptimized with a finer control point resolution under consideration of the final dose distribution of the electron pMLC apertures. This two-step approach has the disadvantage over the one-

step approach, that the first part with the simultaneous optimization cannot tune the photon contribution in the final control point resolution leading potentially to an optimization convergence error. However, there is also an advantage over the one-step approach: the second step including the re-optimization of the photon DTs has the possibility to compensate for discrepancies between optimized and deliverable electron dose distributions. Only an implementation of a one-step approach for DYMBER could answer the question whether a one-step approach could further improve treatment plan quality compared to the two-step approach.

For both TPP, optimizing the photon and electron contributions simultaneously was key. Otherwise, the contributions of the two particle types could not be purposefully tuned dependent on the spatial location in the patient. This is well visible for the ssMBRT plan for the squamous cell carcinoma case in chapter 4, where the PTV electron contributions on eye and on ear level are substantially different. The photon and electron contributions can be followed posteriorly to observe the exploitation of the dosimetric characteristics of photons and electrons. One might also see general tendencies in what geometric target and OAR constellations photon or electron beams have major contributions. However, it is hard to predict the photon and electron contributions in prior justifying the need of a simultaneous optimization.

The dosimetric results in literature of MBRT techniques with sequentially optimized photon and electron contributions also reported better OAR sparing compared to photon-only techniques, but typically on cost of a reduced dose homogeneity in the target (Li *et al* 2000, Mu *et al* 2004, Ge and Faddegon 2011, Rosca 2012, Zhang *et al* 2018). This was not observed in this thesis for simultaneously optimized MBRT plans, which all have a similar or improved dose homogeneity in the target compared to plans of photon-only techniques (see DVH comparisons in chapter 4 and 6). This is in accordance with the findings of Xiong *et al* (2004) that simultaneously optimized photon and electron contributions lead to an improved dose homogeneity compared to sequentially optimized contributions for breast treatments with integrated boost.

7.3. Optimization algorithm

The implemented simulated annealing based direct aperture optimization (DAO) (Shepard *et al* 2002) was used throughout the whole thesis to optimize MERT, photon IMRT, ssMBRT and DYMBER plans. The only exception is the subprocess in the DYMBER TPP used to re-optimize the pMLC sequences of the photon dynamic trajectories. This re-optimization was performed using a research version of the Eclipse VMAT photon optimizer, which is based on the commercially available Eclipse VMAT optimizer (Varian Medical Systems, Palo Alto, CA). However, this VMAT optimizer follows the multi-resolution approach described by Otto (2008), which is also a kind of simulated annealing algorithm. The DTRT and VMAT plans were also created using the research and commercial version of the Eclipse VMAT optimizer (Varian Medical Systems, Palo Alto, CA), respectively. Thus, all plans compared in this thesis were created using a simulated annealing based optimization method and are therefore expected to be compared under undistorted conditions.

The dosimetric results of the MBRT plans indicate that the simulated annealing algorithm is suited to take advantage of the photon and electron beam characteristics. The primary advantage of the simulated annealing algorithm is that both the shapes and weights of photon and electron apertures are simultaneously optimized within the same process. As the DAO is a non-convex optimization problem, it is also of advantage that the simulated annealing algorithm allows to escape local minima of the objective function. However, there are also drawbacks of this stochastic search algorithm. Many iterations are necessary for convergence of the optimization leading to large computation times. Moreover, the number of apertures per field needs to be predefined by the user leading to many pre-optimizations to find an appropriate set of number of apertures per field. A solution to the second issue is to extend the algorithm with a column generation algorithm (Romeijn *et al* 2005) resulting in a hybrid algorithm. Such a hybrid algorithm was developed in-house and applied to generate ssMBRT plans (Risse *et al* 2017, Tessarini *et al* 2016, Mueller *et al* 2017). The hybrid DAO starts with an empty aperture pool and adds apertures iteratively. In one iteration, the optimizer determines for each field the aperture shape with the most negative gradient value on the objective function under consideration of the present aperture pool. Next, each of

these most promising apertures is then separately added to a copy of the present aperture pool, followed by a sequential combination of deterministic aperture weight optimizations and a simulated annealing optimization of the aperture shapes and weights. The aperture pool with the lowest objective function value is then accepted and used for the next hybrid DAO iteration. In figure 1, the DVHs of the ssMBRT plan shown in chapter 4 for the squamous cell carcinoma are compared to those of an ssMBRT plan optimized with the same objectives but using the hybrid algorithm instead of the simulated annealing algorithm. It follows that a more advanced optimization algorithm such as the hybrid algorithm can not only automatize the number of apertures per field but potentially also further increase treatment plan quality.

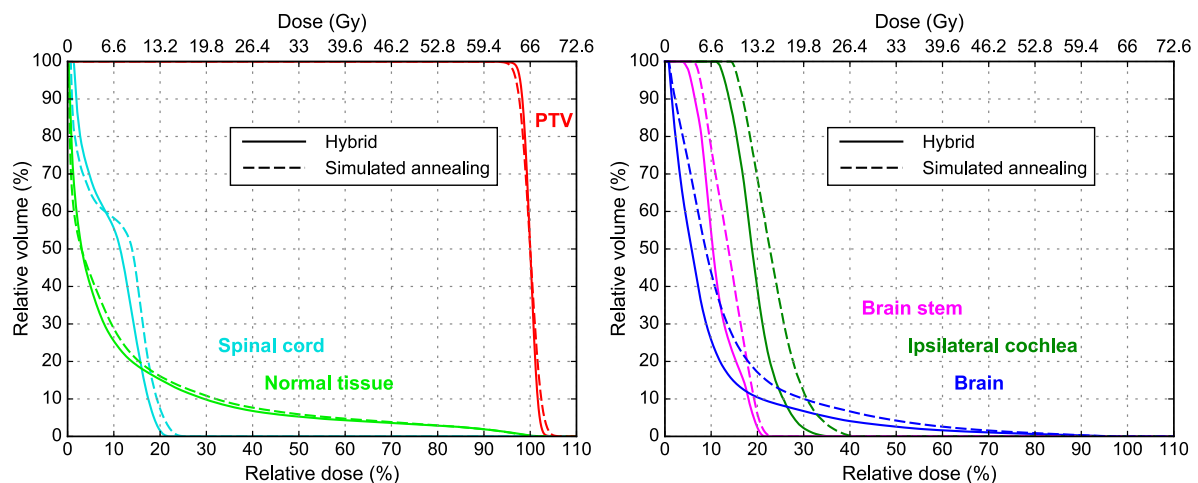


Figure 1. DVH comparison of ssMBRT plans for the squamous cell carcinoma case either optimized with the hybrid algorithm (solid lines) or the simulated annealing algorithm (dashed lines).

7.4. Deliverability

A goal of this thesis was to develop MBRT treatment techniques with efficiently and accurately deliverable treatment plans. All dose distributions of the presented MBRT plans in this thesis were calculated using validated MC algorithms. Additionally, the accuracy of the MC calculations was well demonstrated with the film measurement based validations of the DYMBER plans. These plans contain modulated electron beams and photon beams delivered with dynamic trajectories. Thus, the most advanced delivery types used in this thesis were applied for this validation.

Regarding treatment efficiency, using the pMLC for electron beams is an appropriate solution, which does not need any hardware adaptations on a conventional treatment unit. The treatment room does not need to be entered to switch from photon to electron beams and no custom collimation devices need to be manufactured. Furthermore, MC simulations are capable to maintain dose calculation accuracy for a broad range of SSDs. This is necessary to exploit beam directions that would lead to collisions with the patient or the table using an SSD, which is too short. For electron beams, the dosimetric disadvantage of pMLC collimation compared to collimation with electron applicator based devices is the larger penumbra. However, in the scenario of MBRT this can be compensated to a large extent with the short penumbra of the photon beams. This was demonstrated in this thesis by the MBRT plans, because they have improved near maximal $D_{2\%}$ values to the serial OARs closely located to the target compared to photon-only plans.

The large penumbra of pMLC collimated electron beams has also an advantageous aspect regarding treatment plan robustness. The dose gradients of electron beams are less steep in any direction relative to beam direction compared to the dose gradients at the field edge of photon beams. Thus, the photon and electron contributions within the target cannot be patched to each other with steep dose gradient transitions, if the total dose is homogeneously distributed.

For clinical applications as suggested in the subchapter 7.1, one would need to pay attention that patient position is within tolerance for the following two situations in particular: First, for the isocenter shifts prior to the delivery of the apertures of an electron field and secondly, for the table rotations during the delivery of the photon dynamic trajectories in case of DYMBER. Similar situations are already handled today in clinical routine. Isocenter shifts are applied for photon-only treatment techniques and patient position is verified with image guided radiation therapy solutions. Moreover, translational table movements during beam on are applied for TomoTherapy (Accuray Inc, Sunnyvale, CA) treatments.

For an initial clinical implementation of MBRT, patient-specific pre-treatment quality assurance (QA) could be performed by comparing calculated and measured dose. Potential measurement approaches are films placed within an anthropomorphic phantom

like this was shown in chapter 6 for DYMBER or using the integrated electronic portal imaging device (EPID) as discussed in chapter 4. Both have the advantage that photon and electron beams could be measured with the same measurement device. For later use in clinical routine, independent dose calculations might be an option to replace the time-consuming QA measurements to improve clinical workflow.

In summary, the presented MBRT plans can be efficiently and accurately delivered on a conventional treatment unit. Patient position verification and patient-specific pre-treatment QA could be performed with solutions similar to those applied for other existing treatment techniques.

References

- Devic S, Seuntjens, Abdel-Rahman W, Evans M, Olivares M, Podgorsak E B, Vuong T and Soares C G 2006 Accurate skin dose measurements using radiochromic film in clinical applications *Med. Phys.* **33** 1116-24
- Ge Y and Faddegon B A 2011 Study of intensity-modulated photon–electron radiation therapy using digital phantoms *Phys. Med. Biol.* **56** 6693–708
- Li J G, Williams S S, Goffinet D R, Boyer A L and Xing L 2000 Breast-conserving radiation therapy using combined electron and intensity modulated radiotherapy technique *Radiother. Oncol.* **56** 65–71
- Míguez C, Jiménez-Ortega E, Palma B A, Miras H, Ureba A, Arráns R, Carrasco-Peña F, Illescas-Vacas A and Leal A 2017 Clinical implementation of combined modulated electron and photon beams with conventional MLC for accelerated partial breast irradiation *Radiother. Oncol.* **124** 124–9
- Mu X, Olofsson L, Karlsson M, Sjögren R and Zackrisson B 2004 Can photon IMRT be improved by combination with mixed electron and photon techniques? *Acta Oncol.* **43** 727–35
- Mueller F, Mueller S, Manser P, Fix M K and Stampanoni M F M 2017 Multicriteria optimization for mixed beam radiotherapy *ETH Zürich Master Thesis for Master in Physics*
- Mueller S, Risse T, Fix M K, Tessarini S, Mueller F, Zaugg K, Stampanoni M F M and Manser P 2018a Mixed beam radiotherapy for sternum and lung treatments *Radiother. Oncol.* **127** 1049 EP-1930 presented at ESTRO 37
- Mueller S, Henzen D and Joosten A 2018b Practical usability of a treatment planning process for mixed beam radiotherapy *ETH Zürich Master Thesis for MAS in Medical Physics*
- Otto K 2008 Volumetric modulated arc therapy: IMRT in a single gantry arc *Med. Phys.* **35** 310–7
- Palma B A, Sánchez A U, Salguero F J, Arráns R, Sánchez C M, Zurita A W, Hermida M I R and Leal A 2012 Combined modulated electron and photon beams

- planned by a Monte-Carlo-based optimization procedure for accelerated partial breast irradiation *Phys. Med. Biol.* **57** 1191–202
- Renaud M-A, Serban M and Seuntjens J 2017 On mixed electron–photon radiation therapy optimization using the column generation approach *Med. Phys.* **44** 4287–98
- Risse T, Mueller S, Manser P, Fix M K and Stampanoni M F M 2017 Implementation and application of a hybrid direct aperture optimization for mixed beam radiotherapy *ETH Zürich Master Thesis for Master in Physics*
- Romeijn H, Ahuja R, Dempsey J and Kumar A 2005 A column generation approach to radiation therapy treatment planning using aperture modulation *SIAM J. Optim.* **15** 838–62
- Rosca F 2012 A hybrid electron and photon IMRT planning technique that lowers normal tissue integral patient dose using standard hardware *Med. Phys.* **39** 2964–71
- Shepard D M, Earl M A, Li X A, Naqvi S and Yu C 2002 Direct aperture optimization: a turnkey solution for step-and-shoot IMRT *Med. Phys.* **29** 1007–18
- Tessarini S, Mueller S, Manser P, Fix M K and Stampanoni M F M 2016 Implementation and performance evaluation of a deterministic algorithm used for direct aperture optimization *ETH Zürich Master Thesis for Master in Physics*
- Xiong W, Li J, Chen L, Price R A, Freedman G, Ding M, Qin L, Yang J and Ma C M 2004 Optimization of combined electron and photon beams for breast cancer *Phys. Med. Biol.* **49** 1973–89
- Zhang R, Heins D, Sanders M, Guo B and Hogstrom K 2018 Evaluation of a mixed beam therapy for postmastectomy breast cancer patients: Bolus electron conformal therapy combined with intensity modulated photon radiotherapy and volumetric modulated photon arc therapy *Med. Phys.* **45** 2912–2924

8

Conclusions

In this thesis, two treatment techniques for mixed beam radiotherapy (MBRT) were successfully developed and investigated for different treatment sites. The first is a pMLC based step and shoot technique (ssMBRT) and the second, called dynamic mixed beam radiotherapy (DYMBER), combines step and shoot pMLC segmented electron beams with photon dynamic trajectories. ssMBRT plans were compared to MERT, photon IMRT and VMAT plans for a left chest wall case and a squamous cell carcinoma case in the head and neck region, while DYMBER plans were compared to DTRT and VMAT plans for one brain and two head and neck cases. Both MBRT techniques dosimetrically outperformed the compared treatment techniques demonstrating a substantial dosimetric gain if dose distributions of photon and electron beams are favorably complemented to each other. To achieve this, optimizing the photon and electron contributions simultaneously was key. A simulated annealing based DAO was found to be appropriate for this purpose and could be suitably extended with a column generation algorithm to further automatize the beam direction and modality selection.

Regarding delivery of MBRT, using the pMLC also for electron beam collimation at a reduced SSD beside photon beam collimation is appropriate for a comfortable clinical workflow. An important reason for this is that the operator does not need to enter the treatment bunker to mount and unmount the electron applicator for switching between photon and electron delivery. It was also demonstrated that an accurate dose calculation of pMLC collimated electron beams is not restricted to an SSD of 70 cm, but also at larger SSDs facilitated by MC simulations.

All dose distributions of the presented treatment plans in this thesis were calculated using MC simulations and are accurately deliverable with conventional treatment units. For DYMBER, the calculated dose distributions were shown to agree very well with absolute dose measurements performed with films placed in an anthropomorphic phantom. These film validations demonstrate a high accuracy of conventional treatment

units and MC simulations for treatment techniques utilizing increased degrees of freedom.

In conclusion, this thesis demonstrates the dosimetric value of combining particle types for radiotherapy for the case of photons and electrons. The results of the efficiently and accurately deliverable MBRT plans suggest using MBRT for future clinical applications to treat targets with at least a superficial part of any treatment site with improved treatment plan quality compared to photon-only techniques.

Acknowledgements

I would like to express my thanks to:

Prof. Dr. Marco Stampanoni, for supervising my PhD thesis.

Prof. Dr. Paul Keall, for agreeing to be co-examiner.

In addition, I would like to express my sincere gratitude to:

Dr. Peter Manser and *Prof. Dr. Michael Fix*, who both made my dissertation at the Inselspital possible. They advised me during the whole PhD thesis with many constructive discussions. The brainstorming sessions with them were the origin of many fruitful ideas. They both taught me how to point out the key messages in publications. This increased my pleasure in demonstrating our work substantially. Peter's drive in following and achieving the aspired goals inspired me substantially. I will profit from this for the rest of my life. Michael's passion for medical physics and his optimism influenced my motivation greatly. Already in the very first discussion we had when I was a Physics Master student, he ignited my passion for mixed beam radiotherapy.

Dr. Andreas Joosten and *Dr. Dominik Henzen*, for their previous work about modulated electron radiotherapy and sharing their knowledge about dose measurements, treatment planning and Monte Carlo beam modeling. They always had an open ear for my concerns.

Dr. Daniel Frei and *Dr. Werner Volken*, for their support regarding Monte Carlo simulations and dynamic trajectories. My very favorite day of the week was always Wednesday when both were present on-site, because then, working atmosphere was most inspiring.

Daniel Frauchiger, for his numerous recommendations regarding dose measurements and for answering my detailed questions about the treatment units. I profited a lot from his enormous knowledge.

Reto Kueng, *Stefan Tessarini*, *Dr. Paul-Henry Mackeprang*, *Terence Risse*, *Fabian Mueller* and other students for the countless discussions about any work or non-work related topics and for their contributions to mixed beam radiotherapy, whether it was

about measurements night after night, reducing discrepancies between final and optimized dose, implementing optimization algorithms or sharing numerous Python scripts.

Furthermore, I would like to thank all other physicists, technicians, IT specialists and secretaries at the Division of Medical Radiation Physics (AMS), as well as radio-oncologists and radiation therapy technologists of the Department of Radiation Oncology (UKRO) at the Inselspital. They all shared their knowledge with me and helped me in many tasks such as dose measurements, quality assurance, clinical aspects of treatment techniques, cutting film, fabricating cut-outs, performing CT-scans of phantoms or administrative work. The working environment at the AMS and UKRO was always very pleasant and positive. I appreciated this a lot.

Finally, I would like to thank my family and my friends for their constant encouragement and all their support during these years.

Curriculum Vitae

Silvan Mueller

Born October 16, 1987 in Zug, Switzerland

Citizen of Malters, Switzerland and Ruswil, Switzerland

Education

- 1994-2000 Primary School in Hünenberg, Switzerland
- 2000-2003 Secondary School in Hünenberg, Switzerland
- 2003-2007 Apprenticeship in Information Technology at Oerlikon Assembly
Equipment AG in Cham, Switzerland
- 2003-2007 Technical Vocational Matura in Zug, Switzerland
- 2008-2009 Supplementary Exam Certificate "Passerelle" in Reussbühl, Switzerland
- 2009-2013 Bachelor of Science ETH in Physics
- 2013-2015 Master of Science ETH in Physics
- 2016-2018 Master of Advanced Studies ETH in Medical Physics
- 2015-2018 Ph.D. thesis at the Division of Medical Radiation Physics, Inselspital,
Bern University Hospital, Switzerland

Work Experience

- 2007-2009 Software Engineer at Esec AG, Cham, Switzerland
- 2012 Process Engineer at Esec AG, Cham, Switzerland
- 2015 Medical Physicist at the Division of Medical Radiation Physics,
Inselspital, Bern University Hospital, Switzerland

